UNIVERSITY OF SOUTHAMPTON

FACULTY OF SCIENCE

School of Chemistry

Transition metal complexes of bis(carbene)pyridine 'pincer' ligands: synthesis and reactivity

by

David Charles Pugh

A thesis submitted to the University of Southampton in accordance with the requirements of the degree of Ph.D. in the Faculty of Science

Department of Chemistry, April 2008

UNIVERSITY OF SOUTHAMPTON

ABSTRACT

FACULTY OF PHYSICAL SCIENCES
SCHOOL OF CHEMISTRY

DOCTOR OF PHILOSOPHY

TRANSITION METAL COMPLEXES OF BIS(CARBENE)PYRIDINE 'PINCER' LIGANDS: SYNTHESIS AND REACTIVITY

by David Charles Pugh

A new (CNC) pincer ligand, (2,6-bis(2,6-diisopropylphenyl)imidazol-2-ylidene)-3,5-dimethylpyridine, has been synthesised. Along with the previously reported ligand (2,6-bis(2,6-diisopropylphenyl)imidazol-2-ylidene)pyridine, (CNC) pincer complexes of transition metals across the periodic table, from titanium to iridium, have been synthesised, fully characterised and their reactivity investigated.

A comparison of the σ-donating properties of NHCs, trialkylphosphines and imines as part of pincer ligands has been carried out. Ti(IV) complexes of (CNC) and (PNP) ligands revealed that (CNC) ligands were better σ-donors than (PNP) ligands, in keeping with literature reports. However, Fe(0) complexes of (CNC), (PNP) and (NNN) ligands revealed that (PNP) ligands were better σ-donors, contrary to literature reports.

Novel ring opening reactions of NHCs to coordinated vinyl groups have been observed with nickel and iridium complexes of (CNC) ligands. Proposed mechanisms indicate the former is caused by methyl migration to the C_{NHC} followed by base-catalysed deprotonation whereas it is thought the latter occurs *via* a 4-membered nitrogen-containing heterocycle. An unprecedented binding mode for NHCs has also been observed where the unsaturated backbone of an imidazol-2-ylidene ring bonds in an η^2 fashion to another metal centre.

Acknowledgements

I would first like to thank Dr. Andreas Danopoulos for giving me the opportunity to work on this project. His advice, encouragement and support have been invaluable in allowing me to complete the work.

The past three years would have been much duller without the various 'characters' who have passed through 30:2007. I would like to thank Joseph, Robin, Nikos, Neo, Stephen and Susana for ensuring the Danopoulos group has never been dull to work in. I have also been fortunate to have supervised three very capable undergraduate students, so additional thanks go to Sandra, Hayley and Aimee. Thank you to Lorna, Stuart, Marek, Jo, Thao Nguyen and Dipali who have also had the (mis)fortune to share a lab with me. Or should that be the other way round...? I would also like to thank everyone else on the 2nd floor, past and present.

Several people have collected spectroscopic and structural data on my behalf and I would like to thank them all here: the Southampton NMR service, Joan Street and Dr. Neil Wells, for collecting the VT and ^{29}Si NMR spectra; Dr. David Evans at the John Innes Centre, Norwich, for collecting the Mössbauer data; Dr. Stephen Boyer at London Metropolitan University, for the elemental analysis data and Prof. William Clegg and the EPSRC National Crystallography Service for running my ~~rubbish~~ single(!) crystals at Daresbury. I would also like to thank Dr. Mark Light for being an invaluable source of help with my crystallography problems.

Thanks to Ben, Sarah, Johnny, Wayne and Kate, my housemates over the past three years, for the laughs, card games, pool and general drunken tomfoolery. Thanks to my family for their support, encouragement and financial assistance over the years. I promise I'll get a proper job now!

Finally, thanks to my girlfriend, Ria, for being there for me when I need her. Squawk!

List of Abbreviations

Ac	Acetyl
Acac	Acetylacetonate
Ad	1-Adamantyl
BAr^F	Tetrakis(3,5-bis(trifluoromethyl)phenyl)borate
Bipy	2,2'-Bipyridine
Bu	Butyl
^{t}Bu	*tert*-Butyl
Bz	Benzyl
CIF	Crystallographic information file
COD	1,5-Cyclooctadiene
COE	Cyclooctene
Cp	Cyclopentadienyl
Cp*	Pentamethylcyclopentadienyl
CSD	Cambridge structural database
Ct	Centroid (of two or more atoms)
Cy	Cyclohexyl
DCM	Dichloromethane
DEPT	Distortionless enhancement by polarisation transfer
DiPP	2,6-Bis(diisopropyl)phenyl
DME	1,2-Dimethoxyethane
DMEDA	*N,N'*-Dimethylethylenediamine
Et	Ethyl
Fac	Facial
HMDS	Hexamethyldisilazide
HS	High spin
IPA	Isopropanol
IR	Infra red
LDA	Lithium diisopropylamide
LRMS	Low resolution mass spectrometry
LS	Low spin
Me	Methyl
Mer	Meridional

Mes	Mesityl (2,4,6-trimethylphenyl)
MP	Melting point
MW	Molecular weight
Nbd	1,4-norbornadiene
NHC	*N*-Heterocyclic carbene
NMO	*N*-Methylmorpholine-*N*-oxide
NMR	Nuclear magnetic resonance
Np	Neopentyl
OFN	Oxygen-free nitrogen
ORTEP	Oak Ridge thermal ellipsoid plot
OS	Oxidation state
PE	Petroleum ether
Ph	Phenyl
Ppm	Parts per million
^{i}Pr	*iso*-Propyl
Py	Pyridine
RT	Room Temperature
TBHP	*tert*-Butylhydroperoxide
Tf	Triflyl (trifluoromethanesulfonyl)
THF	Tetrahydrofuran
TMEDA	*N,N,N',N'*-Tetramethylethylenediamine
TMS	Trimethylsilyl
o-tol	*ortho*-Tolyl (2-methylphenyl)
p-tol	*para*-Tolyl (4-methylphenyl)
UV	Ultra violet
Xy	Xylyl (2,6-dimethylphenyl)

Table of contents

Chapter 1

Introduction

1.1 - Background

1.11 History of carbenes

The history of carbenes can be traced back to the mid 1800s, when Dumas and Péligot proposed the synthesis of methylene ($:CH_2$) through the pyrolysis of chloromethane.[1] In 1862, Geuther theorised that the basic hydrolysis of chloroform gave an intermediate of dichlorocarbene ($:CCl_2$),[2] which was not, however, confirmed for nearly 100 years,[3] although plenty of evidence was gathered in the intervening time.[4]

In 1912, Staudinger discovered that pyrolysis of diazomethane in the presence of CO yielded ketene[5] leading to the idea that methylene was the product of the pyrolysis, which combined with CO to afford the ketene. Along with Loose's report of copper-catalysed decomposition of diazo compounds,[5] this work opened up a whole new area of carbene synthesis: the decomposition of diazo compounds is now a widely-used method of synthesising carbenes and their metal complexes.

Although more recent investigations into the copper-catalysed decomposition of diazo compounds indicate that a copper carbene complex is formed,[6] it is generally held that the first stable metal-carbene complex **1** was isolated by Fischer and Maasböl in 1964.[7] However, the first methylidene metal complex **2** was not isolated until 1975 by Schrock (Figure 1).[8]

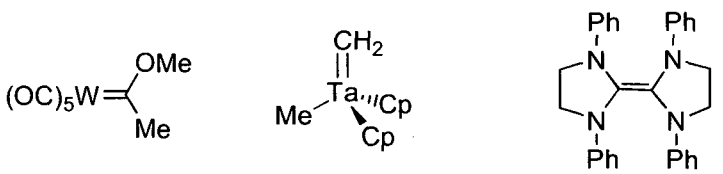

1 **2** **3**

Figure 1: Milestones in early carbene chemistry

In 1962, Wanzlick isolated the dimer bis(1,3-diphenylimidazolin-2-ylidene) **3** (Figure 1), formed formally by the dimerisation of two *N*-heterocyclic carbenes, which exhibited a tendency to dissociate at high temperatures (50% dissociation at 170 °C).[9] However, it was not until 1968 when the first transition metal complexes of *N*-heterocyclic carbenes (NHCs) were isolated independently by Öfele (Figure 2, **4**) and Wanzlick (Figure 2, **5**).[10, 11]

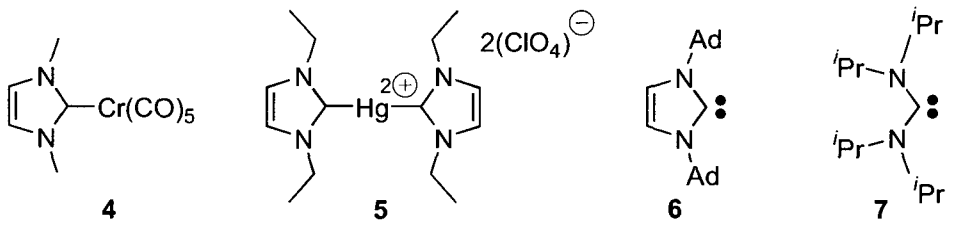

4 5 6 7

Figure 2: Advances in NHC chemistry

A major breakthrough occurred in 1991 when Arduengo isolated and crystallised the first "bottle-able" carbene **6** (Figure 2).[12] Although no metal complexes were reported in this publication, the discovery that carbenes could be isolated and kept, albeit under an inert atmosphere, resulted in a huge growth in the field of carbene chemistry. The isolation of the first non-cyclic diaminocarbene **7** followed in 1996 when Alder reported the synthesis of bis(di*iso*propylamino)carbene.[13] The isolation of **7** demonstrated that ring constraints and/or aromatic stabilisation were not prerequisites for the isolation of stable carbenes. However, most of the research into amine-stabilised carbenes has focussed on NHCs rather than their acyclic analogues.

1.12 What is a carbene?

A carbene is defined as a group with a divalent carbon atom containing only 6 electrons in its valence shell and no overall charge. It can also be thought of as a group with carbon in oxidation state (II). Carbenes themselves can be divided into two subsets depending on their spin-multiplicity: triplet carbenes, where the two non-bonding electrons are unpaired, and singlet carbenes, where the two non-bonding electrons are paired.

Figure 3: Electronic structure of triplet and singlet carbenes

Triplet carbenes are based around an sp hybridised carbon centre, and are linear molecules with two singly occupied p orbitals (Figure 3). As the non-bonding electrons are unpaired, triplet carbenes can also be thought of as diradicals. However, this makes

them extremely difficult species to isolate: triplet methylene, for example, has an enthalpy of dimerisation of –728 kJ mol^{-1}.[14] Electronic stabilisation of triplet carbenes is an ineffective method of isolating them, hence steric crowding of the carbene centre is the method of choice.

Triplet carbenes are sufficiently reactive such that no triplet carbene has yet been synthesised which is indefinitely stable at RT. However, work by Tomioka *et al.* has resulted in triplet carbenes which are indefinitely stable at –40 °C (Figure 4, **10**) and can be stored at RT for up to one week in solution.[15] Structural characterisation of triplet carbenes can also be carried out using single-crystal-to-single-crystal techniques.[16]

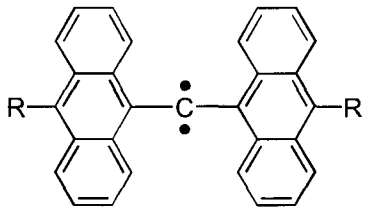

8: R = H, stable <1 sec
9: R = Ph, stable for 19 mins
10: R = 2,6-Me_2-4-^{t}Bu-Ph, stable for 1 week

Figure 4: 'Stable' triplet carbenes

Singlet carbenes are based around an sp^2 hybridised carbon centre and are bent molecules (Figure 3). The non-bonding electrons are paired and the presence of an empty p orbital potentially allows amphiphilic behaviour. Singlet carbenes are much easier to stabilise and isolate by steric and electronic tuning of the carbene carbon substituents than triplet carbenes, with Arduengo's carbene (**6**) a prime example of a stable, isolable singlet carbene.

This extra stabilisation can be a result of steric crowding of the carbene carbon but electronic stabilisation also plays a significant role. Electron-withdrawing substituents bonded to the carbene carbon increase the s-type character of the carbene carbon, hence stabilising the singlet state. However, greater stabilisation is conferred when π-donating substituents, *e.g.* N (**3**) and O (**1**) are bonded to the carbene carbon: the lone pairs on the heteroatoms donate electron density into the empty p-orbital on the carbene carbon, resulting in some multiple-bond character to the C-heteroatom bond and a more electron-rich carbene centre.

1.13 Classification of metal carbene complexes

The pioneering research carried out by Fischer and Schrock (see section 1.11) has resulted in their names being used to classify two different types of carbene complexes of transition metals. Fischer carbene complexes can be thought of as metal complexes of singlet carbenes with an electrophilic carbene carbon, commonly found on transition metals of groups 6-8 (*e.g.* **1**). The lone pair on the carbene carbon renders the carbene as a neutral, 2-electron donor to transition metals and back-donation from the metal to the carbene carbon results in the formation of a metal–carbon double bond, although structural studies indicate the bond length is longer than the typical value for metal–carbon double bonds. Schrock carbene complexes feature a nucleophilic carbene carbon (*e.g.* **2**) and are usually observed on early transition metals (groups 4-6) in high oxidation states.

A subset of singlet carbene complexes is termed NHCs (see section 1.2). In this case, the coordinated carbenes are lone-pair donors with little back-donation from the metal to the carbene carbon. This forms a dative covalent bond between the ligand and metal, best described as a single bond (*e.g.* **4**, **5**) and is analogous to other neutral, 2-electron donors, *i.e.* phosphines and amines. The difference is best illustrated using Grubbs' 2nd generation metathesis catalyst (**11**)[17] which contains both an NHC and an alkylidene (Figure 5).

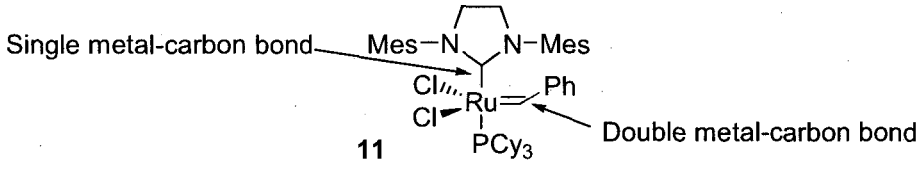

11

Figure 5: Grubbs' 2nd generation metathesis catalyst

1.2 - The NHC as a ligand

NHCs are a subset of singlet carbenes because the non-bonding electrons are paired. However, when complexed to metals, they do not fit the definition of either a Fischer or a Schrock carbene hence they are looked upon as a separate class of singlet carbene.

1.21 Electronic properties

As mentioned previously (section 1.12), there are two methods of stabilising carbenes: electronic stabilisation and steric stabilisation. Arduengo's carbene, **6**, exhibits both: the bulky 1-adamantyl groups prevent dimerisation and the nitrogen atoms flanking the carbene carbon increase the electron density at the electron-deficient carbene centre through the nitrogen lone pairs (Figure 6).

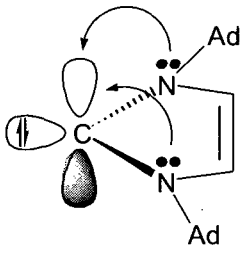

Figure 6: Stabilisation of NHCs

The most common use for NHCs is as a ligand in transition metal chemistry. They are excellent σ-donors and are often considered analogous to electron-rich phosphines. NHCs form a strong bond to transition metals, especially late transition metals. It was initially thought that NHCs did not function as π-acceptors at all based on structural analysis of metal–NHC bond lengths.[18] However, recent work by Jacobsen *et al.* has indicated that NHCs cannot be considered as purely σ-donor ligands.[19]

Two π-interactions contribute to the total orbital interaction between the metal centre and the NHC ligand: π-backdonation, from the metal to the NHC, and π-donation, from the NHC to the metal. This overall π-interaction is present in all NHC complexes of transition metals, with at least 10% of the total orbital interaction (for early TM complexes of NHCs) consisting of π-interactions. This figure rises to over 25% for some late TM complexes of NHCs, indicating that π-interactions make up a substantial part of the total orbital interaction. Even for NHC complexes of d^0 metal centres, a considerable amount of π-bonding exists. For NHC complexes of metal centres with a

low d electron count, the π-bonding consists of both π-donation and π-backdonation but for metals with high d electron counts, the π-bonding is dominated by π-backdonation.

Although NHCs make excellent ligands for transition metals, they have also found uses as organocatalysts due to their nucleophilic character. This area has recently been reviewed by Nolan *et al.*[20] and will not be further discussed.

1.22 Functionalising NHCs

In order for a carbene to be classified as an NHC, two criteria must be met. The carbene carbon must be contained within a ring system and the ring system must contain at least one nitrogen atom. Beyond this, there are no restrictions on what constitutes an NHC.

By far the most common type of NHC is the imidazol-2-ylidene ring (Figure 6) which consists of two nitrogen atoms flanking a carbene carbon (hereafter referred to as C_{NHC}) with an unsaturated 2-carbon linker between the two nitrogen atoms (–CH=CH–) forming a 5-membered heterocyclic ring. In this, an aromatic ring is created (2 π electrons from the backbone, 4 π electrons from the NCN system) which confers additional stability to the NHC. The saturated analogue, imidazolin-2-ylidene, is also widely used. These are not aromatic (only 4 π electrons) and are slightly better σ-donors although they are harder to isolate.

Other, less common, NHCs include those containing other heterocyclic ring sizes (*e.g.* **12**, Figure 7);[21] those containing other heteroatoms (*e.g.* O, S) flanking the C_{NHC} in combination with one nitrogen atom (**13**)[22] and those containing heteroatoms in the backbone (**14**). However, this project is solely concerned with imidazol-2-ylidene rings and the remainder of this introduction will focus solely on the imidazol-2-ylidene type of NHC.

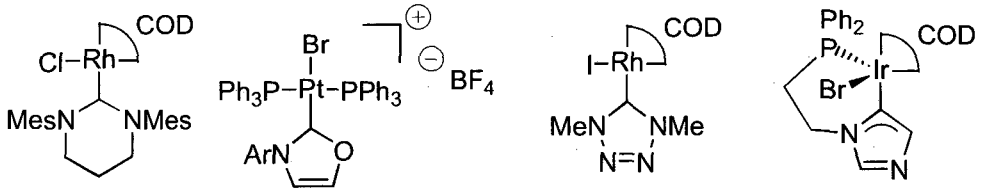

12 **13**: Ar = p-tol **14** **15**

Figure 7: Various types of NHC, including abnormal NHCs

"Normal" NHCs are bound to transition metals through C2 of the ring system. However, there exists another type of NHC which binds to transition metals through the 4- or 5-position of the ring. These are termed "abnormal" carbenes (*e.g.* **15**, Figure 7)[23] and, whilst they are no longer classed as imidazol-2-ylidenes, they are based on a 5-membered ring system containing two nitrogen atoms and an unsaturated backbone. Transition metal complexes of abnormal carbenes are sometimes formed in favour of normal carbenes, though the reasons for this are not fully understood and no mechanism of formation has yet been proposed. The area of abnormal carbenes has recently been reviewed.[24]

The NHC structure lends itself well to functionalisation. The most obvious way to achieve this is by the choice of the groups that are attached to the two nitrogen atoms (R_1, R_4) which can be the same or different. Incorporation of an NHC moiety into a chelating ligand *via* other classical donors bound to R^1 and/or R^4 will be covered in section 1.3 and will not be discussed further here.

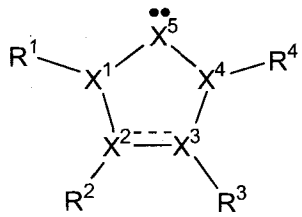

Figure 8: Functionalisation of NHCs

Figure 8 shows the various different points at which the basic 5-membered ring NHC architecture can be altered or functionalised. When none of the atoms X^1–X^4 are nitrogen, the molecule is no longer classed as an NHC, as is the case if X^5 is changed from C. However, it is possible to create molecules such as P-heterocyclic carbenes, (X^1, X^4 = P)[25] group 14 analogues of NHCs (X^1, X^4 = N, X^5 = Si/Ge/Sn)[26] and group 15 analogues of NHCs (X^1, X^4 = N, X^5 = As/Sb/Bi).[27]

Functionalisation at the backbone (R^2, R^3) can be achieved in various ways to tune the electronic properties of the ligand. The use of chlorides (R^2, R^3 = Cl) confers additional stability on the NHC such that the molecule becomes air stable.[28] Alternatively, X^2 and X^3 can be heteroatoms, forming triazole rings, (X^2 = N, X^3 = C)[29] NHCs with a diboron backbone (X^2, X^3 = B, R^2, R^3 = NMe_2)[30] and other substitution patterns are also known.

Other methods of functionalisation include fusing ring systems to the imidazol-2-ylidene ring: R^1-R^2, R^2-R^3 and R^3-R^4 fusion are all possible. Benzimidazol-2-ylidene (R^2-R^3 = Ph) was synthesised and complexed to transition metals.[31] An unstable bipyridine-derived NHC (R^1-R^2, R^3-R^4 = Ph) could only be isolated and not used as a ligand.[32] However, an analogous compound with only one fused benzene ring (R^1-R^2 = Ph) could be isolated and used as a ligand.[33]

1.23 Formation of NHCs and their metal complexes

Despite the plethora of publications containing NHCs either as ligands or as isolated molecules, there are relatively few synthetic methods for preparing them.[34] Most involve deprotonation of an imidazolium salt [a], although thermal α-elimination of volatile molecules [b] and desulfurisation of substituted thioureas [c] are also methods which have found some success (Scheme 1). Metal-based assembly of the NHC heterocycle is a topic which has the potential to yield unusually substituted NHCs but will not be discussed further.[35]

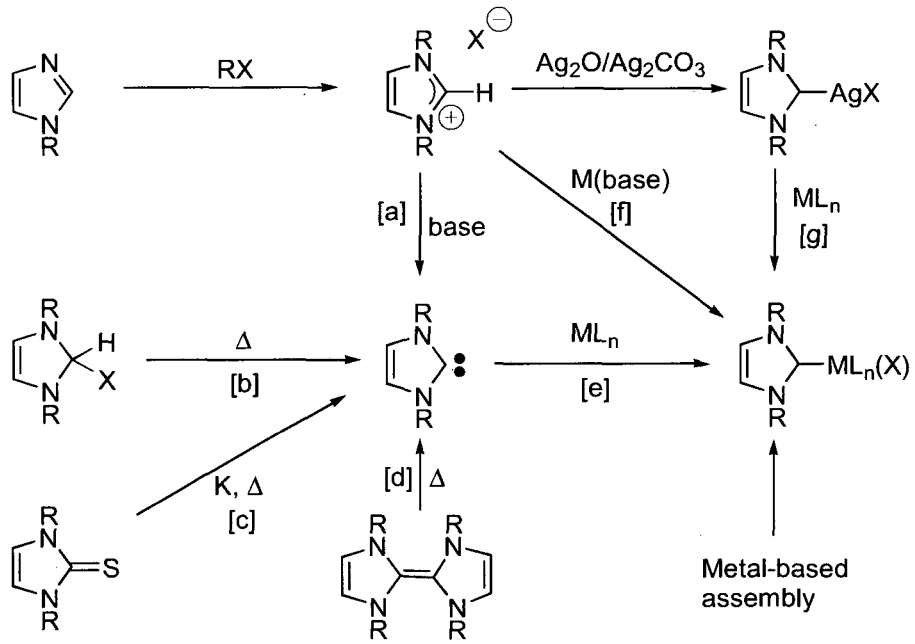

Scheme 1: Synthesis of NHCs and their metal complexes

Isolation of the NHC is not always necessary if the aim is to complex the NHC to a transition metal as a ligand. All of the above synthetic methods of NHC formation (with the exception of desulfurising thioureas) can be carried out in the presence of a metal salt which can trap the NHC as it is formed, yielding an NHC-metal complex *in situ*. This approach avoids manipulating the air and moisture sensitive NHCs, but it restricts

the choice of metal salt to those which can withstand the reaction conditions necessary for generation of the NHC. It can also prove an uneconomical route if the NHC synthesis step is low-yielding.

The most versatile starting material for the synthesis of imidazol-2-ylidenes are imidazolium salts. They are easily synthesised, either from the quaternisation of substituted imidazoles with alkyl halides or from the reaction of anilines, glyoxal and formaldehyde, and are air stable. Imidazolium salts with unusual substitution patterns are also available.[36] Deprotonation with a strong base (*e.g.* KH) yields the free NHC [a] which can be isolated[12] or, if the reaction is carried out in the presence of a metal salt, yields the NHC-metal complex [a,e].[34] If a suitable starting material can be found, it is also possible to deprotonate imidazolium salts using a base coordinated to a metal [f]: Öfele successfully used this method to synthesise complex **4**.[10] This is especially useful when synthesising late transition metal-NHC complexes in low oxidation states, due to the increased basicity of the coordinated ligand originating from reduced π-d backbonding *e.g.* $[Rh(OMe)(COD)]_2$.

Another method which has been widely employed in the synthesis of late transition metal-NHC complexes is transmetallation from Ag-NHC complexes [g].[37] These are easily synthesised from the imidazolium salt and an Ag precursor (usually Ag_2O or Ag_2CO_3) in the presence of 4Å molecular sieves and do not require inert-atmosphere conditions. This makes them especially attractive starting materials for the synthesis of NHC-metal complexes despite the expense of using Ag reagents.

1.3 – NHC donors as part of chelating ligands

This section will focus on tridentate ligands which incorporate at least two NHC moieties. Although there is a great variety of bidentate NHC-containing ligands (R^1 and/or R^4 contains a functional group, Figure 8) functionalised with other "classical" donors (*e.g.* phosphines, amines)[38] and even other carbon-based donors (another NHC,[39] aryl-fused Cp rings[40]), these mixed donor ligands are outside the scope of this project and will not be covered here.

There are two main types of tridentate ligand architecture: facially coordinating ligands and meridionally coordinating (or pseudo-meridionally in the case of 5-coordinate metal complexes) ligands. Facially coordinating ligands are also known as tripodal ligands, the majority of which contain three donor groups bound to a central atom by a linker. They can be divided into two sub-categories: symmetrical tripodal ligands, which contain a C_3-axis originating through the central donor atom, and unsymmetrical tripodal ligands. Meridionally coordinating ligands can also be divided into two sub-categories: linear tridentate (which have a flexible linker between the three donor groups) and pincer ligands, which are rigid species. Tridentate ligands with flexible linkers may alternate between facial and meridional coordination geometries (see section 1.31) but pincer ligands are only capable of coordinating in a meridional fashion.

1.31 Tripodal ligands

Tripodal ligands containing NHCs are not as well studied as pincer ligands containing NHCs. Although some tripodal ligands are only capable of coordinating to transition metals through adopting a facial geometry, tridentate ligands with flexible backbones are sometimes capable of adopting facial or meridional coordination geometries, as evidenced by the bis(phosphine)carbene ligand synthesised by Chiu and Lee (Scheme 2).[41] The flexible 2-carbon linker between the phosphine and NHC moieties results in the ligand switching from facial (**16**) to meridional (**17**) geometry upon addition of CO to bimetallic complex **16**.

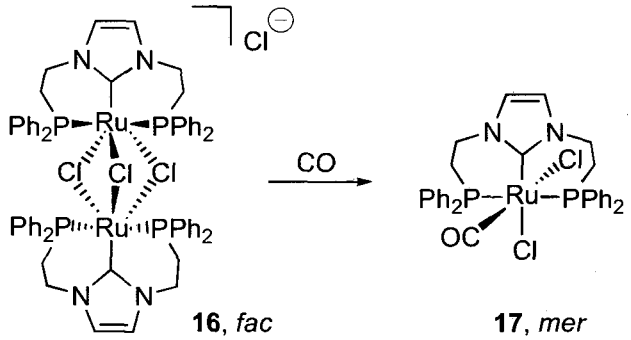

Scheme 2: Facial *vs.* meridional co-ordination

The majority of rigid tripodal ligands containing NHC moieties are based around a common architecture, namely three carbenes as the "legs" of the tripod linked to a common central atom (B, C, N) by a carbon spacer. The first ligand of this type was hydrotris(3-methylimidazol-2-ylidene)borate, synthesised in 1995 by Fehlhammer *et al.*[42] The main use of this ligand was in the synthesis of homoleptic NHC complexes (Scheme 3): hexa(carbene) Fe(III) and Co(III) compounds were structurally characterised, as was a lithium complex with two tripodal ligands.

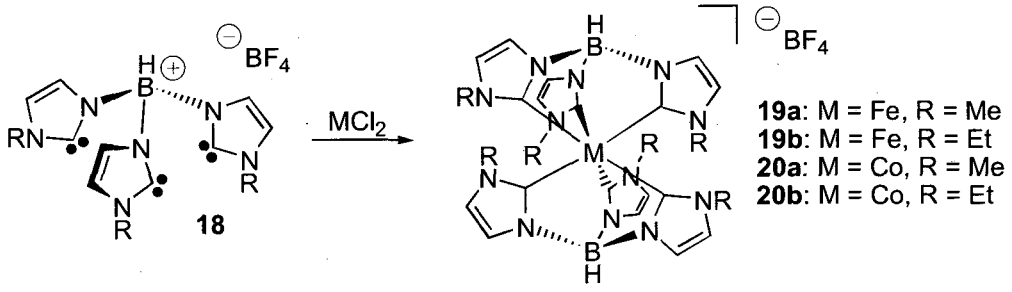

Scheme 3: The first hexacarbene complexes of transition metals

Tripodal ligands with carbon and nitrogen centres have also been synthesised (Figure 9). Dubbed "TIME" (**21**) and "TIMEN" (**22**) these ligands have been complexed to various first-row transition metals. This chemistry has been recently reviewed and will not be discussed further here.[43]

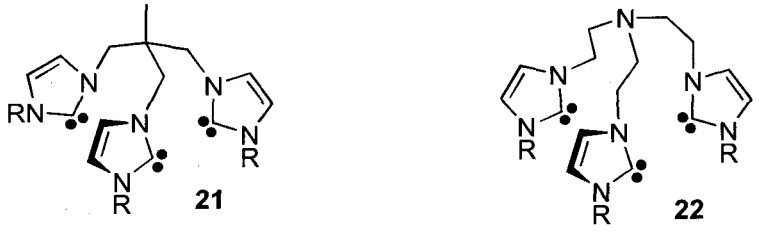

Figure 9: TIME and TIMEN

Attempts to form tripodal complexes of Rh(I) and Ir(I) failed, with bimetallic species the only isolated product.[44] A review of tripodal ligands containing at least two NHC

moieties has recently been published and contains details on the use of metal complexes of **21** and **22** in catalytic transfer hydrogenation reactions.[39]

To date, only two other examples of tripodal ligands containing at least two NHC moieties have been synthesised. Both contain two NHC donors and an aryloxy or alkoxy moiety complete the tripodal geometry.[39]

1.32 Pincer ligands

The first pincer ligand (**23**) was synthesised in 1976 by Moulton and Shaw[45] along with several examples of transition metal complexes. However, it was not until 1995 when the first pincer ligand containing an NHC moiety was synthesised in an unusual method by Matsumura *et al.*[46] (Figure 10). Ligand **24** is still the only pincer ligand containing an NHC moiety which is not based on a 5-membered ring.

The first bis(carbene)pyridine pincer ligand was reported in 2000: Chen and Lin[47] synthesised mercury complexes of ligand **25**, albeit the complexes were helical and the ligand was not acting as a pincer.

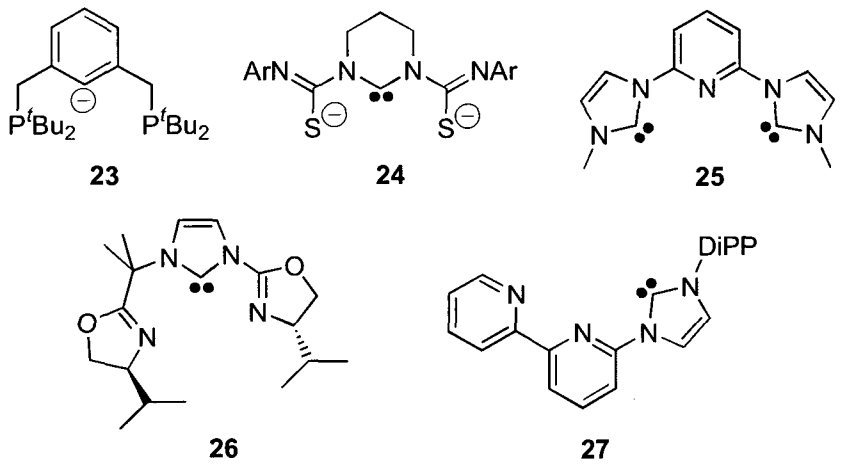

23 **24** **25**

26 **27**

Figure 10: Development of pincer ligands containing NHC moieties, including unsymmetrical pincers

The vast majority of NHC-containing pincer ligands have C_2-symmetry originating through a central donor group; hence there are two identical "arms". This lends itself to two types of architecture: (XCX) where the central donor is an NHC and the "arms" are other donors (*e.g.* **24**) and (CXC) where the "arms" are NHC moieties and the central donor is different (*e.g.* **25**). Rigid ligands also have additional planes of symmetry.

Currently, there are only two examples of pincer ligands where the "arms" are different (Figure 10): Gade *et al.* synthesised oxazoline-based pincer **26**[48] and Danopoulos *et al.* synthesised bipy-based pincer **27**.[49]

Since this section is focussed on pincer ligands with two NHC moieties, the first type of pincer architecture will not be covered here. A review of pincer ligands was recently published and this thoroughly covers the area of pincer ligands with one NHC moiety.[50]

The (CXC) type of pincer architecture can be further subdivided into pincer ligands with a central pyridine donor (see section 1.33) and pincer ligands with other central donor moieties. The latter class includes lutidine-based pincer ligands, pyrrole-based pincer ligands and amido-based pincer ligands as well as phenyl- and xylyl-based pincers.

There are several examples of pincer ligands with a central anionic carbon donor (Figure 11) although in most cases, the only difference is the substituent on the NHC moiety. Crabtree and co-workers synthesised an α,α'-xylyl-based bis(imidazol-2-ylidene) pincer ligand (**28a**)[51] as did Danopoulos *et al.* (**28b,c**)[52] while Hahn *et al.* have synthesised a benzimidazol-2-ylidene analogue (**28d**).[53] Hollis and co-workers have synthesised metal complexes of phenyl-based 1,3-bis(carbene) pincer ligands **29**.[54]

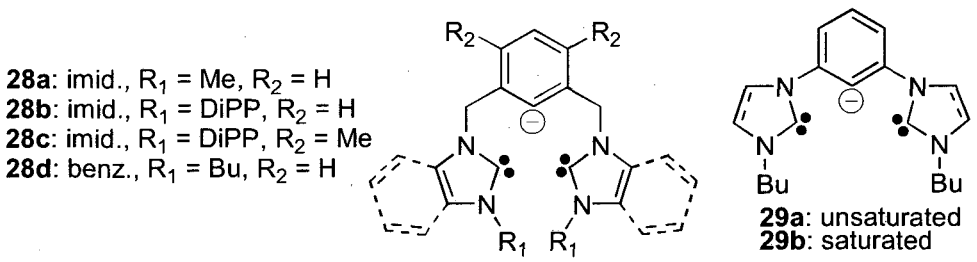

Figure 11: Carbon-based pincer ligands

For the ligands to act as pincers, the central carbon atom must be an anionic donor. Ligands **28a,b,d** were complexed to palladium through C–Br bond activation at the *ipso* carbon of the aryl bromide precursor. Although C–H activation of the bis(imidazolium) arene precursor as a means of introducing **28a** to a metal was attempted, no reaction was observed in the presence of $Pd(OAc)_2$ and NaOAc, even at 160 °C. However, ligand **28c** was introduced to Pd by C–H activation at the *ipso* position under the same conditions: the presence of two methyl groups on the phenyl ring increased the electron density of the aromatic ring and promoted electrophilic attack by Pd. Complexes of ligands **29a**

and **29b** were also synthesised in an analogous manner by activating the aryl C–H bond: reaction of the precursor imidazolium (imidazolinium) salt with $Zr(NMe_2)_4$ led to triple deprotonation and coordination of the ligand in a pincer fashion. The Zr(IV) complexes were also used as transmetallation reagents to form Rh(III) complexes.[55]

The chemistry of lutidine-based pincer ligands (Figure 12) is similarly concentrated on palladium. Most ligands contain two imidazol-2-ylidene rings (**30**), although there is one example containing benzimidazol-2-ylidene moieties (**31**).[56]

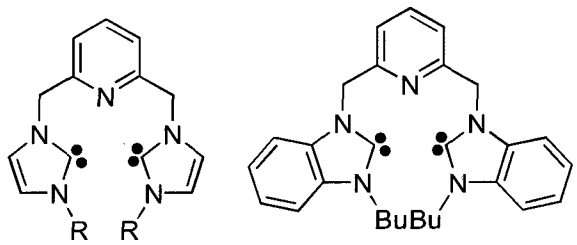

30 **31**

Figure 12: Lutidine-based pincer ligands

All the lutidine-based pincer ligands were complexed to palladium, usually *via* transmetallation from the silver carbene. One rhodium complex was also synthesised (R = Bu)[57] albeit it acted as a bridging ligand between two Rh(I) centres. The palladium complexes of **30** and **31** are similar, each containing a cationic square planar Pd centre with non-coordinating anion. Both aromatic[52] and aliphatic[58] substituents on the NHC moiety have been reported. Each palladium complex showed good catalytic activity in Heck and other cross-coupling reactions.

The CH_2 spacer between the NHC moieties and N-donor (C-donor in the case of **28**) results in the ligand twisting to maintain the square planar geometry, giving the molecule helical chirality (Figure 13). No attempt at resolution of the enantiomers was successful, although heating a Pd complex of **30** (R = DiPP, Figure 13)[59] to 80 °C did not interconvert the enantiomers.

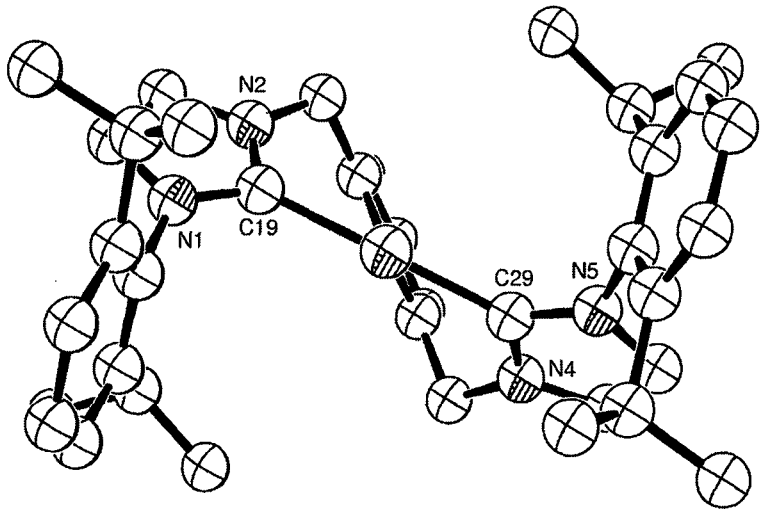

Figure 13: ORTEP representation of **28** (R = DiPP) looking down the Cl–Pd–N_{py} axis, showing the twist of the ligand

To date, there are only two amido-based pincer ligands. Douthwaite synthesised ligand **32** which contains two NHC moieties flanked by an amine donor,[60] while Kunz *et al.* have reported the pyrrole-based "bimca" ligand **33** (Figure 14).[61]

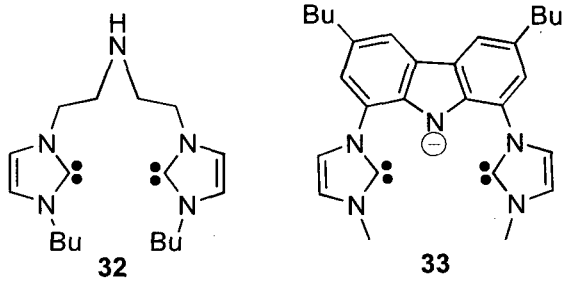

Figure 14: Amine/amide-based pincer ligands

Ligand **32** was coordinated to palladium *via* transmetallation from silver, forming a cationic square planar Pd complex with co-ordinated amine. Deprotonation with NaH resulted in the formation of an anionic amido ligand. Ligand **33** was synthesised by deprotonation of the bis(imidazolium)amine precursor with 3 equivalents of LDA and was subsequently complexed to rhodium.

1.33 (CNC) pincer ligands

By far the most common form of pincer ligand containing two NHC moieties is the pyridine-based dicarbene pincer ligand [hereafter referred to as (CNC)]. The precursor imidazolium salt is easily synthesised in one of two ways (Scheme 4).

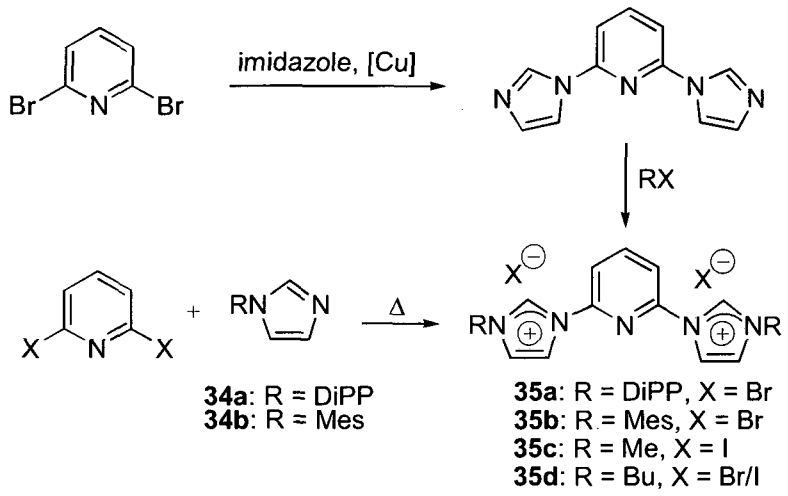

Scheme 4: Synthesis of imidazolium salts

The first method is used for alkyl imidazolium salts; quaternisation of 2,6-bis(imidazolyl)pyridine will only work with primary alkyl halides, usually bromide or iodide. The second method is much more general and can be used for the synthesis of aryl and alkyl imidazolium salts - the only limitation is whether the substituted imidazole can be synthesised. The first method is milder than the second method but the choice of substituent is restricted, whereas the second method uses harsher conditions but can synthesise any imidazolium salt. To date, there are no methods for synthesising a bis(imidazolinium)pyridine salt.

As shown in Scheme 1, there are three methods of synthesising NHC-transition metal complexes from the precursor imidazolium salt: transmetallation from silver, *in situ* deprotonation and reaction of the free carbene with a metal salt. Deprotonation of the imidazolium salt to form the free ligand is usually accomplished by reaction with KHMDS (Scheme 5).[62]

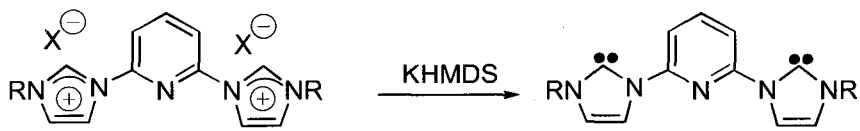

Scheme 5: Deprotonation of imidazolium salts

Gibson *et al.* used this methodology to synthesise a series of first row transition metal complexes with analogues of ligand **36**. It was found that octahedral chromium(III) complexes of **36** (R = ^{i}Pr) were very active ethylene oligomerisation catalysts.[63] Other first row metal complexes of ligand **36** were synthesised (M = Ti, V, Fe, Co)[64] but none proved as active as the Cr complex.

The only other first row transition metal complex of a (CNC) pincer ligand was reported in 2006 by Inamoto *et al.* Reaction of ligand **35c** with $Ni(OAc)_2$ resulted in the isolation of a cationic square planar Ni(II) compound with both coordinated and anionic bromides.[65] Good catalytic activity was noted for both the Heck and Suzuki cross-coupling reactions.

The synthesis of ruthenium complexes of **36** was accomplished by the *in situ* deprotonation method. Refluxing a solution of hydrated $RuCl_3$ with imidazolium salts **35c**[66] and **35d**[67] resulted in the isolation of a 6-coordinate octahedral bis(ligand)ruthenium dication. However, when $[Ru(COD)Cl]_n$ was used as the metal salt in the presence of NEt_3, the monoligated metal complex **37** was isolated in poor yield (Scheme 6). Compound **37** was used as a catalyst for the transfer hydrogenation of ketones and the oxidative cleavage of olefins and performed well in both reactions.

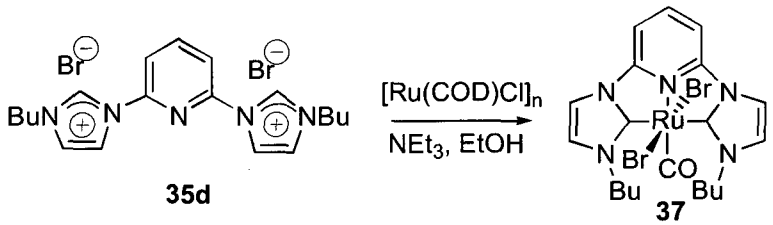

Scheme 6: Synthesis of Ru pincer complex **37**

A similar *in situ* deprotonation method did not afford pincer Rh(I) complexes when **35d** was reacted with $[Rh(COD)Cl]_2$ at 40 °C in the presence of NEt_3.[68] A bimetallic species was isolated which could be converted to a Rh(III) pincer species by addition of another equivalent of **35d** and refluxing in MeCN. However, the bimetallic species was a good catalyst for the hydrosilylation of alkynes and the Rh(III) species was a good catalyst for the transfer hydrogenation of ketones.

The pincer Rh(I) complex **38** was synthesised by the reaction of **35c** (X = PF_6) with $[Rh(CO)_2(OAc)]_2$ in the presence of NEt_3 (Scheme 7). Oxidative addition of MeI was facile, forming a cationic Rh(III) pincer complex.[69]

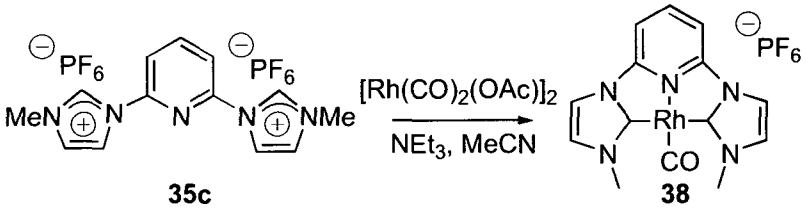

Scheme 7: Synthesis of Rh pincer complex **38**

The first (CNC) complex of palladium was reported in 2001.[70] Reaction of **35c** with $Pd(OAc)_2$ at 160 °C yielded a square planar Pd(II) cation (**39c**) with anionic bromide. A similar reaction could also be performed with **35d** yielding the butyl analogue **39d** (Scheme 8).[71] Both **39c** and **39d** were highly active Heck catalysts.

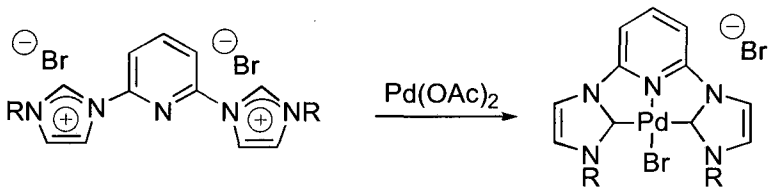

35a: R = DiPP, X = Br
35b: R = Mes, X = Br
35c: R = Me, X = I
35d: R = Bu, X = Br/I

39a: R = DiPP
39b: R = Mes
39c: R = Me
39d: R = Bu

Scheme 8: Synthesis of Pd pincer complexes

An analogue of **39d** with a carboxylate group in the *para* position of the pyridine ring was recently synthesised using the same method. It also proved to be highly catalytically active, this time in the Suzuki cross-coupling reaction under aerobic conditions.[72]

1.34 Danopoulos group work with ligand **36**

Previous work within the Danopoulos group has concentrated on transition metal complexes of ligand **36** and other aryl-substituted analogues (mesityl, 2,6-dimethyl-4-*tert*-butylphenyl). In contrast to other research groups who favour silver transmetallation or *in situ* deprotonation methods for synthesising transition metal complexes, the Danopoulos methodology has concentrated on synthesising and purifying the free ligand **36**. This method has several advantages over the other two methods but perhaps the most important is that it allows the choice of transition metal starting material. This has resulted in the synthesis of compounds which cannot be accessed by other methods, *e.g.* the ruthenium complex **40** which is a good transfer hydrogenation catalyst (Scheme 9).[62] An analogue of Grubbs' catalyst (**41**) has also been synthesised from ligand **36** but it showed limited metathesis activity.[49]

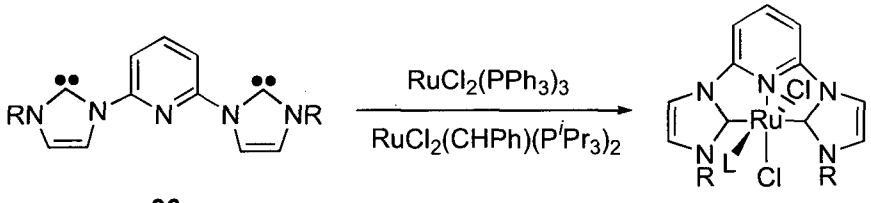

36

40: L = PPh_3
41: L = CHPh

Scheme 9: Synthesis of Ru pincer complexes, R = DiPP

Another advantage of the free ligand methodology is the use of milder reaction conditions for synthesising transition metal complexes. The pincer Rh complexes isolated by Peris[68] and Haynes[69] required elevated temperatures and additives (extra base) in their synthesis. However, reaction of **36** with $[Rh(C_2H_4)_2Cl]_2$ proceeded smoothly at –78 °C to RT to afford the pincer complex **42** in excellent yield (Scheme 10).[73]

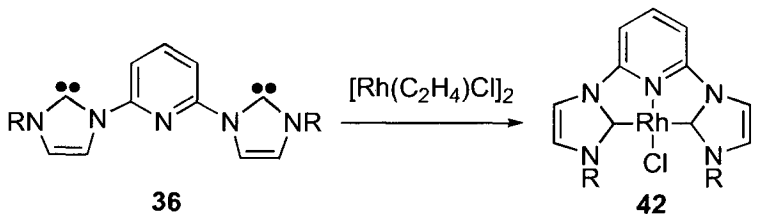

36 **42**

Scheme 10: Synthesis of Rh pincer complex **42**, R = DiPP

Complex **42** was not an active hydroformylation catalyst; this lack of reactivity was thought to be a result of the strongly-bound chloride to the Rh(I) metal. Despite the use of halide abstractors, the only ligand to displace the chloride was CO. However, compound **42** was susceptible to oxidative addition of C–Cl bonds: both CH_2Cl_2 and phosgene reacted to form octahedral Rh(III) pincer complexes.

Palladium complexes of **36** were also prepared by milder reaction conditions than those previously published. Reaction of **36** (and the mesityl analogue) with $Pd(COD)Cl_2$ at RT afforded the square planar cationic complexes **39a** and **39b** (with chloride instead of bromide). However, the reaction of **36** with $PdMe_2(TMEDA)$ yielded a completely different product (Scheme 11).[74]

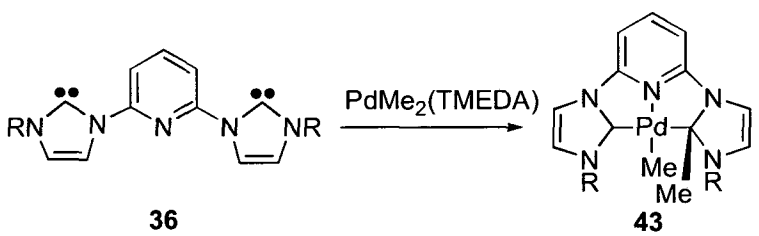

36 **43**

Scheme 11: Me migration to NHC moiety, R = DiPP

Methyl migration from Pd to the NHC moiety had been predicted previously[75] but had not been observed experimentally. DFT studies suggested the formation of an initial 5-coordinate Pd complex followed by methyl migration as a plausible mechanism of formation for **43**.

The majority of work involving (CNC) pincer complexes of transition metals has focused on platinum group metals. However, previous work with ligand **36** has resulted in the synthesis of vanadium, chromium,[76] iron[77] and cobalt[78] complexes, all in oxidation state (II), mainly through aminolysis of the $M(HMDS)_2$ starting material (Scheme 12).

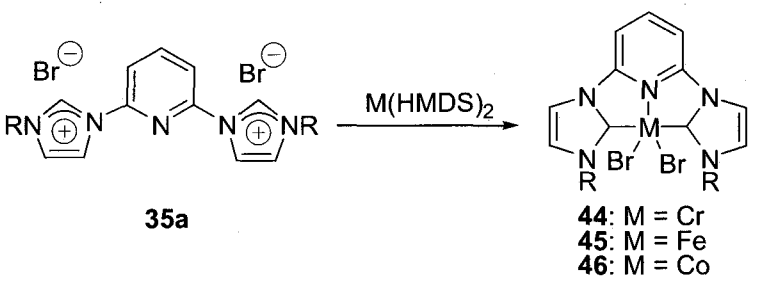

35a

44: M = Cr
45: M = Fe
46: M = Co

Scheme 12: First-row TM pincer complexes, R = DiPP

The vanadium (II) complex was synthesised by reacting **36** with $VCl_2(TMEDA)_2$ but similar reactions between M(II) dihalide salts and **36** did not yield the desired pincer complex. Indeed, the reaction of **36** with $[FeCl_2(TMEDA)]_2$ resulted in an "abnormal" carbene[24] (**47**) being formed (Scheme 13). The fact that $[(CNC)_2Ru]^{2+}$ (R = ^{n}Bu) has been observed[66] but with less bulky substituents on the imidazol-2-ylidene ring indicates the driving force behind the formation of the abnormal carbene is steric in origin.

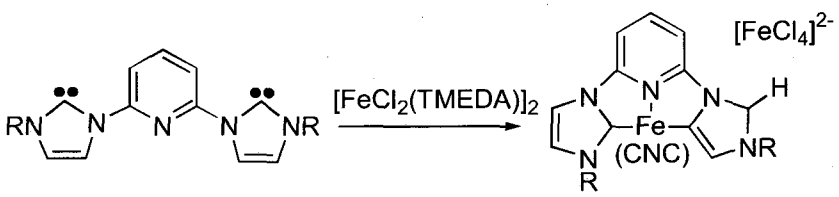

36 **47**

Scheme 13: Synthesis of an "abnormal" carbene, R = DiPP

Oxidation of **45** and **46** with excess Br–HMDS formed the octahedral $[(CNC)FeBr_3]$ and $[(CNC)CoBr_3]$ complexes respectively. Reduction of **46** with Na/Hg yielded a four coordinate square planar Co(I) complex, but performing the same reaction with **45** under 5 bar pressure of N_2 resulted in the formation of a five coordinate Fe(0) bis(dinitrogen) complex $[(CNC)Fe(N_2)_2]$ (Scheme 14).[79]

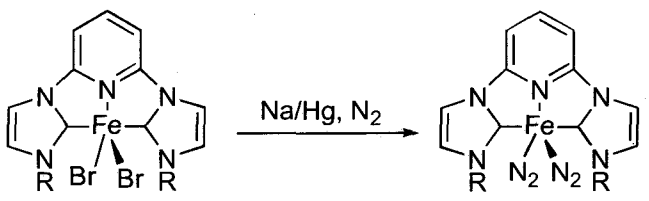

45 **48**

Scheme 14: Synthesis of a Fe(0) dinitrogen complex, R = DiPP

Complex **48** was structurally characterised, showing a distorted square pyramidal geometry. The apical dinitrogen molecule is labile, being displaced by phosphines and ethylene. However, the only ligand to displace the basal dinitrogen ligand was CO which formed a bis(carbonyl) Fe(0) complex. Reduction of **45** under CO also affords the bis(carbonyl) complex. However, if the reduction was carried out under Ar or H_2 then an unexpected product was isolated which was identified by X-ray analysis as the Fe(0) product **49** (Figure 15). C–H activation of the pyridine ring on the ligand was also observed with iridium complex **50** although the assignment was again based on a limited X-ray analysis.[80]

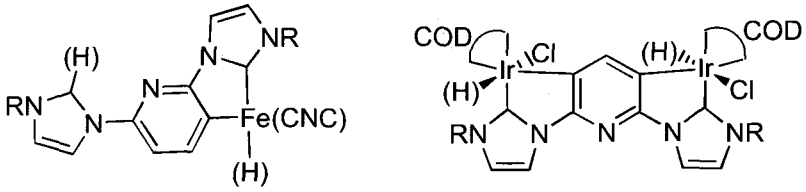

49 **50**

Figure 15: C-H activation of the (CNC) ligand, R = DiPP

1.4 - Aims

The initial aim of this project was to continue investigations into first row transition metal complexes of ligand **36**, building upon previous work with the titanium, vanadium, chromium and iron complexes (see sections 1.33 and 1.34). There had been no reports of manganese or nickel complexes of (CNC) pincer ligands at the time so investigating the chemistry of those two metals with the (CNC) ligand was another target.

Complex **48** was predicted to C–H activate small organic molecules. Another aim of this project was to investigate this. The reactivity of **48** towards substitution by "classic" neutral donor ligands also required further investigation, as did its reactivity towards other X–H bonds (X = Si, Ge, S etc.)

Due to the unwanted C–H activation of ligand **36** hampering efforts to isolate pincer iridium complexes, the synthesis of a new pincer ligand with blocking groups in the 3- and 5-positions of the pyridine ring was a high priority. If this could be accomplished, it would enable studies into the effect that substituted pyridine rings have on the reactivity at the metal centre. It would also allow previously inaccessible compounds to be synthesised (e.g. pincer iridium complexes) as well as analogues of the published pincer complexes of ligand **36**.

1.5 - Table of M–C_{NHC} bond lengths

This project will rely heavily on the use of single crystal X-ray diffraction as a characterisation tool. A large number of structures will be obtained and their analysis will be a significant part of the discussion chapters which follow. To this end, a survey of the CSD has been undertaken in order to find the range of metal–NHC bond lengths for relevant metals and oxidation states. The survey excludes compounds synthesised during the course of this project but includes previously published work involving (CNC) ligand **36**. This table is correct up to the May 2007 update of the CSD.

Metal	OS	Min. length (Å)	CSD code	Max. length (Å)	CSD code
Ag	+1	2.013	OCIGEN	2.460	CAVXON
Ti	+4	2.187	OKOLEF	2.312	ATEWUR
V	+2	2.161	SEDLIX	none	n/a
V	+4	none	n/a	none	n/a
Cr	+3	2.087	BEFJEC	2.120	BEFJEC
Mn	+2	2.204	NADLOU	2.270	UNIXAQ
Fe	0	1.881	FIMVED	2.007	TCIMFE
Fe	+2	1.927	VEWWEA	2.194	IREQOL
Fe	+4	none	n/a	none	n/a
Co	+2	1.901	DEXFAN	2.080	RAJFUE
Co	+3	1.913	IGIMIU	2.052	FEMPIX
Ni	+2	1.835	MOJKEB	2.019	FEGXOF
Nb	+3	none	n/a	none	n/a
Ru	+2	1.911	TZLPRU10	2.168	ABUFAF
Ru	+4	1.955	ALOLAO	2.118	WUWRIP
Rh	+1	1.914	YAXNUG	2.149	CEKSOB
Ir	+1	1.895	FINSOL	2.080	MOKHEZ
Ir	+3	1.905	UCEVEE	2.103	FOJVEG

Table 1: The shortest and longest crystallographically characterised M–C_{NHC} bond lengths for metals and oxidation states pertinent to the project, from a survey of the CSD. The data is correct as of May 2007.

Chapter 2

Ligand synthesis

2.1 - Introduction

In certain reactions of ligand **36** with Fe and Ir metal salts, C–H activation at the 3- and 5-positions of the pyridine ring was observed (see section 1.34). In order to suppress this, a new ligand with blocking groups in the 3- and 5-positions of the pyridine ring was desired. In addition to preventing C–H activation, when the ligand was coordinated to a transition metal, the electronic properties of the blocking group would have an effect on the electronics of the metal centre. It was envisaged that both electron-donating (*e.g.* R' = CH_3) and electron-withdrawing (*e.g.* R' = CF_3) blocking groups could be used hence the electronics at the metal centre could be tuned to specific requirements (Figure 16).

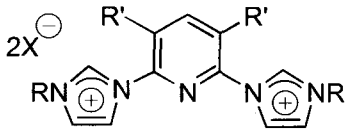

Figure 16: Proposed new ligand system, R = DiPP

Previous attempts at synthesising the new ligand had focussed on the use of 2,6-dibromo-3,5-dimethylpyridine[80] in place of 2,6-dibromopyridine in the quaternisation reaction. Despite the use of elevated temperatures (>200 °C) and lengthy reaction times (2 weeks), only the monosubstituted product was obtained (Scheme 15).

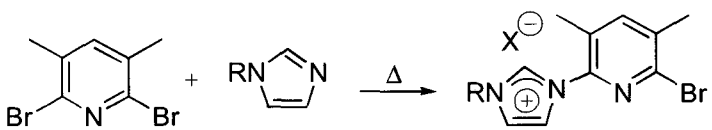

51 **34a** **52**: X = Br

Scheme 15: Attempted synthesis of a new imidazolium salt, R = DiPP

It was not known why the reaction did not proceed as expected, but it was postulated that the electron-donating methyl groups strengthened the C–Br bond sufficiently such that displacement of both bromides by DiPP imidazole was not possible. Other blocking groups were not investigated at this time.

2.2 - Double quaternisation reactions

Initial studies into the synthesis of a new pincer ligand were guided by the easy availability of starting materials. 3,5-bis(trimethylsilyl)-2,6-difluoropyridine was easily accessed in one step from commercially available 2,6-difluoropyridine (Scheme 16).[81]

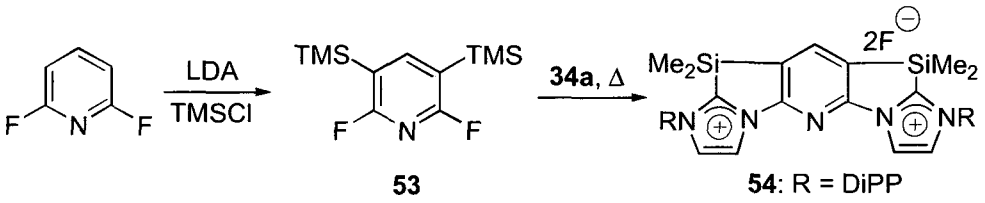

Scheme 16: Attempted use of $SiMe_3$ as a blocking group

However, after the quaternisation reaction was carried out with DiPP imidazole, a beige product was obtained which did not exhibit any resonances for the imidazolium protons (normally found at *ca.* 10-11 ppm in the ^1H NMR spectrum). The signal at 0.28 ppm assigned to '$SiMe_3$' integrated to 12H instead of the expected 18H and, on this basis, structure **54** is proposed. The lack of imidazolium protons precluded the synthesis of a carbene hence the use of $SiMe_3$ as a blocking group was abandoned.

The use of 2,6-dichloro-3,5-dimethylpyridine as a starting material was briefly investigated but no feasible large-scale synthetic route could be found. The procedure of Fort *et al.* did afford the desired starting material in small quantities, but the use of 16 moles of BuLi per mole of 3,5-lutidine rendered this route unsuitable for scale-up.[82]

It was thought that due to the fact that the C–I bond was weaker than the C–Br bond, 2,6-diiodo-3,5-dimethylpyridine would be more susceptible to double quaternisation than **51**. Following the procedure of Sedelmeier and Bolm,[83] halogen exchange of **51** took place in 83% yield (Scheme 17).

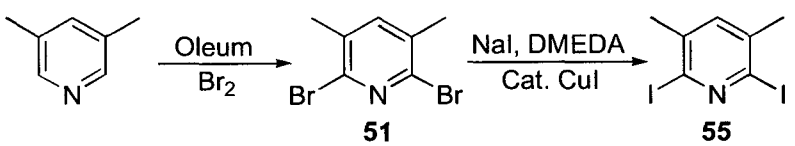

Scheme 17: Synthesis of 2,6-diiodo-3,5-dimethylpyridine

A slight difference in the ^1H NMR signal for the aromatic proton was observed (0.12 ppm difference between **51** and **55**) and microanalysis confirmed that halogen exchange had taken place. The solid state structures of both **51** and **55** were also obtained (Figures 17a and 17b).

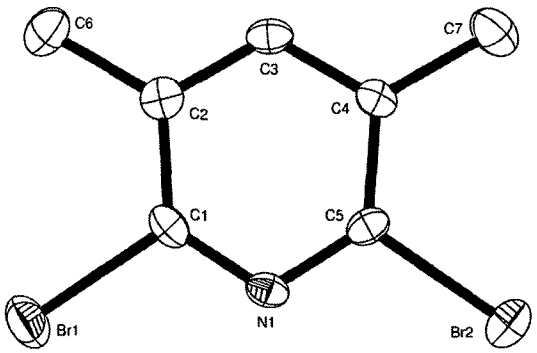

Figure 17a: ORTEP representation of **51**. Thermal ellipsoids at 50% probability, H atoms omitted for clarity.

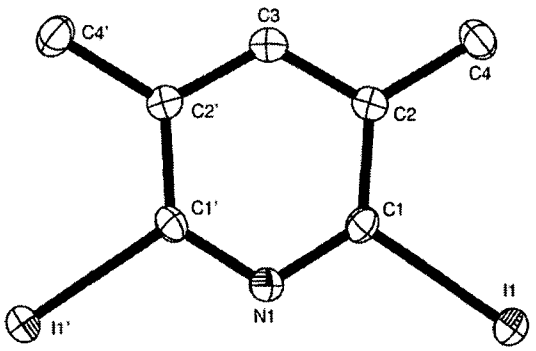

Figure 17b: ORTEP representation of **55**. Thermal ellipsoids at 50% probability, H atoms omitted for clarity.

The structures of both molecules are unremarkable with C–Br and C–I bond lengths consistent with other examples of 2,6-dihalopyridines. Compound **51** is planar whereas compound **55** is slightly deformed into a saddle shape due to the steric interaction between the methyl groups and iodine atoms. The saddle point of the molecule can be found at the centre of the ring.

Compound **51** crystallises as a racemic twin with two independent molecules in the asymmetric unit and compound **55** lies on a C_2 axis within the unit cell. Although the only intermolecular interaction in both compounds is face-face π-stacking, the molecules adopt slightly different packing arrangements in the solid state. Compound **51** is arranged in alternating columns of molecules which result in an X shape when viewed down the b axis (Figure 18a) and compound **55** packs such that the molecules form a zig-zag arrangement when viewed down the b axis (Figure 18b). There are no halogen-halogen interactions.[84]

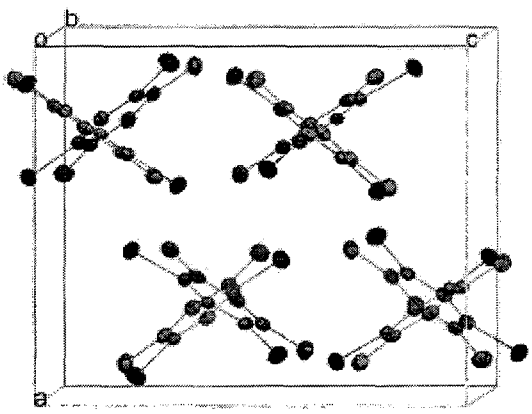

Figure 18a: Packing diagram of **51**.

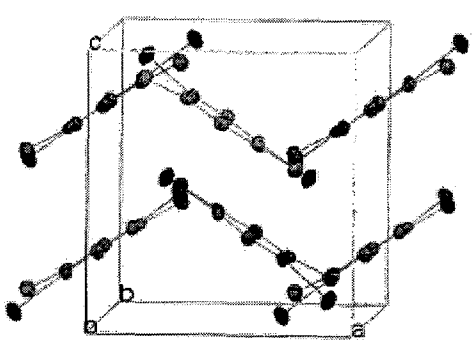

Figure 18b: Packing diagram of **55**.

When quaternisation of compound **55** with 2 equivalents of DiPP imidazole was attempted, after 7 days at 140 °C a mixture of mono- and di-quaternised products was

identified in the ^{1}H NMR spectrum of the reaction product. The presence of two imidazolium peaks at 10.83 and 10.45 ppm in a 1:2 ratio indicated that more forcing conditions were required to drive the reaction to completion. Increasing the amount of DiPP imidazole to 3 molar equivalents and also increasing the reaction temperature to 190 °C resulted in clean conversion to the di-quaternised product **56** after 7 days (Scheme 18). Compound **56** was isolated as a hygroscopic pale grey powder by precipitation with Et_2O from a DCM solution of the reaction product.

55 **34a** **56**

Scheme 18: Synthesis of dimethylated imidazolium salt **56**, R = DiPP

The ^{1}H NMR spectrum of **56** was similar to that of **35a**.[62] The characteristic imidazolium proton resonance was observed at 10.83 ppm (147.61 ppm for the imidazolium carbon in the $^{13}C\{^1H\}$ NMR spectrum) along with a septet and two doublets in the alkyl region of the spectrum corresponding to the ^{i}Pr groups on the DiPP substituents. A sharp singlet at 2.67 ppm was assigned to the methyl groups on the pyridine ring. Microanalysis was consistent with the formation of a bis(imidazolium) salt with iodide counterions. Compound **56** was structurally characterised (Figure 19a) confirming the expected bis(imidazolium) geometry. The structure of compound **35a** (see section 1.33) was also obtained in order to provide a comparison (Figure 19b).

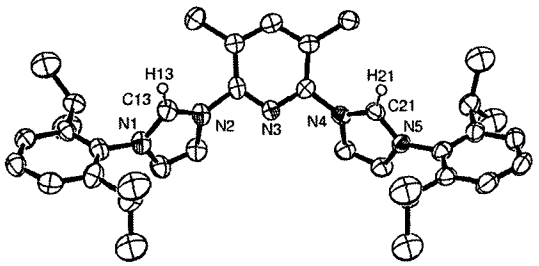

Figure 19a: ORTEP representation of **56**. Thermal ellipsoids at 50% probability: H, I atoms and two $CHCl_3$ solvent molecules omitted for clarity.

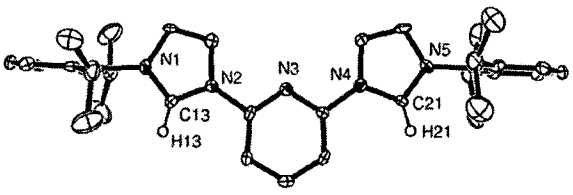

Figure 19b: ORTEP representation of **35a**. Thermal ellipsoids at 50% probability: H, Br atoms (bar imidazolium H), one Et_2O and three CH_2Cl_2 solvent molecules omitted for clarity.

The two imidazolium rings and pyridine ring in **35a** are planar, with the normals to the DiPP rings almost perpendicular to the normal to the plane of the imidazolium ring [84.79(14)° and 88.21(14)°]. The imidazolium proton faces the opposite direction to the lone pair on the pyridine ring: this structural feature is also found in the free carbene **36**.[62]

The main difference between the two molecules is the loss of planarity in **56**: the angle between the planes defined by the imidazolium rings and pyridine ring is *ca.* 44°. This can be attributed to steric interactions between the imidazolium proton and the methyl groups. Again, the normal to the DiPP ring is almost perpendicular to the normal to the imidazolium ring [88.04(25)° and 87.42(26)°].

The C(13)–N and C(21)–N bond lengths for both **35a** and **56** fall within the range 1.318(6) – 1.343(6) Å, which is between the expected values for a C–N single bond and C=N double bond. This is a result of the delocalisation across the N–C–N moiety and is consistent with other structurally characterised imidazolium salts.

2.3 - Deprotonation reactions

Deprotonation of the non-methylated imidazolium salt **35d** required the use of two equivalents of KHMDS (Scheme 5) to yield **36**. When compound **56** was subjected to the same reaction conditions, only a very small amount (<10% yield) of free carbene **58** could be isolated (Scheme 19).

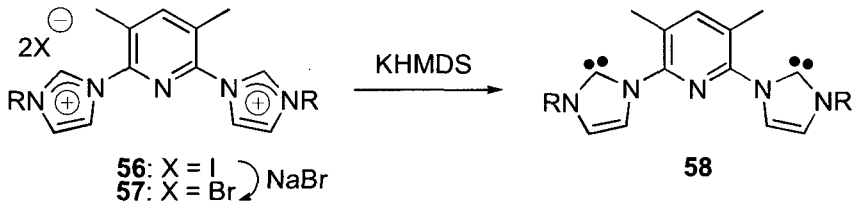

Scheme 19: Synthesis of dimethylated carbene **58**, R = DiPP

Anion exchange with a 20-fold excess of NaBr in MeOH resulted in the replacement of I^- by Br^- and the formation of a new imidazolium salt, **57**. This was also structurally characterised; the geometric parameters of the dication in **57** are identical (within experimental error) to those in **56** (see Appendix 2).

Deprotonation of compound **57** with two equivalents of KHMDS resulted in the isolation of novel ligand **58** in excellent (77%) yield. A slight modification of the published procedure[62] was used; the reaction was carried out in PE rather than THF. This shortened the workup procedure to filtration and concentration, cleanly affording **58** as a beige powder.

The ^{1}H NMR spectrum of **58** is similar to that of **36**: two doublets at 1.25 and 1.15 ppm were characteristic of the ^{i}Pr methyl groups and a septet at 2.92 ppm corresponding to the CH. The major difference between the spectra is the presence of a sharp singlet at 2.76 ppm which is due to the methyl groups on the pyridine backbone. Microanalysis confirmed the loss of two equivalents of HBr from the starting imidazolium salt. The resonance for the C_{NHC} was observed at 221.7 ppm in the $^{13}C\{^1H\}$ NMR spectrum. This is slightly further downfield than the resonance for the C_{NHC} in **36** which was observed at 219.0 ppm. In keeping with imidazolium salts **56** and **57**, the signal assigned to the pyridine methyl groups is the furthest upfield signal at 20.42 ppm.

Compound **58** was also structurally characterised (Figure 20) showing the same non-planar geometry as imidazolium salts **56** and **57**. This is in contrast to compound **36**

which, like its precursor imidazolium salt, contains planar NHC and pyridine rings. The angles between the normals to the planes defined by the imidazol-2-ylidene and pyridine rings are 34.06(12)° and 29.01(10)° – slightly smaller than in the imidazolium salts. This is due to the steric interaction between the methyl groups on the pyridine backbone and the NHC lone pairs being smaller than the interaction between the methyl groups and the imidazolium protons. Positional disorder was observed in one of the DiPP rings; only one of the two positions is shown in Figure 20.

The C_{NHC}–N bond lengths of **58** are slightly longer than for the precursor imidazolium salts. This is due to the formal loss of the C=N double bond after deprotonation, although it can also be viewed as a 1-electron reduction of the delocalisation across the C–N–C functionality.[18]

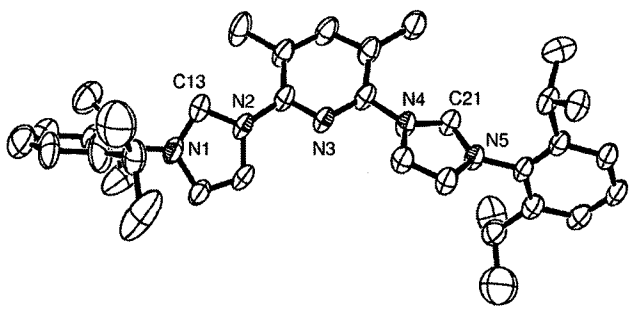

Figure 20: ORTEP representation of **58**. Thermal ellipsoids at 50% probability, H atoms omitted for clarity.

C(13)-N(1)	1.364(4)
C(13)-N(2)	1.374(3)
C(21)-N(4)	1.375(3)
C(21)-N(5)	1.363(3)
N(1)-C(13)-N(2)	101.7(2)
N(5)-C(21)-N(4)	101.1(2)

Table 2: Selected bond lengths (Å) and angles (°) for compound **58**

Due to the initial difficulties in synthesising useful amounts of free ligand **58**, the synthesis of an Ag salt was carried out. Transmetallation from silver is a useful method of synthesising transition metal complexes of NHCs, in particular late metal complexes (see section 1.23). Imidazolium salt **56** and Ag_2O were reacted in DCM in the absence of light and after filtration of the reaction solution, complex **59** was isolated by precipitation with Et_2O (Scheme 20).

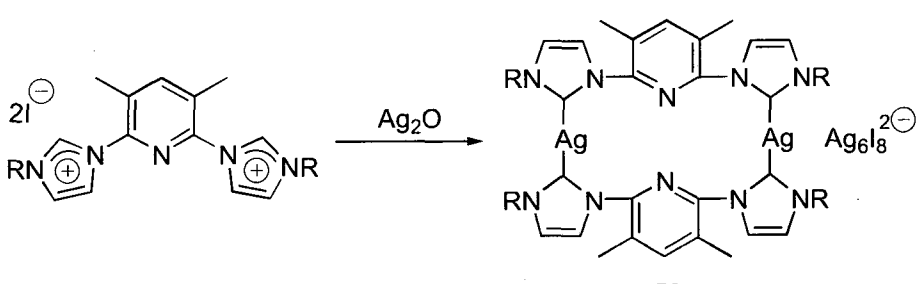

56 **59**

Scheme 20: Synthesis of an Ag carbene complex, R = DiPP

Initially it was thought that a monomeric complex had been formed with linear C_{NHC}–Ag–I functionalities: this was borne out by the ^1H and $^{13}C\{^1H\}$ NMR spectra

which contained all the characteristic peaks of the ligand, albeit slightly broadened. Two doublets and one septet were observed in the ^{1}H NMR spectrum, along with one singlet for the methyl groups. Only one resonance at 188.27 ppm was observed for the C_{NHC} and the rest of the $^{13}C\{^{1}H\}$ NMR spectrum was also consistent with one ligand environment. However, the microanalysis was not consistent with a monomeric complex: the C, H and N values were all much lower than the expected values. X-ray diffraction studies of crystals (which decomposed upon solvent loss) revealed the unusual structure of **59** (Figures 21a and 21b).

The dication is best described as a bis(ligand) bis(silver) 16-membered argentacycle which lies on an inversion centre in the unit cell. The molecule contains two ligands bridged through the NHC moieties by two Ag cations. The pyridine rings do not interact with the Ag cations at all due to the nitrogen lone pair pointing away from the centre of the molecule. The Ag–C_{NHC} bond lengths of 2.079(7) Å and 2.082(7) Å are consistent with the known range of Ag–C_{NHC} bond lengths. The C_{NHC}–Ag–C_{NHC} bond angle is not quite linear at 177.0(3)°.

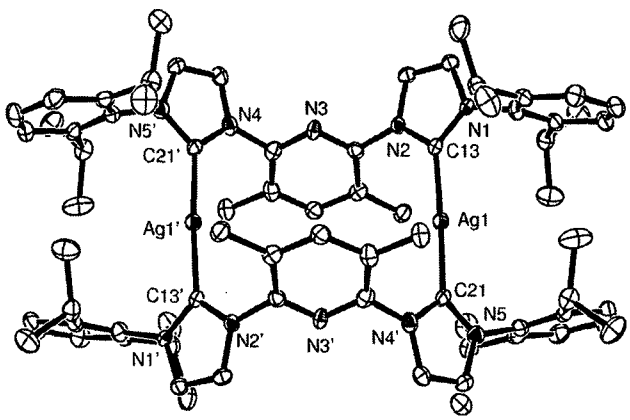

Figure 21a: ORTEP representation of the cation of **58**. Thermal ellipsoids at 50% probability, H atoms omitted for clarity.

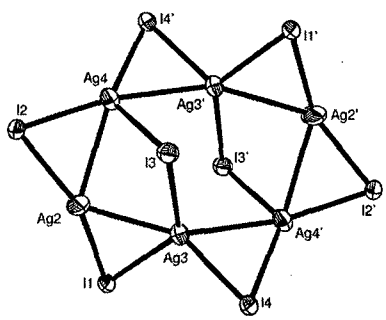

Figure 21b: ORTEP representation of the anion of **58**. Thermal ellipsoids at 50% probability, one Et_2O solvent molecule omitted for claritv.

The $(Ag_6I_8)^{2-}$ anion contains an unusual arrangement of 6 Ag atoms in a planar hexagonal ring. Iodide anions bridge neighbouring Ag atoms alternating 'above' and 'below' and there are also two capping iodides, one directly above and one directly below the plane of the ring. This hexagonal arrangement of Ag atoms has only been structurally characterised once before, in the solid state structure of silver benzenesulfonate.[85] However, the Ag atoms formed an infinite 2D lattice analogous to graphite with capping sulfonate groups whereas the anion in **58** contains a single hexagonal ring with capping iodides.

The capping iodides are 1.830(1) Å out of the plane defined by the six Ag atoms. The Ag–Ag bond distances average 2.966 Å [range 2.9392(11) – 3.0114(11) Å] and are substantially shorter than the sum of the van der Waals radii for Ag (3.44 Å). The terminal Ag–I bond distances are in the range [2.6704(9) – 2.8392(9) Å] and are consistent with previously reported Ag–I bond lengths.

Although no Ag complex of ligand **36** has been structurally characterised, an analogous complex (R = Bz) has been synthesised and structurally characterised.[86] This molecule similarly adopts a dimeric structure with two ligands bridged by two Ag cations. However, in this case, the two ligands twist around each other to form a helicate. When **59** is viewed down the C_{NHC}–Ag–C_{NHC} bond it is obvious that there is no twist in the molecule and it can be described as a mesocate.

There are two points where **59** and the Ag complex reported by Caballero *et al.* differ, but it is likely that the steric bulk of the DiPP substituents is the reason for the formation of a mesocate rather than a helicate. The methyl groups on the pyridine ring point away from the centre of the molecule and do not have any steric effect on the ability of the molecule to twist. However, the ^{i}Pr groups of the NHC substituents of **59** prevent the phenyl rings getting close to each other and, unlike the benzyl-substituted compound, there is no flexible methylene spacer between the phenyl and imidazol-2-ylidene rings to minimise the steric interaction of the phenyl rings.

2.4 - Summary

The synthesis of novel pincer ligand **58** with blocking groups in the 3- and 5-positions of the pyridine ring has been successfully carried out. Switching from 2,6-dibromo-3,5-dimethylpyridine to 2,6-diiodo-3,5-dimethylpyridine resulted in the successful double quaternisation to form the novel imidazolium salt **56**. This was then deprotonated with KHMDS, *via* a halide exchange reaction, to form the free carbene in good yield. Deprotonation of imidazolium salt **56** with Ag_2O resulted in the formation of a novel Ag carbene complex which could be used for transmetallation reactions.

In addition to the known carbene pincer ligand **34** and the novel ligand **58**, a phosphine pincer ligand **60** was also synthesised according to literature procedures.[87]

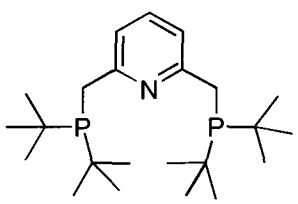

60

Figure 22: *Bis*(phosphine)pyridine pincer ligand **60**

These three ligands were used to prepare complexes of a wide range of transition metals, from titanium to iridium. Ligand **60** was also used in order to compare the electronic and steric features of the "analogous" NHC-containing pincer ligands and trialkylphosphine pincer ligands in real systems. These efforts are described in the following chapters.

Chapter 3

Early transition metal complexes

3.1 - Introduction

At the outset of this project, there were very few reported early transition metal complexes of ligand **36** or its analogues. Some work had been published by Gibson *et al.*, who had synthesised Ti(III), V(III) and Cr(III) complexes of (CNC) pincer ligands (Scheme 21).[64] However, their reactivity towards ligand substitution had not been investigated and only one had been structurally characterised. It had also been discovered that the Cr(III) complexes were good ethylene polymerisation catalysts.[63]

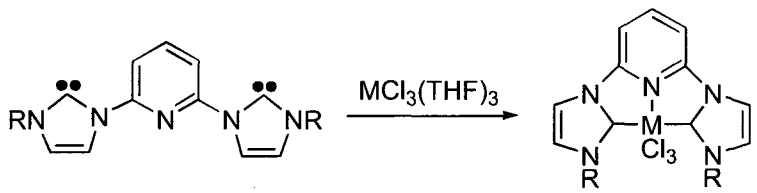

36

61: M = Ti
62: M = V
63: M = Cr

Scheme 21: Synthesis of some early metal pincer complexes; R = DiPP

The remainder of the work into early metal (CNC) pincer complexes was done within the Danopoulos group. Structural characterisation of **61** and **62** was carried out and the synthesis of V(II) and Cr(II) analogues was also accomplished.[76] However, the reactivity of these complexes had not been investigated. The synthesis of new early transition metal complexes of ligands **36** and **58**, in addition to studying the reactivity of all the early metal complexes, was the primary aim of the work reported here.

3.2 - Group 4 metals

Initial investigations into group 4 metals were based on the use of known starting materials in oxidation state +4. The compound $Ti(N^tBu)Cl_2(py)_3$ was chosen with the aim of synthesising a range of neutral pincer complexes with a convenient spectroscopic handle (the Ti=N bond). This would enable a comparison of the electronic properties of ligands **36**, **58** and **60** to be made.

Free ligands **36** and **58** readily reacted with $Ti(N^tBu)Cl_2(py)_3$, forming orange solutions of $(CNC)Ti(N^tBu)Cl_2$ in THF (Scheme 22). The products were crystallised by slow diffusion of PE into a concentrated THF solution, affording air-sensitive, orange crystals which proved to be diamagnetic. Microanalysis was consistent with the reported structure. The ^1H NMR spectrum of both complexes exhibited the usual septet for the ^{i}Pr CH groups and two doublets for the ^{i}Pr methyl groups. The resonance assigned to the ^{t}Bu methyl groups was observed around 0.5 ppm with very little difference (0.05 ppm) between **64** and **65**. There was also very little difference in the position of the C_{NHC} resonance in the $^{13}C\{^1H\}$ NMR spectrum: the signal was observed at 200.72 (**64**) and 200.86 (**65**) ppm.

The structures of both compounds **64** (Figure 23) and **65** (Figure 24) were determined crystallographically, revealing a highly distorted octahedral geometry with mutually *trans* chlorides and the imido functionality *trans* to the pyridine moiety. The ligands adopt the expected meridional coordination geometry. The chlorides in both complexes are bent away from the strongly electronegative nitrogen of the imido functionality to minimise electronic repulsion.

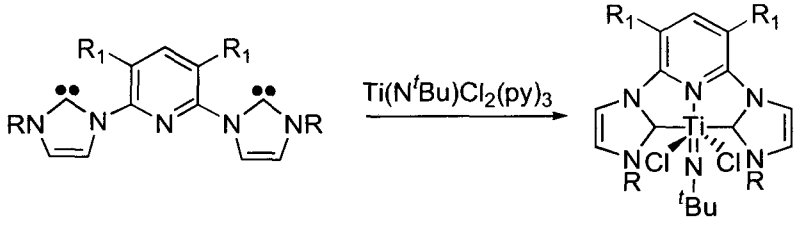

36: R_1 = H
58: R_1 = Me

64: R_1 = H
65: R_1 = Me

Scheme 22: Synthesis of Ti(IV) carbene complexes **64** and **65**, R = DiPP

The Ti=N stretch in the IR spectrum is located at 1037 cm^{-1} in **64** and 1025 cm^{-1} in **65**: this is consistent with ligand **58** being a stronger electron donor than ligand **36**. The presence of two methyl groups on the pyridine ring of ligand **58** results in a more

electron-rich pyridine ring, hence it is a stronger electron donor than a pyridine ring without methyl groups. The Ti=N bond lengths of 1.677(5) Å (**64**) and 1.716(5) Å (**65**) are within the previously reported range of Ti=N^{t}Bu bond lengths [1.656(9) – 1.739(4) Å][88, 89] and are also consistent with the idea that **58** is a stronger electron donor than **36**.

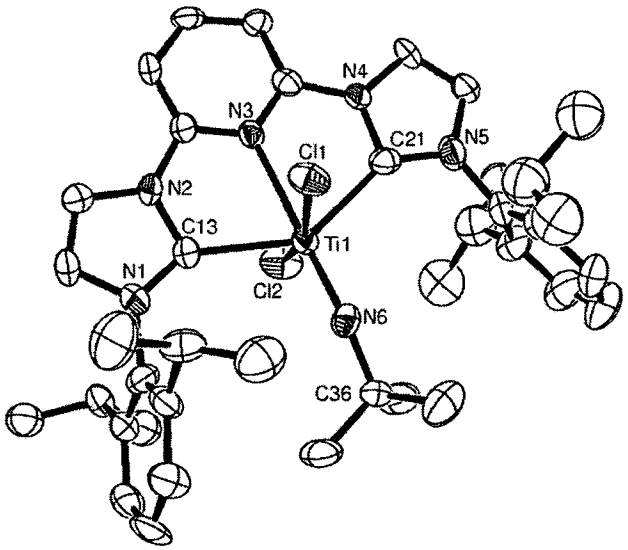

Figure 23: ORTEP representation of **64**. Thermal ellipsoids at 50% probability, H atoms omitted for clarity.

Ti(1)–N(6)	1.677(5)
Ti(1)–C(13)	2.281(6)
Ti(1)–C(21)	2.286(6)
Ti(1)–N(3)	2.332(5)
Ti(1)–Cl(2)	2.415(2)
Ti(1)–Cl(1)	2.433(2)
Cl(2)–Ti(1)–Cl(1)	161.43(9)
N(6)–Ti(1)–N(3)	175.3(2)
C(13)–Ti(1)–C(21)	140.5(2)
C(21)–Ti(1)–Cl(2)	85.6(2)
N(6)–Ti(1)–Cl(1)	102.99(17)
C(13)–Ti(1)–N(3)	70.82(19)

Table 3: Selected bond lengths (Å) and angles (°) for compound **64**

The Ti–C_{NHC} bond lengths in **64** [2.281(6) and 2.286(6) Å] and **65** [2.251(6) and 2.262(6) Å] are identical within experimental error and are consistent with the previously observed range of Ti–C_{NHC} bond lengths. The Ti–N_{py} and Ti–Cl bond lengths are consistent within experimental error and are also consistent with previously reported values.

The distortion away from ideal octahedral geometry is evidenced by the *trans* bond angles around the titanium centres. Although the N–Ti–N angles are almost linear at 175.3(2)° and 179.3(2)°, the Cl–Ti–Cl [161.43(9)° and 161.44(8)°] and C–Ti–C [140.5(2)° and 139.8(2)°] angles are severely distorted away from the ideal 180°. The C–Ti–C distortion is a result of the geometric constraints of the ligand and similar distortion is observed for all other first row transition metal complexes of **36** and **58**. The Cl–Ti–Cl distortion is a result of the chlorides bending away from the strongly electronegative imido nitrogen and possibly due to repulsion between the lone pairs on the chloride anion and the π cloud of the Ti=N bond.

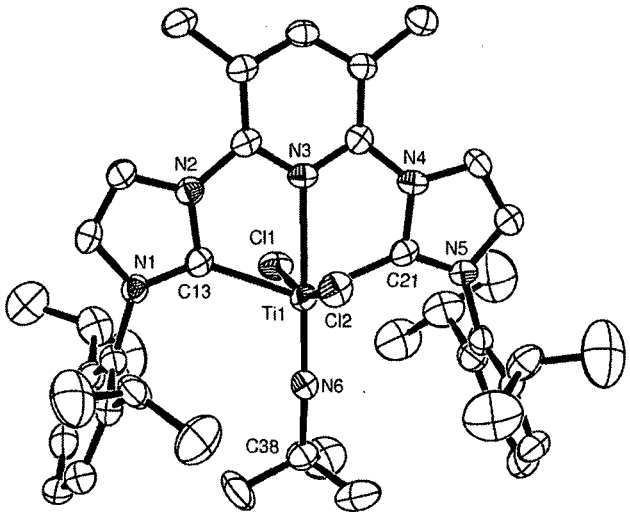

Figure 24: ORTEP representation of **65**. Thermal ellipsoids at 50% probability, H atoms and two THF solvent molecules omitted for clarity.

C(13)–Ti(1)	2.251(6)
C(21)–Ti(1)	2.262(6)
N(3)–Ti(1)	2.350(5)
N(6)–Ti(1)	1.716(5)
Cl(1)–Ti(1)	2.436(2)
Cl(2)–Ti(1)	2.438(2)
C(13)–Ti(1)–C(21)	139.8(2)
Cl(1)–Ti(1)–Cl(2)	161.44(8)
N(6)–Ti(1)–N(3)	179.3(2)
C(13)–Ti(1)–Cl(1)	86.55(16)
N(3)–Ti(1)–Cl(2)	79.40(13)
N(6)–Ti(1)–C(21)	110.0(2)

Table 4: Selected bond lengths (Å) and angles (°) for compound **65**

In order to compare the σ-donating properties of NHC moieties and trialkylphosphines, the bis(phosphine)pyridine (PNP) ligand **60** was also reacted with $Ti(N^tBu)Cl_2(py)_3$ in THF. A diamagnetic, air-sensitive orange complex was obtained after removal of the solvent (Scheme 23).

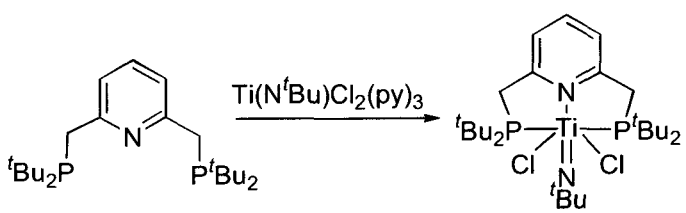

60 **66**

Scheme 23: Synthesis of Ti(IV) imido dichloride phosphine complex **66**

Attempts at crystallising the product failed: the free phosphine ligand was the only isolated product. Microanalytical data are consistent with one (PNP) ligand per titanium centre and an octahedral structure is proposed on the basis of spectroscopic data. One phosphine resonance at 35.9 ppm is found in the $^{31}P\{^1H\}$ NMR spectrum indicating the presence of either a plane of symmetry or a C_2 axis through the molecule. One ^{t}Bu resonance is observed in the ^1H NMR spectrum and only one signal for the ^{t}Bu methyl groups in the $^{13}C\{^1H\}$ NMR spectrum is observed. However, in the absence of structural data, it is impossible to determine whether the (PNP) ligand adopts a meridional or facial coordination mode.

The IR stretch at 1043 cm^{-1} corresponding to the Ti=N bond indicates that (PNP) ligand **60** is a poorer electron donor than either of the two NHC ligands. This is consistent with

previous work which found that NHC ligands were stronger σ-donors than trialkylphosphine ligands.[90]

All attempts at synthesising aryl imido analogues of **64-66** failed. Reaction of $Ti(NMes)Cl_2(NHMe_2)_2$[91] with ligand **36** yielded brown crystals which were identified by single crystal X-ray diffraction as starting material (see Appendix 2). The ^1H NMR spectrum of the crystals showed no indication of the pincer ligand **36**: $Ti(NMes)Cl_2(NHMe_2)_2$ was the only identifiable product. It is likely that the *ortho* methyl groups of the mesityl ring were preventing complex formation due to the steric bulk of the ^{i}Pr groups of the DiPP rings.

Similar experiments with "$Zr(NMes)Cl_2(THF)_2$" yielded yellow crystals but structural characterisation (see Appendix 2) revealed that the starting material, which existed as a dimer, was the only isolated species. The synthesis of monomeric Zr and Hf imido species was accomplished by Arney and co-workers[92] but only through the use of an aryl group with steric bulk in the 2- and 6-positions. The steric bulk of the DiPP substituents on the (CNC) ligands would preclude complex formation hence no further work was carried out in this area.

Reaction of **64** and **65** with one equivalent of water did not result in the formation of a titanium oxychloride species; instead, a white solid precipitated from the reaction mixture which was insoluble in all common organic solvents. Following the method of Jeske *et al.*,[93] a THF solution of **61** was exposed to air but after 3 hours a brown solution had formed. The ^1H NMR spectrum of the product did not contain any of the characteristic peaks of the ligand and no other product could be identified from the spectrum. Attempts at oxidising **61** with excess NMO and PhIO failed; ^1H NMR spectra of the reaction products were all paramagnetic.

The attempted alkylation of **61**, **64** and **65** with $AlMe_3$ or PhMgCl resulted in an intractable mixture from which no product could be isolated. Reduction of **64** and **65** with excess Na/Hg in the presence of PMe_3 afforded a deep blue solution from which no pure product could be isolated. Similar blue solutions were obtained with other donor ligands (*e.g.* MeCN, pyridine) but no product could be isolated: in each case, ^1H NMR spectroscopy indicated the presence of paramagnetic materials.

Stirring ligand **36** or **58** in a THF solution of $MCl_4(THF)_2$ (M = Ti, Zr, Hf) resulted, in each case, in the precipitation of a white solid which did not contain any resonances in the ^1H NMR spectrum. A similar white solid was observed when neat $TiCl_4$ was added dropwise at –78 °C to an Et_2O solution of ligand **36**, even if a halide abstractor (*e.g.* KPF_6) was present. Whilst it is unsurprising that 7-coordinate $(CNC)TiCl_4$ was not obtained, complexes of Zr and Hf with coordination number >6 are known.[94] It is also possible for ligand **36** to be part of a 7-coordinate geometry,[76] albeit uranium(IV) has a larger ionic radius than Zr(IV) or Hf(IV).

3.3 - Group 5 metals

Previous work with vanadium had resulted in the synthesis of V(III) (Scheme 21) and V(II) (Scheme 24) complexes.

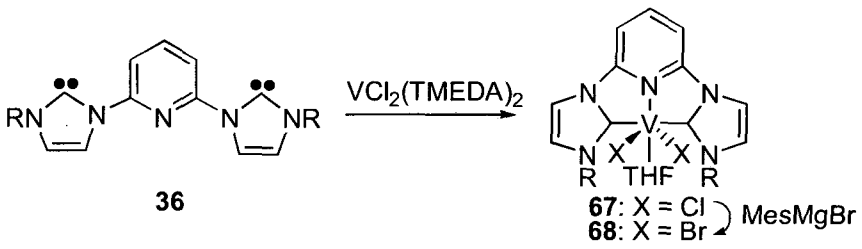

36

Scheme 24: Synthesis of V(II) pincer complexes, R = DiPP

Complex **67** was reacted with MesMgBr in THF and after filtration through Celite, dark blue crystals were obtained by the slow diffusion of PE into a THF solution. However, structural characterisation (Figure 25) revealed that halogen exchange had taken place. Complex **68** has the same distorted octahedral geometry as **67** with mutually *trans* bromides and one THF molecule completing the coordination sphere.

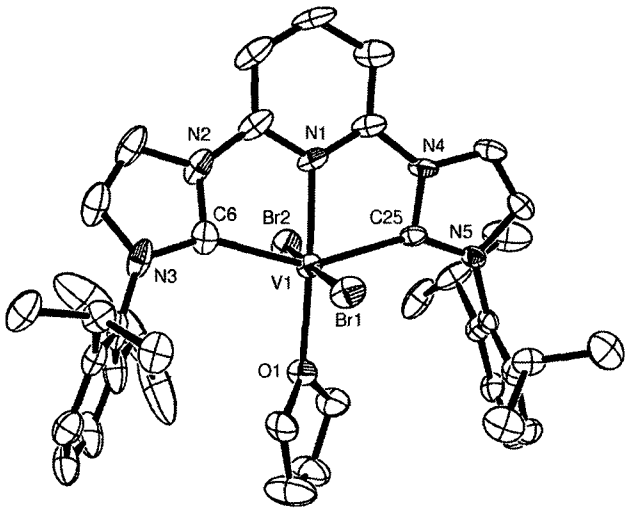

Figure 25: ORTEP representation of **68**. Thermal ellipsoids at 50% probability, H atoms omitted for clarity.

C(6)–V(1)	2.227(6)
C(25)–V(1)	2.224(6)
Br(1)–V(1)	2.6142(11)
Br(2)–V(1)	2.5997(11)
N(1)–V(1)	2.103(5)
O(1)–V(1)	2.162(4)
C(25)–V(1)–C(6)	149.4(2)
Br(2)–V(1)–Br(1)	174.60(5)
N(1)–V(1)–O(1)	177.41(18)
N(1)–V(1)–C(6)	75.1(2)
C(25)–V(1)–Br(1)	84.67(14)
O(1)–V(1)–Br(2)	88.31(11)

Table 5: Selected bond lengths (Å) and angles (°) for compound **68**

The V–C_{NHC} bond lengths are consistent, within experimental error, with those of **67** which is the only previous example of a V(II) NHC complex. Magnetic measurements (Guoy balance) confirmed the presence of 3 unpaired electrons (μ_{eff} = 3.83 B.M.) consistent with a d^3 metal centre and microanalysis was consistent with the reported structure. Attempts to alkylate **67** with other alkylating agents (MeLi, MeMgCl, $AlMe_3$) produced intractable mixtures from which no pure product could be isolated.

Gambarotta *et al.* synthesised 2,6-bis(diisopropylphenyliminomethyl)pyridine vanadium trichloride, (NNN)VCl_3, a bis(imine)pyridine pincer complex analogous to **62**.[95] This underwent reduction with NaH to form a bis(vanadium) dinitrogen complex. A similar reduction of **62** with excess NaH resulted in the formation of an extremely moisture- and oxygen-sensitive blue solution from which no product could be isolated. Attempts to alkylate **62** with MeLi also failed, but the reaction of **62** with $AlMe_3$ in THF afforded weakly-diffracting blue crystals. On the basis of a poor X-ray dataset, the structure is assigned as a V(II) dimer with three bridging chlorides, three THF molecules per vanadium centre and a non-coordinating $[AlCl_2Me_2]^-$ anion (**69**, Scheme 25). The fate of the pincer ligand is not known, though elimination of a methylimidazolium salt has been noted previously with Pd systems.[96]

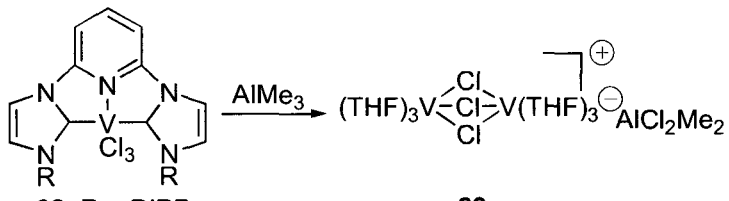

62: R = DiPP **69**

Scheme 25: Reaction of **62** with $AlMe_3$

Oxidation of **67** proved more fruitful: reaction with 1 equivalent of NMO in THF resulted in the formation of a green solution with a green precipitate. The precipitate was dissolved by the addition of more THF and green crystals were isolated by slow diffusion of PE into the THF solution. Solid state magnetic measurements (Guoy balance) revealed they were paramagnetic (μ_{eff} = 1.66 B.M.), consistent with one unpaired electron implying a V(IV), d^1 metal centre had been formed. Structural characterisation of the complex revealed a distorted octahedral structure with mutually *trans* chlorides and an oxo ligand *trans* to the pyridine moiety (Figure 26). Microanalysis was consistent with the solid state structure.

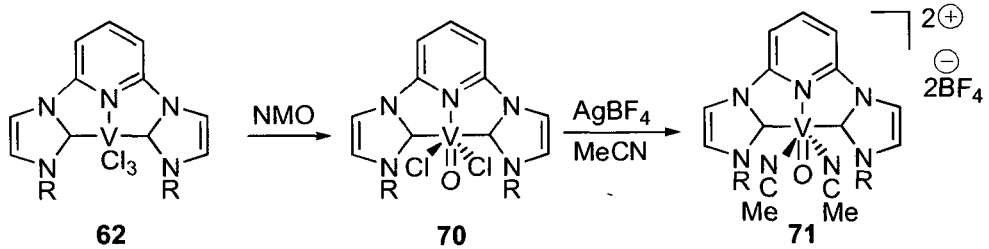

62 **70** **71**

Scheme 26: Synthesis of V(IV) *oxo* complexes, R = DiPP

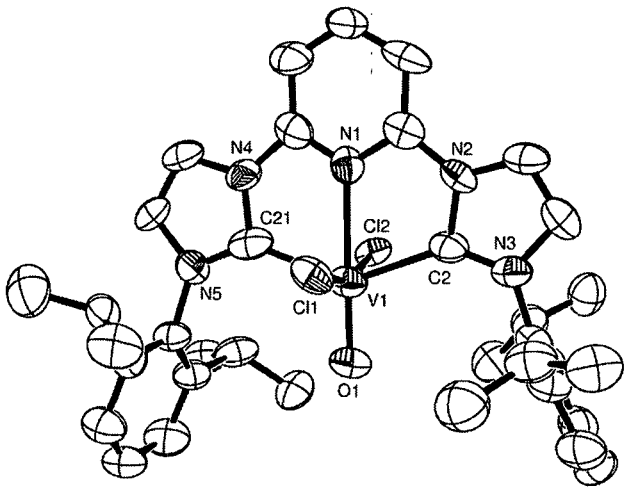

Figure 26: ORTEP representation of **70** showing one of two molecules in the asymmetric unit. Thermal ellipsoids at 50% probability, H atoms omitted for clarity.

C(2)–V(1)	2.169(10)
C(21)–V(1)	2.182(11)
Cl(1)–V(1)	2.398(3)
Cl(2)–V(1)	2.421(3)
N(1)–V(1)	2.275(7)
O(1)–V(1)	1.600(5)
O(1)–V(1)–N(1)	178.9(3)
C(2)–V(1)–C(21)	141.9(4)
Cl(1)–V(1)–Cl(2)	161.97(10)
C(2)–V(1)–N(1)	71.6(3)
O(1)–V(1)–Cl(1)	98.1(2)
C(21)–V(1)–Cl(2)	84.3(2)

Table 6: Selected bond lengths (Å) and angles (°) for compound **70**

Compound **70** is the first NHC complex of V in oxidation state +4. The V–C_{NHC} bond lengths are shorter than in complex **68** which is consistent with oxidation from V(II) to V(IV). The V–N_{py} bond length in **70** is much longer than in **68**, but this is consistent with the greater *trans* effect of an oxo ligand compared to THF. The chlorides are bent away from the strongly electronegative oxo anion; the Cl–V–Cl angle is *ca.* 12° smaller in **70** than the Br–V–Br angle in **68**. The V=O bond length is slightly longer than the only other structurally characterised NHC complex containing a V=O bond [1.5749(16) Å in (IMes)$VOCl_3$],[97] albeit **70** is in oxidation state +4 rather than +5. This is consistent with known V=O bond lengths for V(IV) complexes but the V=O IR stretch at 974 cm^{-1} is at the low end of the known range.[76] This is because NHCs are good σ-donors which results in less V=O π-bonding

Replacement of the chloride ions was accomplished by stirring **70** with MeCN in the presence of 2 equivalents of $AgBF_4$ (Scheme 26). After filtration through Celite, crystallisation occurred by the slow diffusion of Et_2O into a MeCN solution. Magnetic measurements (Guoy balance) revealed the crystals were paramagnetic, the value of 1.79 B.M. (1 unpaired electron) is consistent with retention of the V(IV) oxidation state. Structural characterisation (Figure 27) revealed the distorted octahedral geometry of **70** was retained with MeCN ligands replacing the chlorides. This resulted in a dicationic V(IV) oxo complex with two non-coordinating BF_4^- anions.

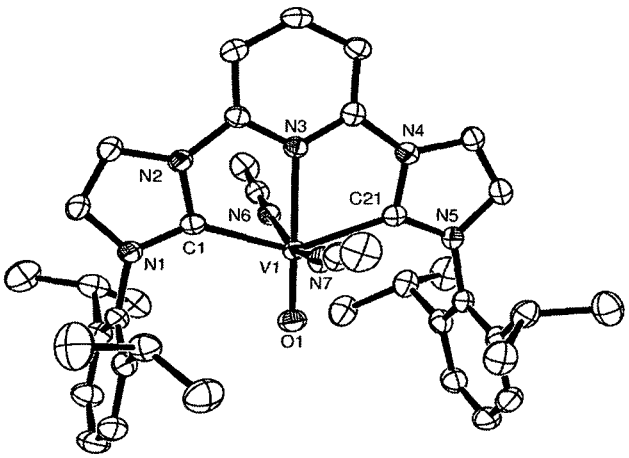

Figure 27: ORTEP representation of the cation of **71**. Thermal ellipsoids at 50% probability, H atoms, BF_4 anions and one MeCN solvent molecule omitted for clarity.

V(1)–O(1)	1.5913(19)
V(1)–C(1)	2.129(3)
V(1)–C(21)	2.136(3)
V(1)–N(3)	2.236(2)
V(1)–N(6)	2.087(2)
V(1)–N(7)	2.091(2)
O(1)–V(1)–N(3)	177.39(9)
N(6)–V(1)–N(7)	162.27(9)
C(1)–V(1)–C(21)	143.63(10)
O(1)–V(1)–C(1)	108.46(10)
N(7)–V(1)–C(21)	87.06(9)
N(6)–V(1)–N(3)	79.87(8)

Table 7: Selected bond lengths (Å) and angles (°) for compound **71**

The V=O bond in **71** is slightly shorter than in **70**, which is consistent with the formation of a dicationic species with increased ionic interaction between V and O. The same is true of the V–C_{NHC} and V–N_{py} bond lengths; they are shorter in **71** than **70** which is due to the increased ionic interaction between the metal centre and the ligand. The *trans* effect of the oxide ligand can be seen by comparing the V–N_{py} and V–N_{MeCN} bond lengths; the former is longer by *ca.* 0.15 Å despite being part of a chelating ligand. In keeping with **70**, the MeCN ligands are bent away from the oxide ligand due to electrostatic repulsion, but the N–V–N angle is comparable to the Cl–V–Cl angle in **70** (within experimental error). The V=O stretch at 976 cm^{-1} in the IR spectrum is almost identical to the V=O stretch of **70**.

Attempts to synthesise a V(V) pincer complex of **36** by oxidising **70** or **71** with NMO, PhIO and O_2 failed. The use of V(V) starting materials ($VOCl_3$, VO_2Cl) similarly failed to furnish a V(V) pincer species. Reaction of **62** with NaN_3 followed by photolysis with a 254 nm UV lamp did not afford the (CNC)$VNCl_2$ species and other attempts to make vanadium nitride starting materials such as $VNCl_2(PMe_2Ph)_2$[98] were unsuccessful.

Although it has been shown that NHCs are capable of stabilising metals in high oxidation states, the use of neutral, tridentate NHC-containing ligands is problematic. This is because the metal centre does not usually coordinate more than six ligands, hence at least one multiply bonded metal–ligand moiety is usually present. Whilst suitable starting materials in oxidation state +4 are relatively easy to obtain, especially

for group 4 metals (see section 3.2), it is much more difficult to obtain suitable starting materials for oxidation states +5 and above. Oxidation of lower oxidation state metal complexes is one way to circumvent this problem but this is dependent on the substrate in question being susceptible to oxidation.

The reaction of **67** with *o*-tolyl azide proceeded slowly in the absence of photolysis (Scheme 27). Crystallisation of the product occurred from slow diffusion of PE into a THF solution but the brown needles were extremely sensitive to solvent loss and structural studies were not possible.

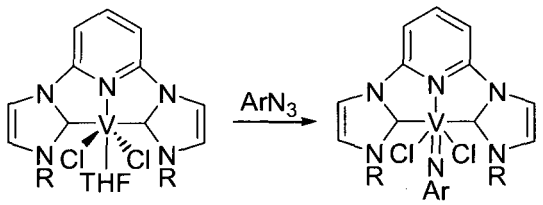

67 **72**: Ar = *p*-C_6H_4Me

Scheme 27: Synthesis of V(IV) imido species, R = DiPP

Microanalysis was consistent with the loss of THF and the presence of an imido moiety rather than an azide. Magnetic measurements (Guoy balance) revealed that compound **72** is paramagnetic (μ_{eff} = 1.66 B.M.), consistent with one unpaired electron and a V(IV) oxidation state. Despite the lack of structural characterisation, **72** is assigned as an octahedral V(IV) species with an imido functionality *trans* to the pyridine moiety and mutually *trans* chlorides, analogous to **70** and **71** in addition to the Ti(IV) imido complexes **64** and **65**. The V=N IR stretch was observed at 970 cm^{-1}.

Complexes **71** and **72** were tested for catalytic epoxidation and aziridination of alkenes (Scheme 28). Despite the use of high catalyst loadings (5 mol%) and high temperatures (70 °C), no functional group transfer to either aliphatic or aromatic alkenes was observed.

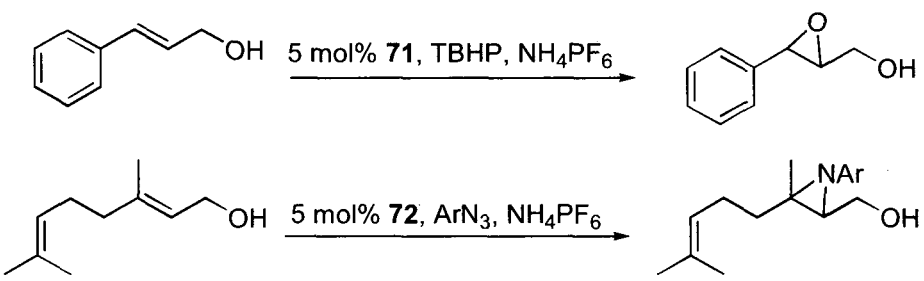

Scheme 28: Attempted oxo- or imido-transfer to alkenes

Stoichiometric epoxidation of citronellol was attempted with **71** but no reaction was observed. It was concluded that **71** and **72** are inert towards alkene functionalisation and no further studies were carried out. The oxidation of PPh_3 with **71** also failed to furnish the desired product.

The reaction of $NbCl_3(DME)$ with **36** in THF resulted in a purple solution which afforded purple crystals by slow diffusion of PE into the THF solution (Scheme 29).

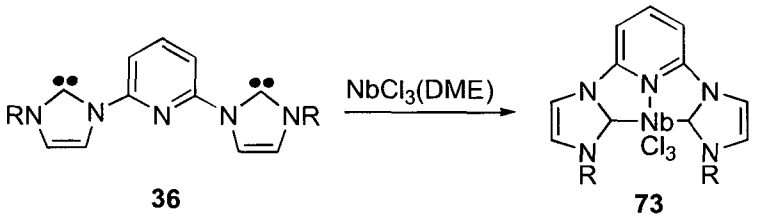

36 **73**

Scheme 29: Synthesis of an Nb(III) pincer complex, R = DiPP

Structural characterisation revealed the expected distorted octahedral geometry with meridionally coordinating ligand and three chlorides (Figure 28). The Cl–M–Cl distortion is much less severe (*ca.* 10°) than the other structurally characterised octahedral complexes of **36** and **58** which is a result of smaller electrostatic repulsion between the mutually *trans* chlorides and the ligand *trans* to the pyridine ring. However, the C–Nb–C angle is consistent with previous structurally characterised complexes of **36** and **58**. The Nb–C_{NHC} bond lengths [2.203(6) and 2.206(6) Å] are longer than the V–C_{NHC} bonds in **62** [2.144(3) and 2.147(3) Å] which is a result of the larger ionic radius of Nb(III) compared to V(III) (0.86 Å and 0.78 Å respectively).

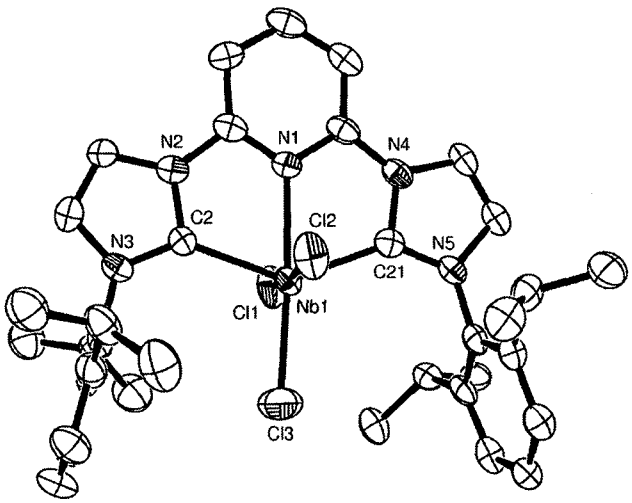

Figure 28: ORTEP representation of **73**. Thermal ellipsoids at 50% probability, H atoms, and one THF solvent molecule omitted for clarity.

C(2)–Nb(1)	2.206(6)
C(21)–Nb(1)	2.203(6)
N(1)–Nb(1)	2.248(5)
Cl(1)–Nb(1)	2.520(2)
Cl(2)–Nb(1)	2.473(2)
Cl(3)–Nb(1)	2.341(3)
N(1)–Nb(1)–Cl(3)	175.79(15)
Cl(2)–Nb(1)–Cl(1)	171.81(6)
C(21)–Nb(1)–C(2)	139.2(2)
Cl(3)–Nb(1)–Cl(2)	92.73(9)
C(2)–Nb(1)–Cl(1)	87.54(15)
C(21)–Nb(1)–N(1)	69.5(2)

Table 8: Selected bond lengths (Å) and angles (°) for compound **73**

The ligand bite angle (the N_{py}–M–C_{NHC} angle) decreases as the ionic radius of the atom increases and moves further out of the pocket of the ligand: the bite angle for **68** of 75.1(2)° is larger than in **73** [69.5(2)°] and compounds **61** and **62** are between the two.

Attempts at alkylating **73** failed, with intractable mixtures obtained with MeLi and $AlMe_3$. Oxidation of **73** with NMO or PhIO failed with starting material the only recovered product. However, ligand **36** did react with $Nb(N^tBu)Cl_3(py)_2$ in THF, forming an orange solution which deposited orange crystals by the slow diffusion of Et_2O into a DCM solution. Attempts at structural characterisation failed due to twinning of the crystals and the ^1H NMR spectrum was broad. Microanalysis was not consistent with an octahedral, cationic Nb(V) complex hence the identity of the reaction product remains unknown.

3.4 - Group 6 metals

As previously mentioned (see section 3.1), 'pincer' complexes of Cr(II) and Cr(III) have been reported. Cr(III) complexes have been synthesised by reacting ligand **36** (and its analogues) with $CrCl_3(THF)_3$[63] whereas the Cr(II) complex has been synthesised by aminolysis of $Cr(HMDS)_2$ with imidazolium salt **35a**. It has also been reported that Cr(III) complexes were exceptionally good ethylene polymerisation catalysts.[63]

Direct reaction of **36** with $CrCl_2$ in THF resulted in the formation of a purple solution after 16 hours. Isolation of the product proved problematic due to decomposition when exposed to vacuum, but slow evaporation of the reaction mixture under partial vacuum resulted in the isolation of a purple solid. On the basis of microanalytical and magnetic data (μ_{eff} = 4.89 B.M.) which corresponded to 4 unpaired electrons, compound **74** was assigned as an octahedral Cr(II) species analogous to **67** and **68** (Scheme 30) with one molecule of THF per complex.

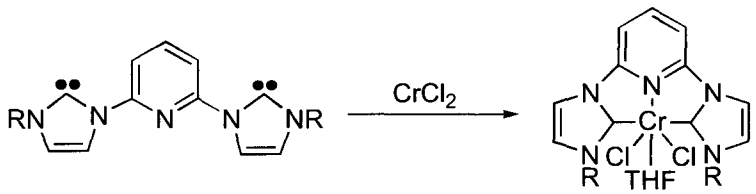

36 **74**

Scheme 30: Synthesis of a Cr(II) pincer complex, R = DiPP

However, structural characterisation of the dibromide analogue of **74**[76] revealed a 5-coordinate geometry. It is unknown whether the THF molecule in **74** is solvating or is actually coordinated to the Cr(II) centre.

In common with other early transition metal complexes of **36**, alkylation of **74** with standard alkylating agents (MeLi, PhMgCl, $AlMe_3$) merely afforded intractable mixtures. Attempts to utilise $CrPh_3(THF)_3$ as a starting material for the synthesis of chromium aryl complexes also failed. However, **74** was susceptible to oxidation; reaction with one equivalent of NMO resulted in the formation of a green solution. Green crystals were deposited from layering a THF solution with PE and were identified as complex **63**, which had previously been reported.[63] Compound **63** is a Cr(III) complex with one meridionally coordinating pincer ligand and three chloride ions completing the octahedral coordination sphere. However, the metrical data (see Appendix 2) were identical to the ^{i}Pr-substituted analogue of **63**.[63] Attempts to reduce

74 with Na/Hg in the presence of donor ligands (PMe_3, pyridine) resulted in the formation of brown solutions from which no identifiable product could be obtained.

Attempts to synthesise Mo(III) complexes of ligand **36** failed, possibly due to the thermal instability of $MoCl_3(THF)_3$. However, a purple, microcrystalline Mo(VI) complex of **36** was synthesised from the reaction of MoO_2Cl_2 with **36**, following the method of Herrmann *et al.* (Scheme 31).[99]

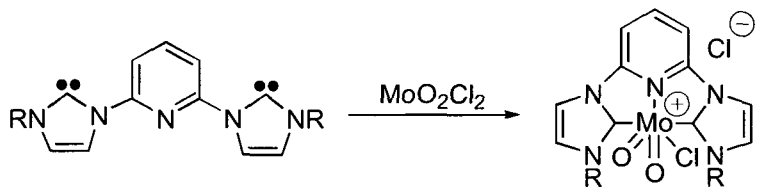

36 **75**

Scheme 31: Synthesis of a Mo(VI) pincer complex, R = DiPP

The empirical composition of **75** was confirmed by microanalytical data and it was also characterised by NMR and IR spectroscopy. The *cis* arrangement of the oxide moieties is borne out by the presence of two Mo=O stretches in the IR spectrum at 951 and 941 cm^{-1}. Further evidence comes in the ^1H NMR spectrum where two broad signals are observed corresponding to the ^iPr septets along with multiple doublet signals for the ^iPr methyl groups. This desymmetrisation of the complex can only be explained by the presence of *cis* oxides: *trans* oxides would retain the plane of symmetry perpendicular to the plane of the *bis*(carbene)pyridine backbone and hence only one septet would appear in the ^1H NMR spectrum.

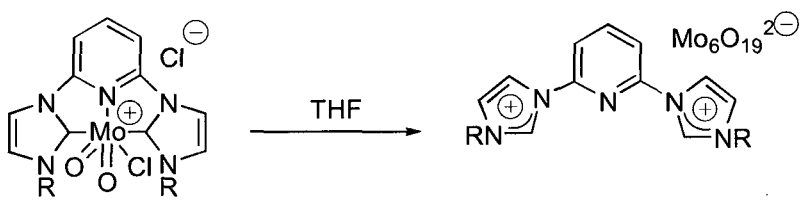

75 **76**

Scheme 32: Decomposition of a Mo(VI) pincer complex, R = DiPP

Attempts to crystallise **75** by slow evaporation of an acetone solution resulted in the formation of colourless crystals. Structural characterisation revealed that decomposition to the bis(imidazolium) salt had taken place (Scheme 32). However, unlike previous structurally characterised imidazolium salts (see section 2.2) the imidazolium protons on the cation are not pointing in the opposite direction to the pyridine lone pair (Figure 29a). This is due to the presence of acetone in the lattice which is hydrogen-bonding to the imidazolium protons [C···O distance 3.208(9) and 3.262(8) Å]. However, there was

no interaction with the pyridine lone pair. Previous imidazolium salts were crystallised from chlorinated solvents which did not undergo H-bonding, hence the preferred *anti* orientation of pyridine lone pair and imidazolium protons was adopted.

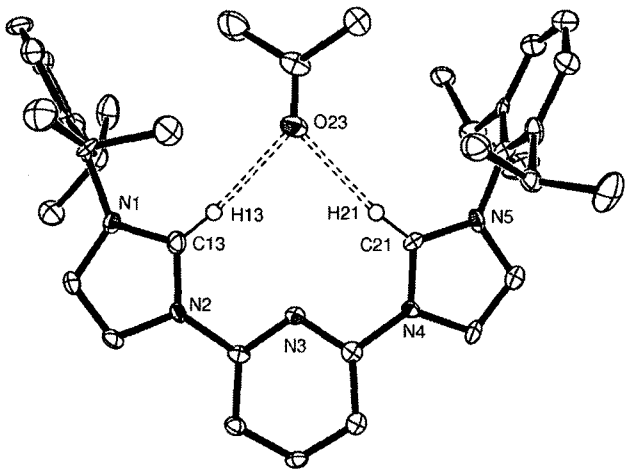

Figure 29a: ORTEP representation of the cation of **76** showing H-bonding. Thermal ellipsoids at 50% probability, H atoms (bar imidazolium protons), and two acetone solvent molecules omitted for clarity.

C(13)–N(1)	1.335(8)
C(13)–N(2)	1.344(9)
C(21)–N(4)	1.330(8)
C(21)–N(5)	1.335(8)
N(1)–C(13)–N(2)	107.8(6)
N(4)–C(21)–N(5)	108.3(6)
C(13)–N(1)–C(1)	127.7(6)
C(21)–N(5)–C(24)	127.1(6)

Table 9a: Selected bond lengths (Å) and angles (°) for the cation of compound **76**

Microanalysis confirmed the presence of one molecule of acetone per molecule of imidazolium salt.

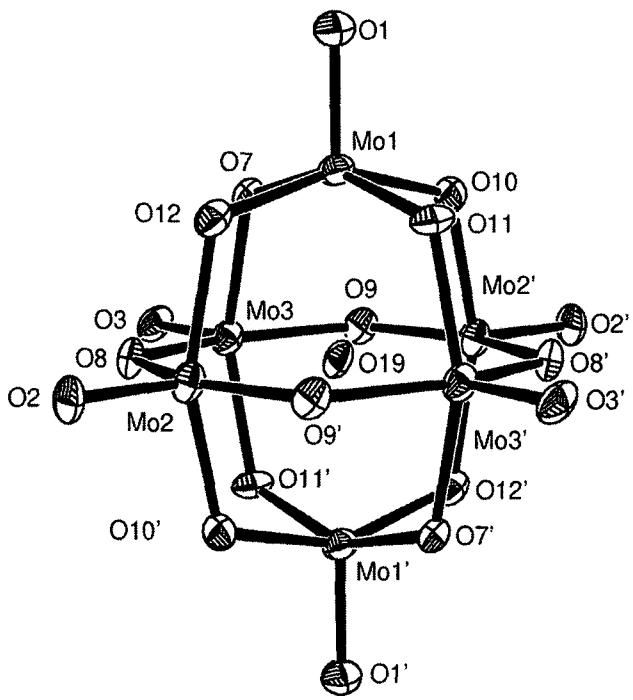

Figure 29b: ORTEP representation of the anion of **76**. Thermal ellipsoids at 50% probability.

O(1)–Mo(1)	1.684(5)
O(2)–Mo(2)	1.684(5)
O(7)–Mo(1)	1.910(5)
O(8)–Mo(2)	1.958(5)
O(19)–Mo(1)	2.3192(6)
O(19)–Mo(2)	2.3257(6)
O(1)–Mo(1)–O(7)	102.6(2)
O(7)–Mo(1)–O(10)	87.4(2)
Mo(1)–O(7)–Mo(3)	116.4(2)
Mo(3)–O(19)–Mo(1)	89.91(2)
Mo(1)–O(12)–Mo(2)	116.5(2)
O(1)–Mo(1)–O(19)	179.42(18)
O(7)–Mo(1)–O(19)	77.05(13)

Table 9b: Selected bond lengths (Å) and angles (°) for the anion of compound **76**

The $[Mo_6O_{19}]^{2-}$ anion (Figure 29b) is a cage structure with overall O_h symmetry and lies on an inversion centre in the unit cell. There are three different oxide environments: terminal oxide, bridging oxide and central oxide. Each molybdenum atom is 6-coordinate distorted octahedral if the interaction to the central oxide is counted as a bond. However, if it is not counted as a bond then the geometry becomes 5-coordinate square-based pyramidal. Each of the bridging oxides is bonded to two molybdenum atoms and there are no other interactions.

The terminal Mo=O bonds [1.684(5) – 1.687(5) Å] are notably shorter than the bridging Mo–O bonds [1.888(5) – 1.961(5) Å], which are in turn shorter than the Mo–O interactions for the central oxide [2.3138(6) – 2.3257(6) Å]. The central oxide has interactions with all six molybdenum atoms but the bond lengths are too long to be counted as a formal Mo–O single bond. All bond lengths are of similar lengths to other literature examples.[100]

3.5 - Group 7 metals

Prior to the start of this project there were no group 7 complexes of (CNC) pincer ligands. The lack of reports is unsurprising for technetium and rhenium, complexes of which have little synthetic usefulness, but manganese salen complexes have found various applications, *e.g.* the epoxidation of olefins and oxidation of organosulfur compounds.[101]

Attempts to synthesise manganese complexes of ligand **36** were undertaken with the reaction of anhydrous $MnBr_2$ with **36** in THF. After 16 hours all the $MnBr_2$ had dissolved, affording an orange solution (Scheme 33).

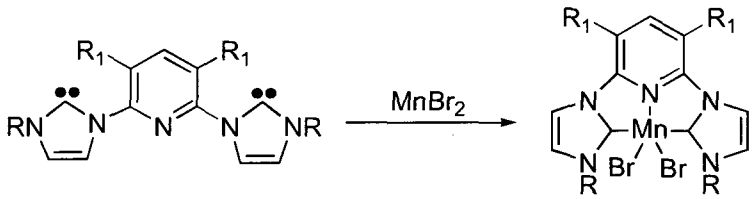

36: R_1 = H
58: R_1 = Me

77: R_1 = H
78: R_1 = Me

Scheme 33: Synthesis of a Mn(II) pincer complex, R = DiPP

Complex **77** was crystallised by slow diffusion of PE into a THF solution, yielding orange crystals. Microanalytical data on these crystals indicated that one molecule of THF was present in the complex (despite extensive drying *in vacuo*) but structural characterisation revealed a 5-coordinate Mn(II) complex with no coordinated THF (Figure 30). The magnetic data (μ_{eff} = 5.87 B.M.) was consistent with a d^5 species with 5 unpaired electrons, confirming the first Mn(II) complex of a (CNC) pincer ligand had been formed.

The diffraction pattern clearly showed discontinuous planes of diffuse scattering at (*h*, 0.5*k*, *l*), indicating significant disorder of the molecules within the crystal. From initial refinements it was obvious that the manganese and bromine sites were split over 2 positions. To retain a chemically sensible geometry it was necessary to refine the structure with whole molecule disorder. This entailed the use of geometrical and thermal parameter restraints but some less than ideal features remained and the refinement did not fully converge. As the model clearly did not account for the diffuse scattering, some imperfections in the refinement were inevitable.

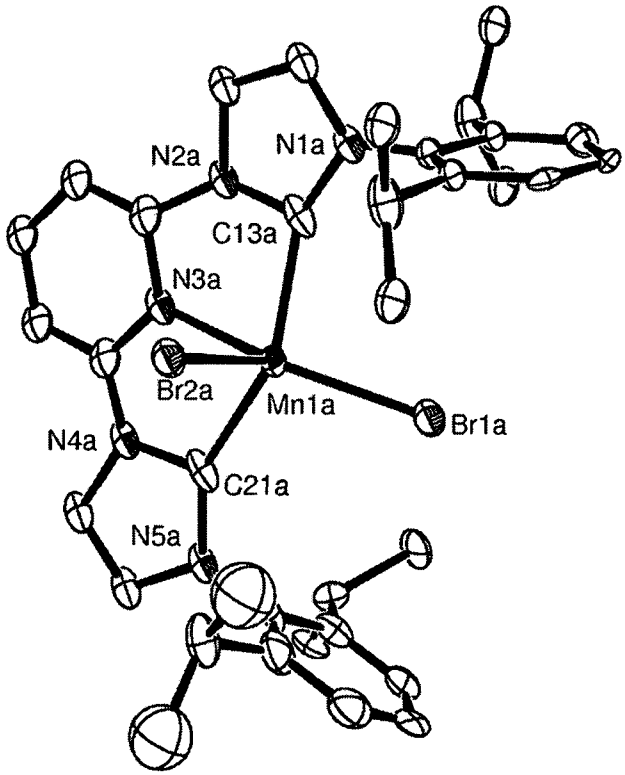

Figure 30: ORTEP representation of **77** showing one refined orientation of the molecule. Thermal ellipsoids at 50% probability, H atoms, and one THF solvent molecule omitted for clarity.

Mn(1A)–N(3A)	2.2574(16)
Mn(1A)–C(13A)	2.206(2)
Mn(1A)–C(21A)	2.210(2)
Mn(1A)–Br(1A)	2.5458(7)
Mn(1A)–Br(2A)	2.5708(7)
C(13A)–Mn(1A)–C(21A)	143.58(8)
C(13A)–Mn(1A)–N(3A)	74.99(7)
C(13A)–Mn(1A)–Br(1A)	99.12(6)
C(13A)–Mn(1A)–Br(2A)	97.41(6)
N(3A)–Mn(1A)–Br(1A)	150.91(5)
N(3A)–Mn(1A)–Br(2A)	84.52(4)
Br(1A)–Mn(1A)–Br(2A)	124.57(3)

Table 10: Selected bond lengths (Å) and angles (°) for compound **77**

The 'degree of trigonality', τ,[102] is a measure of how close a 5 coordinate complex is to either an ideal trigonal bipyramidal or an ideal square-based pyramidal geometry. For an ideal square-based pyramid, the two largest angles at the metal centre, denoted β and α, are equal (180° between two *trans* basal ligands) hence $(\beta - \alpha) = 0$. For an ideal trigonal bipyramid, the two largest angles at the metal centre are 180° (between the two axial substituents) and 120° (between two of the three equatorial ligands) hence $(\beta - \alpha) = 60$. Thus, the formula $(\beta - \alpha)/60$ gives a value between 0 and 1 showing how close a 5 coordinate complex is to an ideal square based pyramidal geometry ($\tau = 0$) and a trigonal bipyramidal geometry ($\tau = 1$).

For complex **77**, $\tau = 0.122$ ($\beta = 150.91°$ and $\alpha = 143.58°$) hence it can be best described as a distorted square based pyramid. This can clearly be seen from Figure 30 where Br(1A) is the basal bromide and Br(2A) is the apical bromide.

In keeping with other 5 coordinate complexes of **36**, the metal atom is out of the plane defined by the N_{py} and two C_{NHC} atoms, here by 0.3873 Å. The Mn–C_{NHC} bond lengths are at the lower end of the range previously observed for Mn(II) NHC complexes.

An analogous complex with ligand **58** was also synthesised following the same method (Scheme 33). Crystallisation occurred from slow diffusion of Et_2O into a DCM solution affording orange blocks in good yield. Microanalysis was consistent with the reported structure and there was no THF in the crystalline solid. Complex **78** was structurally characterised (Figure 31a).

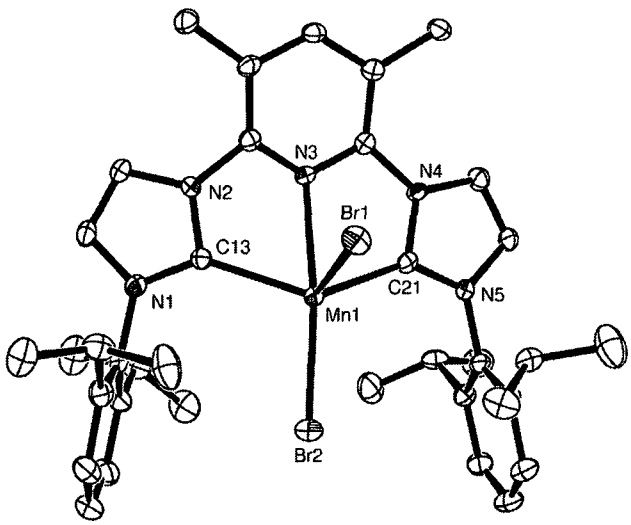

Figure 31a: ORTEP representation of **78**. Thermal ellipsoids at 50% probability, H atoms and two DCM solvent molecules omitted for clarity.

C(13)–Mn(1)	2.263(4)
C(21)–Mn(1)	2.250(4)
N(3)–Mn(1)	2.439(3)
Mn(1)–Br(2)	2.4925(7)
Mn(1)–Br(1)	2.5397(7)
C(21)–Mn(1)–C(13)	132.47(14)
C(13)–Mn(1)–N(3)	68.10(12)
C(13)–Mn(1)–Br(1)	100.83(10)
N(3)–Mn(1)–Br(2)	158.17(8)
Br(2)–Mn(1)–Br(1)	114.57(3)
N(3)–Mn(1)–Br(1)	87.25(8)

Table 11: Selected bond lengths (Å) and angles (°) for compound **78**

The τ value of 0.43 indicates that the complex is almost half-way between square-based pyramidal and trigonal bipyramidal so neither description is really appropriate. However, it is slightly closer to square-based pyramidal than trigonal bipyramidal. The Mn–C_{NHC} bond lengths are at the higher end of the known range of Mn(II)–C_{NHC} bond lengths.

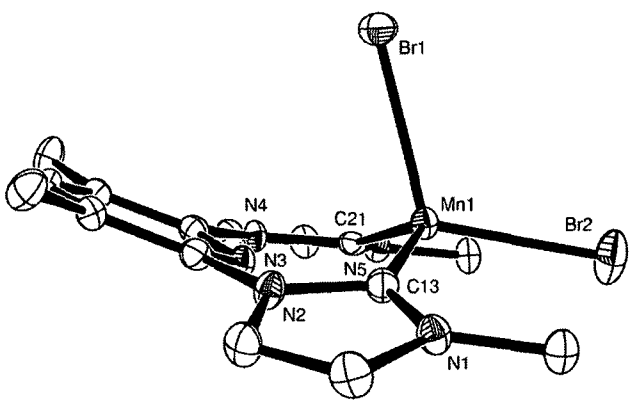

Figure 31b: ORTEP representation of **78** showing the pyridine ring pointing "away" from the manganese centre. Thermal ellipsoids at 50% probability, H atoms, DiPP group (bar ipso carbons) and two DCM solvent molecules omitted for clarity.

An unusual feature of complex **78** in the solid state is the direction in which the pyridine ring is pointing (Figure 31b). All 5 coordinate complexes of **36** contain the metal atom lying above the plane defined by the three coordinating atoms in the ligand, with the three rings pointing toward the metal atom. However, in **78**, the pyridine ring is pointing "down" away from the metal and the two NHC rings are pointing "up" towards the metal. This resulted in the metal atom being further out of the coordination plane than usual, at 0.505(4) Å. There are no intramolecular interactions which could cause this unusual geometry and its origin remains unknown.

The reactivity of complexes **77** and **78** was studied. Attempts at oxidising both complexes failed: despite the use of strong oxidants (NMO, PhIO) no reaction was observed. In an attempt to synthesise a (CNC) complex of manganese in a higher oxidation state, **78** was reacted with NaN_3 with the intention of photolysing the resulting azide to the nitride. However, the only product which could be obtained was colourless crystals which rapidly decomposed when removed from the solvent (THF). Attempts at using $Mo(N)Cl_3(MeCN)_2$[103] as a nitride transfer reagent did not afford any oxidised product. Finally, the use of aromatic azides with photolysis did lead to a reaction taking place, but intractable mixtures were obtained. Reduction of **77** with Na/Hg in the presence of PMe_3 yielded a brown solution from which no pure product could be isolated.

Attempts to alkylate **77** and **78** with MeLi, MeMgBr and $AlMe_3$ resulted in the formation of black solutions from which no product could be isolated. In an attempt to synthesise alkyl manganese complexes of ligand **36**, the disproportionation of $Mn(acac)_3$ with MeLi (Scheme 34)[104] to $(CNC)MnMe_2$ and $(CNC)MnMe_4$ was attempted in the presence of **36**. Although the reaction proceeded according to the literature description, no product could be isolated. The reaction was repeated with monodentate NHC ligands to investigate whether it was the tridentate nature of **36** or the NHC itself which was causing the reaction to fail (Scheme 34).

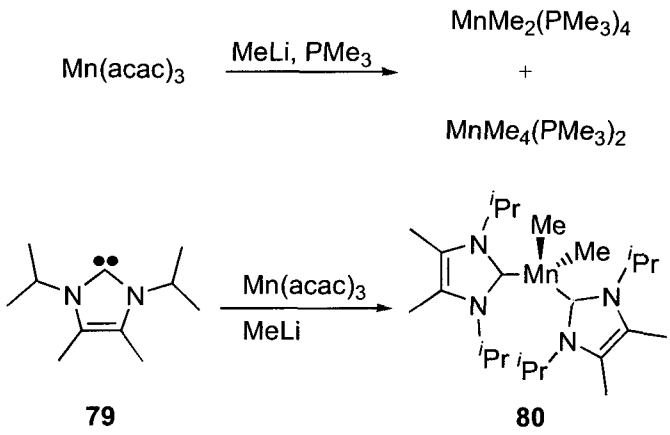

Scheme 34: Synthesis of Mn(II) alkyls stabilised by PMe_3 and NHCs

The reaction proceeded as per the literature description, but crystallisation from Et_2O afforded orange crystals in 93% yield, instead of the expected yellow crystals. Despite the extremely reactive nature of the compound (the crystals reacted with Fomblin®), structural characterisation revealed the formation of a Mn(II) dialkyl complex stabilised by two monodentate NHC ligands (Figure 32). The oxidation state was confirmed by magnetic measurements (μ_{eff} = 5.88 B.M.) indicating 5 unpaired electrons consistent with a Mn(II), d^5 metal centre.

No Mn(IV) product was isolated from the reaction: this is in contrast to the literature example with PMe_3 where the only isolated product was the Mn(IV) complex $MnMe_4(PMe_3)_2$ (Scheme 34). The anomalously high yield of **80** (93%: the expected maximum yield was 50% based on $Mn(acac)_3$) indicates that it is likely the Mn(IV) complex is formed, but reductively eliminates ethane to form **80**.

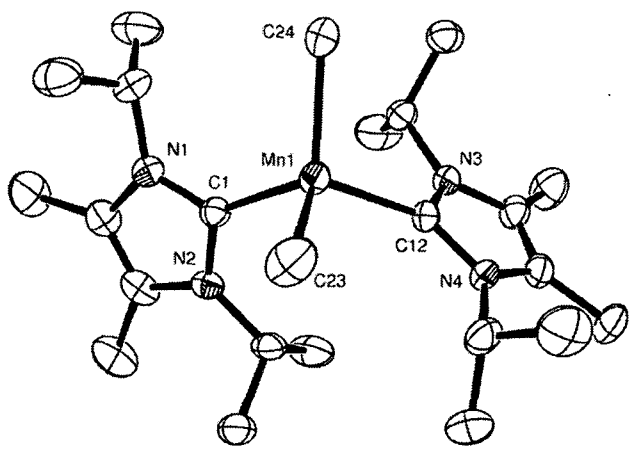

Figure 31: ORTEP representation of **80**. Thermal ellipsoids at 50% probability, H atoms omitted for clarity.

C(1)–Mn(1)	2.264(3)
C(12)–Mn(1)	2.282(3)
C(23)–Mn(1)	2.150(3)
C(24)–Mn(1)	2.182(3)
C(23)–Mn(1)–C(24)	117.95(14)
C(1)–Mn(1)–C(12)	101.08(10)
C(23)–Mn(1)–C(1)	104.29(14)
C(24)–Mn(1)–C(12)	107.67(11)

Table 11: Selected bond lengths (Å) and angles (°) for compound **80**

Compound **80** is a 13-electron, 4 coordinate species which adopts a distorted tetrahedral geometry. The Mn–C_{Me} bond lengths are notably shorter than the Mn–C_{NHC} bond lengths, which are at the longer end of the observed range of Mn^{II}–C_{NHC} bond lengths. The Mn–Me bond lengths are amongst the longest terminal Mn–Me bond lengths observed [the longest literature bond length is 2.173(10) Å].[105] Microanalysis is consistent with the reported structure.

Although the successful isolation of **80** proves that the presence of NHCs does not prevent the disproportionation reaction from occurring, repeated attempts at carrying out the reaction in the presence of **36** failed to yield any product. No further attempts at synthesising manganese alkyl complexes of **36** and **58** were carried out.

3.6 - Summary

A range of early transition metal complexes with the pincer ligands **36**, **58** and **60** have been synthesised and fully characterised. The reactivity of these complexes (and previously synthesised literature complexes) has also been explored.

The Ti=N bond in complexes **64-66** was a convenient spectroscopic handle which allowed comparisons between the σ-donating properties of ligands **36**, **58** and **60** to be made by comparing the IR stretches and Ti=N bond lengths. In keeping with the received notion that NHCs are better σ-donors than trialkylphosphines, the spectroscopic evidence suggested that the best donor ligand was **58** (with 2 extra methyl groups on the pyridine ring compared to **36**) and the worst donor ligand was the trialkylphosphine-containing ligand **60**. Attempts to synthesise 2^{nd}- and 3^{rd}-row transition metal analogues with similar spectroscopic handles failed.

The vanadium complexes **62** and **67** were susceptible to oxidation, allowing access to V(IV) complexes of **36**. However, it was not possible to oxidise complexes to V(V). The first NHC complex of Nb (in any oxidation state) was synthesised.

A new Cr(II) complex has been synthesised by reacting free **36** with $CrCl_2$. This was also susceptible to oxidation although the only isolated product was the previously reported complex **63**.

The first (CNC) complexes of Mn were synthesised but were inert towards substitution and oxidation. However, a 13 electron Mn(II) complex stabilised by two NHC ligands was synthesised: this proved to be very reactive, even reacting with perfluorinated polyethers.

Chapter 4

Cobalt and nickel complexes

4.1 - Introduction

A significant amount of work on cobalt complexes of **36** was published by Danopoulos and co-workers in 2004.[78] Starting from a 5-coordinate Co(II) pincer complex, synthesised by aminolysis of imidazolium salt **35a** with $Co(HMDS)_2$ (Scheme 35), its substitution, oxidation and reduction chemistry was studied. Work by Gibson *et al.* had also established that Co(III) complexes of (CNC) ligands were not catalytically active in the polymerisation of ethylene.[64]

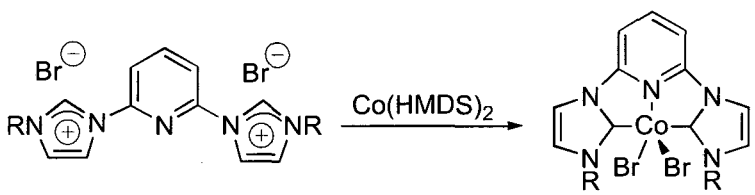

35a **46**

Scheme 35: Synthesis of a Co(II) complex, R = DiPP

Prior to 2006, there were no (CNC) pincer complexes of nickel in the literature. However, during the course of this work, one publication by Inamoto and co-workers appeared (Scheme 36).[65] Although complex **81** showed good catalytic activity in the Heck and Suzuki reactions, its stoichiometric reactivity was not reported.

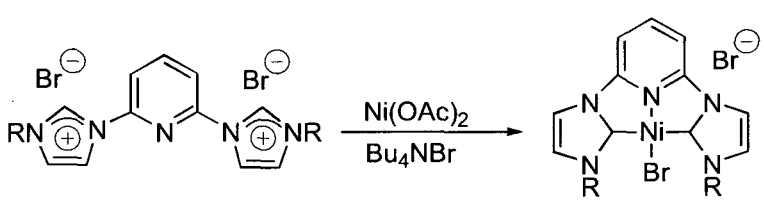

35c **81**

Scheme 36: Synthesis of a Ni(II) complex, R = Me

4.2 - Cobalt

Initial studies into cobalt complexes of ligand **58** started from aminolysis of the precursor imidazolium salt **57** with $Co(HMDS)_2$ in THF (Scheme 37), in an analogous reaction to that of **35a**.

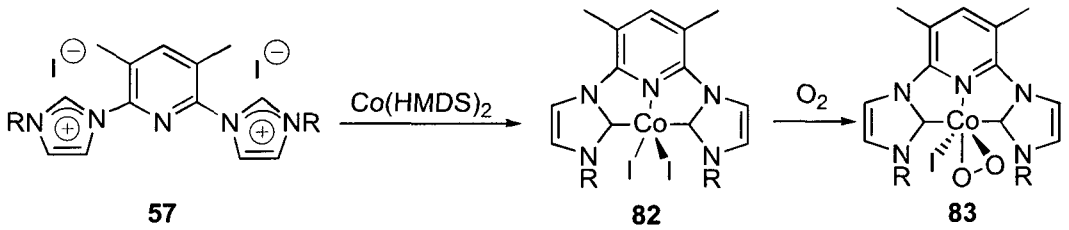

57 **82** **83**

Scheme 37: Synthesis of Co(II) and Co(III) complexes, R = DiPP

Compound **82** was isolated as a brown air-sensitive solid in quantitative yield. Microanalysis was consistent with a Co(II) diiodide pincer complex but, as expected, compound **82** was paramagnetic. By the Evans' method, the magnetic moment of **82** was measured as 2.95 B.M., corresponding to 2 unpaired electrons. Solid-state measurements were also consistent with this value. Magnetic moments of up to 2.90 B.M. have been previously noted for Co(II) systems with one unpaired electron,[106] but it is still mid-way between the ideal values for low-spin Co(II) (1.73 B.M., one unpaired electron) and high-spin Co(II) (3.87 B.M., three unpaired electrons). It is possible that the interconversion between a LS- and HS-d^7 arrangement takes place readily at RT and the magnetic measurement records an average of the two values. Compound **46**, which is a 5-coordinate Co(II) system, has a magnetic moment of 2.00 B.M. which is consistent with one unpaired electron.[78]

The slow diffusion of PE into a THF solution of **82** resulted in the formation of purple rods after 14 days. These were structurally characterised (Figure 32) but instead of the expected 5-coordinate Co(II) diiodide, a 5-coordinate Co(III) peroxo species was formed (Scheme 37).

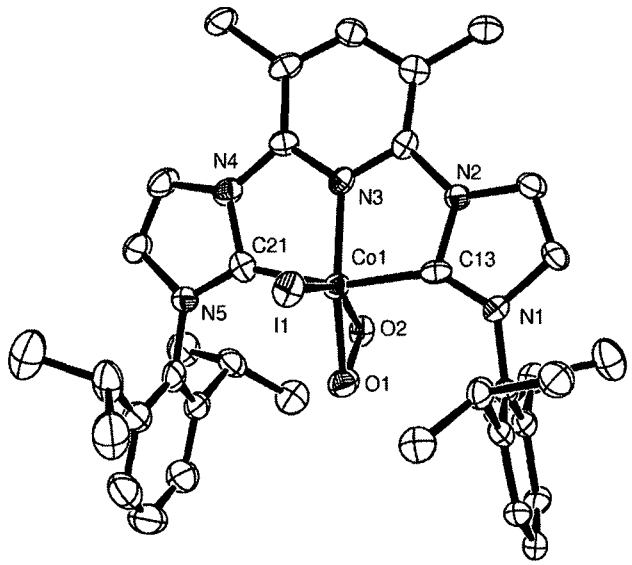

Figure 31: ORTEP representation of **83**. Thermal ellipsoids at 50% probability, H atoms omitted for clarity.

C(13)–Co(1)	1.928(6)
C(21)–Co(1)	1.909(6)
N(3)–Co(1)	1.897(5)
Co(1)–O(1)	1.887(4)
Co(1)–O(2)	1.921(4)
Co(1)–I(1)	2.6060(9)
O(1)–O(2)	1.409(5)
C(21)–Co(1)–C(13)	161.4(3)
O(1)–Co(1)–N(3)	155.49(19)
O(2)–Co(1)–I(1)	152.89(12)
C(13)–Co(1)–I(1)	90.24(16)
O(1)–Co(1)–C(13)	99.3(2)

Table 11: Selected bond lengths (Å) and angles (°) for compound **83**

If the peroxo ligand is assumed to occupy one coordination site (through the centre of the O–O bond), compound **83** is a 5-coordinate complex with a τ value of 0.46, almost half-way between square-based pyramidal and trigonal bipyramidal. However, if the peroxo ligand is assumed to occupy two coordination sites then compound **83** is a severely distorted 6-coordinate octahedral species. The extent of the distortion can be seen from the bond angles around the metal centre: none of the three "*trans*" angles are above 162°.

The Co–C_{NHC} bond lengths of 1.928(6) and 1.909(6) Å are at the low end of the previously observed range of Co(III)–C_{NHC} bond lengths (section 1.5). The Co–O bond lengths are within the expected range for Co–O_{peroxo} species.[107] The O–O bond length of 1.409(5) Å is also consistent with the expected range for a Co(III)–peroxo species.[107]

Microanalysis was consistent with the addition of two oxygen atoms and the loss of one iodine atom from **82**. The ^{1}H NMR spectrum is unremarkable, with two doublets and one septet corresponding to the ^{i}Pr methyl and CH groups respectively, along with a sharp singlet at 2.84 ppm which is assigned to the methyl groups on the pyridine backbone. The signal in the $^{13}C\{^{1}H\}$ spectrum at 198.0 ppm is assigned to the C_{NHC}. Oxidation of **46** with O_2 also results in the formation of a Co(III) peroxo species, although the only characterisation data which was obtained was a poor quality X-ray dataset.[80]

The addition of 0.5 equivalents of I_2 to a THF solution of **82** results in the controlled oxidation of **82** to **84**, a Co(III) triiodide species (Scheme 38). This is analogous to the reactivity of **46** towards Br–HMDS where oxidation to a Co(III) tribromide was observed.[78] However, compound **84** is much more soluble than the tribromide analogue of ligand **36** hence NMR data could be obtained.

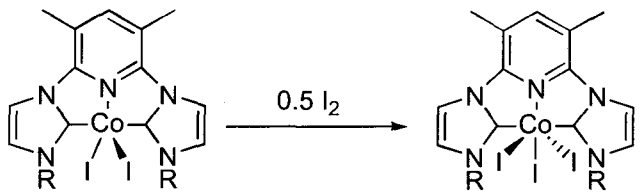

82 **84**

Scheme 38: Formation of a Co(III) triiodide, R = DiPP

Microanalysis was consistent with the addition of one I atom to **82**. The ^1H NMR spectrum exhibits the expected resonances for the ^{i}Pr groups: two doublets at 1.15 and 1.09 ppm, along with a septet at 3.28 ppm. The signal assigned to the methyl groups on the pyridine backbone is observed at 2.90 ppm. The signal for the C_{NHC} is found at 195.25 ppm in the $^{13}C\{^1H\}$ NMR spectrum: slightly further upfield than in **83**, which is a result of the smaller electronegativity of two I^- anions rather than a peroxide dianion. No further studies into the reactivity of **82** were carried out.

Attempts at synthesising an analogue of **46** and **82** with ligand **60** proceeded smoothly. Addition of $CoBr_2(THF)_2$ to ligand **60** in THF resulted in the formation of a purple solution, from which purple crystals could be isolated by the slow diffusion of Et_2O into a concentrated DCM solution (Scheme 39).

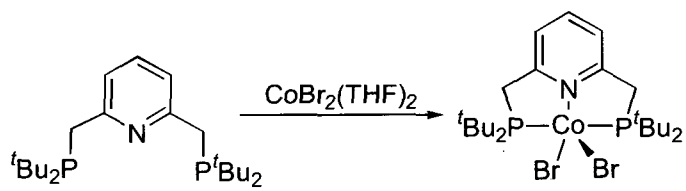

60 **85**

Scheme 39: Synthesis of a Co(II) (PNP) complex

Microanalysis was consistent with the reported structure and, as expected, complex **85** was paramagnetic: a solid state magnetic moment of 1.71 B.M. corresponds to 1 unpaired electron and a low-spin d^7 Co(II) species. This is in agreement with the value for complex **46** but does not agree with the value for complex **82**. Structural characterisation of compound **85** was carried out (Figure 32).

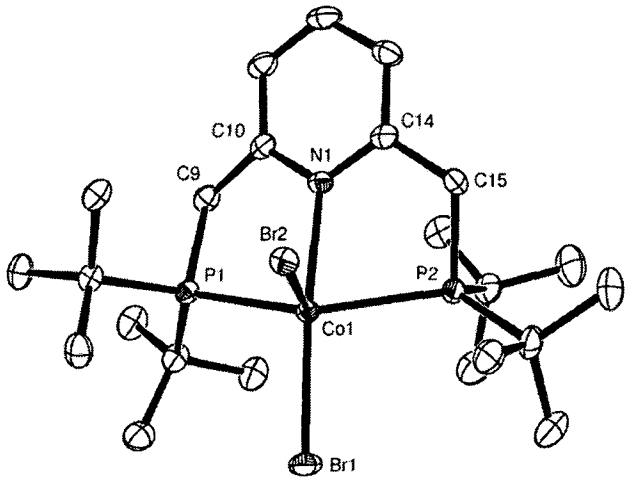

Figure 32: ORTEP representation of **85** showing one of two molecules in the asymmetric unit. Thermal ellipsoids at 50% probability, H atoms omitted for clarity.

N(1)–Co(1)	2.2560(18)
P(1)–Co(1)	2.4596(7)
P(2)–Co(1)	2.4860(7)
Co(1)–Br(1)	2.4630(4)
Co(1)–Br(2)	2.4625(4)
N(1)–Co(1)–Br(1)	166.53(5)
P(1)–Co(1)–P(2)	139.97(2)
Br(2)–Co(1)–P(2)	101.531(19)
Br(2)–Co(1)–Br(1)	102.706(14)
N(1)–Co(1)–Br(2)	90.50(5)

Table 12: Representative bond lengths (Å) and angles (°) for compound **85**

Complex **85** is a 5-coordinate complex with a τ value of 0.44, indicating geometry almost exactly half-way between square-based pyramidal and trigonal bipyramidal. The deviation away from ideal geometry can be seen from the Br–Co–Br bond angle which is mid-way between the angle expected for ideal trigonal bipyramidal (120°) and ideal square-based pyramidal (90°). The Co–P bond lengths of 2.4596(7) and 2.4860(7) Å are shorter than the only other structurally characterised examples of (PNP)Co(II) complexes [range 2.542(2)–2.6200(13) Å].[108] This may be a result of a smaller cone angle around the phosphine: the literature complexes are diarylalkylphosphines with substituents on the *ortho*-positions of the aryl rings whereas ligand **60** is a trialkylphosphine.

4.3 - Nickel complexes of ligand 36

At the outset of this project, no nickel complexes of (CNC) pincer ligand **36** had been reported in the literature. A significant amount of work into palladium complexes of (CNC) pincer ligand **36** had been carried out (see section 1.34): the typical complex geometry was a distorted square planar Pd(II) centre with three of the coordination sites occupied by the pincer ligand, the fourth by a halide and a non-coordinating anion was also present.[52] It was thought that a similar coordination geometry would be found for nickel(II) complexes.

Addition of a THF solution of **36** to $NiBr_2(DME)$ resulted in the formation of an orange solution (Scheme 40). After removal of solvents, air-stable orange crystals were isolated from the slow diffusion of Et_2O into a concentrated DCM solution.

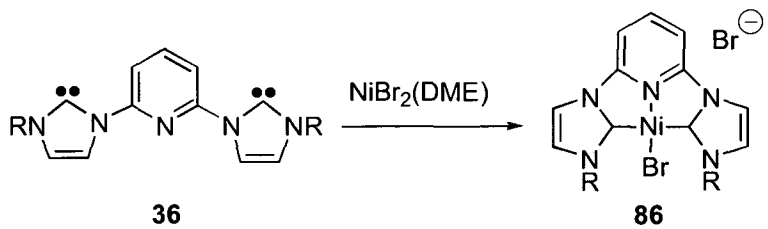

36 **86**

Scheme 40: Synthesis of the first Ni (CNC) pincer complex, R = DiPP

Surprisingly, the ^1H NMR spectrum of these orange crystals consisted of very broad signals. Only two resonances could be distinguished: one multiplet between 6.0 and 9.2 ppm and one multiplet between 0.5 and 3.0 ppm. The multiplet in the aromatic region of the spectrum integrated to 13H, which was consistent with the number of aromatic protons in **86**, and the multiplet in the aliphatic region of the spectrum integrated to 28H, which is the number of protons on the ^{i}Pr groups. Attempts at carrying out magnetic measurements (both in solution and in the solid state) did not result in the detection of a magnetic moment. The $^{13}C\{^1H\}$ NMR spectrum exhibited 9 resonances between 164.6 and 109.8 ppm which is consistent with the expected number of aromatic carbon resonances, but DEPT experiments did not distinguish between the quaternary and CH carbons. There were also three resonances between 28.6 and 22.9 ppm which corresponded to the two different environments for the ^{i}Pr methyl groups and the ^{i}Pr methine group. The resonance for the C_{NHC} was not observed. Structural characterisation of **86** was carried out (Figure 33).

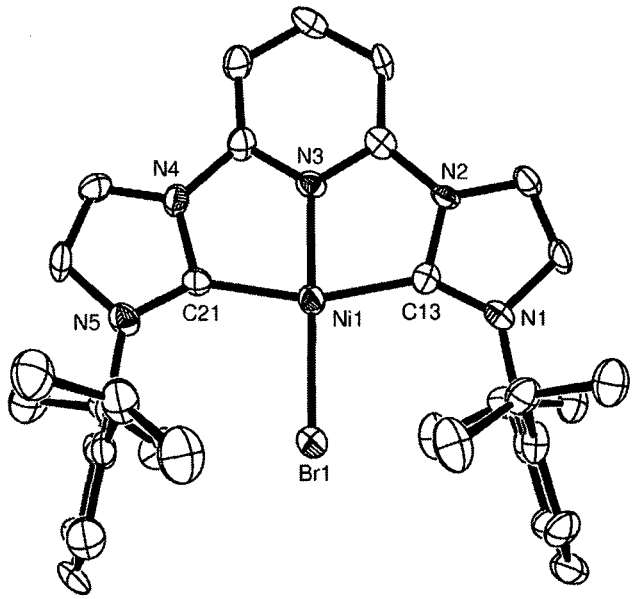

Figure 33: ORTEP representation of **86** showing one of two molecules in the asymmetric unit. Thermal ellipsoids at 50% probability, non-coordinating bromide anion, H atoms and two DCM solvent molecules omitted for clarity.

C(13)–Ni(1)	1.920(7)
C(21)–Ni(1)	1.914(7)
N(3)–Ni(1)	1.872(5)
Ni(1)–Br(1)	2.2813(11)
C(21)–Ni(1)–C(13)	161.1(3)
N(3)–Ni(1)–Br(1)	174.43(18)
N(3)–Ni(1)–C(13)	80.3(3)
N(3)–Ni(1)–C(21)	80.8(3)
C(13)–Ni(1)–Br(1)	99.8(2)
C(21)–Ni(1)–Br(1)	99.1(2)

Table 13: Representative bond lengths (Å) and angles (°) for compound **86**

Compound **86** is a 4-coordinate distorted square planar complex with three of the coordination sites taken up by the ligand and the fourth occupied by a bromide anion. There is also a non-coordinating bromide anion present in the asymmetric unit along with two DCM solvent molecules. The distortion away from ideal square planar is caused by the steric demands of the ligand: the metal cannot move any further into the pocket of the ligand and as a result, the C–Ni–C angle is 161.1(3)° rather than the ideal 180°. The Ni–C_{NHC} bond lengths of 1.920(7) and 1.914(7) Å are within the range of previously observed Ni(II)–C_{NHC} bond lengths. The metal lies out of the coordination plane [C(13), C(21), N(3) and Br(1)] by 0.050(3) Å.

Microanalysis was also consistent with the reported structure. As a result of this and the solid-state structure confirming the expected Ni(II) square planar geometry, it was thought that the reason for the broad peaks in the ^{1}H NMR spectrum was the non-coordinating bromide reversibly binding to the nickel centre in solution. However, VT NMR studies showed that the spectrum remained broad as low as –70 °C hence experimental confirmation of this hypothesis could not be obtained.

Attempts at studying the reactivity of **86** initially focussed on removing the bromide anions in favour of more labile ligands. The reaction of **86** with 2.1 equivalents of $AgBF_4$ in MeCN resulted in the formation of a green solution from which green needles could be obtained after filtration through Celite. Unfortunately, due to the size of the

needles, only a poor-quality X-ray dataset could be obtained. This showed the 4-coordinate square planar geometry was retained, with a dicationic Ni(II) metal centre, acetonitrile occupying the fourth coordination site and two non-coordinating BF_4^- anions (Scheme 41).

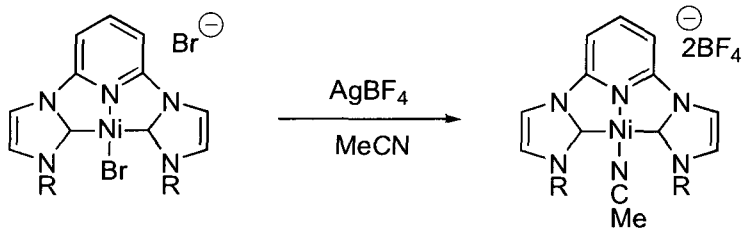

86 **87**

Scheme 41: Anion exchange in complex **86**, R = DiPP

Microanalysis was consistent with the formation of an acetonitrile adduct with two BF_4^- anions. The ^1H NMR spectrum had the expected resonances for the ^{i}Pr groups; two doublets at 1.08 and 1.19 ppm and one septet at 2.54 ppm. A signal integrating to 3H, corresponding to the coordinated acetonitrile, could be observed at 1.94 ppm. Unfortunately, no resonance for the C_{NHC} could be observed in the $^{13}C\{^1H\}$ NMR spectrum.

The reaction of **86** with 2 equivalents of AgOTf in THF also resulted in the formation of a green solution, implying both bromides had been exchanged for triflate anions. After filtration through Celite, green blocks were obtained from the slow diffusion of PE into a concentrated THF solution (Scheme 42). However, these crystals were paramagnetic: a magnetic moment of 2.86 B.M. was observed, which corresponds to 2 unpaired electrons.

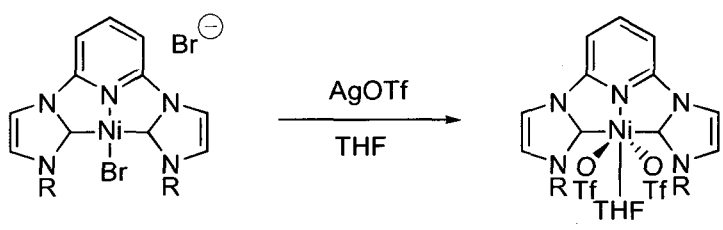

86 **88**

Scheme 42: Synthesis of an octahedral Ni(II) complex, R = DiPP

Structural characterisation of the green crystals was carried out (Figure 34). This revealed an unexpected slightly distorted octahedral geometry with ligand **36** occupying three meridional coordination sites, a THF molecule trans to the N_{py} and two mutually trans triflate molecules, each coordinating to the nickel through one oxygen. Microanalysis was consistent with this elemental composition.

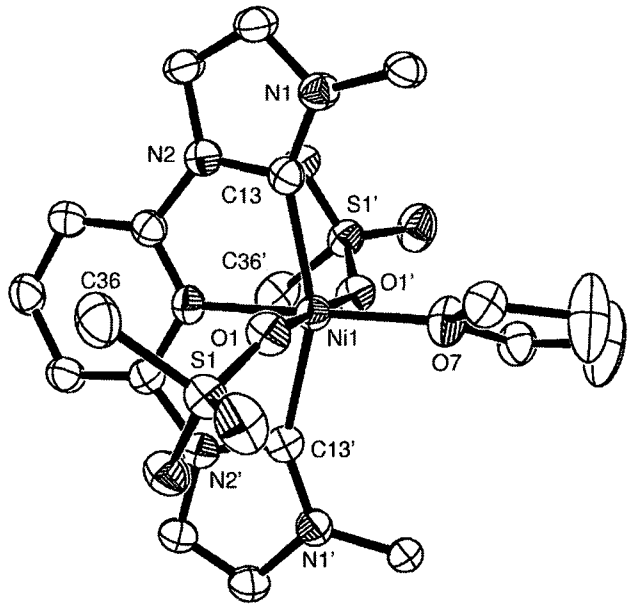

Figure 34: ORTEP representation of **88**. Thermal ellipsoids at 50% probability, H and F atoms, DiPP groups (bar ipso carbons) and two THF solvent molecules omitted for clarity.

C(13)–Ni(1)	2.103(4)
N(3)–Ni(1)	2.017(4)
O(1)–Ni(1)	2.190(3)
O(7)–Ni(1)	2.069(4)
C(13)–Ni(1)–C(13')	155.3(2)
O(1)–Ni(1)–O(1')	179.03(15)
N(3)–Ni(1)–O(7)	180.0
C(13)–Ni(1)–O(1)	87.49(12)
O(7)–Ni(1)–C(13)	102.37(11)
O(7)–Ni(1)–O(1)	89.52(8)
N(3)–Ni(1)–O(1)	90.48(8)
N(3)–Ni(1)–C(13)	77.63(11)

Table 14: Selected bond lengths (Å) and angles (°) for compound **88**

Complex **88** lies on a C_2 axis within the unit cell and has crystallographically imposed C_2 symmetry. It is only the second structurally characterised example of an octahedral nickel species containing NHC ligands.[109] The Ni–C_{NHC} bond length of 2.103(4) Å is substantially longer (*ca.* 0.84 Å) than the longest literature example in the other structurally characterised octahedral complex. This indicates that the geometry at the metal centre has an effect on the bond lengths at the metal centre. Further evidence comes from the Ni–N_{py} bond lengths; the Ni–N_{py} bond length in **88** is *ca.* 0.14 Å longer than the Ni–N_{py} bond in **86**, which is a square planar compound.

Within experimental error, there is no difference between the non-coordinating S–O bonds and the coordinated S–O bond. However, there is a difference between the Ni–O bonds at the metal centre: despite THF being a neutral ligand, the Ni–O_{THF} bond is significantly shorter (*ca.* 0.12 Å) than the Ni–O_{Tf} bond. This is probably a result of steric crowding at the metal centre: the bulky triflate anions cannot closely approach the nickel centre due to the ^{i}Pr groups of the DiPP substituents. However, the Ni–O_{Tf} bond length is one of the longest structurally characterised Ni–O_{Tf} bonds.[110]

The distortion away from ideal octahedral geometry in complex **88** is mainly a result of the steric restrictions of the pincer ligand. The C–Ni–C bond angle of 155.3(2)° is *ca.* 6° smaller than the same angle in square planar complex **86**, but the other two trans angles

are 180°. The fact that the triflate anions adopt an ideal geometry indicates that they are not sterically or electronically influenced by the other atoms around the metal centre.

Attempts at oxidation of Ni(II) pincer complexes focussed on those complexes which contained labile ligands. Both complexes **87** and **88** were suitable substrates for attempts at oxidation. Addition of NMO, PhIO and aromatic azides to THF solutions of **87** did not result in any reaction, even after photolysis: starting material was recovered in each case. However, when NMO was added to a THF solution of **88**, a very small amount of pale green crystals were deposited after the reaction was left standing for 72 hours. An X-ray diffraction study indicated that loss of ligand **36** had occurred and a $[Ni_4O_4]$ distorted cube-type structure had been formed (Figure 35, Scheme 43).

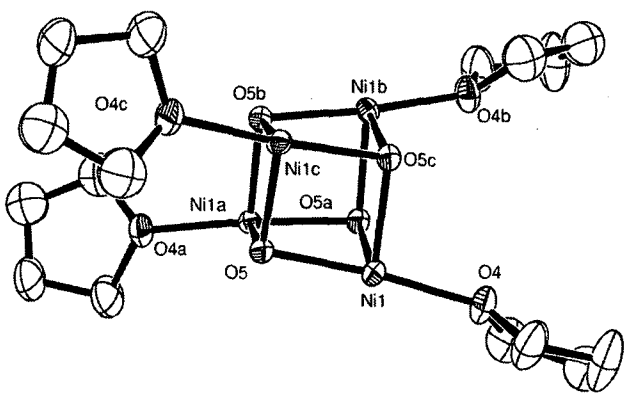

Figure 35: ORTEP representation of the $[Ni_4O_4]$ core. Thermal ellipsoids at 50% probability, H atoms and bridging triflates omitted for clarity.

O(4)–Ni(1)	2.041(3)
O(3)–Ni(1)	2.121(3)
O(5)–Ni(1)	2.032(3)
Ni(1)–O(5a)	2.038(3)
Ni(1)–O(5c)	2.037(3)
O(1)–Ni(1)	2.119(3)
O(5)–Ni(1)–O(4)	173.78(13)
O(5a)–Ni(1)–O(1)	169.26(12)
O(5c)–Ni(1)–O(3)	168.32(12)
O(4)–Ni(1)–O(3)	87.77(14)
O(5)–Ni(1)–O(5c)	84.57(12)
O(5c)–Ni(1)–O(1)	93.93(11)

Table 15: Selected bond lengths (Å) and angles (°) for compound **89**

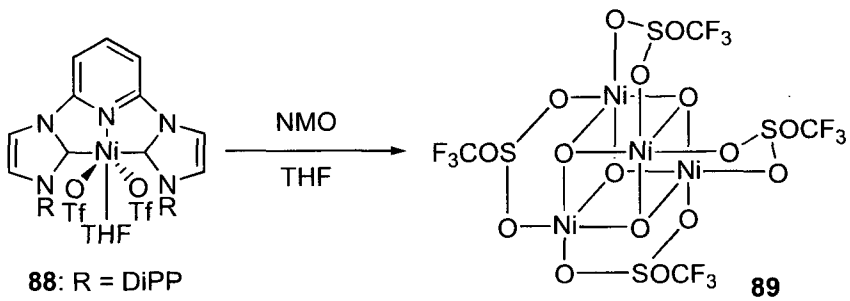

Scheme 43: Synthesis of the $[Ni_4O_4]$ cubane-type structure. THF groups omitted for clarity

The core of the molecule is a nickel oxide cube-type structure with 4 nickel atoms and 4 oxygen atoms. There are 4 triflate groups, each of which bridges two nickel atoms on the same face of the cube, four faces being occupied in total. The octahedral coordination sphere of each nickel atom is completed by one THF molecule. The four THF molecules occupy the faces of the cube (two THF molecules per face) which do not contain triflate anions and are diametrically opposite each other.

Compound **89** lies on two 4-fold rotoinversion axes in the unit cell (the asymmetric unit is one quarter of the molecule). The $[Ni_4O_4]$ core has been previously observed several times, although the oxygen atoms are usually part of an alkoxide moiety,[111] although some hydroxide-containing structures are known.[112]

As drawn, compound **89** contains nickel in oxidation state +3. However, it is possible that the nickel atoms are in oxidation state +2 and that the oxides are hydroxides. There is a Q-peak in the difference map which is in the expected position for a proton, however it does not refine to a position consistent with a hydroxide proton.

The Ni–O bond lengths for the cubane-type core range from 2.032(3) Å to 2.038(3) Å. This is consistent with other examples of Ni(II) cubane-type structures where the bond lengths range from 1.977(6) Å to 2.168(3) Å.[113, 114] However, no Ni(III) cubane-type structures exist in the literature so the oxidation state cannot be unequivocally determined by bond-length analysis. Unfortunately, despite repeated attempts, compound **89** could not be remade in large enough quantities to enable further characterisation, so the oxidation state of the nickel atoms remains in doubt.

Further attempts to synthesise (CNC)Ni=X type complexes (X = O, NR) were made using the reaction of compound **86** with 2.5 equivalents of lithium mesitylamide in THF. The aim was to synthesise a nickel mesitylimide species *via* deprotonation of the intermediate nickel mesitylamide (Scheme 44). A small amount of yellow crystals were isolated from a brown solution by cooling a saturated Et_2O solution to 5 °C.

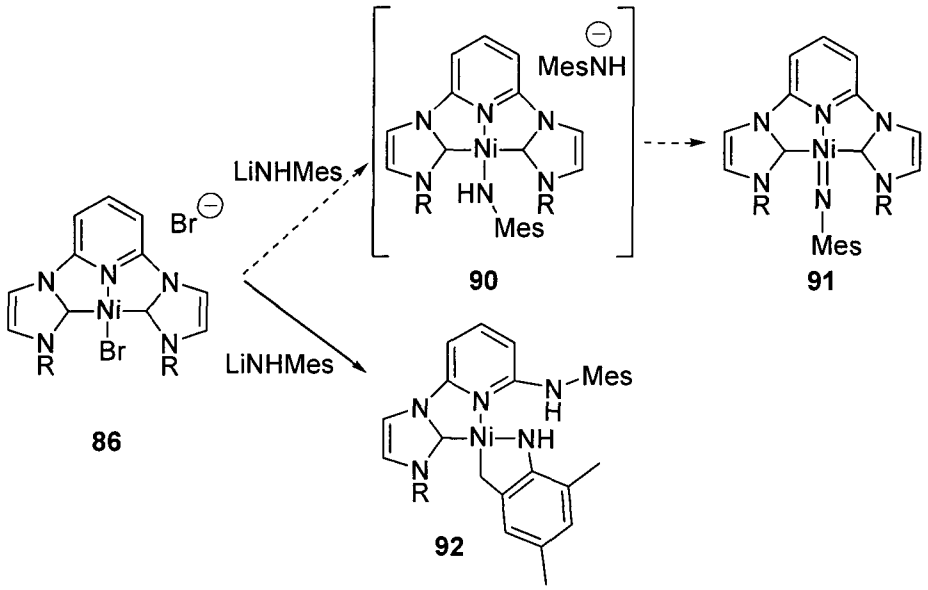

Scheme 44: Attempted synthesis of a Ni(II) imido species, R = DiPP

The yellow crystals were structurally characterised, but the product was not the expected Ni(II) imido species. Instead, ligand decomposition and C–H activation of a mesityl group had taken place (Figure 36).

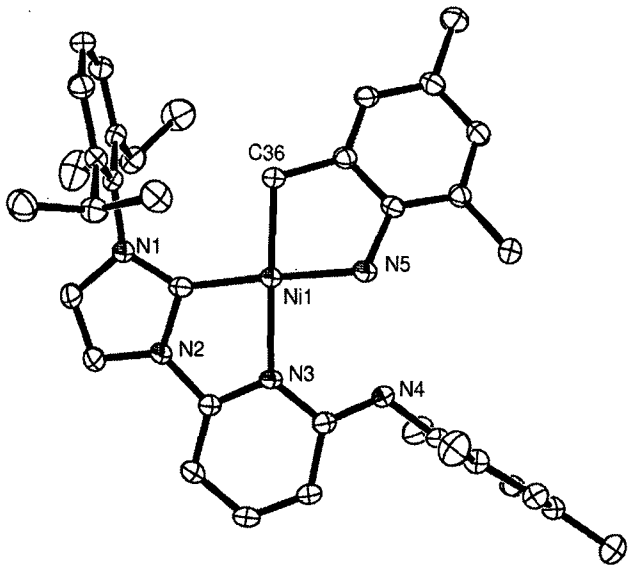

Figure 36: ORTEP representation of **92** showing one of two molecules in the asymmetric unit. Thermal ellipsoids at 50% probability, H atoms omitted for clarity.

C(13)–Ni(1)	1.852(2)
C(36)–Ni(1)	1.9418(19)
N(3)–Ni(1)	2.0238(16)
N(5)–Ni(1)	1.9395(18)
C(13)–Ni(1)–N(5)	173.31(8)
C(36)–Ni(1)–N(3)	171.30(8)
C(13)–Ni(1)–C(36)	97.32(9)
N(5)–Ni(1)–C(36)	85.10(8)
C(13)–Ni(1)–N(3)	82.79(8)
N(5)–Ni(1)–N(3)	95.76(7)

Table 16: Representative bond lengths (Å) and angles (°) for compound **92**

Compound **92** is a 4-coordinate, distorted square planar species containing two bidentate ligands: one composed of an NHC ring and a pyridine ring, the other composed of an amide functionality and an alkyl group. The NHC-containing ligand is derived from ligand **36** whilst the other ligand is generated by one equivalent of lithium mesitylamide. The second equivalent of lithium mesitylamide has displaced one of the

"arms" of the pincer, resulting in an amine functionality in the 6-position of the pyridine ring and, presumably, diisopropylimidazole as the byproduct. The N-bound protons were located in the difference map, one close to N(4) and one close to N(5) but after refinement, both protons were found bonded to N(5). The Ni–N(5) bond length of 1.9395(18) Å is consistent with an amine functionality,[115] but in the absence of further corroborating evidence for the location of the protons, their position remained undetermined.

The Ni–C_{NHC} bond length of 1.852(3) Å is at the lower end of the previously observed range of Ni–C_{NHC} lengths. It is also notably shorter than the Ni–C_{Mes} bond length. The distortion away from ideal square planar geometry is a result of the constraints of the two bidentate ligands: both the ligand bite angles are less than 90°.

The mechanism of formation is unknown. The first step is presumably ion exchange between the non-coordinating bromide of **86** and LiNHMes, forming LiBr and a Ni-containing species with $^{-}$NHMes as the anion. This reactive anion could then either displace the NHC from the 6-position of the pyridine ring (forming the neutral ligand first) or it could bind to the metal centre, leaving the NHC pendant. However, in the absence of further experimental evidence, it is impossible to say which pathway is more likely.

The reaction of **86** with alkylating agents (MeLi, MeMgBr or $AlMe_3$) resulted in the formation of brown solutions from which no identifiable product could be isolated. Attempts to synthesise alkyl nickel complexes of **36** utilised $NiMe_2$(TMEDA) as a starting material.[116] Reaction of **86** with $NiMe_2$(TMEDA) in THF at –78 °C led to the formation of a brown solution, from which a brown solid could be isolated.

Microanalysis of the solid product revealed the elemental composition was consistent with the formulation (CNC)$NiMe_2$, but the ^{1}H NMR spectrum was extremely complicated. The usual sharp doublets corresponding to the ^{i}Pr methyl groups were not present; instead a complex multiplet was observed which integrated to 24H. Three septets corresponding to the ^{i}Pr methine protons were observed in a 1:1:2 ratio. One singlet, integrating to 3H, was observed for the NiMe protons and several resonances in the olefinic region of the spectrum were also present. Cooling a saturated Et_2O solution

of the brown solid led to the formation of extremely small crystals from which an X-ray crystal structure could be obtained (Figure 37).

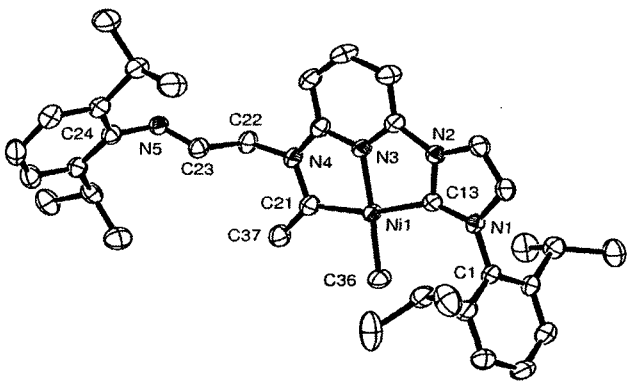

Figure 37: ORTEP representation of **93** showing one of two molecules in the asymmetric unit. Thermal ellipsoids at 50% probability, H atoms omitted for clarity.

C(13)–Ni(1)	1.912(2)
C(21)–Ni(1)	1.930(2)
C(36)–Ni(1)	1.924(2)
N(3)–Ni(1)	1.8725(19)
C(21)–C(37)	1.337(3)
C(23)–N(5)	1.259(3)
C(13)–Ni(1)–C(21)	164.05(10)
N(3)–Ni(1)–C(36)	177.77(10)
N(3)–Ni(1)–C(13)	81.50(9)
C(36)–Ni(1)–C(21)	95.21(11)
N(4)–C(22)–C(23)	111.8(2)
C(37)–C(21)–N(4)	117.9(2)

Table 17: Representative bond lengths (Å) and angles (°) for compound **93**

The structure of the molecule revealed an unexpected ring-opening of the NHC moiety had taken place accompanied by methyl migration from nickel to the C_{NHC}. Compound **93** is a 4-coordinate, distorted square planar species containing one NHC moiety, one pyridine moiety, one vinyl group and one methyl group surrounding the metal centre. The nickel centre is in oxidation state +2 and there are 16 valence electrons, consistent with the distorted square planar geometry.

The presence of a vinyl group is confirmed from the C(37)–C(21) bond length of 1.337(3) Å, which is typical of a C=C double bond. The C–C–N angle around C(21) of 117.9(2)° also indicates the presence of an sp^2 hybridised carbon atom. The C(23)–N(5) bond length of 1.259(3) Å is consistent with an imine, whilst the C–C–N angle at C(22) of 111.8(2)° indicates an sp^3 hybridised carbon centre. These functional groups explain the observed ^{1}H NMR spectrum: the presence of only one methyl group coordinated to nickel and the olefinic resonances are a result of the methyl migration and ring-opening. The loss of symmetry by ring-opening explains the multiplet in place of sharp doublets for the ^{i}Pr methyl protons, and also the presence of three signals for the ^{i}Pr methine protons.

Of the three Ni–C bonds, the Ni–C_{NHC} bond length is the shortest. It is also consistent with the previously observed range of Ni–C_{NHC} bond lengths. The Ni–C_{Me} bond length

is slightly shorter than the Ni–C_{vinyl} bond length, although it is possible that within experimental error it is the other way round. However, the geometric constraints of the ligand are a likely explanation for this apparent anomaly.

The mechanism for the rearrangement is not clear. However, an analogous palladium system reported in 2004[74] contained a square planar Pd(II) pincer species which had undergone methyl group migration from Pd to the C_{NHC}, resulting in a pincer ligand with one NHC and one alkyl group. Based on a similar process occurring with the nickel system, a possible mechanism of formation is proposed (Scheme 45). The first step is formation of an intermediate 5-coordinate nickel centre by coordination of the pincer ligand and displacement of TMEDA. The "axial" methyl group is aligned to undergo migration to the C_{NHC} and results in the formation of a 4-coordinate square planar species analogous to the reported palladium structure.

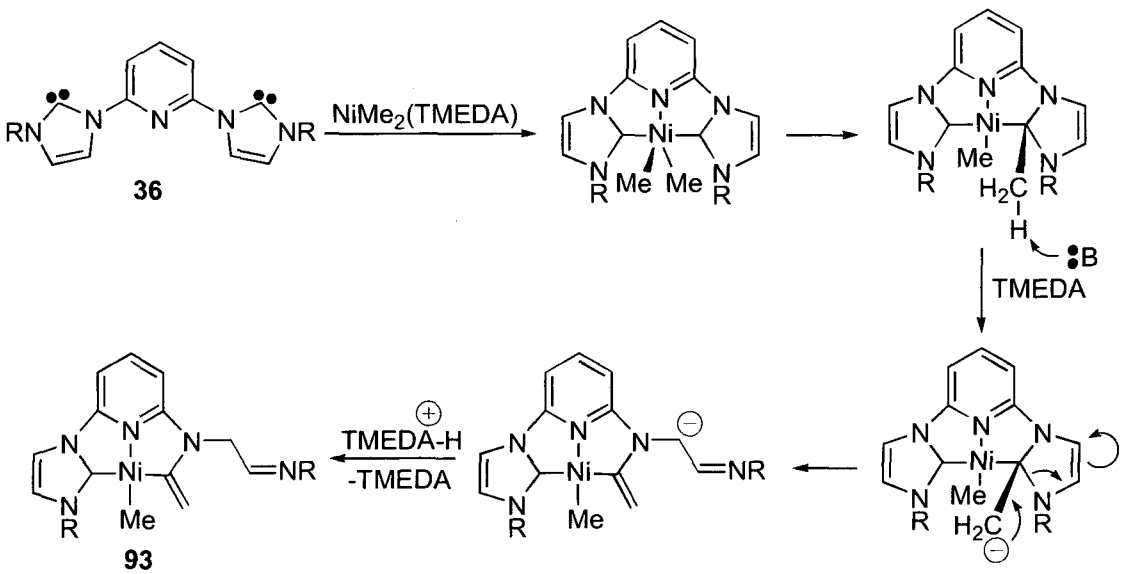

Scheme 45: Proposed mechanism of formation of complex **93**, R = DiPP

However, the presence of base (TMEDA) in the system may result in deprotonation of the migrated methyl group bearing β-hydrogens, forming a primary carbanion and TMEDA·H^+ cation. The unstable carbanion immediately forms the olefin moiety, in the process opening the 5-membered ring forming the imine and a more stable secondary carbanion. The secondary carbanion is further stabilised by the presence of the adjacent electron-withdrawing nitrogen atom and is eventually reprotonated by the ammonium salt, forming the methylene group at C(22).

A recent publication by Grubbs *et al.* reported the decomposition of a saturated NHC ring coordinated to nickel.[117] It was thought that migration of an aryl group to the C_{NHC}

was the first step, leading to ring-opening and the formation of a Fischer carbene. The use of methyl nickel complexes stabilised by non-basic ligands was attempted [*e.g.* $NiMe_2(PMe_3)_2$], but no product could be identified from the reaction.

Attempts at synthesising aryl complexes of nickel pincer species focussed on the use of $PhNiCl(PPh_3)_2$ with the aim of synthesising a phenylnickel cation stabilised by (CNC) ligand **36** and a non-coordinating chloride anion. However, the brown solid which was isolated from the reaction did not contain any resonances for the ^{i}Pr groups (either septet or doublets) and the product could not be identified.

Complex **86** was tested as a catalyst for the coupling of bromobenzene and phenylmagnesium chloride with the use of KPF_6 as a halide abstractor: however the only reaction product was a brown solution which yielded a brown solid. This contained no cross-coupled product when analysed by ^{1}H NMR, but slowly diffusing PE into a THF solution of the brown solid yielded a very small amount of yellow crystals. Structural characterisation revealed that exchange of the non-coordinated bromide anion for PF_6^- had taken place (Figure 38).

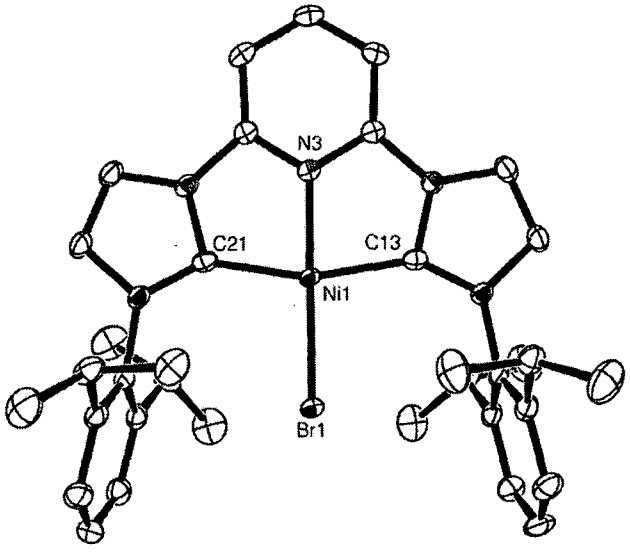

Figure 38: ORTEP representation of the cation of **94**. Thermal ellipsoids at 50% probability, H atoms and PF_6^- anion omitted for clarity.

C(13)–Ni(1)	1.925(2)
C(21)–Ni(1)	1.925(2)
Ni(1)–Br(1)	2.2746(4)
N(3)–Ni(1)	1.8667(19)
C(13)–Ni(1)–C(21)	162.36(10)
N(3)–Ni(1)–Br(1)	179.64(7)
N(3)–Ni(1)–C(13)	81.46(9)
N(3)–Ni(1)–C(21)	80.92(9)
C(13)–Ni(1)–Br(1)	98.24(7)
C(21)–Ni(1)–Br(1)	99.38(7)

Table 18: Selected bond lengths (Å) and angles (°) for compound **94**

Compound **94** is a 4-coordinate distorted square planar species with non-coordinating PF_6^- anion. The bond lengths at the metal centre are identical to the cation in **86** within experimental error, with the exception of the Ni–Br bond which is slightly shorter. The Ni–C_{NHC} bond lengths are within the range of previously observed Ni–C_{NHC} bond

lengths. The distortion away from ideal square planar is slightly less than in **86**: the C–Ni–C angle is *ca.* 1° larger in **94** and the N–Ni–Br angle is closer to 180° by *ca.* 5°.

A systematic synthesis of **94** involved stirring complex **86** with 3.5 equivalents of KPF_6 in THF (Scheme 46). Despite the use of excess halide abstractor, only the non-coordinated bromide anion was exchanged for PF_6^-. This is in contrast to the use of AgOTf where both bromides were substituted.

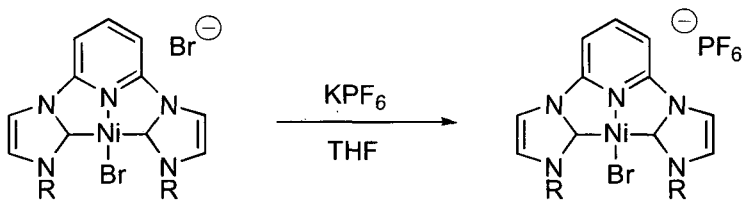

86 **94**

Scheme 46: Anion exchange in complex **86**, R = DiPP

The ^{1}H NMR spectrum of **94** exhibited the usual sharp doublets and septet for the ^{i}Pr groups. Full assignment of the aryl region was possible, with the *para* protons of the pyridine ring and phenyl rings appearing as triplets (1:2 ratio) and the *meta* protons appearing as doublets (2:4 ratio). An unusually high-field (165.22) resonance for the C_{NHC} was observed in the $^{13}C\{^1H\}$ NMR spectrum. Microanalysis was consistent with the reported structure.

Two routes to synthesising a Ni(0) complex of ligand **36** were attempted. The first was reduction of **86** with Na/Hg in the presence of PMe_3. However, the only reaction product was a brown solution, affording a brown paramagnetic solid which could not be identified. The second route was to add an Et_2O solution of **36** to $Ni(COD)_2$ at –78 °C. After warming to RT and removal of solvents, a paramagnetic yellow solid was obtained. However, elemental analysis showed the product to be severely deficient in carbon from the expected [(CNC)Ni] empirical formula.

4.4 - Nickel complexes of ligand 58

Due to initial difficulties in synthesising **58** in gram quantities, a Ag complex of ligand **58** was synthesised with the aim of using it as a transmetallation reagent (see section 2.3). Ag complex **59** was reacted with $NiBr_2(DME)$ in THF and an orange solution resulted. After filtration through Celite, an orange crystalline material was obtained by diffusion of PE into a concentrated THF solution. The ^1H NMR spectrum exhibited the usual doublets and septet for the ^{i}Pr groups, along with a singlet at 3.02 ppm for the methyl groups on the pyridine ring. No signal for the C_{NHC} was observed in the $^{13}C\{^1H\}$ NMR spectrum although a resonance at 168.6 ppm which was assigned as a high-field quaternary aromatic carbon could be due to the C_{NHC}. However, microanalysis was inconsistent with a (CNC)NiBr(Br) formulation and the orange crystals were structurally characterised (Figure 39).

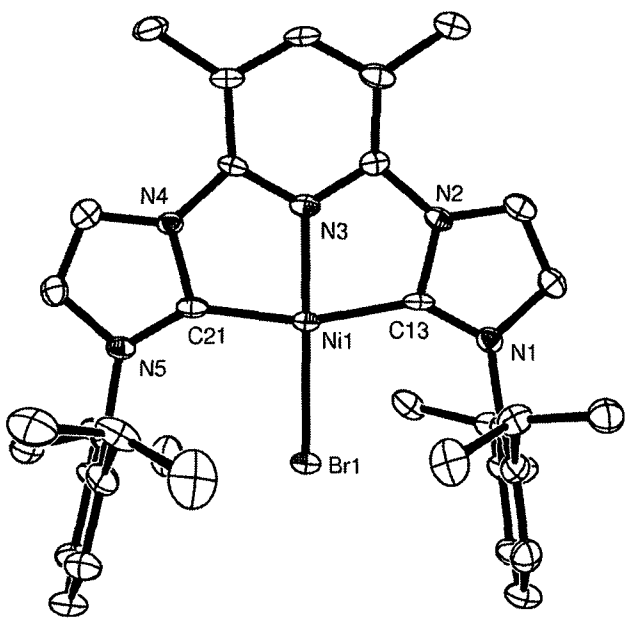

Figure 39: ORTEP representation of one of the cations of **95**. Thermal ellipsoids at 50% probability, H atoms and $Ag_2I_4^{2-}$ anion omitted for clarity.

C(13)–Ni(1)	1.911(8)
C(21)–Ni(1)	1.895(8)
Ni(1)–Br(1)	2.2761(11)
N(3)–Ni(1)	1.860(6)
I(1)–Ag(1)	2.5404(12)
I(2)–Ag(1)	2.6278(12)
C(13)–Ni(1)–C(21)	163.3(3)
N(3)–Ni(1)–Br(1)	178.99(19)
N(3)–Ni(1)–C(13)	81.1(3)
N(3)–Ni(1)–C(21)	82.2(3)
C(13)–Ni(1)–Br(1)	99.5(2)
C(21)–Ni(1)–Br(1)	97.2(2)
Ag(1)–I(2)–Ag(1a)	71.21(4)
I(1)–Ag(1)–I(2)	138.28(5)

Table 19: Representative bond lengths (Å) and angles (°) for compound **95**

Compound **95** contains the expected (CNC)NiBr distorted square planar cation, but contains a disilver tetraiodide dianion instead of the expected bromide anion. The stoichiometry of the compound is two nickel-containing cations to one dianion. The Ni–C_{NHC} bond lengths are identical within experimental error and are within the previously observed range of Ni–C_{NHC} bond lengths.

The dianion contains two Ag^+ cations in a distorted trigonal planar geometry and four I^- anions; two bridging between the Ag^+ cations and two terminal, hence each Ag^+ cation is bonded to three I^- anions. The Ag–I bond lengths are slightly shorter than in the $[Ag_6I_8]^{2-}$ dianion observed with compound **59**. The distortion away from ideal trigonal planar geometry of the Ag^+ cations can be seen from the angles around the Ag centre: the I–Ag–I angle is *ca.* 18° larger than the ideal 120° whilst the Ag–I–Ag angle is very small at 71.21(4)°. Elemental analysis is consistent with the empirical formula (CNC)NiBr(AgI_2).

Compound **95** was reacted with AgOTf in an attempt to synthesise an analogous octahedral complex to **88**. Upon addition of cold THF (–78 °C) to a mixture of **95** and AgOTf, a precipitate immediately formed. After stirring for 48 hours and filtration through Celite, a brown solution remained. This was crystallised by the slow diffusion of PE into a THF solution and colourless crystals were deposited. The molecule was diamagnetic indicating an octahedral nickel-containing compound had not been formed, but the ^1H and $^{13}C\{^1H\}$NMR spectra were almost identical to that of **59** (Scheme 47).

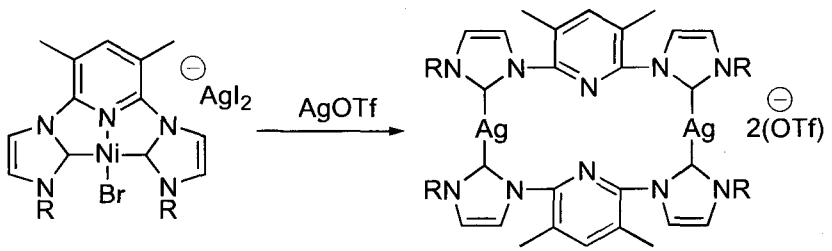

95: R = DiPP **96**: R = DiPP

Scheme 47: Reverse transmetallation from Ni to Ag

As with compound **59**, the colourless crystals decomposed slowly when removed from the solvent, but structural characterisation was possible (Figure 40).

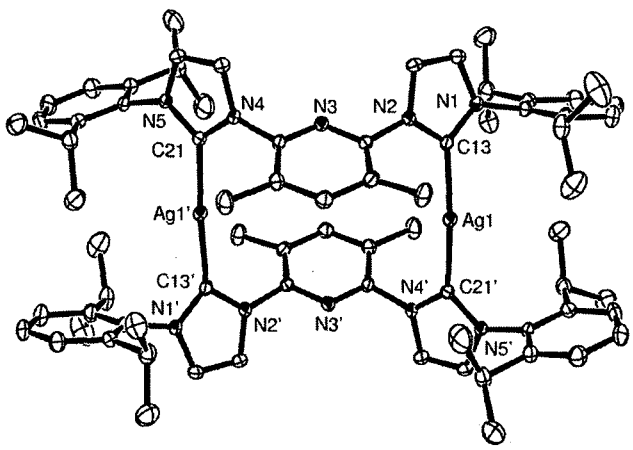

Figure 40: ORTEP representation of the cation of **96**. Thermal ellipsoids at 50% probability, H atoms and $^-$OTf anions omitted for clarity.

C(13)–Ag(1)	2.089(2)
C(21)–Ag(1')	2.094(2)
C(13)–Ag(1)–C(21')	173.42(9)
C(13)–Ag(1)	2.079(7)
C(21)–Ag(1')	2.082(7)
C(13)–Ag(1)–C(21')	177.0(3)

Table 20: Selected bond lengths (Å) and angles (°) for compound **96** (top) and compound **59** (bottom)

The geometry of the dication is almost exactly the same as that of **59**. The cation lies on an inversion centre in the unit cell and it also can be described as a mesocate. A comparison of the bond lengths and angles between **96** and **59** (Table 20) shows that the Ag–C_{NHC} bond lengths are identical within experimental error, but the C–Ag–C angle is slightly closer to 180° in complex **59**. Microanalysis is consistent with the reported structure.

Although transmetallation of NHCs from Ag to other transition metals is a widely used technique for NHC complex synthesis, the reverse process has not been previously observed. The review by Lin and Vasam[37] contains a few examples where transmetallation from Ag to other metals has failed. One particular case, reported by Herrmann *et al.*, states that the reason transmetallation to Pd(II) fails is due to the unusually strong Ag–C_{NHC} bond,[118] as measured by the chemical shift of the C_{NHC} resonance in the $^{13}C\{^1H\}$ NMR spectrum. The shifts of **59** and **96** are almost 190 ppm, which is *ca.* 10 ppm downfield from the literature average,[118] but still *ca.* 15 ppm upfield from those reported by Herrmann *et al.* Another example comes from Crabtree and co-workers who found that switching the counterion enabled the controlled formation of normal or abnormal carbenes bound to iridium.[119] In this case, it is possible that the excess Ag present in the reaction from the anion of **95** is having an effect on the reactivity.

In order to prevent the reverse transmetallation, all traces of silver were removed from the reaction. A new Ni(II) starting material was required, hence free ligand **58** was reacted with $NiBr_2$(DME) in THF. This resulted in the formation of an orange solution after 16 hours and after removal of solvents, complex **97** was isolated as an orange powder (Scheme 48).

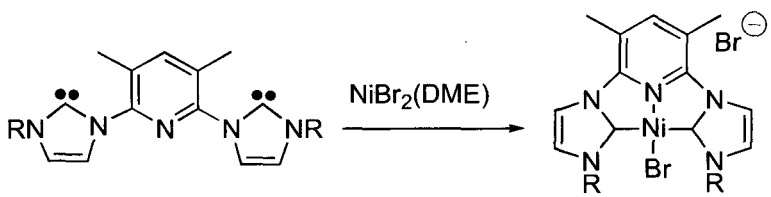

58: R = DiPP **97**: R = DiPP

Scheme 48: Synthesis of a silver-free Ni complex of ligand **58**

Microanalysis was consistent with the structure as drawn and, unlike complex **86**, the ^1H NMR spectrum of complex **97** exhibited all the expected resonances. The doublets at 1.05 and 1.19 ppm and the septet at 2.46 ppm are indicative of the ^{i}Pr groups and the

singlet at 2.89 ppm is from the methyl groups on the pyridine ring. The resonance due to the C_{NHC} was observed at 182.2 ppm in the $^{13}C\{^1H\}$ NMR spectrum. Although crystallisation did occur from the slow diffusion of Et_2O into a concentrated DCM solution, complex **97** was not structurally characterised.

The reaction of **97** with two equivalents of TlOTf was carried out in THF. After stirring for 16 hours, an orange solution with a white precipitate had formed (Scheme 49). After filtration through Celite and removal of solvents, crystallisation occurred from the slow diffusion of PE into a concentrated THF solution.

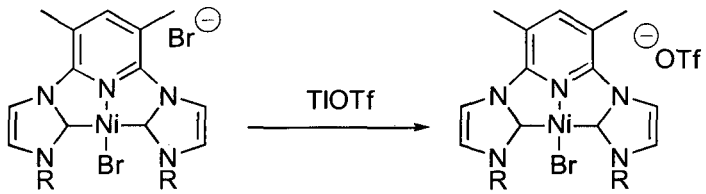

97: R = DiPP **98**: R = DiPP

Scheme 49: Attempted synthesis of an octahedral Ni(II) compound

Microanalysis was consistent with the expected [(CNC)NiBr][OTf] structure. Confirmation that only one bromide had been substituted came from an X-ray diffraction study on the orange crystals (Figure 41).

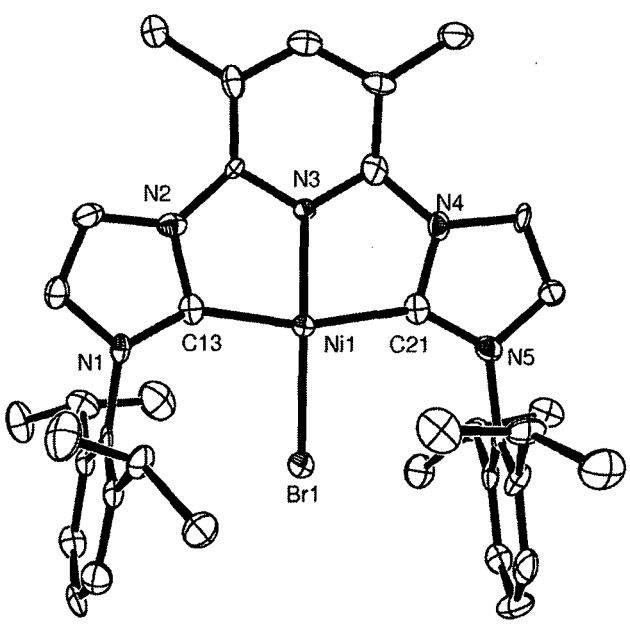

Figure 41: ORTEP representation of the cation of **98**. Thermal ellipsoids at 50% probability, H atoms and $^-$OTf anion omitted for clarity.

C(13)–Ni(1)	1.897(10)
C(21)–Ni(1)	1.901(9)
Ni(1)–Br(1)	2.2717(15)
N(3)–Ni(1)	1.877(7)
C(13)–Ni(1)–C(21)	163.2(4)
N(3)–Ni(1)–Br(1)	176.6(2)
N(3)–Ni(1)–C(13)	82.0(4)
N(3)–Ni(1)–C(21)	81.5(4)
C(13)–Ni(1)–Br(1)	98.0(3)
C(21)–Ni(1)–Br(1)	98.6(3)

Table 21: Selected bond lengths (Å) and angles (°) for compound **98**

As expected, complex **98** is a 4-coordinate, distorted square planar species with a $(CNC)NiBr^+$ cation and non-coordinating triflate anion. Within experimental error, the bond lengths of the cation are identical to the cation in **95**. The only difference between

the two cations is the N–Ni–Br angle: it is slightly closer to 180° in **95**. The Ni–C_{NHC} bond lengths are within the previously observed range of Ni(II)–C_{NHC} bond lengths.

The ^{1}H NMR spectrum of **98** contains the usual two doublets and septet assigned to the ^{i}Pr groups. It also contains a singlet at 2.78 ppm which is assigned to the methyl groups on the pyridine ring. The resonance for the C_{NHC} was not observed in the $^{13}C\{^{1}H\}$ NMR spectrum but in keeping with complex **95**, there is a resonance at 167.22 ppm which is assigned to a high-field aromatic quaternary carbon which could also be from the C_{NHC}.

4.5 - Summary

A Co(II) complex with ligand **58** has been synthesised and characterised. The oxidation of complex **82**, forming (CNC)CoI_3 and (CNC)$CoI(O_2)$ complexes, is analogous to the reactivity of the published compound **46**. An unusual magnetic moment was observed for **82**: a value of 2.95 B.M. corresponding to 2 unpaired electrons was almost half-way between the expected value of 1 or 3 unpaired electrons.

The reactivity of the first (CNC) pincer complex of nickel(II), complex **86**, has been explored. Although no Ni(0) complexes could be synthesised, substitution of one or both bromide anions in **82** could be accomplished by judicious choice of the halide abstractor. The formation of only the second octahedral Ni(II) species stabilised by NHCs was also accomplished.

(CNC) complexes of Ni(II) with ligand **58** were also synthesised. However, only the non-coordinating bromide anion could be substituted irrespective of the choice of halide abstractor. A novel reverse transmetallation reaction was also observed from the reaction of **95** with AgOTf to form a bis(ligand) bis(silver) bis(triflate) species analogous to compound **59**.

Finally, two novel ligand decomposition products have been observed. Substitution of one of the 'arms' of pincer ligand **36** has been noted with LiNHMes whilst the reaction of **36** with $NiMe_2$(TMEDA) results in complete decomposition of an NHC ring.

Chapter 5

Iron complexes

5.1 – Introduction

The first NHC pincer complex of Fe was reported in 2004 by Danopoulos *et al.*,[77] when aminolysis of $Fe(HMDS)_2$ with imidazolium salt **35a** led to the formation of complex **45** (Scheme 50). Gibson later reported the same compound, but *via* direct combination of $FeBr_2$ and ligand **36** in THF at –78 °C.[64]

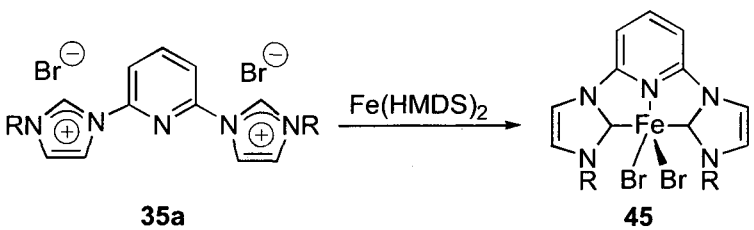

35a **45**

Scheme 50: Synthesis of the first (CNC)Fe complex, R = DiPP

Reduction of compound **45** with Na/Hg under 5 bar pressure of N_2 led to the formation of the Fe(0) bis(dinitrogen) complex **48** (Scheme 51).[79] The labile N_2 ligands could be substituted by CO, ethylene and phosphines. However, no studies towards X–H activation (X = C, Si) were carried out. C–H activation is important to convert cheap and readily available alkanes into synthetically useful reagents whereas Si–H activation may lead to the synthesis of novel hydrosilylation catalysts.[120]

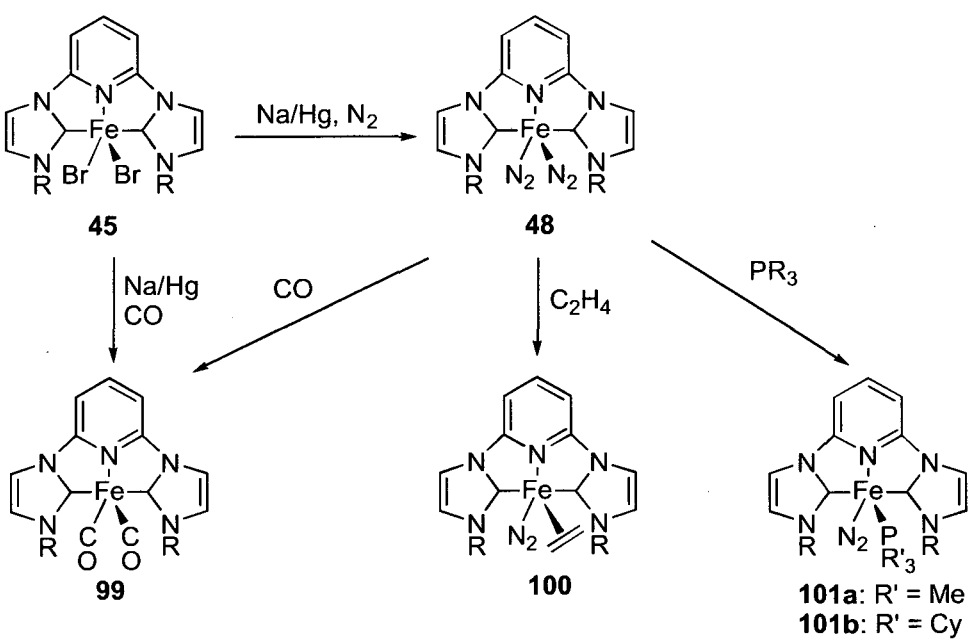

Scheme 51: Reactivity of the Fe(0) dinitrogen complex **48**, R = DiPP

5.2 – An electronic comparison of NHCs and trialkylphosphines

5.21 – Previously synthesised complexes

In addition to the Fe(0) dinitrogen complex **48** and dicarbonyl complex **99**, several other structurally characterised 'pincer' complexes of Fe(0) with convenient spectroscopic handles have been reported in the literature. The most well-studied is the bis(imine)pyridine (NNN) Fe(0) dinitrogen complex **104**,[120] which was also reacted with CO to form the bis(carbonyl) compound **105** (Scheme 52).

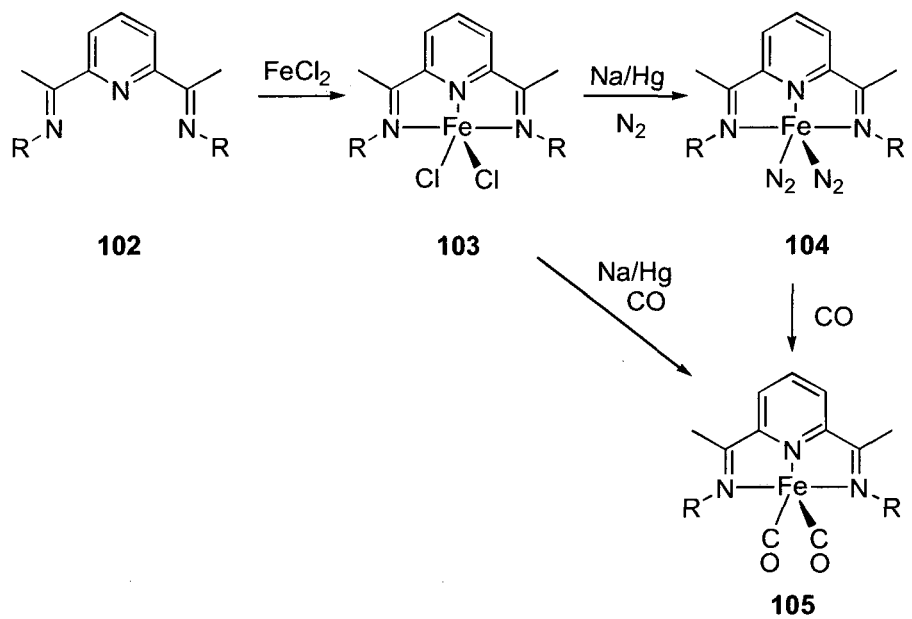

Scheme 52: Synthesis of (NNN) pincer complexes of Fe(0), R = DiPP

Although both aryl[108] and alkyl[121] bis(phosphine)pyridine (PNP)$FeCl_2$ complexes have been synthesised (**107**), none have been reduced to the corresponding bis(dinitrogen) complex. However, one bis(carbonyl) complex (**108**) was isolated and structurally characterised from the reduction of (PNP)$FeCl_2$ under 1 bar CO pressure (Scheme 53).[121]

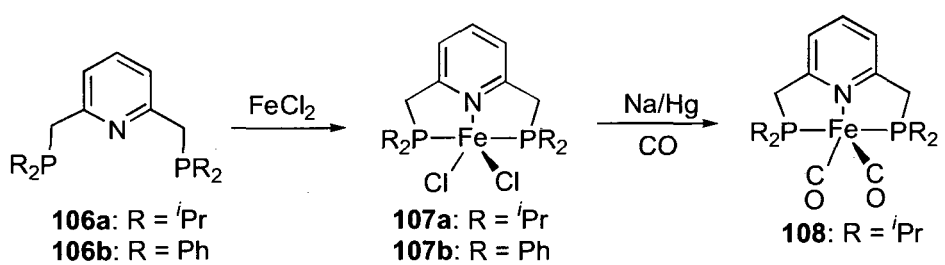

Scheme 53: Synthesis of (PNP)Fe complexes

Several comparisons between the σ-donating properties of NHCs and trialkylphosphine ligands have been drawn and all have concluded that NHCs are at least as good σ-donors as trialkylphosphines.[90] However, the υ(CO) of compound **108** (1794 and 1842 cm^{-1}) is lower than the υ(CO) of compound **99** (1865 and 1928 cm^{-1}), indicating that the (PNP) ligand is a better σ-donor than the (CNC) ligand. In order to investigate this apparent abnormality, Fe(0) dinitrogen and dicarbonyl complexes of ligands **58** and **60** were synthesised and analysed spectroscopically.

5.22 – Synthesis of novel (CNC) complexes

A new Fe(II) complex of ligand **58** was synthesised by following the published procedure[77] with imidazolium salt **56** instead of **35a** (Scheme 54). Reacting $Fe(HMDS)_2$ with imidazolium salt **56** in THF at –78 °C resulted in the formation of a purple solution, from which a purple powder could be isolated by removal of solvents.

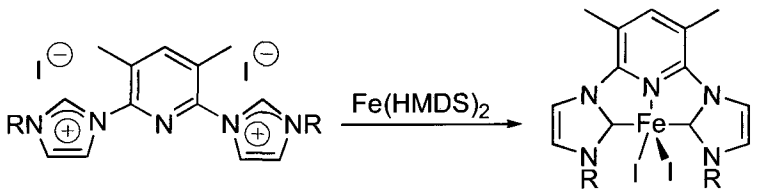

56 **109**

Scheme 54: Synthesis of a novel Fe complex, R = DiPP

Microanalysis was consistent with the expected formulation of $(CNC)FeI_2$. A magnetic susceptibility of 4.84 B.M. was measured for compound **109**, which is consistent with a high-spin Fe(II) centre containing 4 unpaired electrons. Crystallisation occurred from the slow diffusion of PE into a concentrated THF solution, enabling structural characterisation of **109** to be carried out (Figure 42).

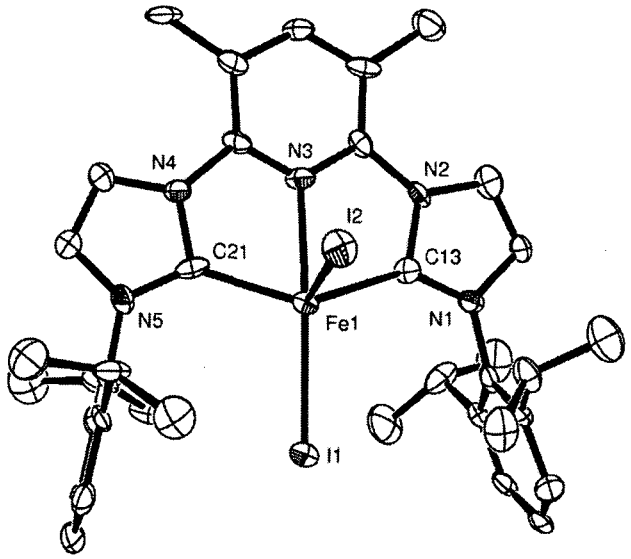

Figure 42: ORTEP representation of **109**. Thermal ellipsoids at 50% probability, H atoms omitted for clarity.

C(13)–Fe(1)	2.164(11)
C(21)–Fe(1)	2.134(11)
N(3)–Fe(1)	2.279(8)
Fe(1)–I(1)	2.6607(17)
Fe(1)–I(2)	2.7254(16)
C(21)–Fe(1)–C(13)	138.4(4)
C(13)–Fe(1)–N(3)	70.6(4)
C(13)–Fe(1)–I(1)	103.1(3)
N(3)–Fe(1)–I(2)	86.6(2)
I(1)–Fe(1)–I(2)	114.47(5)
N(3)–Fe(1)–I(1)	158.8(2)

Table 22: Selected bond lengths (Å) and angles (°) for compound **109**

Compound **109** has a 5-coordinate distorted square-based pyramidal structure. The τ value of 0.34 indicates severe distortion but the description of square-based pyramidal is still appropriate: I(2) is the apical iodide and I(1) is the basal iodide, as evidenced by the bond angles around the metal centre between I(2) and other coordinating atoms. The τ value is almost the same as that for complex **45** (0.33). The metal centre is out of the basal coordination plane by 0.442(4) Å in keeping with other 5-coordinate complexes of ligands **36** and **58**. The Fe–C_{NHC} bond lengths of 2.164(11) and 2.134(11) Å are within the range of previously observed Fe(II)–C_{NHC} bond lengths (see section 1.5).

In an attempt to synthesise a novel Fe(0) dinitrogen complex of ligand **58**, compound **109** was reduced using the method for compound **45** (Scheme 55).[79] After pressurising a Fischer-Porter bottle containing a THF solution of **109** above excess Na/Hg to 5 bar N_2 pressure, a green solution formed. The solution was decanted away from unreacted amalgam, concentrated to dryness, extracted into Et_2O and filtered through Celite. Removal of solvents afforded a green-brown powder.

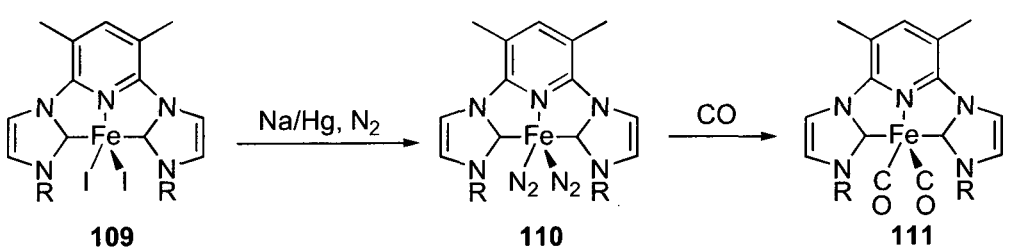

Scheme 55: Synthesis of a novel Fe(0) dinitrogen complex, R = DiPP

As expected for a 5-coordinate Fe(0) d^8 complex, **110** is diamagnetic. The ^{1}H NMR spectrum contains the expected two doublets and septet for the ^{i}Pr groups whilst the resonance assigned to the methyl groups on the pyridine ring is observed at 2.38 ppm. The C_{NHC} resonance is observed at 204.64 ppm in the $^{13}C\{^1H\}$ NMR spectrum, slightly downfield from the observed resonance in compound **48**.[79] Cooling the Et_2O solution to 4 °C resulted in the formation of green crystals which were structurally characterised (Figure 43).

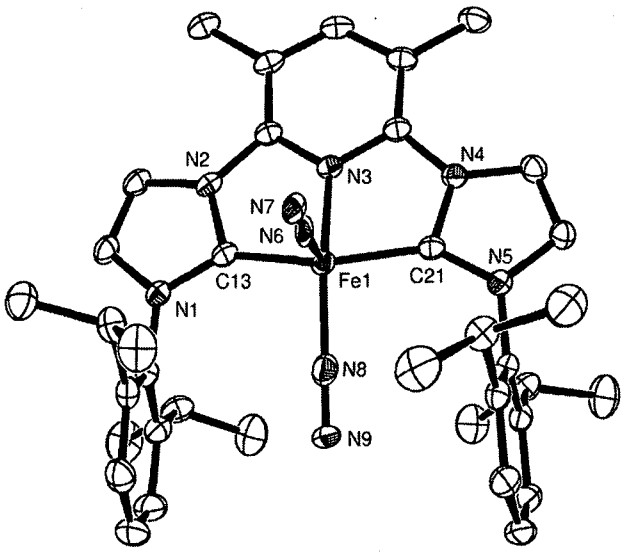

Figure 43: ORTEP representation of **110**. Thermal ellipsoids at 50% probability, H atoms and one Et_2O solvent molecule omitted for clarity.

C(13)–Fe(1)	1.9057(16)
C(21)–Fe(1)	1.9063(16)
N(3)–Fe(1)	1.9008(13)
Fe(1)–N(8)	1.8116(16)
Fe(1)–N(6)	1.912(2)
N(6)–N(7)	0.966(2)
N(8)–N(9)	1.124(2)
C(21)–Fe(1)–C(13)	154.61(7)
C(13)–Fe(1)–N(3)	79.24(6)
C(13)–Fe(1)–N(8)	97.18(7)
N(3)–Fe(1)–N(6)	103.10(6)
N(8)–Fe(1)–N(6)	101.10(6)
N(3)–Fe(1)–N(8)	155.80(6)

Table 23: Selected bond lengths (Å) and angles (°) for compound **110**

Compound **110** has a 5-coordinate square-based pyramidal structure. The τ value of 0.02 indicates that distortion away from ideal square-based pyramidal is minimal: this can be seen from the C–Fe–C and N(3)–Fe–N(8) bond angles around the metal centre [154.61(7)° and 155.80(6)° respectively], which are almost identical. The metal centre is out of the basal coordination plane by 0.3403(8) Å. The Fe–C_{NHC} bond lengths of 1.9063(16) and 1.9008(13) Å are within the previously observed range of Fe(0)–C_{NHC} bond lengths.

The basal N≡N bond length of 1.124(2) Å is slightly longer than the N≡N bond length of free N_2 (1.0968 Å); this is consistent with other examples of N_2 coordinated to transition metals. However, the apical N≡N distance of 0.966(2) Å is substantially shorter than the N≡N distance in free N_2. Whilst several examples of short N≡N bonds coordinated to transition metals have been observed in the literature, notably one of 0.744 Å for the complex [Cp*MoCl(PMe_3)(N_2)],[122] no explanation has yet been offered

for this apparent abnormality. However, the possibility that it is merely a crystallographic artefact cannot be ruled out.

The N≡N stretches in the IR spectrum are observed at 2107 and 2026 cm^{-1}, corresponding to the basal and apical N_2 molecules respectively. These are slightly lower (3–5 cm^{-1}) than the corresponding stretches for **48**, which is consistent with ligand **58** being a better σ-donor than **36** on account of the methyl groups on the pyridine ring. It also implies that the abnormally short N≡N bond length is merely a crystallographic artefact. Microanalysis is consistent with a (CNC)Fe formulation after loss of two N_2 molecules.

Stirring a THF solution of complex **109** over Na/Hg at 1 atm. pressure of N_2 led to the formation of a green solution of **110** after 4 hours. Attempts at reducing **109** under H_2 or Ar led to the formation of a red-brown solution which turned green upon exposure to N_2. It was thought that the red-brown solution was an unstable (CNC)Fe$(THF)_2$ species which reacted quickly with N_2 to form the stable complex **110**, however no spectroscopic data could be gathered to verify this theory.

The analogous dicarbonyl complex **111** was synthesised by bubbling CO through a PE/Et_2O solution of **110** for 15 minutes (Scheme 55). After concentration to *ca.* 10 mL, purple crystals were deposited which were structurally characterised (Figure 44).

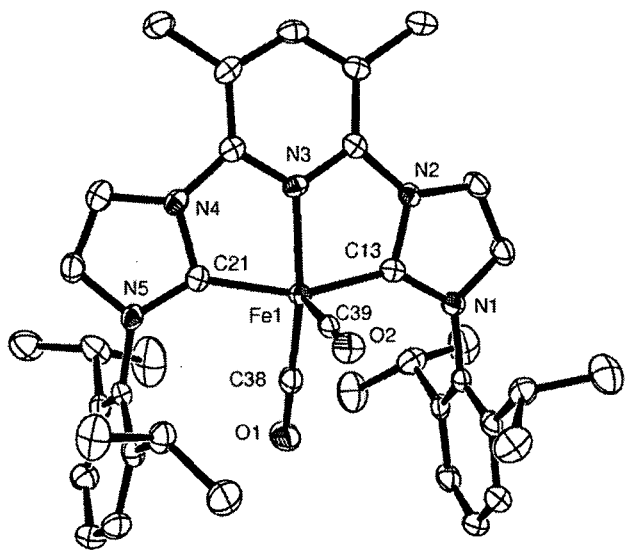

Figure 44: ORTEP representation of **111**. Thermal ellipsoids at 50% probability, H atoms omitted for clarity.

C(13)–Fe(1)	1.904(3)
C(21)–Fe(1)	1.901(3)
N(3)–Fe(1)	1.921(3)
C(38)–Fe(1)	1.766(4)
C(39)–Fe(1)	1.781(4)
C(38)–O(1)	1.154(4)
C(39)–O(2)	1.111(4)
C(21)–Fe(1)–C(13)	154.79(14)
C(13)–Fe(1)–N(3)	78.89(13)
C(38)–Fe(1)–C(13)	97.65(15)
C(38)–Fe(1)–N(3)	151.00(14)
C(39)–Fe(1)–N(3)	109.69(13)
C(38)–Fe(1)–C(39)	99.31(16)

Table 24: Selected bond lengths (Å) and angles (°) for compound **111**

Compound **111** is a 5-coordinate square-based pyramidal complex: the τ value of 0.06 indicates that distortion is slightly greater than that for **110** but it is still minimal. The metal centre is out of the basal coordination plane by 0.3682(17) Å. The Fe–C_{NHC} bond lengths are identical (within experimental error) to those in **110** and are within the previously observed range of Fe(0)–C_{NHC} bond lengths.

In a similar manner to complex **110**, the basal CO ligand has a bond length slightly elongated when compared to free CO [1.154(4) and 1.13 Å respectively]. However, the apical CO ligand has a bond length shorter than free CO of 1.111(4) Å. Whilst the disparity of 0.02 Å is much less than the disparity in **110** (*ca.* 0.13 Å), it provides evidence that this effect may be more than merely a crystallographic artefact. There are many structurally characterised examples of CO complexes of transition metals with a bond length shorter than free CO: these are termed "nonclassical carbonyl complexes".[123]

Complex **111** is also diamagnetic and the ^{1}H NMR spectrum contains all the expected ligand resonances. There are two doublets at 1.39 and 1.11 ppm and one septet at 3.10 ppm corresponding to the ^{i}Pr groups. The singlet at 2.31 ppm is assigned to the methyl groups on the pyridine ring. There are two resonances in the $^{13}C\{^1H\}$ NMR spectrum above 200 ppm (215.86 and 210.84 ppm); in keeping with the assignment for complex **99**,[79] the former is assigned to the carbonyl groups and the latter is assigned to the C_{NHC}. Presumably there is an equilibrium in solution between the apical and basal carbonyl groups hence only one resonance is observed.

There are two carbonyl stretches in the IR spectrum at 1925 and 1858 cm^{-1}, corresponding to the basal and apical CO ligands respectively. These are slightly lower (3–7 cm^{-1}) than the corresponding stretches for **99**, providing further evidence that ligand **58** is a better σ-donor than ligand **36**. The fact that no unusual carbonyl stretch is observed lends further credence to the idea that the abnormal CO bond distance is a crystallographic artefact, but it cannot be completely dismissed. The IR stretch also indicates that a "non-classical" carbonyl complex[123] has not been formed, although more evidence is needed to completely rule out the idea. Microanalysis was consistent with the observed structure.

5.23 – Synthesis of novel (PNP) complexes

An analogous Fe(II) complex of ligand **60** was synthesised by stirring **60** and $FeBr_2(THF)_{1.5}$ in ^{i}PrOH for 16 hours (Scheme 56).

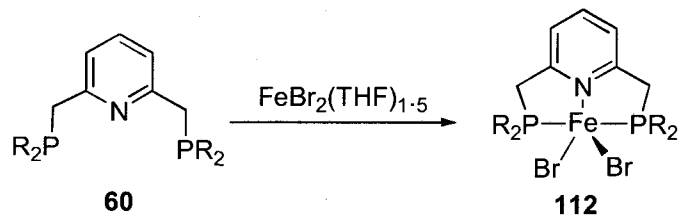

60 **112**

Scheme 56: Synthesis of a (PNP)$FeBr_2$ complex, R = ^{t}Bu

A yellow precipitate with a grey contaminant was isolated by filtration. The yellow solid was extracted into DCM, filtered and crystallised by the slow diffusion of Et_2O into the DCM solution. The grey solid proved to be pyrophoric and it was thought to be metallic iron, an impurity left over from the synthesis of $FeBr_2(THF)_{1.5}$. Structural characterisation was carried out on the yellow crystals (Figure 45).

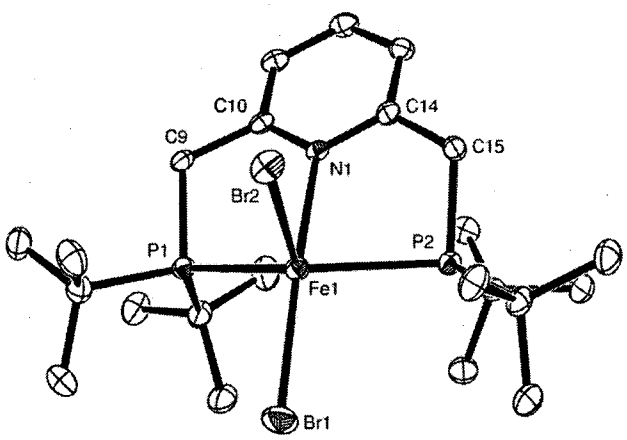

Figure 45: ORTEP representation of **112** showing one of two molecules in the asymmetric unit. Thermal ellipsoids at 50% probability, H atoms omitted for clarity.

P(1)–Fe(1)	2.5078(8)
P(2)–Fe(1)	2.5621(8)
N(1)–Fe(1)	2.309(2)
Fe(1)–Br(1)	2.4695(5)
Fe(1)–Br(2)	2.4923(5)
P(1)–Fe(1)–P(2)	132.17(3)
N(1)–Fe(1)–Br(1)	165.08(6)
Br(1)–Fe(1)–P(1)	96.01(2)
Br(2)–Fe(1)–P(1)	110.02(2)
Br(1)–Fe(1)–Br(2)	109.822(18)
N(1)–Fe(1)–P(2)	75.29(6)

Table 25: Representative bond lengths (Å) and angles (°) for compound **112**

Complex **112** is a 5-coordinate complex which is almost mid-way between trigonal bipyramidal and square-based pyramidal geometries, although the τ value of 0.55 indicates that it is slightly closer to trigonal bipyramidal. The range of Fe–P bond lengths [2.5019(8) – 2.5621(8) Å] is at the long end of the range of previously observed Fe(II)–P bond lengths [2.145(3) – 2.583(2) Å].[124, 125] Compound **112** is paramagnetic but has an unusually high magnetic moment of 6.09 B.M., corresponding to 5 unpaired

electrons. However, a HS Fe(II) d^6 molecule can only have a maximum of 4 unpaired electrons. One possible explanation is the presence of a small amount of metallic iron impurity in the sample. Microanalysis was consistent with the observed structure. Due to the undesired metallic iron contaminant, the analogous Fe(II) dichloride was synthesised directly from $FeCl_2$ and (PNP) ligand **60** (Scheme 57).

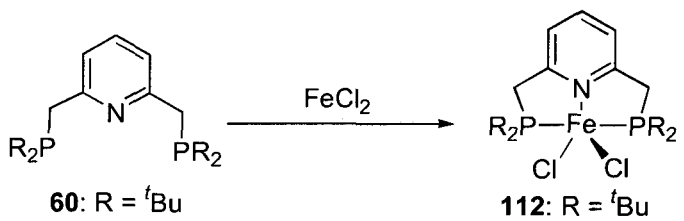

60: R = ^{t}Bu **112**: R = ^{t}Bu

Scheme 57: Synthesis of a (PNP)$FeCl_2$ complex

Similarly to the synthesis of **112**, after stirring **60** and $FeCl_2$ in ^{i}PrOH for 16 hours, a yellow solid was obtained which was recovered by filtration. No iron contaminant was observed and after drying *in vacuo*, elemental analysis was consistent with a (PNP)$FeCl_2$ formulation. Compound **113** was crystallised in the same manner as **112** and structural characterisation was carried out (Figure 46).

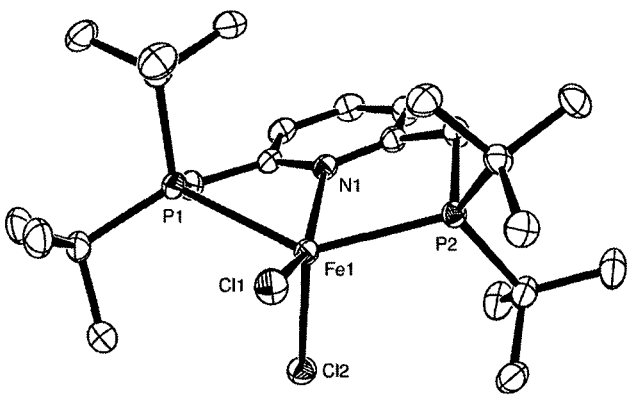

Figure 46: ORTEP representation of **113**. Thermal ellipsoids at 50% probability, H atoms omitted for clarity.

P(1)–Fe(1)	2.5210(4)
P(2)–Fe(1)	2.5176(4)
N(1)–Fe(1)	2.3249(12)
Fe(1)–Cl(1)	2.3817(4)
Fe(1)–Cl(2)	2.3056(4)
P(1)–Fe(1)–P(2)	139.811(15)
N(1)–Fe(1)–Cl(1)	154.05(3)
Cl(1)–Fe(1)–P(1)	93.436(15)
Cl(2)–Fe(1)–P(1)	104.692(15)
Cl(1)–Fe(1)–Cl(2)	107.524(16)
N(1)–Fe(1)–P(2)	77.16(3)

Table 26: Selected bond lengths (Å) and angles (°) for compound **113**

Complex **113** is a 5-coordinate complex and the τ value of 0.24 indicates that the geometry can be described as distorted square-based pyramidal. The Fe–P distances are within the same range as **112** and are consistent with previously observed Fe(II)–P bonds. There is a difference between the apical and basal Fe–Cl bonds (ca. 0.075 Å) which is *ca.* 3 times greater than the difference in **112**. The magnetic susceptibility is again unusually high (5.94 B.M.) corresponding to 5 unpaired electrons.

Attempts at reducing both complexes **112** and **113** to the corresponding Fe(0) bis(dinitrogen) complex **114** failed (Scheme 58). Both complexes were subjected to the same conditions as **45** and **109** but after decanting the supernatant from the unreacted amalgam, a colourless solution with a grey suspension was formed. The grey suspension was extremely pyrophoric and it was assumed to be finely divided iron particles. $^{31}P\{^{1}H\}$ NMR spectroscopy of the colourless solution revealed the presence of many phosphorus-containing compounds, but free ligand **60** was the major product.

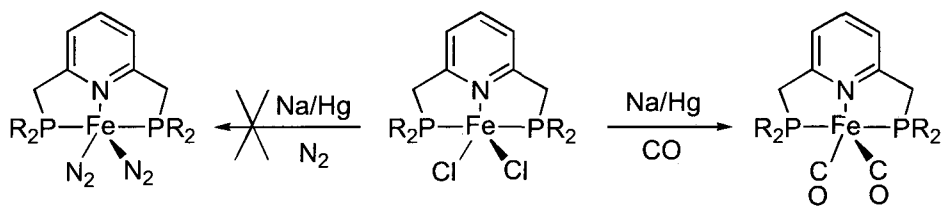

114 **113** **115**

Scheme 58: Synthesis of (PNP)Fe(0) complexes, R = ^{t}Bu

Chirik *et al.* also failed to synthesise a (PNP)Fe$(N_2)_2$ complex, obtaining instead an intractable mixture of iron-containing products and free (PNP) ligand similar to that described above.[121] However, isolation of an unstable Fe(II) dinitrogen complex was possible when the dichloride complex **107b** was reacted with $NaBEt_3H$, forming an Fe(II) dihydride containing one equivalent of molecular N_2.[121] Reduction of **107b** under 4 atm. pressure CO led to the formation of a red solid which was identified as complex **108** (Scheme 53).

When complex **112** or **113** was reduced by excess Na/Hg in the presence of 1 bar CO, using CO-saturated THF as solvent, a green-brown solution was obtained with no grey precipitate. After decanting the solution away from unreacted amalgam and evaporation of solvents, a green-brown solid was formed (Scheme 58). After extraction into PE and filtration through Celite, slow cooling of the PE solution to –35 °C led to the formation of green crystals.

The ^{1}H NMR spectrum of the green crystals contained the expected ligand resonances: a doublet at 1.14 ppm corresponding to the ^{t}Bu methyl groups and a doublet at 2.99 ppm corresponding to the methylene protons. Only one carbonyl resonance in the $^{13}C\{^{1}H\}$ NMR spectrum was observed at 204.68 ppm, substantially (*ca.* 10 ppm) downfield from (CNC)Fe$(CO)_2$ complexes **99** and **111**. The $^{31}P\{^{1}H\}$ NMR spectrum contains one resonance at 37.3 ppm, which is consistent with the resonance observed for titanium

complex **66** (35.9 ppm). Elemental analysis was consistent with a $(PNP)Fe(CO)_2$ formulation. Structural analysis confirmed the desired complex had been synthesised.

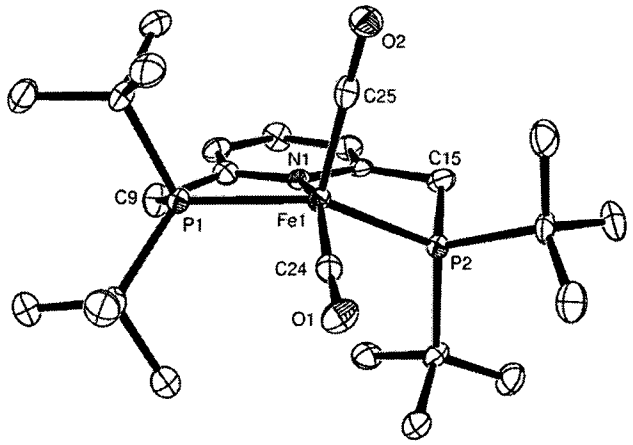

Figure 47: ORTEP representation of **115**. Thermal ellipsoids at 50% probability, H atoms omitted for clarity.

P(1)–Fe(1)	2.2369(10)
P(2)–Fe(1)	2.2096(10)
N(1)–Fe(1)	2.054(3)
C(24)–Fe(1)	1.721(4)
C(25)–Fe(1)	1.761(4)
C(24)–O(1)	1.180(4)
C(25)–O(2)	1.171(4)
P(2)–Fe(1)–P(1)	153.08(4)
N(1)–Fe(1)–P(1)	83.89(9)
C(24)–Fe(1)–P(1)	92.20(13)
C(24)–Fe(1)–N(1)	153.01(14)
C(25)–Fe(1)–N(1)	101.03(14)
C(24)–Fe(1)–C(25)	105.86(16)

Table 27: Selected bond lengths (Å) and angles (°) for compound **115**

Compound **115** is a 5-coordinate square-based pyramid. The τ value of 0.00 indicates that there is virtually no distortion away from ideal square-based pyramidal geometry: this is not accurate, as can be seen from the basal cis angles [N–Fe–P(1) and P(1)–Fe–C(24)] which are different. However, the two biggest angles at the metal centre [P–Fe–P and N–Fe–C(24)] are identical within experimental error, hence the "ideal" square-based pyramidal nature of **115**.

The Fe–P bond distances are substantially (*ca.* 0.2 Å) shorter than the distances in **112** and **113**, although they are longer than the Fe–P bond length in complex **108**. This is probably due to the sterics of the system: the bulky *tert*-butyl groups prevent the phosphine getting as close to the metal centre as the smaller ^{i}Pr groups. However, they are consistent with the previously observed range of Fe(0)–P bond distances [2.1364(13) – 2.393(1) Å].[126, 127] The $Fe–C_{CO}$ distances are consistent with the $Fe–C_{CO}$ distances in complex **111**. No shortening of the CO bond was observed, both the apical and basal CO bond lengths [1.180(4) and 1.171(4) Å respectively] are longer than free CO. The CO stretches in the IR spectrum (1847 and 1797 cm^{-1}) are consistent with the CO stretch for complex **108**.

5.24 – Comparison of the electronic properties of (CNC), (PNP) and (NNN) ligands

The novel Fe(0) compounds described above, along with compounds **48**, **99**, **104**, **105** and **108** which have previously been reported in the literature, can be divided into two classes on the basis of the coordinated diatomic ligand: N_2 complexes and CO complexes. Although the synthesis of (PNP)Fe$(N_2)_2$ complexes has not been accomplished, a comparison of (CNC) and (NNN) ligands can still be made using the dinitrogen complexes depicted in Figure 48.

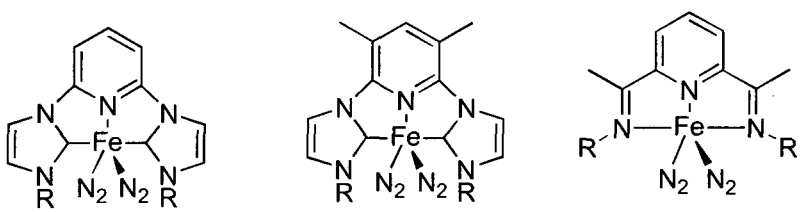

48 **110** **104**

Figure 48: The Fe(0) dinitrogen complexes being compared, R = DiPP

	(CNC)		(NNN)
Complex	**48**	**110**	**104**
$\nu(N_2)$ (basal) (cm^{-1})	2031	2026	2053
$\nu(N_2)$ (apical) (cm^{-1})	2109	2107	2124
(N≡N) (basal) (Å)	1.113(3)	1.124(2)	1.090(2)
(N≡N) (apical) (Å)	1.115(3)	0.966(2)	1.104(3)
Fe–N (basal) (Å)	1.820(2)	1.8116(16)	1.8341(16)
Fe–N (apical) (Å)	1.847(2)	1.912(2)	1.8800(19)

Table 28: Spectroscopic and structural data for dinitrogen complexes **48**, **110** and **104**

As the σ-donating ability of the pincer ligands increases the metal centre becomes more electron-rich, hence the degree of π-donation to the dinitrogen ligands increases. This is manifested in the IR stretch of the dinitrogen ligands: the lower the stretch in wavenumbers, the more electron-rich the metal centre. It is shown by the N≡N bond lengths: the longer the bond, the more electron-rich the metal centre. Finally, the length of the Fe–N bond provides another indication of how electron-rich the metal centre is: more electron-rich metal centres exhibit shorter Fe–N distances.[121]

From table 28, it is immediately obvious that the poorest σ-donating ligand is the (NNN) ligand **102**. The N_2 stretches for complex **104** occur at the highest wavenumbers

in the IR spectrum (when comparing basal N_2 ligands with basal N_2 ligands and *vice versa* for apical N_2 ligands). The N≡N bonds are the shortest of all three complexes, excluding the abnormal length in complex **110**. The Fe–N bond distances also indicate that the (NNN) ligand is the poorest σ-donor: the basal Fe–N distance is the longest of all three complexes and, barring the abnormally long Fe–N distance in **110**, the apical Fe–N distance is also the longest of all three complexes.

The best σ-donating ligand is the (CNC) ligand **58**. This is consistent with expectations: the methyl groups on the pyridine ring create a more electron-rich pyridine ring, hence there is greater σ-donation from the pyridine moiety to metal centres than there is in metal complexes of **36**. The N_2 stretches in the IR spectrum occur at the lowest wavenumbers of all three complexes when comparing ligands in the same position. The basal N≡N distance is the longest of all three complexes and the basal Fe–N distance is the shortest of all three complexes.

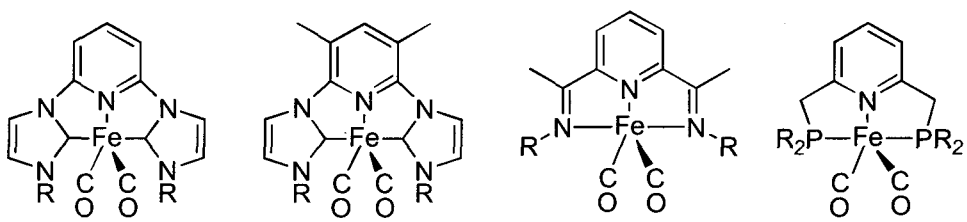

Figure 49: The Fe(0) dicarbonyl complexes being compared

	(CNC)		(PNP)		(NNN)
Complex	**99**	**111**	**115**	**108**	**105**
ν(CO) (basal) (cm^{-1})	1865	1858	1797	1794	1894
ν(CO) (apical) (cm^{-1})	1928	1925	1847	1842	1950
(C≡O) (basal) (Å)	1.165(4)	1.154(4)	1.180(4)	1.1734(11)*	1.147(2)*
(C≡O) (apical) (Å)	1.161(4)	1.111(4)	1.171(4)		
Fe–C_{CO} (basal) (Å)	1.746(3)	1.766(4)	1.721(4)	1.7325(9)*	1.7809(19)
Fe–C_{CO} (apical) (Å)	1.767(4)	1.781(4)	1.761(4)		1.7823(19)
$^{13}C\{^{1}H\}$ CO (ppm)	215.57	215.86	204.68	223.07	*

Table 29: Spectroscopic and structural data for carbonyl complexes **99**, **111**, **115**, **108** and **105**. Entries marked with an asterisk are incomplete literature data.

The same criteria can be used to compare the carbonyl complexes displayed in Figure 49. Better σ-donating ligands result in the metal centre becoming more electron rich,

therefore the CO stretch in the IR occurs at lower wavenumbers, the CO bond lengthens and the Fe–C_{CO} bond shortens.

As expected, the (NNN) ligand is still the poorest σ-donor. The CO stretches occur at the highest wavenumbers (when comparing like for like stretches) and the CO bond length is the shortest of all the reported CO lengths. The Fe–C distances are also the longest of all the reported distances.

The IR data indicates that (CNC) ligand **58** is still a better σ-donor than ligand **36** because the CO stretches occur at slightly lower wavenumbers. However, the crystallographic data appears to indicate otherwise: even discounting the abnormally short apical CO bond in **111**, the basal CO bond appears to be shorter than the basal bond in **99**, indicating that it is a poorer σ-donor. However, within experimental error, the bond lengths are the same so strong conclusions cannot be drawn from the data.

The IR data for the (PNP) complexes indicates that complex **108** is a stronger σ-donor than complex **115**. This is slightly surprising given that **115** contains two P^tBu_2 groups whereas **108** contains two P^iPr_2 groups. The crystallographic data does indicate that **115** is the stronger σ-donor, due to the longer CO bond and shorter Fe–C_{CO} bond, but only one CO and Fe–C_{CO} bond length is available. However, this is due to the molecule lying on a C_2 axis within the unit cell.

Due to the fact that the IR and crystallographic data for the new (CNC)$Fe(CO)_2$ complex **111** is similar to the published complex **99**, and the same being true of **115** and **108**, the apparent abnormality of the (PNP) ligand being a better σ-donor than the (CNC) ligand is confirmed. The CO stretches of both **115** and **108** occur at significantly lower wavenumbers than the CO stretches of **99** and **111**. The CO bond lengths are also longer and the Fe–C_{CO} bond lengths are shorter.

Currently, no explanation can be offered for this abnormality. It is not merely a consequence of the NHC and PR_3 moieties being part of a chelating ligand: complexes of Ti(IV) with ligands **36**, **58** and **60** indicated that the (PNP) ligand was a worse σ-donor than the (CNC) ligands, in line with literature expectations (see section 3.2). Much more work with (CNC) and (PNP) ligands is needed in order to satisfactorily explain this phenomenon.

5.25 – Synthesis of Fe(0) isocyanide complexes

It was hoped that the C=N bond of coordinated isocyanides would be another spectroscopic handle to enable a comparison of the σ-donor abilities of ligands **36**, **58** and **60**. However, due to the inability to synthesise a dinitrogen complex of **60**, no Fe(0) (PNP) complex of isocyanides could be synthesised. However, one isocyanide complex with ligand **36** was synthesised: reaction of **48** with 2 equivalents of 2,6-xylyl isocyanide led to the formation of a brown solution from which brown crystals could be isolated at –35 °C (Scheme 59).

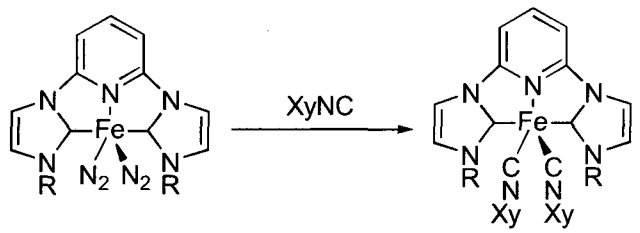

48 **116**

Scheme 59: Formation of an Fe(0) isocyanide complex, R = DiPP

Compound **116** exhibited two IR stretches at 1901 and 1837 cm^{-1} corresponding to the C=N bond. It was also diamagnetic and the ^{1}H NMR spectrum contained the expected resonances for ligand **36**: two doublets at 1.14 and 1.34 ppm and a septet at 3.30 ppm. A singlet integrating to 12H was also observed at 2.05 ppm which was assigned to the methyl groups on the isocyanide. Two resonances above 200 ppm in the $^{13}C\{^{1}H\}$ NMR spectrum were observed, one at 208.6 and one at 203.6. These were assigned to the C_{NHC} and the isocyanide respectively. Structural characterisation of **116** was also carried out (Figure 50).

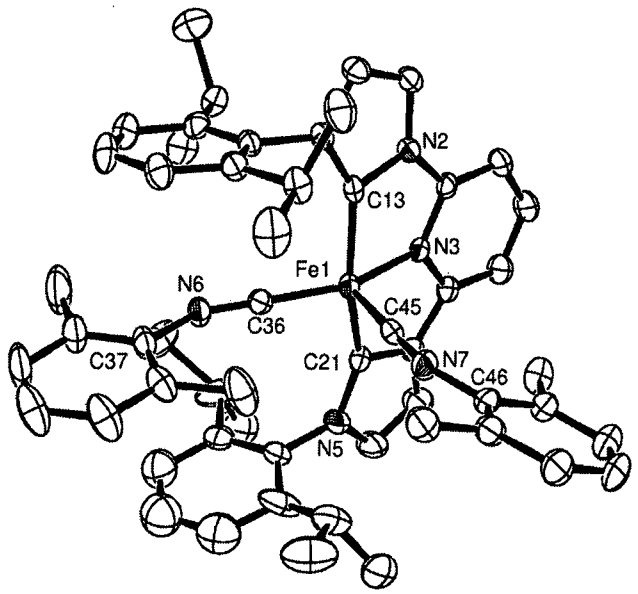

Figure 50: ORTEP representation of **116**. Thermal ellipsoids at 50% probability, H atoms omitted for clarity.

Fe(1)–C(13)	1.918(3)
Fe(1)–C(21)	1.918(3)
Fe(1)–N(3)	1.909(3)
Fe(1)–C(36)	1.798(3)
Fe(1)–C(45)	1.796(3)
N(6)–C(36)	1.204(4)
N(7)–C(45)	1.198(4)
C(21)–Fe(1)–C(13)	155.16(13)
N(3)–Fe(1)–C(13)	78.49(12)
C(36)–Fe(1)–N(3)	154.69(12)
C(45)–Fe(1)–N(3)	104.35(12)
C(45)–Fe(1)–C(13)	100.41(14)
C(45)–Fe(1)–C(36)	100.97(14)

Table 30: Selected bond lengths (Å) and angles (°) for compound **116**

Compound **116** is a 5-coordinate square-based pyramidal species with a τ value of 0.01 indicating virtually no distortion. However, as with complex **115**, the basal *cis* angles indicate that compound **116** does not adopt an ideal square-based pyramidal geometry. The Fe centre is 0.3278(15) Å out of the basal coordination plane.

The Fe–C_{NHC} bond distances of 1.918(3) Å are within the range of previously observed Fe(0)–C_{NHC} bond lengths. Interestingly, the Fe–C_{CN} bond lengths are almost 0.1 Å shorter than the Fe–C_{NHC} bond lengths. The Fe–C_{CN} bond lengths are consistent with the previously observed range of Fe(0)–C_{CN} bond lengths [1.770(3) – 1.831(6) Å].[128] Microanalysis was consistent with the observed structure.

5.3 – Oxidative transformations of Fe(0) bis(dinitrogen) complexes

5.31 – Reactivity towards CO_2

The activation of CO_2 is one of the most important reactions currently being studied, mainly for the environmental benefits but also for the possibility of using CO_2 as a feedstock for chemicals derived from petroleum.[129] It was thought that the labile N_2 ligands in complex **48** would allow access to the reactive "(CNC)Fe" fragment, hopefully enabling the activation of CO_2. Compound **45** was dissolved in THF and reduced over Na/Hg. The THF solution of **48** was decanted from the amalgam and without further purification, one pellet of solid CO_2 was added to the THF solution. After stirring for 16 hours, a brown solution had formed from which a brown solid was isolated. The crystals were paramagnetic, with a magnetic moment of 4.79 B.M. corresponding to 4 unpaired electrons. This implied a d^6, Fe(II) centre had been formed. Crystallisation occurred by cooling an Et_2O solution to –35 °C and structural characterisation was possible (Figure 51).

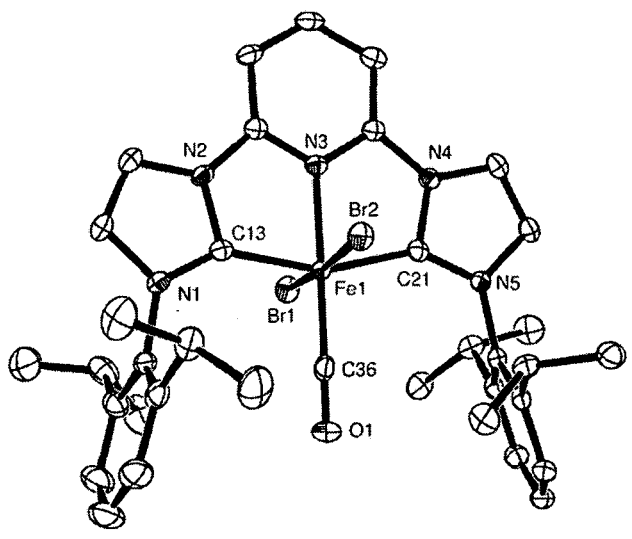

Figure 51: ORTEP representation of **117**. Thermal ellipsoids at 50% probability, H atoms and one DCM solvent molecule omitted for clarity.

C(13)–Fe(1)	1.958(2)
C(21)–Fe(1)	1.955(2)
N(3)–Fe(1)	1.9427(19)
C(36)–Fe(1)	1.765(2)
Fe(1)–Br(1)	2.4557(4)
Fe(1)–Br(2)	2.4626(4)
C(36)–O(1)	1.144(3)
C(21)–Fe(1)–C(13)	158.97(9)
C(36)–Fe(1)–N(3)	178.11(10)
Br(1)–Fe(1)–Br(2)	174.928(16)
N(3)–Fe(1)–C(13)	79.38(9)
C(21)–Fe(1)–Br(1)	90.17(7)
C(36)–Fe(1)–Br(2)	95.67(8)

Table 31: Selected bond lengths (Å) and angles (°) for compound **117**

Compound **117** is a 6-coordinate distorted octahedral species with one CNC ligand, two bromides and one CO ligand completing the coordination sphere. The octahedral geometry is consistent with the magnetic moment and indicates the presence of a high spin d^6 Fe(II) metal centre. The Fe–C_{NHC} bond lengths are within the previously

observed range of Fe(II)–C_{NHC} bond lengths. The CO bond length of 1.144(3) Å indicates the metal centre is slightly less electron rich than the Fe(0) complex **105**. However, the IR stretch of 1975 cm^{-1} occurs at a higher wavenumber than any of the Fe(0) dicarbonyl complexes described above (section 5.24) indicating that, as expected, the Fe(II) metal centre is much less electron rich than any of the Fe(0) metal centres.

The bromide anions in complex **117** come from NaBr dissolved in the freshly reduced THF solution of **48**. The CO can only come from reduction of CO_2, leaving two Na^+ cations and one O^{2-} anion unaccounted for. Whilst formation of Na_2O is highly likely, in the presence of excess CO_2 it is more likely that Na_2CO_3 is the actual byproduct. Unfortunately no inorganic products could be quantified from the reaction. Compound **117** was also synthesised systematically by bubbling CO through a THF solution of **45**.

A similar reaction using excess CS_2 instead of CO_2 resulted in the formation of a brown solution, but microanalysis of the resulting paramagnetic brown solid was inconsistent with a (CNC)$FeBr_2$(CS) formulation.

5.32 – C–H activation

Achieving the reliable C–H activation of organic substrates was one of the main aims of this project. Similarly to the reaction with CO_2, it was thought that the labile N_2 ligands would allow access to a reactive "(CNC)Fe" fragment which would accomplish C–H activation of simple organic substrates.

When benzaldehyde anilide was added to a solution of **48** in THF and photolysed with 254 nm UV light, a colour change from green to dark blue was observed along with the evolution of gas (Scheme 60). After removal of solvents and extraction into PE, dark crystals were deposited at –35 °C.

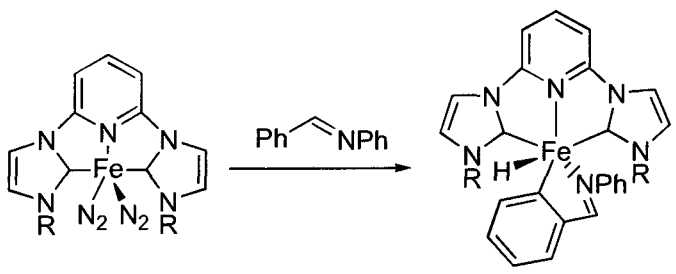

48 **118**

Scheme 60: C-H activation of benzaldehyde anilide, R = DiPP

The ^{1}H NMR spectrum of the product was complicated, with several resonances corresponding to the ^{i}Pr groups and a large number of aromatic peaks. Two septets, each integrating to 2H, were observed along with three doublets in a 1:1:2 ratio. A singlet at 8.24 ppm was observed corresponding to the imine CH, implying that C–H activation had not taken place at that position. A singlet at -14.14 ppm was observed which was assigned to the iron hydride. Structural characterisation was carried out (Figure 52).

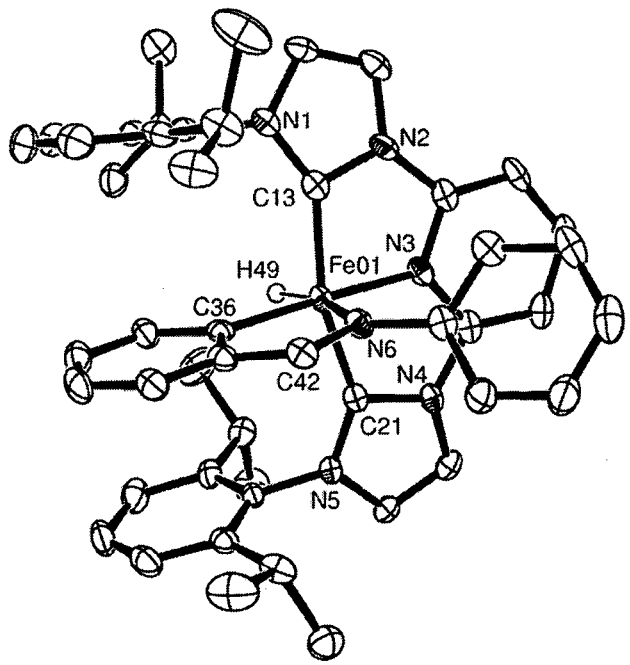

Figure 52: ORTEP representation of **118** showing one of two molecules in the asymmetric unit. Thermal ellipsoids at 50% probability, H atoms (bar H49) omitted for clarity.

C(13)–Fe(01)	1.890(3)
C(21)–Fe(01)	1.907(3)
N(3)–Fe(01)	1.903(2)
C(36)–Fe(01)	1.944(3)
Fe(01)–N(6)	2.036(2)
Fe(01)–H(49)	1.47(3)
C(21)–Fe(01)–C(13)	154.68(12)
C(36)–Fe(01)–N(3)	176.35(10)
N(6)–Fe(01)–H(49)	163.6(10)
N(3)–Fe(01)–C(13)	79.50(11)
C(21)–Fe(01)–H(49)	86.1(10)
C(36)–Fe(01)–N(6)	81.14(10)

Table 32: Selected bond lengths (Å) and angles (°) for compound **118**

Complex **118** is a distorted octahedral species with one (CNC) ligand, one hydride, one imine and one phenyl ring making up the coordination sphere. The hydride next to the Fe centre was located in the difference map. The distortion is evident from the *trans* angles around the metal centre with only one above 170°. The phenyl ring and hydride are *cis* to each other and the imine coordinates to the metal centre forming a 5-membered metallacyclic ring. The Fe–C_{NHC} bond lengths are the shortest Fe(II)–C_{NHC} bonds observed. The Fe–N_{py} distance is significantly shorter (ca. 0.1 Å) than the Fe–N_{imine} distance, which is a result of the constraints of the chelating ligand. The C(36)–Fe–N(6) angle of 81.14(10)° is slightly larger than the ideal angle for a 5-membered ring of 72°.

The observed structure accounts for the loss of symmetry in complex **118**: the normally equivalent methine protons from the DiPP substituents are now in two environments. There are two methine protons on the hydride side of the molecule and two on the imine side of the molecule. This also explains the ^{i}Pr methyl groups splitting into four doublets: on the hydride side, there are two methyl groups facing away from the C–H activated phenyl ring and two methyl groups facing towards the phenyl ring, which is repeated on the imine side giving rise to four environments. Overlapping doublets accounts for the observed ratio. There are also two resonances over 200 ppm in the $^{13}C\{^{1}H\}$ NMR spectrum (225.1 and 214.5 ppm), which are assigned to the C–H activated phenyl ring and the C_{NHC} respectively. Microanalysis is consistent with the observed structure.

The addition of other unsaturated organic substrates to a solution of **48** in THF (*e.g.* benzophenone imine, 2-vinylpyridine, acetophenone, diallyl ether) all resulted in a colour change to dark brown, accompanied by the evolution of gas. Photolysis was unnecessary, however the substrates had to be stirred for at least 16 hours to complete the reaction. After concentration to dryness and extraction into Et_2O, cooling the Et_2O solution to 5 °C resulted in the deposition of brown crystals. Structural characterisation revealed the same product was formed in each case (Figure 53).

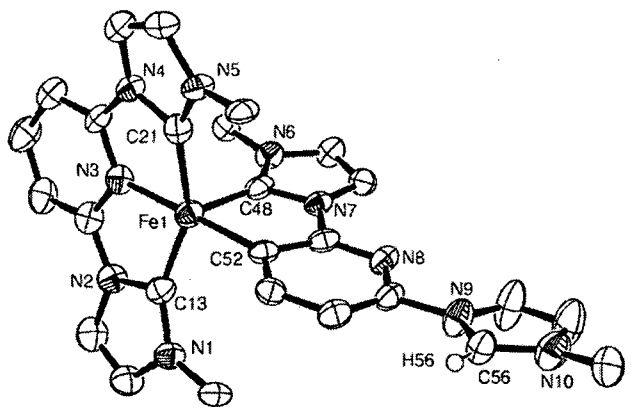

Figure 53: ORTEP representation of **119**. Thermal ellipsoids at 50% probability, H atoms (bar H56) and DiPP groups (bar ipso carbons) omitted for clarity.

C(13)–Fe(1)	1.908(4)
C(21)–Fe(1)	1.906(5)
N(3)–Fe(1)	1.909(4)
C(48)–Fe(1)	1.966(5)
C(52)–Fe(1)	1.979(4)
C(21)–Fe(1)–C(13)	154.73(19)
N(3)-Fe(1)-C(52)	178.55(17)
C(48)-Fe(1)-C(52)	81.13(18)
C(13)-Fe(1)-N(3)	79.72(17)
C(13)-Fe(1)-C(48)	100.86(18)

Table 33: Selected bond lengths (Å) and angles (°) for compound **119**

Compound **119** is a 5-coordinate zwitterionic complex containing two (CNC) ligands: one is coordinated to the metal in the usual manner and the other is coordinated through one NHC ligand and one C–H activated pyridine ring. The other NHC ring has gained a

proton from the C–H activation process and become protonated, forming an imidazolium salt. The τ value of 0.40 indicates that severely distorted square-based pyramidal is the most appropriate description of the compound. The proton attached to C56 was added as an idealised aromatic proton but it was located in the difference map. Although C–H activation of the pyridine ring has taken place, the oxidation state of the metal centre is still Fe(0) and the overall complex is neutral due to the imidazolium ring being positively charged.

The Fe–C_{NHC} bond lengths are within the range of previously observed Fe(0)–C_{NHC} bond lengths. There is a notable difference between the Fe–C_{NHC} bond lengths arising from the tridentate (CNC) ligand (*ca.* 1.907 Å) and the Fe–C_{NHC} bond length from the bidentate ligand [1.966(5) Å]. The Fe–C_{NHC} and Fe–C_{py} bond lengths from the bidentate ligand are identical within experimental error.

All attempts at obtaining NMR spectra of complex **119** failed, usually due to paramagnetic impurities in the sample which broadened the resonances. However, complex **119** is not paramagnetic: no magnetic moment was detected using a Guoy balance or by using the Evans method. Microanalysis is consistent with the $(CNC)_2Fe$ formulation.

Due to the unwanted ligand decomposition, C–H activation with dinitrogen complex **110** was attempted. Although a colour change from green to dark brown was observed when organic substrates were added to THF solutions of **110**, no pure product could be isolated. All solids were contaminated by small amounts of paramagnetic impurity and crystallisation was not possible, hence the identity of the products remains unknown.

5.33 – Attempted synthesis of alkyl and aryl Fe(II) complexes

The C–X activation (X = halogen) to form Fe(II) alkyl or aryl halide complexes was attempted with complex **110**. Reaction of a THF solution of **110** with DCM or PhI led to the formation of brown solutions (Scheme 61).

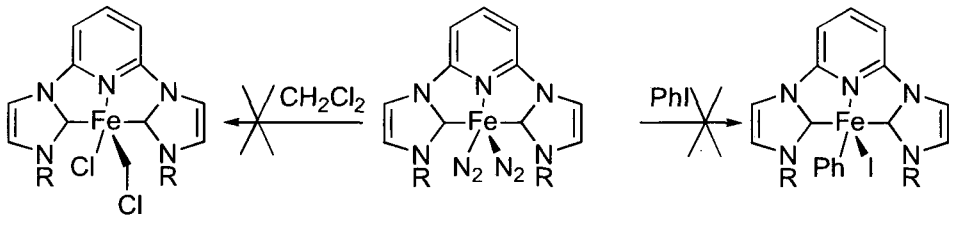

120 **48** **121**

Scheme 61: Attempted formation of Fe(II) alkyl and aryl complexes, R = DiPP

However, despite the fact that microcrystalline deposits were obtained in each case, no structural characterisation was possible and elemental analysis was inconsistent with the expected product.

Attempts at alkylating **45**, **109** and **113** with MeLi, MeMgBr or $AlMe_3$ all failed, with intractable mixtures the only products. In an attempt to synthesise Fe(II) alkyls, THF solutions of ligands **36** and **113** were added to a solution of $FeNp_2(py)_2$ (Np = neopentyl). An intractable mixture was the only product with (PNP) ligand **113**, but a red solution was obtained with ligand **36**. Removal of solvents led to the formation of a paramagnetic red solid which was not crystallised. However, elemental analysis was not consistent with a $(CNC)FeNp_2$ formulation.

Complexes of Fe in oxidation state –2 have been reported in the literature by adding alkali metals to complexes of Fe(0).[130] THF solutions of **48** were added to Li sand in the presence of TMEDA, Na/Hg in the presence of 15-crown-5 and C_8K in the presence of 18-crown-6. However, in each case, no reduced product was obtained and crystals of the starting material were recovered.

Attempts to synthesise Fe=O and Fe=NAr complexes of ligand **36** did not result in the isolation of pure products. Addition of excess NMO (or mesityl azide, with photolysis of the resulting solution) to a THF solution of **48** resulted in a colour change from green to red-brown. However, after removal of solvents, the red-brown solids obtained were paramagnetic. Despite repeated attempts, crystallisation of either product was not possible.

5.4 – The reactivity towards Si–H bonds

5.41 – Background

One of the applications of the (NNN)Fe(N_2)$_2$ dinitrogen complex reported by Chirik *et al.* was the catalytic hydrosilylation of olefins.[120] Upon reaction with phenylsilane, two equivalents of $PhSiH_3$ displaced the dinitrogen ligands, forming a bis(η^2–phenylsilane) Fe(0) complex (Scheme 62). Although it was not possible to synthesise a (PNP)Fe(N_2)$_2$ complex, the (PNP)FeH_2(N_2) complex **123** could be reacted with $PhSiH_3$ to give an iron silyl species stabilised by the (PNP) ligand (**124**, Scheme 62).

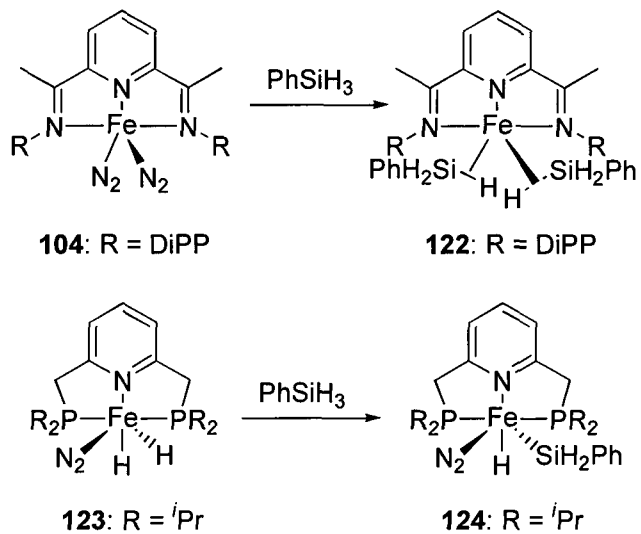

Scheme 62: Synthesis of (NNN) and (PNP) Fe silane and silyl complexes

5.42 – Reactivity with $PhSiH_3$

An excess of $PhSiH_3$ was added dropwise to a freshly synthesised THF solution of **48**. The solution immediately changed from green to orange and after removal of solvents, an orange solid remained. After extraction into PhMe, the solution was filtered through Celite and cooled to –35 °C where orange crystals were deposited.

The ^{1}H NMR spectrum contains many aromatic resonances and also the expected resonances for the ligand, notably two doublets at 1.42 and 1.01 ppm and one septet at 3.44 ppm corresponding to the ^{i}Pr groups. Two resonances for Si–H protons are found at 4.97 (2H) and 4.62 (4H) ppm. The signal at –12.03 ppm integrating to 1H is

indicative of an iron hydride. The $^{13}C\{^1H\}$ NMR spectrum contains many aromatic resonances, but the resonance at 211.9 ppm is assigned to the C_{NHC}. The $^{29}Si\{^1H\}$ NMR spectrum contains two resonances at –1.18 and –19.35 ppm. Compound **125** was also structurally characterised (Figure 54).

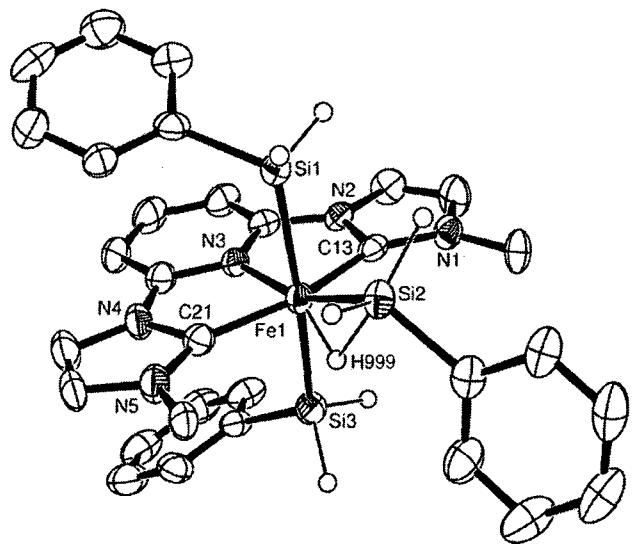

Figure 54: ORTEP representation of **125**. Thermal ellipsoids at 50% probability, H atoms (bar protons attached to heteroatoms) omitted for clarity.

C(13)–Fe(1)	1.965(5)
C(21)–Fe(1)	1.958(5)
N(3)–Fe(1)	1.914(3)
Fe(1)–Si(1)	2.391(3)
Fe(1)–Si(2)	2.3389(18)
Fe(1)–Si(3)	2.369(3)
Fe(1)–H(999)	1.29(5)
C(21)–Fe(1)–C(13)	160.36(17)
N(3)–Fe(1)–Si(2)	160.20(11)
Si(3)–Fe(1)–Si(1)	169.83(5)
N(3)–Fe(1)–H(999)	144(2)
Si(3)–Fe(1)–H(999)	60(2)
N(3)–Fe(1)–C(13)	80.60(17)

Table 34: Selected bond lengths (Å) and angles (°) for compound **125**

Complex **125** contains two mutually *trans* phenylsilyl groups, one (CNC) ligand and one "$PhSiH_3$" moiety which can be described as either η^2-phenylsilane or phenylsilyl hydride depending on the oxidation state of the Fe centre. The Si(2)–H(999) bond distance of 1.92(5) Å is significantly longer than the range of other Si–H bonds [1.38(4) – 1.49(4) Å] but elongation of Si–H bonds upon coordination to a metal in η^2 fashion is not uncommon.[120] The Fe–C_{NHC} bond lengths are in the range previously observed for Fe(II)–C_{NHC} bonds but no structurally characterised Fe(IV)–C_{NHC} bonds have been reported. The Fe–H distance is equal to the Fe–H distance in complex **118**, within experimental error. Microanalysis is consistent with the observed structure.

The two Si–H resonances in the ^1H NMR spectrum are assigned to the two silicon environments: the mutually *trans* silyl groups contain 4 protons and the silicon atom trans to the N_{py} is bonded to two protons. It is obvious that the resonance at –12.03 ppm corresponds to H(999). The two resonances in the $^{29}Si\{^1H\}$ NMR spectrum are also indicative of two different silicon environments: the signal at –1.18 ppm is assigned to Si(2) and the signal at –19.35 ppm is assigned to Si(1)/Si(3).

Mössbauer spectroscopy of complex **125** was carried out at two temperatures: 80 K (Figure 55a) and 273 K (Figure 55b).

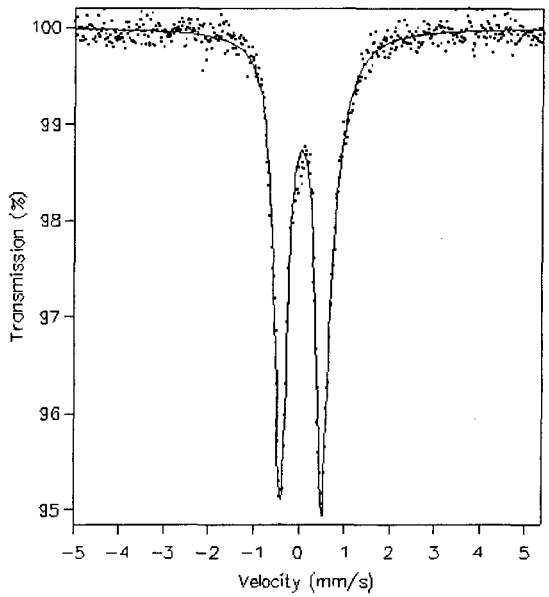

Figure 55a: Mössbauer spectrum of **125** measured at 80 K.

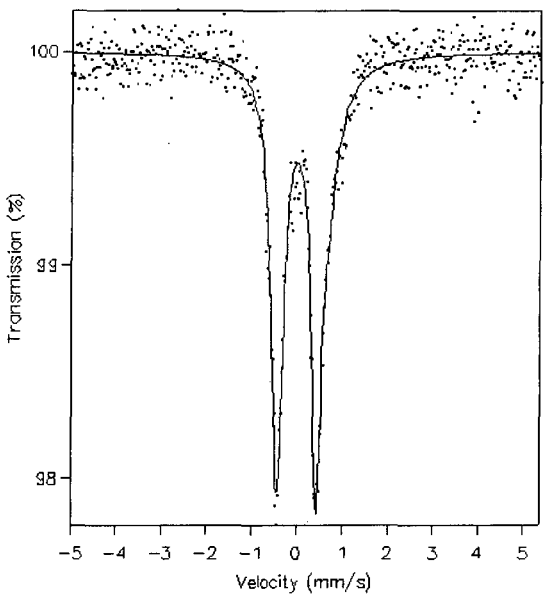

Figure 55b: Mössbauer spectrum of **125** measured at 273 K.

At each temperature, the spectra are best fit by overlapping quadropole-split doublets. The parameters (Table 35) show that some HS Fe(III) is present in the sample as an impurity, presumably as a decomposition product. The parameter range for LS Fe(II) [i.s. –0.2 to +0.4; q.s. 0 to 2 mms^{-1}] and HS Fe(IV) [i.s. –0.2 to +0.2; q.s. 0 to 1 mms^{-1}] both fit the data, within experimental error, thus the oxidation state cannot be unequivocally determined by Mössbauer spectroscopy. However, the data does indicate that LS Fe(II) is more likely.

Temp. (K)	i.s.	q.s.	h.w.h.m.	%
80	0.06	0.92	0.15	70(3)
	0.31(5)	1.01(3)	0.40(3)	30(5)
273	0.00	0.89	0.13	53(4)
	0.17(3)	1.05(3)	0.38(3)	47(8)

Table 35: Parameters for the Mössbauer spectroscopy of **125**. i.s. = isomer shift; q.s. = quadropole splitting; h.w.h.m. = half-width at half-maximum; units = mms^{-1}; errors ±0.01 mms^{-1} or less, unless otherwise stated.

In order to distinguish between Fe(II) and Fe(IV) oxidation states, the T_1 relaxation time of the hydride signal in the ^1H NMR spectrum –12.03 ppm) was measured. If the minimum relaxation time was consistent with a classical hydride (>>100 ms) then complex **125** can be described as a silyl hydride and the oxidation state of the iron centre is +4. However, if the minimum relaxation time is not consistent with a classical

hydride (<100 ms), then complex **125** is best described as an η^2-silane and the oxidation state of the iron centre is +2.[131]

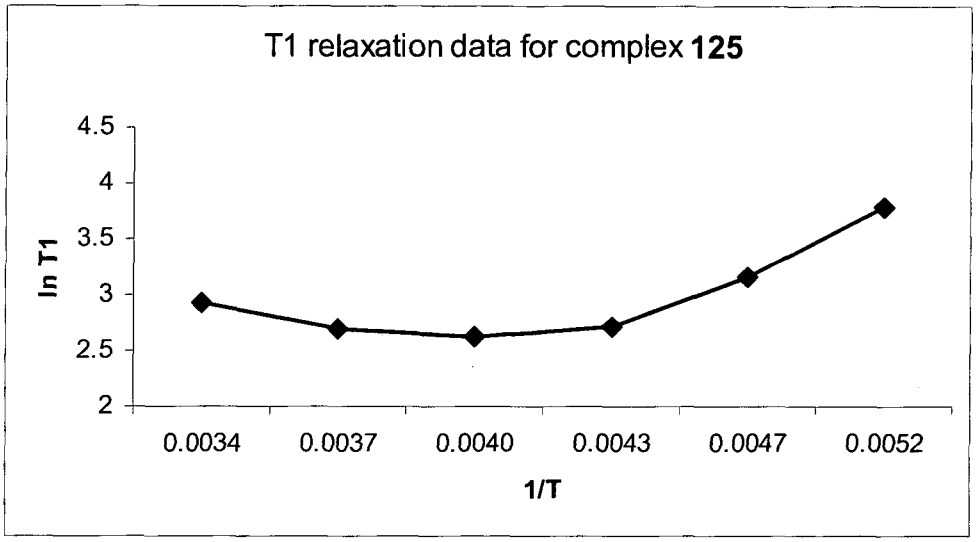

Figure 56: Plot of ln(T_1) against temperature^{-1} for complex **125**

Temp. (K)	$^1/_T$ (K^{-1})	T_1 (ms)	ln T_1
298	3.4×10^{-3}	18.8	2.93
273	3.7×10^{-3}	14.7	2.69
253	4.0×10^{-3}	13.8	2.62
233	4.3×10^{-3}	15.2	2.72
213	4.7×10^{-3}	23.7	3.17
193	5.2×10^{-3}	43.9	3.79

Table 36: T_1 relaxation data for complex **125** collected at different temperatures

The data clearly shows a minimum relaxation time of 13.8 ms at 253 K, indicating that the hydrogen signal in complex **125** is not consistent with a classical hydride. Complex **125** is therefore an Fe(II) species with two phenylsilyl groups and one η^2-phenylsilane group.

A large excess of $PhSiH_3$ (>10 equivalents) was also reacted with a THF solution of complex **110**. An instantaneous colour change from green to dark orange was observed. After removal of solvents and extraction into Et_2O, cooling to 5 °C resulted in the formation of orange crystals suitable for X-ray diffraction studies (Figure 57).

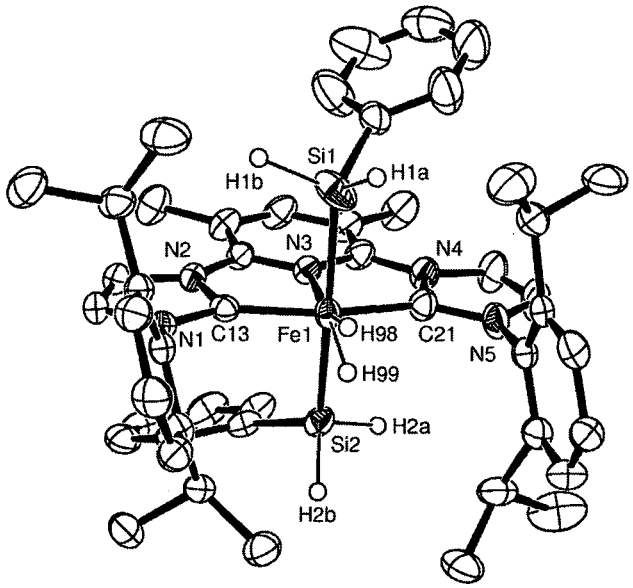

Figure 57: ORTEP representation of **126**. Thermal ellipsoids at 50% probability, H atoms (bar protons attached to heteroatoms) omitted for clarity.

C(13)–Fe(1)	1.883(3)
C(21)–Fe(1)	1.887(3)
N(3)–Fe(1)	1.882(2)
Fe(1)–Si(1)	2.3228(10)
Fe(1)–Si(2)	2.3299(9)
Fe(1)–H(98)	1.53(4)
Fe(1)–H(99)	1.57(3)
C(21)–Fe(1)–C(13)	162.71(12)
Si(2)–Fe(1)–Si(1)	171.86(4)
N(3)–Fe(1)–H(99)	164.6(11)
N(3)–Fe(1)–H(98)	163.6(14)
C(13)–Fe(1)–Si(1)	88.24(8)
N(3)–Fe(1)–C(13)	81.16(10)

Table 37: Selected bond lengths (Å) and angles (°) for compound **126**

Compound **126** is a 7-coordinate species which adopts a severely distorted pentagonal bipyramidal geometry. The two H atoms, two phenylsilyl groups and pyridine nitrogen atom form the equatorial ligands and the C_{NHC} atoms are the axial ligands. The Fe–H distances of 1.53(4) and 1.57(3) Å are consistent with other observed Fe–H distances (complexes **118** and **125**). The range of Si–H distances [1.37(4) – 1.50(4) Å] is consistent with the range of Si–H distances observed in complex **126**. The Fe–C_{NHC} bond distances are in the same range as those observed for complex **118** [1.890(3) – 1.907(3) Å], making them the shortest Fe(II)–C_{NHC} bond distances observed. The Fe–Si bond distances are shorter than the Fe–Si distances observed for the silyl groups in complex **125** [2.369(3) – 2.391(3) Å] and the Fe–Si distance for the silane moiety in complex **125** [2.3389(18) Å]. The distortion around the metal centre is evident from the trans angles, none are greater than 175°. As with complex **125**, this can be put down to steric factors: the phenylsilyl groups are bending away from the ^{i}Pr groups on the phenyl rings.

The ^{1}H NMR spectrum contains the expected ligand resonances: doublets at 1.54 and 1.18 ppm and a septet at 3.50 ppm from the ^{i}Pr groups and a singlet at 2.04 ppm corresponding to the Me groups on the pyridine ring. A singlet at 4.56 ppm corresponds to the silyl protons and the H atoms attached to iron can be found at –12.92 ppm. One

C_{NHC} resonance at 218.8 ppm is observed in the $^{13}C\{^1H\}$ NMR spectrum. Microanalysis is consistent with the observed structure.

To determine whether the H atoms were two hydrides or molecular hydrogen, the T_1 relaxation time of the signal at –12.92 ppm was measured (Figure 58).

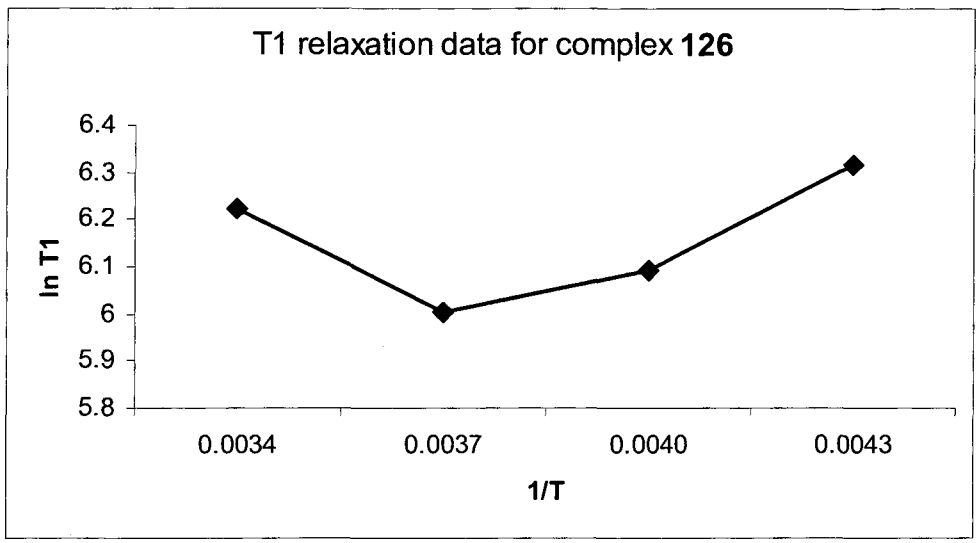

Figure 58: Plot of $\ln(T_1)$ against temperature^{-1} for complex **126**

Temp. (K)	$^1/_T$ (K^{-1})	T_1 (ms)	ln T_1
298	3.4×10^{-3}	503	6.22
273	3.7×10^{-3}	405	6.00
253	4.0×10^{-3}	443	6.09
233	4.3×10^{-3}	553	6.32

Table 38: T1 relaxation data for complex **126** collected at different temperatures

Surprisingly, the data showed a minimum T_1 relaxation time of 405 ms at 273 K, indicating that the H_2 ligand is actually two hydrides rather than dihydrogen. Based on this evidence, complex **126** contains iron in oxidation state +4 with two hydrides and two phenylsilyl groups. This is not the first example of an Fe(IV) silyl hydride, but compounds of this type are rare.[131]

Complexes **125** and **126** were tested for catalytic activity in the hydrosilylation of olefins. Following the procedure reported by Chirik *et al.*,[120] addition of $PhSiH_3$ and the olefin to dinitrogen complexes **48** and **110** resulted in the formation of complexes **125** and **126** respectively: no hydrosilylation activity was observed.

5.43 – Reactivity with other silanes

Complex **48** was reacted with 5 equivalents of Ph_2SiH_2. The colour change from a green solution to a dark orange solution occurred over 10 minutes, rather than being instantaneous as with $PhSiH_3$. After removal of solvents and extraction into PhMe, cooling to –35 °C led to the formation of orange crystals suitable for X-ray diffraction (Figure 59a).

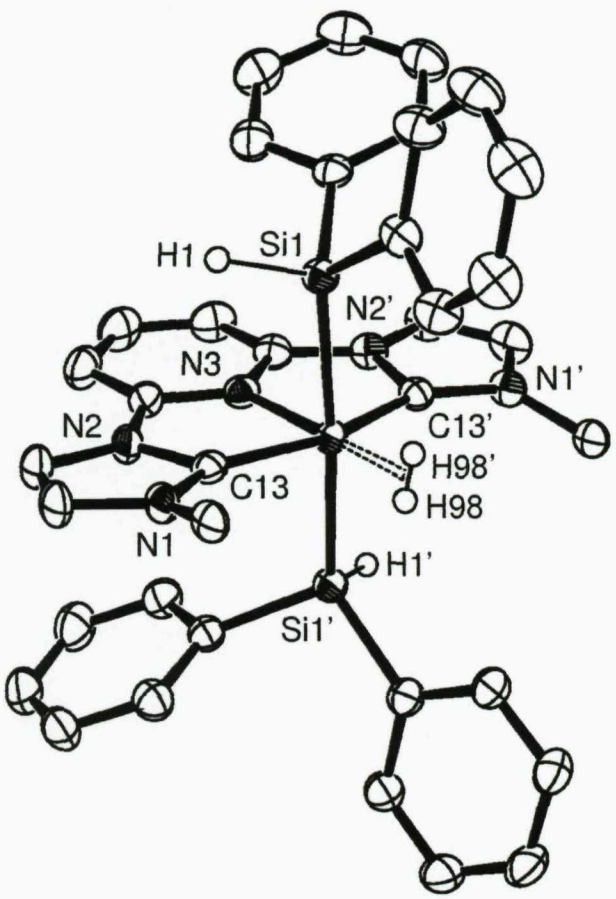

Figure 59a: ORTEP representation of **127**. Thermal ellipsoids at 50% probability, H atoms (bar protons attached to heteroatoms) and DiPP groups (bar ipso carbons) omitted for clarity.

C(13)–Fe(1)	1.9160(19)
N(3)–Fe(1)	1.882(2)
Fe(1)–Si(1)	2.3210(10)
Fe(1)–H(98)	1.616(15)
C(13)–Fe(1)–C(13')	161.17(12)
Si(1)–Fe(1)–Si(1')	174.37(3)
N(3)–Fe(1)–H(98)	168.4(6)
C(13)–Fe(1)–Si(1)	85.26(6)
N(3)–Fe(1)–C(13)	80.59(6)

Table 39: Selected bond lengths (Å) and angles (°) for compound **127**

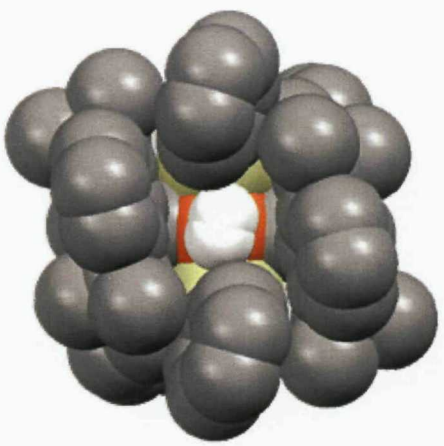

Figure 59b: Space-filling representation of **127** showing the H_2 molecule residing in the cleft. DiPP groups on the left and right, Si–Ph groups at the top and bottom.

Complex **127** is a 6-coordinate distorted octahedral species which lies on a C_2 axis in the unit cell. The coordination sphere around the metal centre is similar to complex **126**, containing one (CNC) ligand, two silyl groups and what appears to be dihydrogen trans to the pyridine ring. The Fe–H distance of 1.616(15) Å is consistent, within experimental error, with the Fe–H distances in complex **126**. The Si–H distance of 1.45(2) Å is consistent with the previously observed range of Si–H distances for

complexes **125** and **126**. The Fe–C_{NHC} distance of 1.9160(19) Å is within the previously observed range of Fe(II)–C_{NHC} bond distances.

The postulated molecular H_2 resides in a cleft created by the DiPP groups and one of the phenyl rings from the diphenylsilyl groups (Figure 59b). Unlike complexes **125** and **126** where the phenyl ring of the $PhSiH_2$ group can bend back from the ^{i}Pr groups to minimise steric repulsion, complex **127** contains two $SiHPh_2$ groups where both phenyl rings cannot bend away from the ^{i}Pr groups. This results in π-stacking effects where one of the phenyl rings from the diphenylsilyl ligand (top and bottom) inserts into the gap between the phenyl rings of the DiPP groups (left and right), completely blocking access to the metal centre. It therefore becomes impossible for a third equivalent of Ph_2SiH_2 to displace the coordinated dihydrogen in an analogous manner to that for complex **125** hence it is likely that the presence of molecular hydrogen in complex **127** is mainly a result of steric protection of the metal centre.

The ^{1}H NMR spectrum contains the usual ligand resonances of two doublets and one septet. The resonance due to the Si–H protons is found at 4.72 ppm and the molecular hydrogen signal occurs at –12.63 ppm. The C_{NHC} resonance was not observed in the $^{13}C\{^{1}H\}$ NMR spectrum. Microanalysis was consistent with the observed structure.

Attempts to synthesise the analogous complex with ligand **58** instead of **36** were unsuccessful. Although a colour change was observed when Ph_2SiH_2 was added to a THF solution of **110**, the orange product could not be isolated in pure form. ^{1}H NMR spectroscopy of the crude reaction product contained several sets of doublets and septets, and more than one signal corresponding to the pyridine methyl groups, indicating more than one product had been formed. No reaction of either **48** or **110** with Ph_3SiH was observed.

The effect of substitution on the aromatic rings of the silanes was investigated. Reaction of excess *ortho*-tolylsilane with a THF solution of **110** resulted in an instantaneous colour change from green to orange. After stirring for 16 hours and removal of solvents, the resulting orange solid was extracted into PhMe and filtered through Celite. After standing for 72 hours, orange crystals were deposited (Scheme 63).

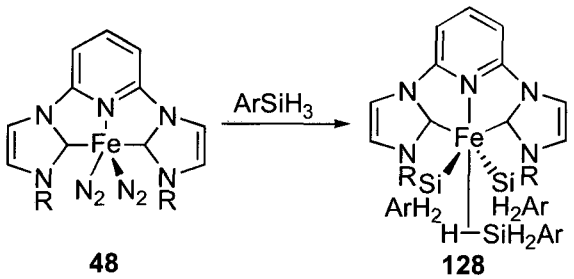

48 128

Scheme 63: Formation of Fe(II) silyl complexes, R = DiPP, Ar = *o*-tolyl

The ^{1}H NMR spectrum of the orange crystals contained two doublets at 1.39 and 1.04 ppm, one septet at 3.55 ppm and one singlet at 2.32 ppm indicating that one (CNC) ligand was bonded to the metal. There were two Si–H resonances at 4.54 and 4.52 ppm, integrating to 2H and 4H respectively, along with a singlet at –13.62 ppm integrating to 1H. This is indicative of a structure similar to that of **125** with an η^2–*o*-tolylSiH$_3$ trans to the pyridine ring. Further evidence comes from two singlets at 2.04 and 1.70 ppm integrating to 3H and 6H respectively, indicating two methyl group environments from the silyl rings. One C_{NHC} resonance was observed in the ^{13}C{^{1}H} NMR spectrum at 213.55 ppm.

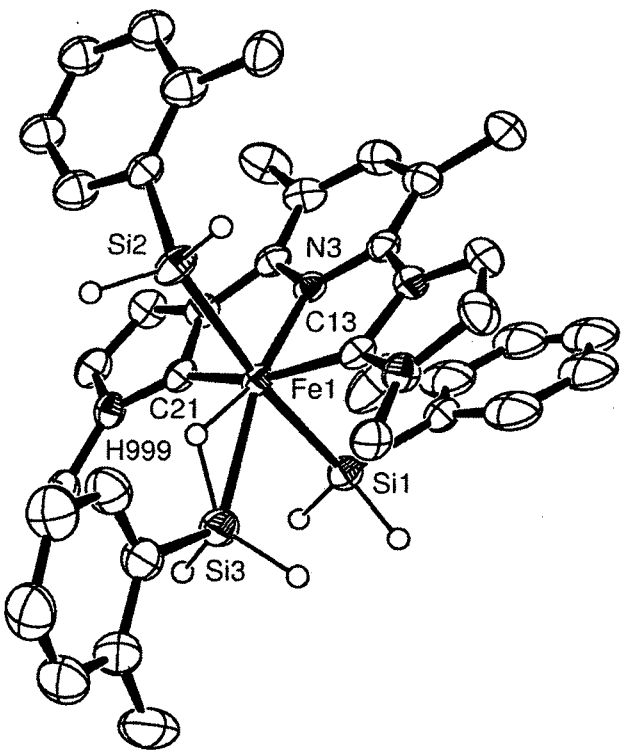

Figure 60: ORTEP representation of **128**. Thermal ellipsoids at 50% probability, H atoms (bar protons attached to heteroatoms) and DiPP groups (bar *ipso* carbons) omitted for clarity.

C(13)–Fe(1)	1.921(3)
C(21)–Fe(1)	1.916(3)
N(3)–Fe(1)	1.908(2)
Fe(1)–Si(1)	2.3475(10)
Fe(1)–Si(2)	2.3412(10)
Fe(1)–Si(3)	2.3727(11)
Fe(1)–H(999)	1.58(3)
C(21)–Fe(1)–C(13)	160.86(14)
N(3)–Fe(1)–Si(3)	162.55(8)
Si(2)–Fe(1)–Si(1)	170.94(4)
N(3)–Fe(1)–H(999)	160.9(10)
C(13)–Fe(1)–H(999)	97.0(10)
C(13)–Fe(1)–Si(3)	99.70(10)
N(3)–Fe(1)–C(13)	80.48(12)

Table 40: Selected bond lengths (Å) and angles (°) for compound **128**

Structural characterisation (Figure 60) confirmed the structure was analogous to complex **125**. A distorted octahedral species (no *trans* angles at the metal centre greater

than 175°) containing one (CNC) ligand, two *o*-tolylsilyl groups and one η^2–*o*-tolylsilane group trans to the pyridine ring. The *o*-tolylsilyl groups are bent away from the DiPP groups in order to minimise steric repulsion. The Fe–C_{NHC} bond lengths are within the range of previously observed Fe(II)–C_{NHC} bond lengths and the Fe–H distance is also within the range of previously observed Fe–H distances (complexes **118**, **125**, **126** and **127**). The Si–H distances are consistent with the Si–H distances observed for complexes **125**, **126** and **127**, likewise for the Fe–Si distances. The Si(3)–H(999) distance of 1.45(3) Å is not significantly longer than the other Si–H distances, unlike complex **125** where elongation of the coordinated Si–H bond was observed.

Attempts at synthesising an analogous complex with ligand **36** rather than **58** were unsuccessful. Addition of *o*-tolylsilane to a THF solution of **48** resulted in a colour change from green to orange, but no pure product could be isolated. The ^{1}H NMR spectrum of the reaction product contained many doublets and singlets between 1.00 and 2.25 ppm, indicating the presence of at least three compounds in the crude product.

An excess of mesityl silane was added to a freshly reduced THF solution of **48**, resulting in an instantaneous colour change from green to orange. Removal of solvents and extraction into PhMe resulted in an orange solution which crystallised at –35 °C. Structural characterisation was carried out (Figure 61).

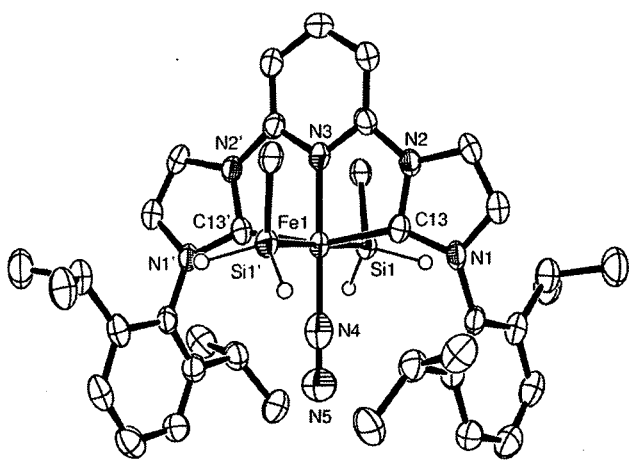

Figure 61: ORTEP representation of **129**. Thermal ellipsoids at 50% probability, H atoms (bar protons attached to heteroatoms) and mesityl groups (bar *ipso* carbons) omitted for clarity.

C(13)–Fe(1)	1.922(4)
N(3)–Fe(1)	1.882(5)
Fe(1)–Si(1)	2.3805(12)
Fe(1)–N(4)	1.827(7)
N(4)–N(5)	1.147(9)
C(13)–Fe(1)–C(13')	160.4(3)
Si(1)–Fe(1)–Si(1')	179.67(7)
N(3)–Fe(1)–N(4)	180.000(1)
C(13)–Fe(1)–Si(1)	92.86(12)
N(4)–Fe(1)–Si(1)	90.17(3)
N(3)–Fe(1)–C(13)	80.21(13)

Table 41: Selected bond lengths (Å) and angles (°) for compound **129**

Complex **129** is a 6-coordinate slightly distorted octahedral species which lies on a C_2 axis within the unit cell. One (CNC) ligand, two mesitylsilyl groups and one end-on-bound dinitrogen molecule make up the coordination sphere around the metal. The mesitylsilyl groups are bent away from the DiPP groups in order to minimise steric repulsion. The Fe–C_{NHC} bond length is consistent with previously observed Fe(II)–C_{NHC} bond lengths, likewise for the Fe–Si bond length. The range of Si–H bond lengths [1.35(4) – 1.41(5) Å] is consistent with the range of Si–H bond lengths observed for complexes **125** through **128**. Unlike previous octahedral Fe(II) disilyl complexes stabilised by (CNC) ligands, the distortion away from ideal octahedral is minimal with two trans angles of 180°, within experimental error. The only non-180° trans angle (the C–Fe–C angle) is caused by the limitations of the (CNC) ligand.

The Fe–N_2 bond distance of 1.827(7) Å is consistent with other Fe–N_2 bond distances (see section 5.24). The N≡N distance of 1.147(9) Å is significantly longer than the N≡N distances in Fe(0) dinitrogen complexes (Table 28). The N≡N stretch in the IR spectrum occurs at 2149 cm^{-1}, at significantly higher wavenumbers than the Fe(0) dinitrogen complexes which is consistent with the Fe(II) metal centre being less electron rich than the Fe(0) metal centres.

All attempts at obtaining a ^1H NMR spectrum of complex **129** resulted in broadening of the signals. It is possible that the N_2 ligand is fluxional on the NMR timescale, but the lack of resonances below 0 ppm is consistent with the observed structure. Microanalysis was consistent with loss of N_2 from the observed structure.

Attempts to synthesise an analogous complex with ligand **58** instead of **36** did not result in the isolation of a pure complex: the ^1H NMR spectrum of the crude reaction product was broad and no ligand peaks could be distinguished.

5.44 – Proposed mechanism of formation

Complexes **125** through **129** are all octahedral complexes containing one (CNC) ligand, two mutually *trans* silyl groups and a variety of groups occupying the position *trans* to the pyridine ring (η^2–silane, two hydrides, dihydrogen and dinitrogen). However, it is likely that the formation of these complexes follows a common mechanism.

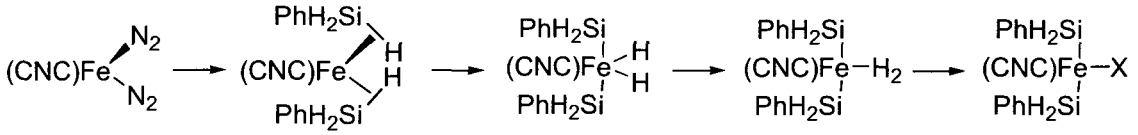

Scheme 64: Postulated mechanism of formation of Fe(II) silyl complexes

The most plausible mechanism (Scheme 64), given the direct observation of Fe(IV) complex **126**, is a double oxidative addition of $PhSiH_3$ to the Fe(0) centre. Displacement of N_2 and coordination of two phenylsilyl ligands in an η^2–fashion leads to the Fe(0) intermediate which, for steric reasons, has the phenylsilyl groups pointing away from the ^{i}Pr groups. This is followed by the oxidative addition of the coordinated Si–H bonds to form the Fe(IV) complex. In some cases this Fe(IV) product is stable enough to be isolated, in others the two hydride ligands reductively eliminate to form a Fe(II) dihydrogen complex. Substitution (or retention) of the molecular H_2 ligand with other groups (silane, dinitrogen) is the final step. A successive oxidative addition mechanism, following the pathway Fe(0)–Fe(II)–Fe(IV)–Fe(II) is also plausible in place of the concerted double oxidative addition.

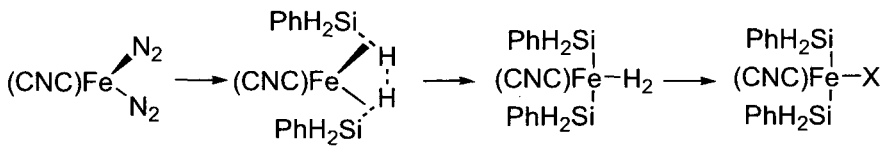

Scheme 65: Alternative mechanism of formation of Fe(II) silyl complexes

The alternative mechanism of formation (Scheme 65) is also based on the observed complex **122** reported by Chirik *et al.*[120] However, the next step is the coordinated hydrogens undergoing σ–bond metathesis. This results in oxidation of the metal centre, forming the two phenylsilyl groups and coordinated dihydrogen as possibly seen in complex **127**. The dihydrogen can then be reduced to two hydrides with oxidation of the metal centre (complex **126**) or displacement with other coordinating ligands (*e.g.* silane).

The factors governing the occupancy of the position *trans* to the pyridine ring are not well understood. Although sterics probably play a part in the formation of certain complexes, notably **127**, they are not the deciding factor. Even if steric interactions preclude the synthesis of η^2–silane species, as may be the case for compound **129** due to the interaction between the DiPP groups and the methyl groups on the mesityl silane, the reason for N_2 binding instead of H_2 is not known.

The only difference between dinitrogen complexes **48** and **110** is the greater σ-donating ability of ligand **58**. It is possible that the slight difference between the two ligands is enough to stabilise the Fe(IV) centre and enable isolation of the dihydride species **126**. Although attempts to react **48** and **110** with other silanes were carried out, it was not possible to isolate the products from both reactions, hence the effect of changing the ligand on the isolated product is not fully understood.

Chirik and co-workers have shown that iron silyl complexes stabilised by (NNN) and (PNP) ligands can be synthesised (Scheme 62).[120, 121] It has also been shown (section 5.24) that the (PNP) ligand is more electron-donating than the (CNC) ligand, which in turn is more electron-donating than the (NNN) ligand. This is also manifested in the reactivity towards phenylsilane (Figure 62).

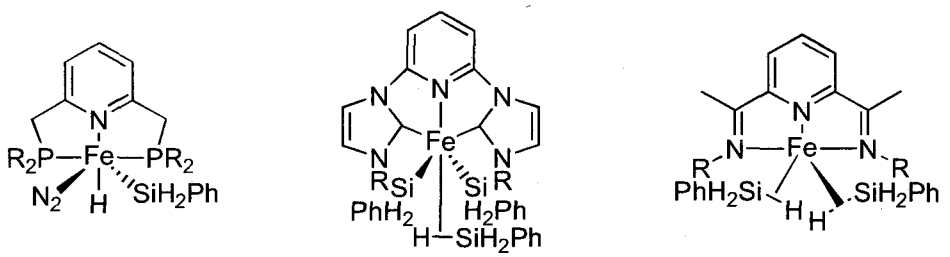

124: R = ^{i}Pr **125**: R = DiPP **122**: R = DiPP

Figure 62: Silyl and silane complexes of (XNX) pincer Fe species, X = P, C, N

The only species isolated with the (PNP) ligand is the Fe(II) silyl compound **124**, despite the presence of labile N_2. The only species isolated with the (NNN) ligand is the Fe(0) disilane complex **122**. However, the (CNC) ligand exhibits both silyl and silane coordination (**125**). Therefore, the reactivity of the (CNC) ligand lies between the (PNP) and (NNN) ligand and the reactivity changes as the σ-donor abilities of the pincer ligand decreases.

5.5 – Summary

Novel Fe(0) bis(dinitrogen) and dicarbonyl species with ligand **58**, and an Fe(0) dicarbonyl complex of ligand **60**, have been synthesised and characterised. Added to the complexes previously synthesised in the literature, it enabled a comparison of the σ-donating properties of trialkylphosphines, NHCs and imines to be made by studying the structural and spectroscopic data of the complexes. Contrary to the literature findings (and the work carried out in section 3.2), the trialkylphosphine pincer ligand was discovered to be a better σ-donor than the NHC ligand. No explanation for this apparent anomaly can be offered.

The dinitrogen complexes **48** and **110** are very reactive species and **48** undergoes C–H activation of benzaldehyde anilide. Despite repeated attempts, no other organic molecules could be C–H activated. Complex **48** will also reduce CO_2 to CO, although much more work into the mechanism of the reaction needs to be carried out before it can be understood.

Both **48** and **110** will react with a range of aryl silanes affording a variety of octahedral disilyliron products. Although Si–H activation has occurred twice, the nature of the ligand trans to the pyridine nitrogen varies. The reason for the difference in reactivity is not known, although sterics probably play a small part in some cases. However, it appears that changing the electron-donating properties of the (CNC) ligand results in a big difference in the reactivity: ligand **58** is capable of stabilising the Fe(IV) dihydride complex **126** whereas ligand **36** can only stabilise the Fe(II) bis(silyl)silane species **125**. Excessively bulky silanes will not react with either dinitrogen complex, presumably as a result of steric clashes with the DiPP groups.

Chapter 6

Platinum group metal complexes

6.1 – Introduction

The first ruthenium complex of ligand **36** was reported in 2002 by Danopoulos *et al.*, who discovered that complex **40** was a good catalyst for the transfer hydrogenation of ketones.[62] However, (CNC) analogues of Grubbs' catalyst (**41**) showed poor metathesis activity (Figure 63).[49]

40: R = DiPP **41**: R = DiPP

Figure 63: Previously synthesised Ru pincer complexes

The rhodium(I) complex **42** was reported in 2006 and tested as a hydroformylation catalyst. No activity was noted and the only observed product was a cationic Rh(I) carbonyl species which did not bind H_2 or olefins. However, complex **42** was susceptible to the addition of C–Cl bonds, affording Rh(III) species (Scheme 66).[73]

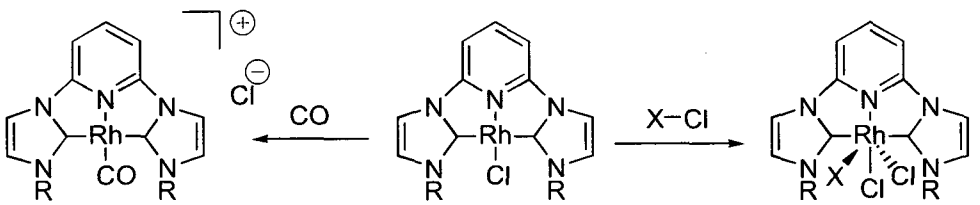

130 **42** **131a**: X = CH_2Cl **131b**: X = COCl

Scheme 66: Reactivity of Rh complex **42**

The synthesis of an Ir(I) analogue of complex **42** failed. The only isolated product was tentatively assigned as **50**, based on weakly-diffracting crystals, indicating C–H activation of the pyridine ring had occurred (Scheme 67).[80] It was hoped that ligand **58** would prevent C–H activation and allow access to Ir(I) pincer complexes.

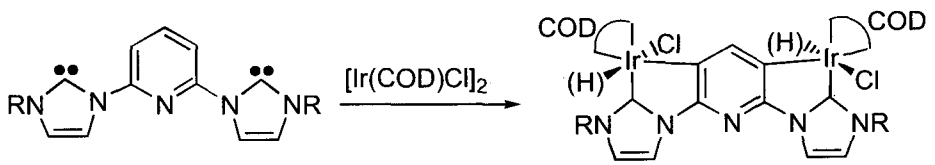

36: R = DiPP **50**: R = DiPP

Scheme 67: C-H activation of the pyridine moiety of ligand **36**

6.2 – Ruthenium

Although several complexes of ruthenium with (CNC) ligand **36** have been reported and their catalytic activity investigated, the substitution chemistry of complex **40** had not been reported. It was also desirable to obtain Ru complexes in oxidation state +3 and above. To this end, the reactivity of **40** with NaN_3 was investigated in an attempt to synthesise nitride complexes by photolysis of the azide. One equivalent of NaN_3 was reacted with **40** in THF under aerobic conditions (Scheme 68).

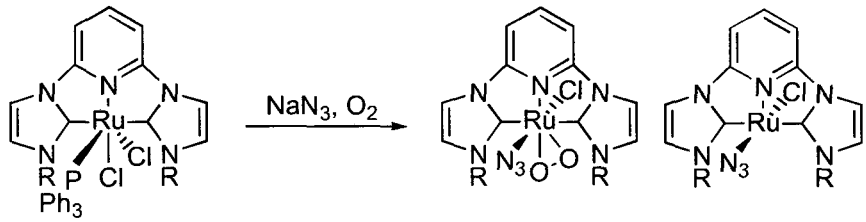

Scheme 68: Partial formation of a Ru(IV) peroxide, R = DiPP

After removal of the THF and extraction of the red solid into DCM, filtration afforded a red solution from which crystals were deposited by the slow diffusion of Et_2O. Surprisingly, the $^{31}P\{^1H\}$ NMR spectrum of complex **132** contained no resonances. Although the ^1H NMR spectrum was broad, the resonances corresponding to the aromatic protons integrated to 13H, also implying no PPh_3 was present. Structural characterisation revealed an unexpected peroxo species had been formed (Figure 64).

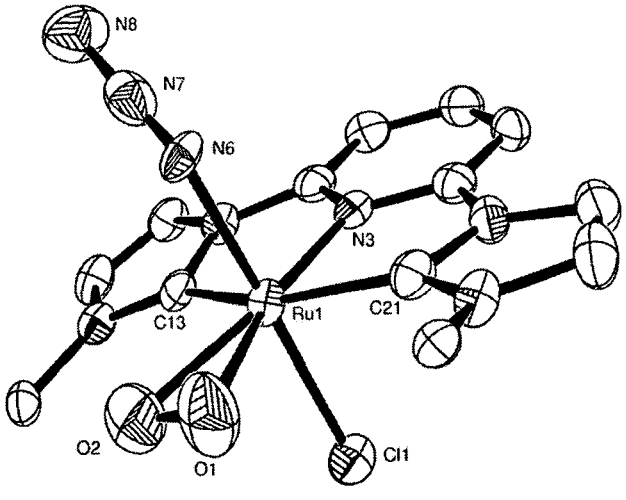

Figure 64: ORTEP representation of **132a**. Thermal ellipsoids at 50% probability, H atoms and DiPP groups (bar *ipso* carbons) omitted for clarity.

C(13)–Ru(1)	2.066(5)
C(21)–Ru(1)	2.058(5)
N(3)–Ru(1)	2.016(4)
Cl(1)–Ru(1)	2.3970(14)
N(6)–Ru(1)	2.163(4)
O(1)–Ru(1)	2.213(6)
O(2)–Ru(1)	2.196(6)
O(2)–O(1)	1.297(9)
C(21)–Ru(1)–C(13)	154.30(19)
N(6)–Ru(1)–Cl(1)	176.18(12)
N(3)–Ru(1)–O(1)	162.0(2)
N(3)–Ru(1)–O(2)	163.5(2)
C(21)–Ru(1)–Cl(1)	87.00(14)
N(6)–Ru(1)–O(1)	88.3(2)
N(3)–Ru(1)–C(13)	77.21(18)

Table 42: Selected bond lengths (Å) and angles (°) for compound **132**

Complex **132** is a co-crystallised mixture of two ruthenium-containing products, one a 7-coordinate Ru(IV) peroxo chloride azide species (**132a**) and the other a 5-coordinate Ru(II) chloride azide species with no ligand *trans* to the N_{py} (**132b**) The two compounds occupy the same environment in the unit cell in a 3:1 ratio, resulting in 75% partial occupancy for the oxygen atoms and full occupancy for the remaining atoms. The presence of two compounds explains the broad resonances in the ^{1}H NMR spectrum: the two species have very similar overlapping resonances. The $^{13}C\{^{1}H\}$ NMR spectrum contained the expected number of aromatic carbon resonances but extra resonances corresponding to the ^{i}Pr groups, consistent with the desymmetrisation of the molecule. Microanalysis is consistent with the formulation $(CNC)RuCl(N)(O_{1.5})$ after loss of N_2 from the azide.

The $Ru–C_{NHC}$ bond lengths are consistent with the range of previously observed $Ru(II)–C_{NHC}$ bond lengths. No NHC complexes of Ru(IV) have been structurally characterised (see section 1.5). The $Ru–N_{py}$ distance is shorter than the $Ru–N_3$ distance by *ca.* 0.15 Å – this is a result of the chelating ligand forcing the pyridine moiety closer to the metal centre. The Ru–O distances are longer than the only other two structurally characterised Ru–O bond lengths from Ru(IV) peroxide species [range 1.991(3) – 2.048(3) Å].[132, 133] The O–O distance in complex **132** is shorter than both the O–O bond distances for other structurally characterised Ru(IV) peroxide species [1.363(4) – 1.416(5) Å]. Unfortunately, all attempts at photolysing and thermolysing the azide did not result in the formation of a Ru(IV) nitride species.

Compound **40** was also reacted with an excess of NaN_3, under the same aerobic conditions, with the ultimate aim of synthesising a Ru(VI) azide after photolysis (Scheme 69). After removal of solvents, extraction into DCM and filtration, a red solution was isolated which afforded a red solid after removal of solvents.

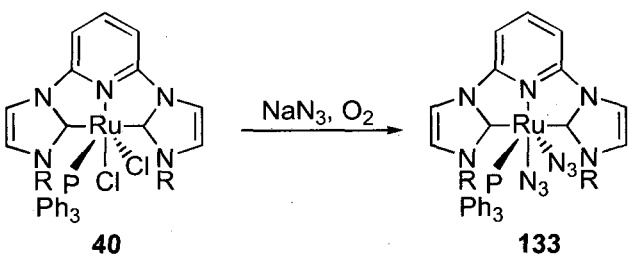

40 **133**

Scheme 69: Formation of a bis(azide) complex, R = DiPP

Surprisingly, the ^{1}H NMR spectrum of the red solid contained many aromatic resonances. The spectrum was broad and provided poor resolution, however it appeared

that there were at least two signals for the ^{i}Pr CH protons and at least 4 signals for the ^{i}Pr CH_3 protons. There was one resonance in the $^{31}P\{^{1}H\}$ NMR spectrum at 36.99 ppm, indicative of coordinated PPh_3. Crystallisation of the red solid by slow diffusion of Et_2O into a concentrated DCM solution enabled an X-ray diffraction study to be carried out (Figure 65).

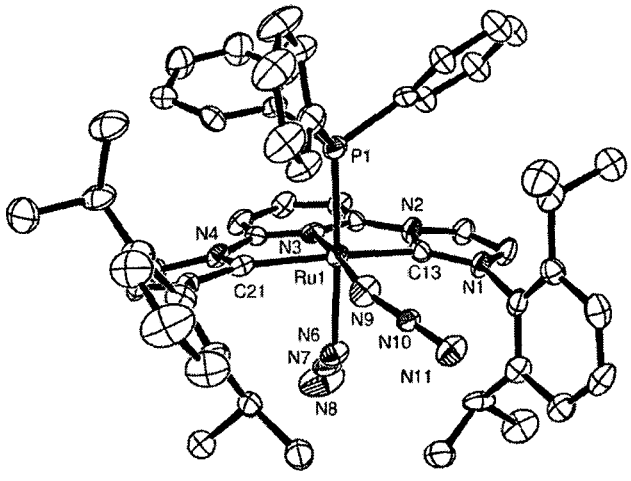

Figure 65: ORTEP representation of **133**. Thermal ellipsoids at 50% probability, H atoms omitted for clarity.

C(13)–Ru(1)	2.048(5)
C(21)–Ru(1)	2.063(6)
N(3)–Ru(1)	1.982(4)
N(6)–Ru(1)	2.165(4)
N(9)–Ru(1)	2.107(4)
Ru(1)–P(1)	2.3103(14)
C(21)–Ru(1)–C(13)	155.3(2)
N(3)–Ru(1)–N(9)	174.85(17)
N(6)–Ru(1)–P(1)	176.66(14)
C(21)–Ru(1)–N(6)	84.30(19)
N(9)–Ru(1)–P(1)	93.84(13)
N(3)–Ru(1)–C(13)	78.7(2)

Table 43: Selected bond lengths (Å) and angles (°) for compound **133**

Complex **133** is a 6-coordinate octahedral Ru(II) species with one (CNC) ligand, two azides and one PPh_3 ligand making up the coordination sphere. The DiPP groups are distorted from their usual geometry of normal to the plane of the NHC ring in order to accommodate the steric bulk of the PPh_3 ligand, a feature common to complex **40**.[62] The presence of PPh_3 in the complex accounts for the higher than expected number of aromatic resonances in the $^{13}C\{^{1}H\}$ NMR spectrum.

The Ru–C_{NHC} bond lengths are consistent with those in complex **132** and also with other structurally characterised examples of Ru(II)–C_{NHC} bond lengths. The Ru–N_3 distance *trans* to the pyridine nitrogen is slightly shorter than the Ru–N_3 distance *trans* to the PPh_3 ligand and both are longer than the Ru–N_{py} distance. The Ru–P distance of 2.3103(14) Å is consistent with the Ru–P distance in complex **40** of 2.318(2) Å. Microanalysis is consistent with the formulation (CNC)Ru(PPh_3)$(N)_2$ after loss of two molecules of N_2 from the azide ligands. Neither photolysis nor thermolysis of complex **133** resulted in decomposition of the azide moieties.

It is not known why the PPh_3 ligand was still bound to the Ru centre in complex **133** but not **132**. The synthesis of both complexes was carried out under exactly the same conditions, apart from the amount of NaN_3 present. Due to this apparent inconsistency, it was decided to synthesise a new ruthenium starting material with no phosphines. The reaction of **36** with $[RuCl_2(nbd)(py)_2]$ in THF afforded a red solution, from which a red solid was isolated (Scheme 70).

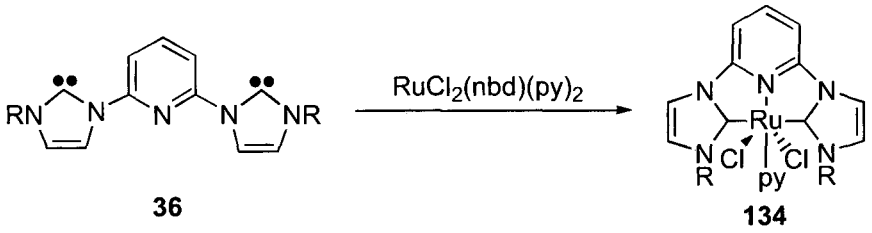

36 **134**

Scheme 70: Synthesis of a Ru complex without PPh_3, R = DiPP

The ^1H NMR spectrum of the red solid contained the expected ligand peaks of 2 doublets and a septet corresponding to the ^{i}Pr groups, indicating that the product contained mutually *trans* chlorides and a pyridine ligand *trans* to the pyridine from the (CNC) ligand. The aromatic resonances integrated to 18 protons, which is consistent with 13 from the (CNC) ligand and 5 from the pyridine. The $^{13}C\{^1H\}$ NMR spectrum contained one resonance for the ^{i}Pr CH carbon and two for the ^{i}Pr CH_3 carbons, further evidence that the two pyridine rings are trans to each other. The C_{NHC} resonance was observed at 204.3 ppm. Crystallisation of the red solid occurred from the slow diffusion of Et_2O into a DCM solution and structural characterisation was carried out (Figure 66).

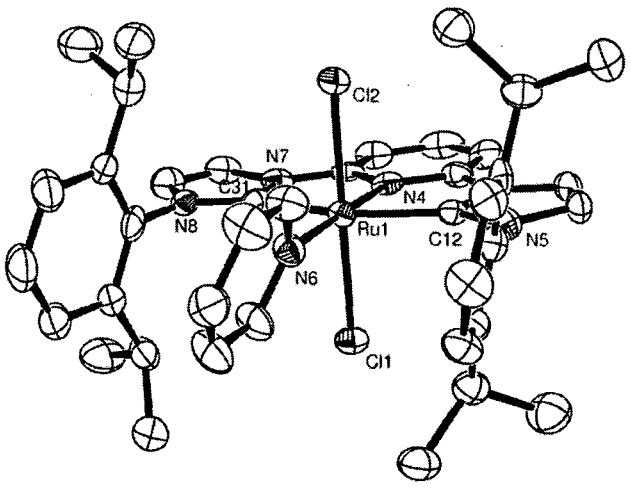

Figure 66: ORTEP representation of **134**. Thermal ellipsoids at 50% probability, H atoms omitted for clarity.

Ru(1)–C(12)	2.049(6)
Ru(1)–C(31)	2.043(5)
N(4)–Ru(1)	1.973(5)
N(6)–Ru(1)	2.120(5)
Ru(1)–Cl(1)	2.4398(15)
Ru(1)–Cl(2)	2.4176(15)
C(31)–Ru(1)–C(12)	157.2(2)
N(4)–Ru(1)–N(6)	179.50(18)
Cl(2)–Ru(1)–Cl(1)	175.64(5)
N(6)–Ru(1)–Cl(2)	91.76(13)
C(31)–Ru(1)–Cl(1)	89.12(15)
N(4)–Ru(1)–C(12)	78.3(2)

Table 44: Selected bond lengths (Å) and angles (°) for compound **134**

Complex **134** is a 6-coordinate slightly distorted octahedral species with one (CNC) ligand, two chlorides and one pyridine ligand comprising the coordination sphere. The distortion is small, as evidenced by the Cl–Ru–Cl and N–Ru–N angles which are close to 180°. The Ru–C_{NHC} bond lengths are consistent with complexes **132** and **133** and are also consistent with the known range of Ru(II)–C_{NHC} bond lengths. Microanalysis was consistent with the observed structure.

The long Ru–N_{py} bond length of 2.120(5) Å for the non-chelating pyridine ring, compared to the Ru–N_{py} length of 1.973(5) Å for the (CNC) pyridine ring, is in part due to the chelating nature of the (CNC) ligand forcing the short Ru–N_{py} bond length. However, another effect of note is face to face π–stacking of the phenyl rings and the pyridine ring. The Ru–N_{py} bond is slightly extended in order to allow the aromatic rings to stack in a non-eclipsing manner.

Complex **134** was dissolved in THF and refluxed under aerobic conditions for 72 hours in an attempt to synthesise a peroxo species. After removal of solvents, crystallisation occurred by diffusion of Et_2O into a DCM solution. However, the unit cell was identical to that of the starting material. Using one equivalent of NaN_3 with the same reaction conditions produced the same result; crystals of the starting material only. Bubbling O_2 through a DCM solution also failed to furnish a Ru(IV) dichloride peroxide. Oxidation with TBHP resulted in decomposition of **134** to a paramagnetic black solid.

Attempts to form a Ru(II) species with ligand **58** were unsuccessful. Unlike complex **40**, which is air stable in solution, decomposition occurred when ligand **58** was reacted with $RuCl_2(PPh_3)_3$ and exposed to air during the workup. Surprisingly, even when the reaction was kept under a dinitrogen atmosphere, a brown solution formed and no (CNC) species could be isolated.

6.3 – Rhodium

The Rh(I) pincer species **42** contains a chloride ion which is strongly bound to the rhodium centre, with only CO capable of displacing it. It was hoped that the more electron-donating ligand **58** would result in a weaker Rh–Cl bond, allowing access to cationic Rh(I) species stabilised by more labile ligands.

Following the published procedure,[73] $[Rh(COD)Cl]_2$ was reacted with ligand **58** in THF, forming a purple solution. After removal of solvents, a purple solid was isolated which was redissolved in THF and PE was slowly diffused in. Yellow needles were deposited and structural characterisation was carried out (Figure 67).

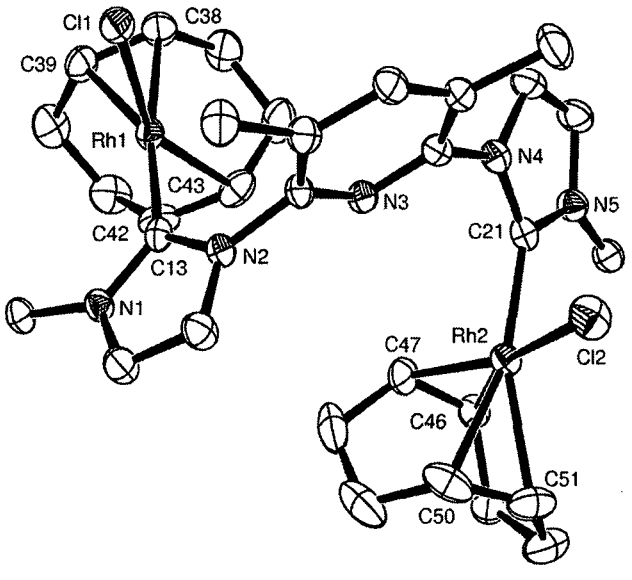

Figure 67: ORTEP representation of **136**. Thermal ellipsoids at 50% probability, H atoms and DiPP groups (bar ipso carbons) omitted for clarity.

C(13)–Rh(1)	2.033(2)
C(21)–Rh(2)	2.037(3)
C(38)–Rh(1)	2.214(3)
C(43)–Rh(1)	2.088(3)
Cl(1)–Rh(1)	2.3686(7)
Cl(2)–Rh(2)	2.3666(8)
C(13)–Rh(1)–Cl(1)	89.79(7)
C(21)–Rh(2)–Cl(2)	86.77(7)
C(42)–Rh(1)–C(38)	89.14(11)
C(46)–Rh(2)–C(50)	89.24(11)
C(13)–Rh(1)–C(38)	172.06(10)
C(21)–Rh(2)–C(50)	162.10(12)

Table 45: Selected bond lengths (Å) and angles (°) for compound **136**

Complex **136** contains one (CNC) ligand and two 4-coordinate square planar rhodium centres, each with one NHC, one chloride and chelating COD. There is very little distortion away from ideal square planar geometry, as evidenced by the *cis* angles at the rhodium centre. The Rh–C_{NHC} bond lengths are within the range of previously observed Rh(I)–C_{NHC} bond lengths (section 1.5) and are shorter than the range of Rh–C_{COD} bond lengths.

The isolated product was not the expected Rh(I) pincer complex **135** (Scheme 71). Instead, the bis(rhodium) species **136** had been formed. The formation of bis(rhodium)

complexes with (CNC) pincer ligands is common, especially when starting from the precursor imidazolium salt and using the *in situ* deprotonation methodology.[68] However, when starting from the free ligand, formation of the pincer complex is favoured. The purple colouration of the solid is consistent with the purple colouration of complex **42**, indicating that the majority of the isolated complex is the pincer complex **135**. ^{1}H NMR spectroscopy of the purple solid indicated this to be the case: although the solid was not pure, the resonances associated with the (CNC) ligand were dominant. There were some signals characteristic of the COD ligand, indicating that a small amount of the bis(rhodium) species was present, but it was a minor impurity.

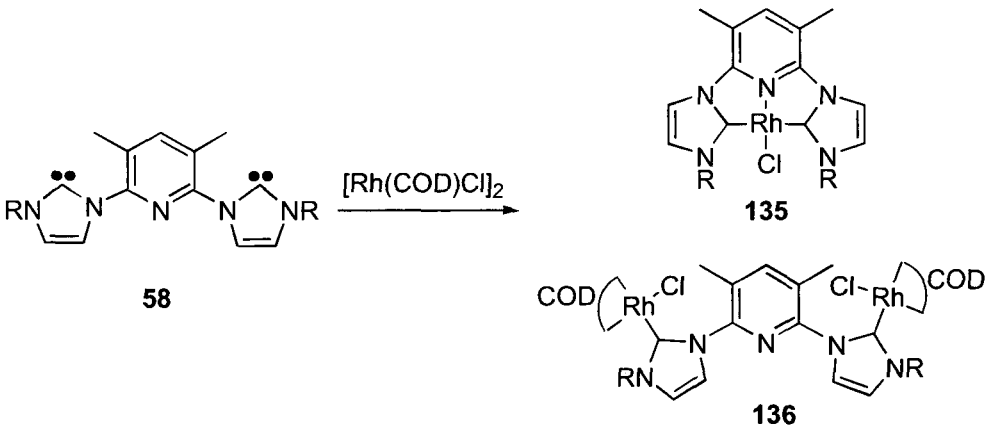

Scheme 71: Synthesis of new Rh complexes **135** and **136**, R = DiPP

Attempts at purifying the purple solid were not successful hence no studies into its reactivity were carried out.

6.4 – Iridium

6.41 – Background

All previous attempts at synthesising Ir complexes of (CNC) ligands were unsuccessful. The reaction of $[Ir(COD)Cl]_2$ with **36** led to the formation of a green solution at –30 °C but upon warming to RT, decomposition to a brown solution took place. Crystallisation of the green solution at low temperatures resulted in the deposition of thermally sensitive crystals but X-ray diffraction studies indicated C–H activation of the pyridine ring had taken place, forming a dinuclear $[Ir(III)]_2$ species (Scheme 67).[80] It was thought that ligand **58** would not undergo C–H activation and would furnish an Ir(I) pincer species.

6.42 – Synthesis of a novel Ir(I) compound

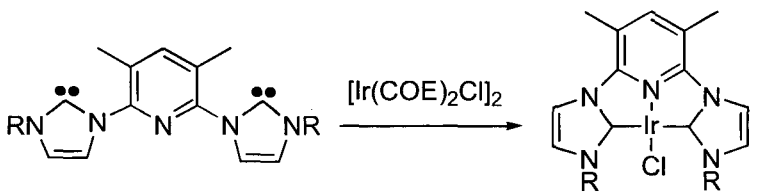

58 **137**

Scheme 72: Synthesis of a novel Ir pincer complex, R = DiPP

A THF solution of ligand **58** was added to a THF solution of $[Ir(COE)_2Cl]_2$ at –78 °C (Scheme 72). A green solution quickly formed which retained its green colour as the solution was warmed to RT. Removal of solvents resulted in the isolation of a green solid which was washed with PE and dried *in vacuo* to remove all traces of alkene.

Elemental analysis of the green solid was consistent with a (CNC)IrCl formulation. The ^1H NMR spectrum contained the characteristic signals associated with ligand **58**, notably two doublets at 1.31 and 1.13 ppm, a septet at 3.11 ppm (^{i}Pr CH_3 and CH respectively) and a singlet at 2.16 ppm (py-Me). The resonance for the C_{NHC} was observed at 188.43 ppm in the $^{13}C\{^1H\}$ NMR spectrum.

Complex **137** was dissolved in THF and Et_2O was slowly diffused in. Clusters of very small green needles formed which were too small for X-ray diffraction studies. Interestingly, if PE was used instead of Et_2O, decomposition to an unidentified brown

solid was observed over a period of several days. The same decomposition occurred with pentane, indicating **137** was intolerant of hydrocarbon solvents.

6.43 – Oxidative chemistry

Much like rhodium complex **42**, complex **137** was extremely susceptible to transformations leading to Ir(III) species. Dissolution of **137** in DCM resulted in the formation of a green solution which turned yellow after less than 10 minutes (Scheme 73), indicating oxidative addition across the C–Cl bond had taken place.

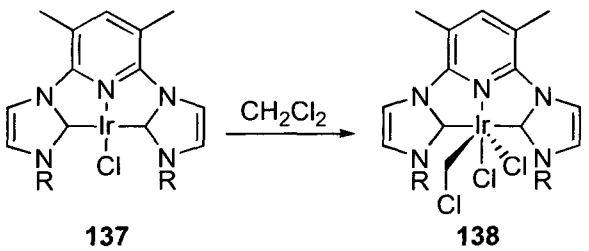

Scheme 73: Oxidative addition of DCM, R = DiPP

Diffusion of Et_2O into the DCM solution resulted in the formation of small yellow needles, which enabled structural characterisation of **138** to take place (Figure 68).

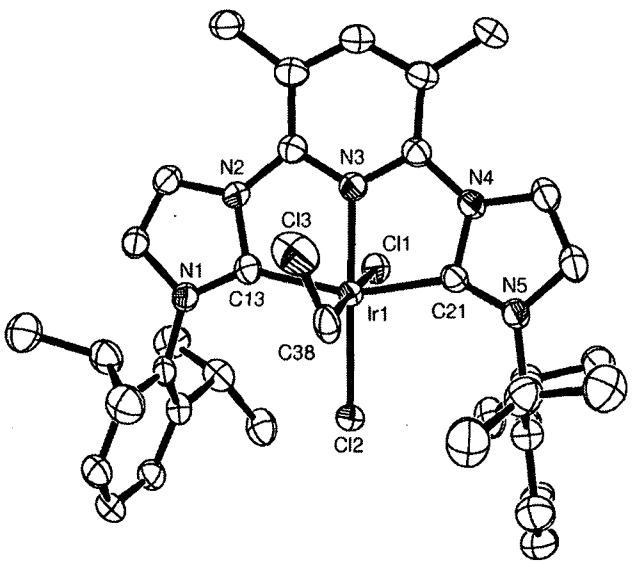

Figure 68: ORTEP representation of **138**. Thermal ellipsoids at 50% probability, H atoms and one DCM solvent molecule omitted for clarity.

C(13)–Ir(1)	2.031(4)
C(21)–Ir(1)	2.017(4)
N(3)–Ir(1)	1.979(3)
C(38)–Ir(1)	2.096(5)
Cl(1)–Ir(1)	2.4783(11)
Cl(2)–Ir(1)	2.3584(11)
C(21)–Ir(1)–C(13)	158.28(17)
N(3)–Ir(1)–Cl(2)	176.13(10)
C(38)–Ir(1)–Cl(1)	176.90(15)
C(21)–Ir(1)–C(38)	90.62(17)
Cl(2)–Ir(1)–Cl(1)	89.86(4)
N(3)–Ir(1)–C(13)	79.32(16)

Table 46: Selected bond lengths (Å) and angles (°) for compound **138**

Complex **138** is a 6-coordinate slightly distorted octahedral compound containing one (CNC) ligand, two chlorides and one chloromethyl ligand. The distortion is mainly due to the constraints of the (CNC) ligand: the C–Ir–Cl and N–Ir–Cl *trans* angles are both

close to 180°. The Ir–C_{NHC} bond lengths are shorter than the Ir–CH_2Cl bond and are consistent with the range of previously observed Ir(III)–C_{NHC} bond lengths (section 1.5). The increased trans influence of a chloromethyl group over pyridine is evident from the Ir–Cl bond lengths: the Ir–Cl(2) bond length is substantially shorter than the Ir–Cl(1) bond length (*ca.* 0.12 Å). Microanalysis is consistent with the observed structure.

The ^{1}H NMR spectrum of **138** is consistent with the low symmetry of the complex. Four doublets are present (instead of two) and two septets (instead of one) corresponding to the ^{i}Pr groups. However, only one singlet corresponding to the pyridine methyl groups is observed. A singlet due to the methylene group is present at 1.47 ppm. The C_{NHC} resonance is observed at 175.57 ppm in the $^{13}C\{^1H\}$ NMR spectrum. A very shielded signal at 13.46 ppm corresponds to the chloromethyl group.

Oxidation of **137** to the (CNC)$IrCl_3$ complex **139** was achieved by adding $PhICl_2$ to a THF solution of **137** under a counterflow of N_2 (Scheme 74). A colour change from green to yellow occurred after *ca.* 1 hour. After removal of solvents, the resulting yellow solid was dissolved in DCM and precipitated with Et_2O. Attempts at crystallising **139** by the slow diffusion of Et_2O into DCM or MeCN solutions failed.

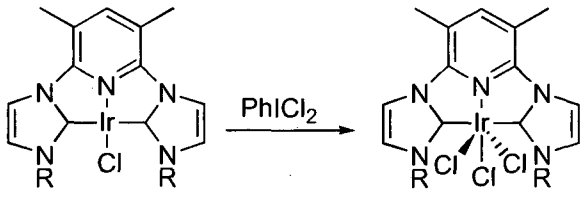

137 **139**

Scheme 74: Oxidative addition of "Cl_2", R = DiPP

The ^{1}H NMR spectrum of the yellow solid contained the expected ligand peaks: two doublets (1.22 and 1.11 ppm) and one septet (3.04 ppm) corresponding to the ^{i}Pr groups and a singlet at 2.95 ppm corresponding to the methyl groups on the pyridine ring. The resonance for the C_{NHC} was observed at 167.72 ppm in the $^{13}C\{^1H\}$ NMR spectrum. Microanalysis was consistent with a (CNC)$IrCl_3$ formulation.

6.44 – Substitution chemistry

Due to the fact that no Ir(I) (CNC) complexes had previously been synthesised, the substitution chemistry of **137** was completely unknown. It was thought that replacing

the chloride anion with other coordinating anions (*e.g.* alkoxide, alkyl, amide, triflate) should lead to some interesting substitution chemistry and could potentially lead to ligands multiply bonded to iridium (*e.g.* nitride from azide).

Complex **137** was reacted with one equivalent of NaO^iPr in THF with the intention of replacing the chloride with an isopropoxide moiety (**140**, Scheme 75). After stirring for 16 hours, removal of solvents, filtration and cooling to 5 °C led to the deposition of brown crystals.

Scheme 75: Formation of an Ir(I) hydride, R = DiPP

Analysis of the ^{1}H NMR spectrum of the reaction product indicated that a hydride was present (resonance at –12.97 ppm). The expected ligand peaks of two doublets and one septet corresponding to the ^{i}Pr groups of the DiPP substituents were present, but no septets or doublets corresponding to the isopropoxy group could be located. It was thought that β-hydrogen elimination had occurred, forming an iridium hydride species and acetone. Structural characterisation confirmed that no isopropoxide was present (Figure 69).

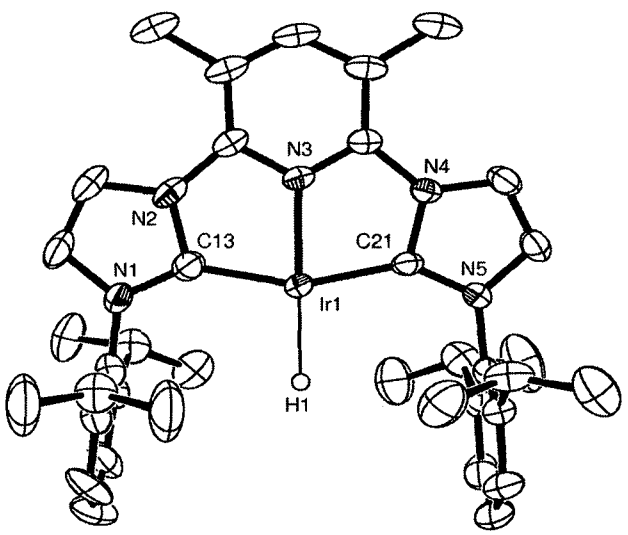

Figure 69: ORTEP representation of **141**. Thermal ellipsoids at 50% probability, H atoms (bar Ir–H) omitted for clarity.

C(13)–Ir(1)	1.972(4)
C(21)–Ir(1)	1.964(4)
N(3)–Ir(1)	2.008(3)
Ir(1)–H(1)	1.73(3)*
C(21)–Ir(1)–C(13)	157.36(16)
N(3)–Ir(1)–H(1)	177.4(16)
N(3)–Ir(1)–C(13)	78.93(16)
N(3)–Ir(1)–C(21)	78.44(14)
C(13)–Ir(1)–H(1)	101.9(16)
C(21)–Ir(1)–H(1)	100.7(16)

Table 47: Selected bond lengths (Å) and angles (°) for compound **141**.

* = Bond length fixed using the DFIX command

Complex **141** is a 4-coordinate square planar complex with one (CNC) ligand and one hydride comprising the coordination sphere. The hydride was located in the difference map but it was necessary to restrain the Ir–H bond distance in the refinement in order to retain a sensible Ir–H bond length. The Ir–C_{NHC} bond lengths are consistent with other Ir(I)–C_{NHC} bond lengths. Microanalysis was consistent with the observed structure.

Complex **137** was reacted with one equivalent of $NaNH_2$ in THF with the aim of synthesising an Ir(I) amide complex (Scheme 76).

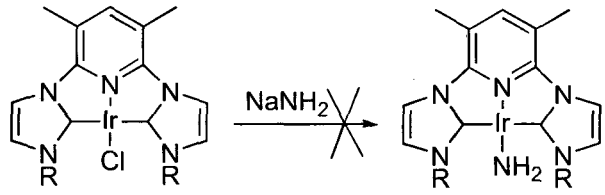

137 **142**

Scheme 76: Attempted formation of an Ir(I) amide, R = DiPP

A colour change from green to dark red was observed almost immediately and the reaction was then stirred for 16 hours. After this time, solvents were removed, the solid extracted into Et_2O and cooled to 5 °C where a very small amount of red crystals were deposited. These crystals were structurally characterised (Figures 70a and 70b: each Figure shows one of two 'pincer' ligands around the metal centre).

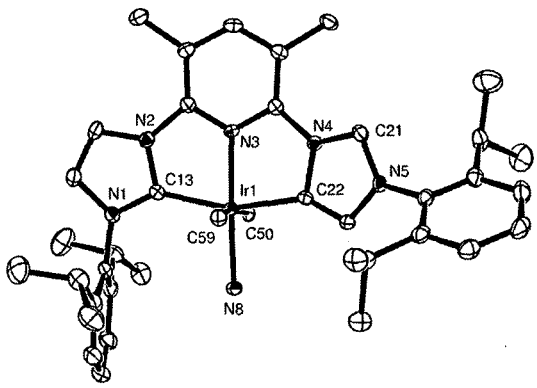

Figure 70a: ORTEP representation of **143** showing the pincer ligand containing the abnormal NHC. Thermal ellipsoids at 50% probability, H atoms omitted for clarity. C(50), C(59) and N(8) are the donor atoms of the other pincer ligand.

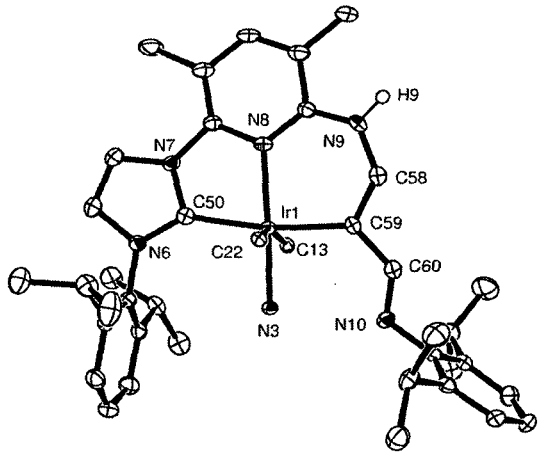

Figure 70b: ORTEP representation of **143** showing the pincer ligand containing the destroyed NHC. Thermal ellipsoids at 50% probability, H atoms (bar N–H) omitted for clarity. C(13), C(22) and N(3) are the donor atoms of the other pincer ligand.

Complex **143** is a 6-coordinate distorted octahedral species with two (CNC) pincer ligands surrounding one Ir(I) centre. The distortion is fairly severe, as evidenced by the *trans* angles at the metal centre: only one is above 170°. One of the pincer ligands

(Figure 70a) is comprised of one normal NHC and one abnormal NHC. The other pincer ligand (Figure 70b) comprises one normal NHC and one vinyl group which arose from complete opening of an NHC ring. The vinyl ring is linked to an imine [C(60) – N(10)] by a conjugated C–C single bond which is evident from the observed bond lengths (Table 48).

C(13)–Ir(1)	2.018(3)	C(50)–Ir(1)	2.043(3)
C(22)–Ir(1)	2.046(3)	C(59)–Ir(1)	2.100(3)
N(3)–Ir(1)	1.996(2)	N(8)–Ir(1)	2.082(2)
C(22)–Ir(1)–C(13)	157.36(16)	C(58)–C(59)	1.369(4)
N(3)–Ir(1)–N(8)	177.10(9)	C(59)–C(60)	1.441(4)
N(3)–Ir(1)–C(13)	78.86(10)	C(60)–N(10)	1.293(4)
C(22)–Ir(1)–N(8)	96.99(10)	C(50)–Ir(1)–C(59)	168.65(11)
C(13)–Ir(1)–C(50)	99.33(11)	N(8)–Ir(1)–C(59)	91.63(10)
C(22)–Ir(1)–C(59)	84.46(11)	C(50)–Ir(1)–N(8)	78.22(10)

Table 48: Selected bond lengths (Å) and angles (°) for comp ound **143**

The Ir–C_{NHC} bond lengths are within the range of previously observed Ir(I)–C_{NHC} bond lengths (see section 1.5). The Ir–C distances for the abnormal and normal NHCs are the same within experimental error and are shorter than the Ir–C distance to the vinyl group.

Attempts to isolate the originally targeted (CNC)Ir(NH_2) species from the dark red supernatant failed due to decomposition to a green solution when exposed to common NMR solvents [C_6D_6, C_4D_8O, $(CD_3)_2CO$]. No characteristic ligand peaks could be identified in the ^1H NMR spectrum of the green solution.

The reaction of **137** with one equivalent of TlOTf in THF produced a yellow solution which deposited yellow crystals after PE was slowly diffused in. X-ray diffraction studies revealed that the same octahedral Ir-containing product had formed (Figure 71), except the iridium centre was in oxidation state +3 and there were two non-coordinating triflate anions in the asymmetric unit to balance the charge (Scheme 77).

The metrical data of complexes **143** and **144** are almost identical (within experimental error). The only difference between the two complexes is the Ir–C_{ab} distance, which is *ca.* 0.06 Å longer in **143** than in **144**.

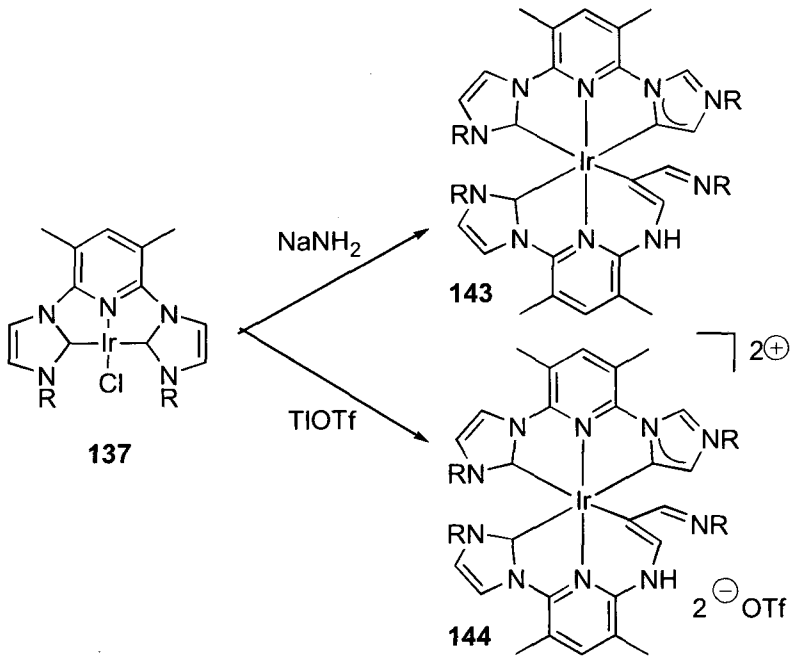

Scheme 77: Formation of bis(ligand)Ir(I) and Ir(III) complexes, R = DiPP

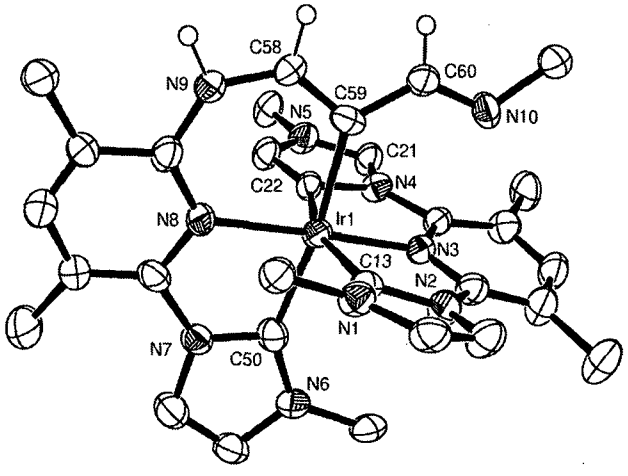

Figure 71: ORTEP representation of the cation of **144**. Thermal ellipsoids at 50% probability, H atoms and DiPP groups (bar ipso carbons) omitted for clarity.

C(13)–Ir(1)	2.016(6)	C(50)–Ir(1)	2.034(6)
C(22)–Ir(1)	1.984(7)	C(59)–Ir(1)	2.096(6)
N(3)–Ir(1)	1.982(5)	N(8)–Ir(1)	2.086(5)
C(22)–Ir(1)–C(13)	160.0(2)	C(58)–C(59)	1.358(8)
N(3)–Ir(1)–N(8)	173.1(2)	C(59)–C(60)	1.443(8)
N(3)–Ir(1)–C(13)	80.3(2)	C(60)–N(10)	1.280(8)
C(22)–Ir(1)–N(8)	94.6(2)	C(50)–Ir(1)–C(59)	171.0(2)
C(13)–Ir(1)–C(50)	94.8(2)	N(8)–Ir(1)–C(59)	93.1(2)
C(22)–Ir(1)–C(59)	88.5(2)	C(50)–Ir(1)–N(8)	78.0(2)

Table 49: Selected bond lengths (Å) and angles (°) for comp ound **144**

6.45 – Chemistry of cationic Ir(I) complexes

The synthesis of cationic Ir(I) complexes by replacing the chloride from **137** with other donor ligands (*e.g.* pyridine, CO) was facile. Initial attempts focussed on $(BAr^F)^-$ as the counterion; it was thought that using a large anion would enable easier crystallisation of the resulting complexes due to the presence of a large (CNC)Ir cation. Reaction of **137** with $NaBAr^F$ in pyridine led to the formation of a bright green solution. After removal of solvents, a green powder was formed which was extracted into Et_2O, filtered through Celite to remove NaCl and thoroughly dried *in vacuo* (Scheme 78).

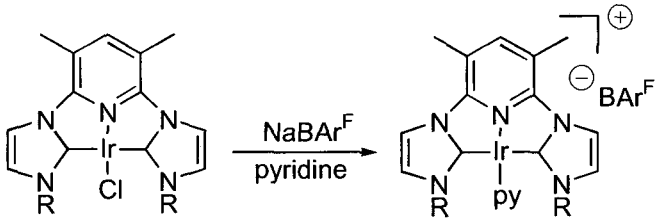

137 **145**

Scheme 78: Formation of a cationic Ir(I) species, R = DiPP

The ^1H NMR spectrum of **145** contains the expected doublets at 0.95 and 1.03 ppm, a septet at 2.86 ppm (the ^{i}Pr groups) and a singlet at 2.81 ppm (pyridine methyl groups). Two singlets in a 2:1 ratio were observed at 7.72 and 7.60 ppm corresponding to the *ortho* and *para* aromatic protons respectively of the $(BAr^F)^-$ anion. The presence of one equivalent of pyridine could also be determined from the resonances at 7.85 and 6.47 ppm. The resonance corresponding to the C_{NHC} was observed at 188.57 ppm in the $^{13}C\{^1H\}$ NMR spectrum. A very deshielded quartet for the CF_3 carbon was observed at 130.24 ppm and a quartet corresponding to the ipso carbon of the $(BAr^F)^-$ anion was observed at 162.82 ppm.

The slow diffusion of PE into a THF solution of complex **145** resulted in deposition of green crystals which were suitable for X-ray diffraction studies (Figure 72a).

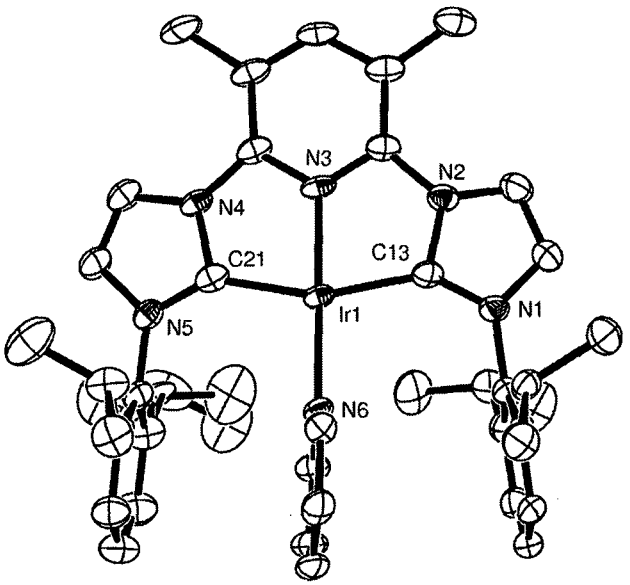

Figure 72a: ORTEP representation of the cation of **145**. Thermal ellipsoids at 50% probability, H atoms and $(BAr^F)^-$ anion omitted for clarity.

C(13)–Ir(1)	1.998(4)
C(21)–Ir(1)	1.994(4)
N(3)–Ir(1)	1.973(3)
N(6)–Ir(1)	2.058(3)
C(21)–Ir(1)–C(13)	156.90(16)
N(3)–Ir(1)–N(6)	173.31(13)
N(3)–Ir(1)–C(13)	79.03(15)
N(3)–Ir(1)–C(21)	78.91(16)
C(13)–Ir(1)–N(6)	101.33(14)
C(21)–Ir(1)–N(6)	101.38(15)

Table 50: Selected bond lengths (Å) and angles (°) for compound **145**

Complex **145** is a four-coordinate distorted square planar species with one (CNC) ligand and one pyridine ligand comprising the coordination sphere. The distortion is evident from the cis angles around the pyridine ring, none of which are within 10° of the ideal 90°. However, the true extent of the distortion is only apparent from viewing the cation parallel to the plane of the (CNC) ligand (Figure 72b).

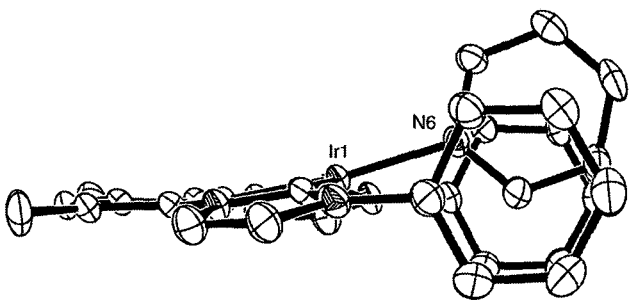

Figure 72b: ORTEP representation of the cation of **145**. Thermal ellipsoids at 50% probability, H atoms, $(BAr^F)^-$ anion and ^{i}Pr groups omitted for clarity.

It is obvious that complex **145** is severely distorted away from the ideal square planar geometry. The iridium centre is out of the plane defined by the two C_{NHC} and N_{py} atoms of the (CNC) ligand by 0.1462(35) Å. N(6) is even further out of the plane at 0.5365(90) Å. It is likely that this distortion is a result of π-stacking effects: face to face π-stacking is disfavoured when the aromatic rings are perfectly eclipsed, compared to π-stacking when the aromatic rings are only partially overlapping.[134]

One consequence of the distortion away from ideal geometry is that the Ir–N_{py} bond length for the non-chelating pyridine ring is not lengthened in order to minimise eclipsing of the aromatic rings. The difference in Ru–N_{py} bond lengths for the octahedral complex **134** was *ca.* 0.15 Å. This was a consequence of the octahedral geometry where the presence of two chlorides prevented the pyridine ring from distorting in the manner seen in **145**. Therefore, the only available distortion was lengthening the Ru–N_{py} bond to the non-chelating pyridine ring in order to minimise overlap of the aromatic rings. The square planar geometry of **145** allowed the non-chelating pyridine ring to adopt a staggered geometry with respect to the phenyl rings hence the difference in Ir–N_{py} bond lengths for **145** is *ca.* 0.08 Å. The Ir–C_{NHC} bond lengths are within the range of previously observed Ir(I)–C_{NHC} bond lengths.

Attempts at synthesising (CNC)Ir(I) carbonyl and ethylene complexes with $(BAr^F)^-$ as the anion were unsuccessful. Dissolving **137** and $NaBAr^F$ in THF, then bubbling either CO or ethylene through the solution resulted in a colour change from green to brown and green to orange respectively. However, after removal of solvents, sticky oils were the only isolated products which contained many impurities in the ^1H NMR spectrum. It was thought that the $(BAr^F)^-$ anion was preventing the product from crystallising so the anion was switched from $(BAr^F)^-$ to PF_6^-.

Bubbling CO through a solution of **137** and KPF_6 in THF for five minutes resulted in a colour change from green to brown. The reaction was left to stir under N_2 for 15 minutes after the bubbling of CO stopped and the solution changed colour from brown to purple. Addition of further CO to the purple solution resulted in a reversible reaction to a brown solution, which changed back to purple 15 minutes after removal of the CO source. All attempts at isolating the brown product were unsuccessful, however it is postulated that the brown product is a 5-coordinate Ir(I) dicarbonyl cation and the purple product is a 4-coordinate Ir(I) monocarbonyl cation (Scheme 79).

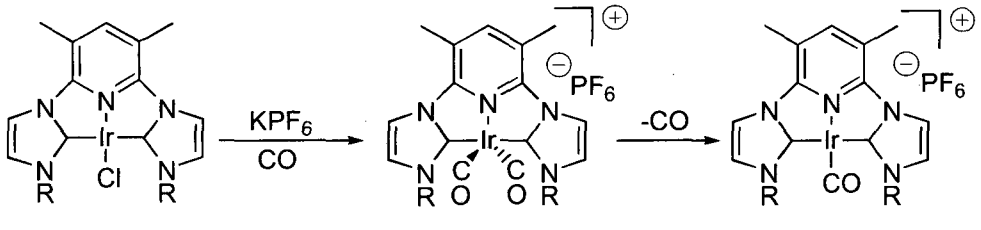

137 **146** **147**

Scheme 79: Formation of an Ir(I) monocarbonyl complex, R = DiPP

Removal of solvents resulted in the formation of a purple powder, which was extracted into MeCN and filtered through Celite to remove KCl. Slow diffusion of Et_2O into the MeCN solution resulted in the deposition of purple needles, which enabled structural characterisation to take place (Figure 73).

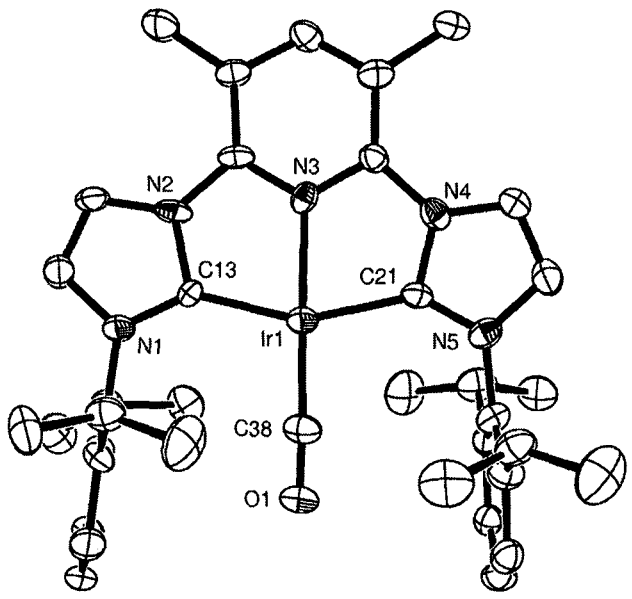

Figure 73: ORTEP representation of the cation of **147**. Thermal ellipsoids at 50% probability, H atoms and PF_6^- anion omitted for clarity.

C(13)–Ir(1)	1.982(8)
C(21)–Ir(1)	2.017(9)
N(3)–Ir(1)	2.033(7)
C(38)–Ir(1)	1.810(8)
C(38)–O(1)	1.178(10)
C(21)–Ir(1)–C(13)	155.3(3)
N(3)–Ir(1)–N(6)	178.8(4)
N(3)–Ir(1)–C(13)	77.9(3)
N(3)–Ir(1)–C(21)	77.4(3)
C(13)–Ir(1)–C(38)	103.3(4)
C(21)–Ir(1)–C(38)	101.4(4)

Table 51: Selected bond lengths (Å) and angles (°) for compound **147**

Complex **147** is a 4-coordinate distorted square planar species with one (CNC) ligand and one carbonyl ligand making up the coordination sphere. The distortion is solely a result of the geometric constraints of ligand **58** and is less severe than in complex **145**. The Ir–C_{NHC} bond lengths are consistent with the range of structurally characterised Ir(I)–C_{NHC} bond lengths. The C–O bond length of 1.178(10) Å is *ca.* 0.05 Å longer than the bond length of free CO (1.13 Å) and indicates substantial back-bonding from the electron rich Ir(I) centre to the carbonyl ligand.

The ^{1}H NMR spectrum contains all the expected ligand peaks, including two doublets at 1.13 and 1.16 ppm, a septet at 2.63 ppm (^{i}Pr groups) and a singlet at 2.77 ppm (pyridine methyl groups. There are two resonances above 185 ppm in the $^{13}C\{^1H\}$ NMR spectrum at 193.08 and 189.69 ppm. The former is assigned to the carbonyl and the latter the C_{NHC}. The IR stretch for the carbonyl is found at 1983 cm^{-1} and microanalysis is consistent with the reported structure.

The attempted synthesis of an ethylene complex was run under the same conditions as for compound **147**, substituting ethylene for CO. A colour change from green to orange

took place with no further change observed when the ethylene source was removed from the reaction. Crystallisation occurred from the slow diffusion of PE into a THF solution, affording yellow needles which were structurally characterised (Figure 74).

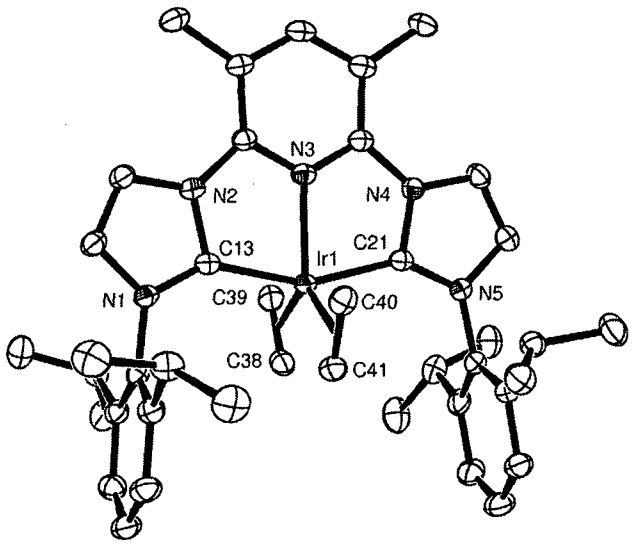

Figure 74: ORTEP representation of the cation of **148**. Thermal ellipsoids at 50% probability, H atoms and PF_6^- anion omitted for clarity.

C(13)–Ir(1)	2.019(3)
C(21)–Ir(1)	2.018(3)
N(3)–Ir(1)	2.046(2)
Ir(1)–Ct(1)	2.0372(1)
Ir(1)–Ct(2)	2.0271(2)
C(38)-C(39)	1.439(5)
C(40)-C(41)	1.422(4)
C(21)–Ir(1)–C(13)	156.64(11)
N(3)–Ir(1)–Ct(1)	117.53(7)
N(3)–Ir(1)–Ct(2)	117.53(7)
Ct(1)–Ir(1)–Ct(2)	126.17(1)
N(3)–Ir(1)–C(13)	78.42(10)
C(21)–Ir(1)–Ct(2)	96.04(7)

Table 52: Selected bond lengths (Å) and angles (°) for compound **148**. Ct = centre of C=C bond

Compound **148** is a 5-coordinate complex with one (CNC) ligand and two ethylene molecules (assuming each ethylene molecule occupies one coordination site) comprising the coordination sphere. The τ value of 0.51 (measurements of angles around the metal centre were taken from the centre of the ethylene C=C bond) indicates neither trigonal bipyramidal nor square-based pyramidal is an accurate description of the geometry. The Ir–C_{NHC} bond lengths are within the range of previously observed Ir(I)–C_{NHC} bond lengths. The ethylene C=C bond lengths are consistent with previously observed Ir(I) ethylene complexes.[135]

The ^{1}H NMR spectrum contains the expected ligand peaks of two doublets, one septet (^{i}Pr groups) and one singlet at 2.97 ppm integrating to 3H for the pyridine methyl groups. A large singlet at 1.90 ppm integrating to 8H was assigned to the protons of the ethylene groups. The C_{NHC} resonance in the $^{13}C\{^1H\}$ NMR spectrum was observed at 167.9 ppm. Two CH_2 resonances at 32.5 and 31.0 ppm were observed, which were assigned to the coordinated ethylene carbons.[136]

The ethylene C=C stretch is observed at 1598 cm^{-1}, consistent with other examples of ethylene coordinated to Ir(I).[137] Microanalysis was consistent with the observed structure.

A small amount of orange plates were also deposited along with the yellow needles. Unfortunately the diffraction pattern was smeary due to the crystals being multiply twinned and structural characterisation was not accomplished. However, the unit cell was notably different to that for complex **148**.

Attempts at synthesising an acetonitrile adduct were successful: after dissolving **137** in acetonitrile without KPF_6, a bright green solution was obtained. This implied the chloride anion was very labile – dissolving **137** in pyridine without the presence of a halide abstractor also resulted in the formation of a bright green solution analogous to the formation of **145**. However, to facilitate crystallisation, the chloride anion was abstracted with KPF_6 and complex **149** was isolated as a green powder (Scheme 80).

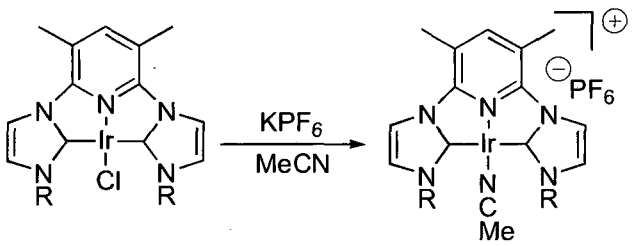

137 **149**

Scheme 80: Formation of an Ir(I) acetonitrile complex, R = DiPP

^{1}H NMR spectroscopy of compound **149** indicated the presence of one acetonitrile ligand, a singlet at 1.77 ppm integrating to 3H. The expected ligand peaks were present: two doublets at 1.15 and 1.12 ppm, a septet at 2.79 ppm (^{i}Pr groups) and a singlet at 2.84 ppm (pyridine methyl groups). The C_{NHC} resonance was observed at 188.71 ppm in the $^{13}C\{^1H\}$ NMR spectrum. Green crystals were grown from the slow diffusion of Et_2O into a MeCN solution of **149**, enabling structural characterisation (Figure 75).

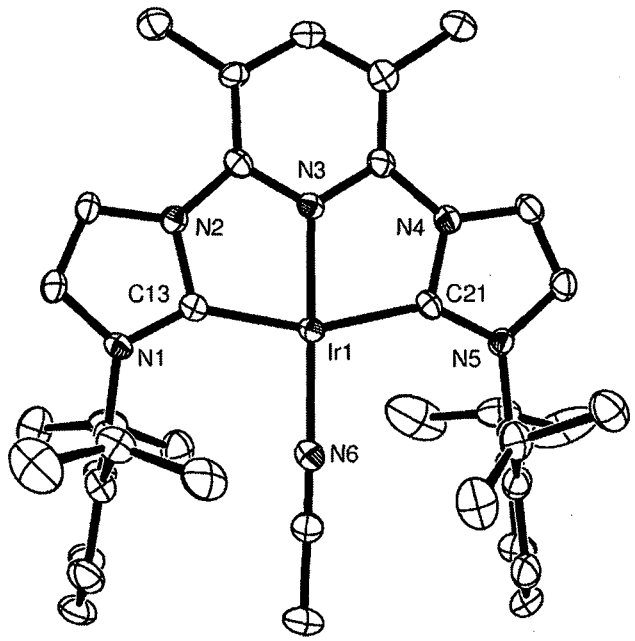

Figure 75: ORTEP representation of the cation of **149** showing one of four molecules in the asymmetric unit. Thermal ellipsoids at 50% probability, H atoms and PF_6^- anion omitted for clarity.

C(13)–Ir(1)	1.975(6)
C(21)–Ir(1)	1.990(6)
N(3)–Ir(1)	1.968(5)
N(6)–Ir(1)	1.980(5)
C(21)–Ir(1)–C(13)	158.1(2)
N(3)–Ir(1)–N(6)	178.3(2)
N(3)–Ir(1)–C(13)	79.5(2)
N(3)–Ir(1)–C(21)	78.6(2)
C(13)–Ir(1)–N(6)	99.4(2)
C(21)–Ir(1)–N(6)	102.5(2)

Table 53: Representative bond lengths (Å) and angles (°) for compound **149**

Complex **149** is a four-coordinate distorted square planar species with one (CNC) ligand and one acetonitrile ligand comprising the coordination sphere. Interestingly, there are four molecules in the asymmetric unit: a survey of the CDS carried out after the January 2007 update revealed that there were slightly more than 1200 compounds which crystallise with $Z'= 4$, out of over 400,000 total entries.[138]

The range of Ir–C_{NHC} bond lengths is consistent with the range of Ir–C_{NHC} bond lengths previously observed. Within experimental error, there is no difference between the Ir–N_{py} and Ir–N_{MeCN} bond lengths. Microanalysis was consistent with the observed structure.

Attempts at synthesising a less stable cationic Ir(I) species, through the use of an O-donor ligand, were undertaken using acetone. Dissolution of **137** and KPF_6 in dry acetone was accompanied by a colour change from a dark green, characteristic of solutions of **137**, to a very bright green, characteristic of cationic complexes of $(CNC)Ir^+$ cations. Crystallisation was attempted from the slow diffusion of Et_2O into the acetone solution but no green crystals were deposited. Instead, three different crystal types were deposited: very pale grey, yellow and orange, which could not be separated by chemical means. They were characterised structurally by picking crystals.

Structural characterisation of the pale grey crystals revealed a twinned species with a cell almost identical to that of complex **148**. Initially it was thought that an Ir(V) bis(peroxide) species had been formed, but further experiments using a small non-twinned crystal and synchrotron radiation revealed that complex **148** had actually been formed. The origin of the ethylene is not certain, although thermal decomposition of both acetone[139] and diethyl ether[140] have been known to produce ethylene. In both cases, molecular hydrogen was also observed as a byproduct. The yellow crystals turned out to be analogous to complex **144**, with PF_6^- anions replacing the triflate anions.

The orange crystals contained the same unit cell as the twinned orange plates which crystallised at the same time as complex **148**. No twinning was present this time and structural characterisation was possible (Figure 76).

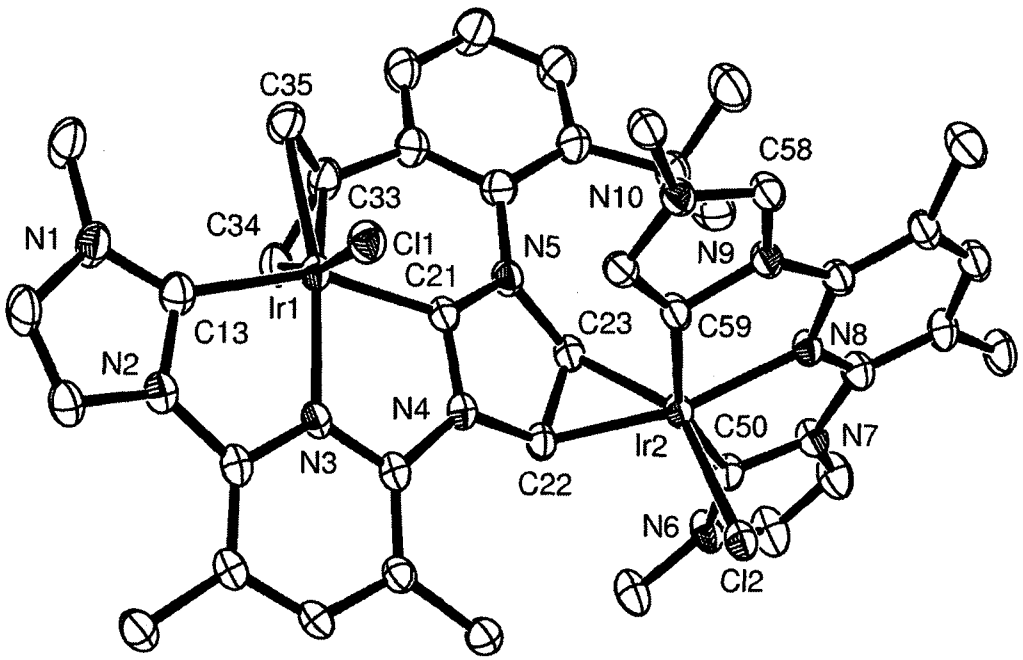

Figure 76: ORTEP representation of the cation of **150**. Thermal ellipsoids at 50% probability, H atoms, DiPP groups (bar *ipso* carbons and the decomposed DiPP group) and PF_6^- anion omitted for clarity.

C(13)–Ir(1)	2.065(3)	C(50)–Ir(2)	2.002(3)
C(21)–Ir(1)	2.015(3)	C(59)–Ir(2)	2.033(3)
N(3)–Ir(1)	2.026(3)	N(8)–Ir(2)	2.042(2)
C(33)–Ir(1)	2.117(3)	C(22)–Ir(2)	2.061(3)
C(34)–Ir(1)	2.129(4)	C(23)–Ir(2)	2.061(3)
C(35)–Ir(1)	2.187(4)	Ct(1)–Ir(2)	1.9277(4)
Cl(1)–Ir(1)	2.4460(9)	Cl(2)–Ir(2)	2.5187(11)
C(21)–Ir(1)–C(13)	155.55(13)	C(50)–Ir(2)–C(59)	156.77(12)
N(3)–Ir(1)–C(33)	141.46(13)	N(8)–Ir(2)–Ct(1)	140.40(7)
C(21)–Ir(1)–Cl(1)	96.10(9)	C(50)–Ir(2)–N(8)	77.94(11)
N(3)–Ir(1)–C(13)	77.62(12)	C(59)–Ir(2)–Cl(2)	88.22(9)
C(35)–C(33)–C(34)	116.7(3)	Ct(1)–Ir(2)–Cl(2)	127.50(2)

Table 54: Selected bond lengths (Å) and angles (°) for comp ound **150**. Ct = centre of C(22)–C(23) bond

Complex **150** contains two iridium centres, one in oxidation state +1 and one as a cationic +3 iridium centre. One PF_6^- anion is present in the asymmetric unit. The Ir(III) centre [crystallographic Ir(1)] contains two normally bound NHCs as part of a (CNC) pincer ligand, one chloride anion and one η^3-allyl group which comes from an unprecedented triple C–H activation of one of the isopropyl groups. Overall, it is a 5-coordinate 18-electron centre and the geometry is best described as distorted square-based pyramidal. The τ value, taking the middle carbon of the allyl moiety as representative of the whole group, is calculated to be 0.23, indicating a moderate amount of distortion is present.

The Ir(I) centre [crystallographic Ir(2)] contains an η^2 interaction of the unsaturated backbone of an NHC normally-bound to an Ir(III) centre [crystallographic Ir(1)]. This coordination mode is unprecedented for an NHC. The Ir(I) centre also contains one chloride and one (CNC) pincer ligand where one of the 'arms' has formed an abnormal carbene. Overall, it is also a 5-coordinate 18-electron species which can be described as distorted square-based pyramidal. The τ value of 0.27, taking the centre of the imidazol-2-ylidene C=C bond as representative of the whole group, indicates the distortion away from ideal square-based pyramidal is slightly more severe than the other Ir centre.

The Ir–C_{NHC} bond lengths range from 2.002(3) to 2.065(3) Å and are consistent with other structurally characterised Ir–C_{NHC} bond lengths in both +1 and +3 oxidation states. All the Ir–C_{NHC} bond lengths are shorter than the Ir–C_{allyl} bond lengths. The abnormal

Ir–C_{NHC} bond length is longer than the corresponding length in complex **144** but consistent with complex **133**, within experimental error. The Ir–C_{imid} bond lengths for the η^2 interaction are consistent with the longer range of the Ir–C_{NHC} bond lengths and, surprisingly, are shorter than the Ir–C_{allyl} bond lengths. Insufficient sample was recovered to enable elemental analysis.

6.46 – Possible mechanism of formation for **143**, **144** and **150**

Complexes **143** and **144** contain two unusual structural features (abnormal NHC and an opened imidazol-2-ylidene ring). Complex **150** contains three unusual structural features (abnormal NHC, η^2-interaction and formation of an allyl group from a DiPP moiety). It is unlikely that the unusual features are formed in one concerted step, hence the mechanisms of formation consist of several steps leading to the unusual features. One mechanism is proposed below and is speculative since no experimental evidence for any of the steps has yet been accumulated.

All three complexes contain one common feature, namely the abnormal NHC. The fact that NHCs are capable of coordination in an η^2 fashion through the unsaturated backbone opens up a possible mechanism of formation for abnormal NHCs in general. The first step is reductive elimination of an imidazolium salt from a metal centre containing a proton and a normally bound NHC: spontaneous loss of a free NHC is unlikely due to the strength of the Ir–C_{NHC} bond. The imidazolium salt next coordinates to the metal centre through the unsaturated backbone in an η^2 fashion. C–H activation in the 4- or 5-position of the pyridine ring reforms the metal hydride moiety, this time with an abnormal NHC bound to it (Scheme 81).

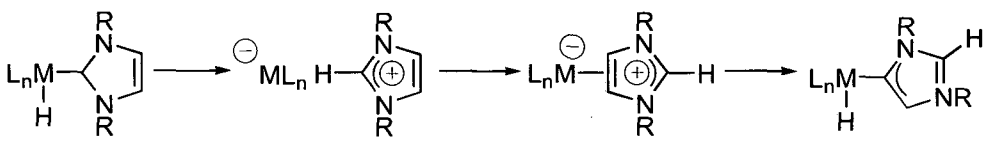

Scheme 81: Possible mechanism of formation for abnormal NHCs

Apart from the allyl moiety, the coordination sphere around the Ir(III) centre in complex **150** is similar to that of **137**, with only one normally bound (CNC) ligand and one chloride. Due to the fact that complex **137** has been isolated and does not undergo

spontaneous triple C–H activation to form an allyl group, it is likely that formation of the allyl moiety is the result of other driving forces within the reaction system.

It is also conceivable that the decomposed NHC ring in complexes **143** and **144** could have its origins in the η^2 interaction observed in complex **150**. If formation of the abnormal carbene is the first step, following the mechanism described above, the resultant lessening of the steric crowding at the metal centre may enable η^2-coordination of another molecule, forming intermediate **152** (Scheme 82).

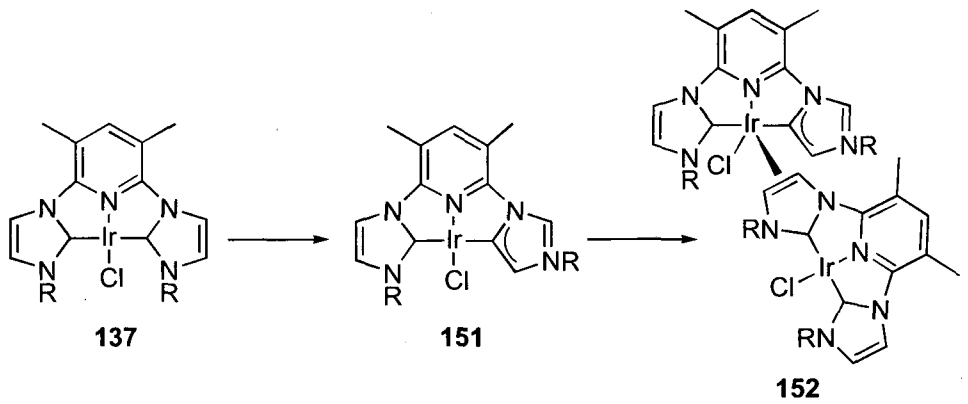

Scheme 82: Possible mechanism of formation leading to the imidazol-2-ylidene η^2 interaction, R = DiPP

From this point the mechanistic pathways diverge. It is possible that the deciding factor could be the amount of halide abstractor present in the reaction: complex **150** retains two chloride anions in addition to containing one non-coordinating anion, whereas complexes **143** and **144** do not contain any chloride anions.

If insufficient halide abstractor is present then intermediate **152** cannot lose the chloride anions. It is also very sterically encumbered around the 5-coordinate Ir centre, with the ^{i}Pr groups of the normally bound NHC clashing with the ^{i}Pr groups of the DiPP moiety attached to the η^2-coordinated NHC. Twisting of this DiPP group to relieve strain brings a methyl group into close proximity with the Ir centre, enabling C–H activation to take place.

However, if the DiPP group twists further, the methine carbon of the activated ^{i}Pr group bears a β-hydrogen which can also be C–H activated. Reductive elimination of H_2 leads to the formation of an olefin bound to the Ir centre in an η^2 fashion. A third C–H activation leads to the formation of an allyl group bound to Ir, along with a hydride

attached to Ir. Loss of H^- (and replacement with a PF_6^- anion to retain the Ir(III) oxidation state) results in the formation of **150** (Scheme 83).

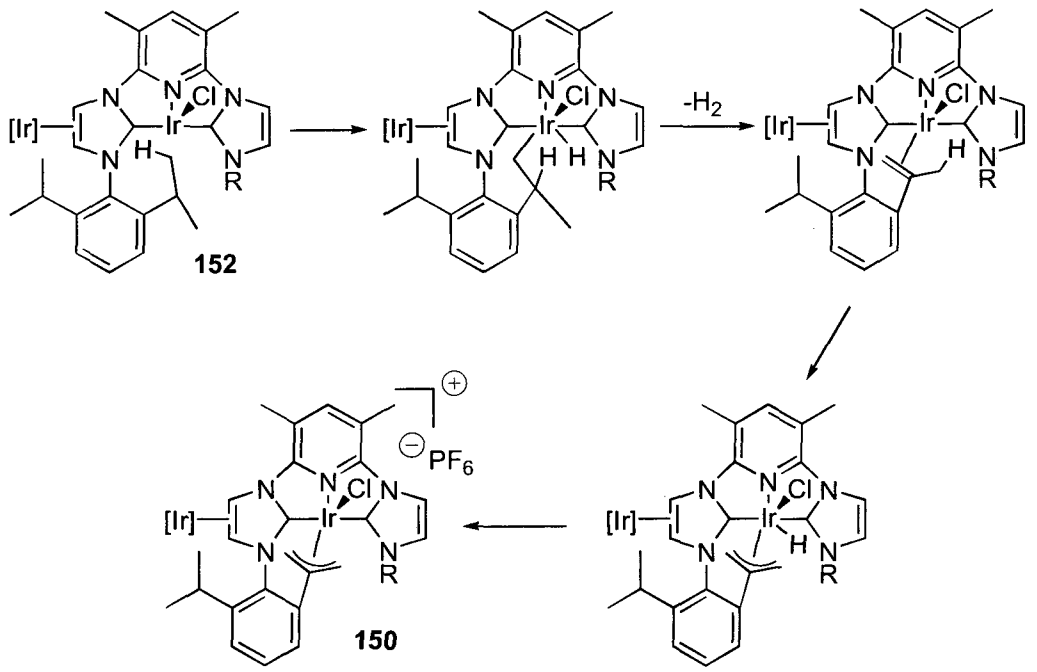

Scheme 83: Possible mechanism of formation for complex **150**, R = DiPP, [Ir] = $(CNC_{ab})IrCl$

However, if sufficient halide abstractor (MX) is present in the reaction, then the steric crowding of intermediate **152** can be relieved through loss of chloride from the Ir(I) centre bearing the η^2-coordinated NHC. This enables C–H activation of the η^2-coordinated NHC to take place, forming an Ir(III) vinyl hydride.

The next step is attack of the NHC lone pair on the vinyl carbon, also resulting in loss of coordination to the second Ir centre. This forms a zwitterionic species containing a cationic 4-membered nitrogen-containing ring, bound to the iridium centre in the 3-position, with an amide group in the 4-position. The zwitterionic nature of the intermediate is quickly lost, forming intermediate **153** which contains an imine functionality bound to a 4-membered ring in the 4-position (Scheme 84). The 4-membered ring is bound in the 3-position to a cationic Ir(III) centre which also contains a hydride.

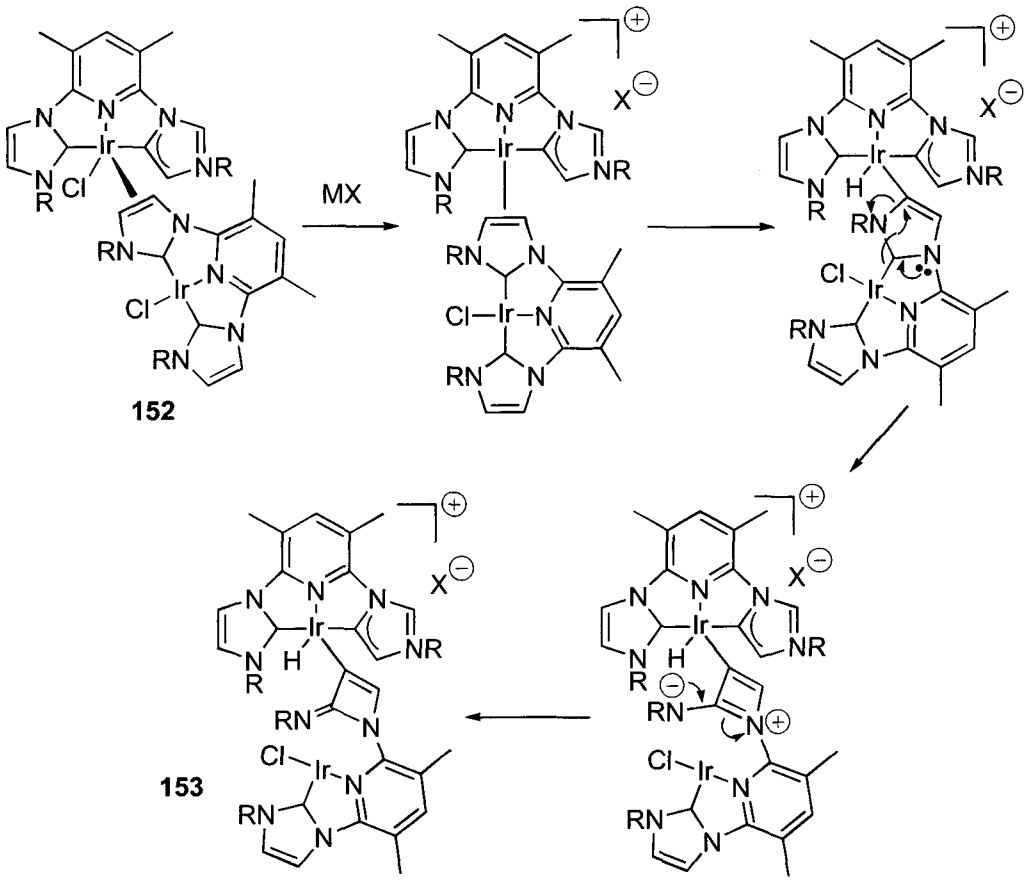

Scheme 84: Possible mechanism of formation of key intermediate **153**, R = DiPP

At this point, the mechanisms of formation of **143** and **144** differ. Complex **143** is an Ir(I) species, implying reduction from Ir(III) to Ir(I) had taken place. This is accomplished by abstraction of H^+ from the metal centre by the imine lone pair. The resulting cationic imine product tautomerises so the ring nitrogen is protonated, allowing attack of hydride at the imine carbon. This breaks open the 4-membered ring and forms the coordinated vinyl group.

The final step is transfer of pyridine and the normally bound NHC from one iridium centre to the other, resulting in the formation of compound **143** (Scheme 85).

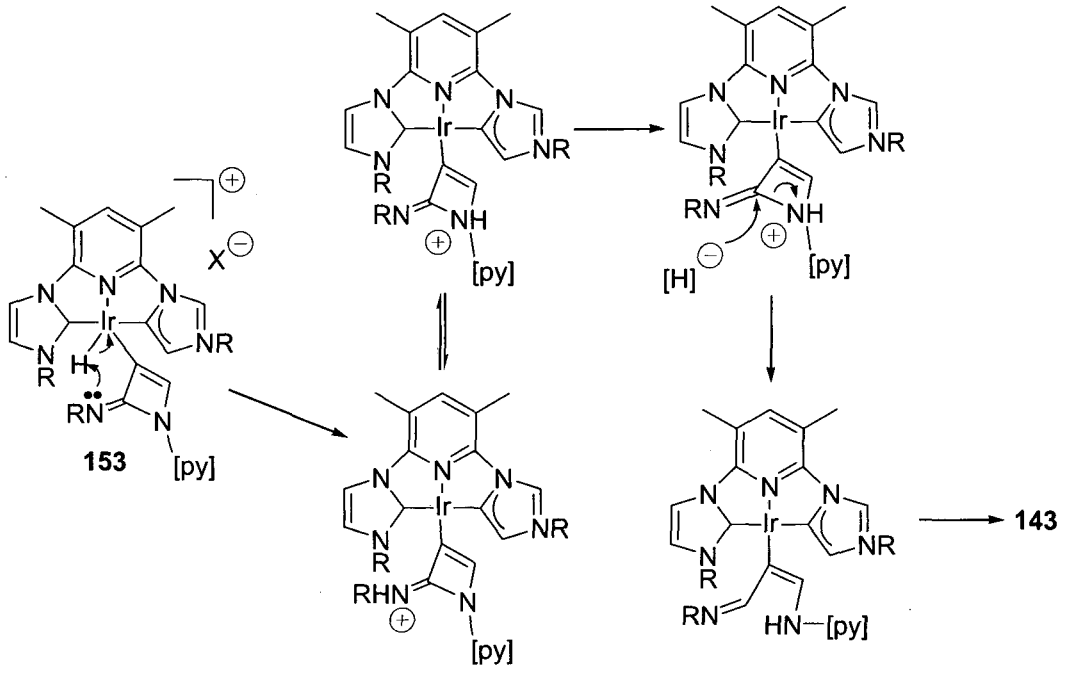

Scheme 85: Possible mechanism of formation of compound **143**, R = DiPP, [py] = (-NC)IrCl

However, complex **144** is an Ir(III) species which implies no reduction of intermediate **153** has taken place. This is accomplished by hydride shift from the iridium centre to the imine carbon, forming a dicationic Ir(III) centre. The non-coordinating anion (X^-) and the reformed amide anion balance the dicationic charge.

The next step is reformation of the imine, which breaks open the 4-membered ring and forms an amide anion on the pyridine-substituted nitrogen. Whilst this amide anion is stabilised by coordination to M^+, resulting in the second equivalent of X^- balancing the extra negative charge, subsequent protonolysis forms the coordinated vinyl group with the metal centre still in a +3 oxidation state and two equivalents of non-coordinating anion. Transfer of pyridine and NHC proceeds as above, affording complex **144** (Scheme 86).

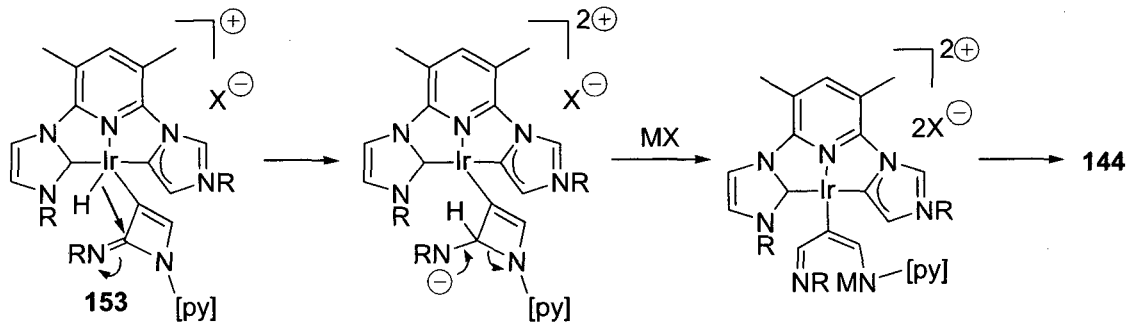

Scheme 86: Possible mechanism of formation of compound **144**, R = DiPP, [py] = (-NC)IrCl

6.47 – Catalysis

Complexes **137** and **145** were briefly screened for catalytic activity in the transfer hydrogenation of acetophenone. Many Ir(I) complexes of NHCs are good catalysts for this reaction (Scheme 87).[141]

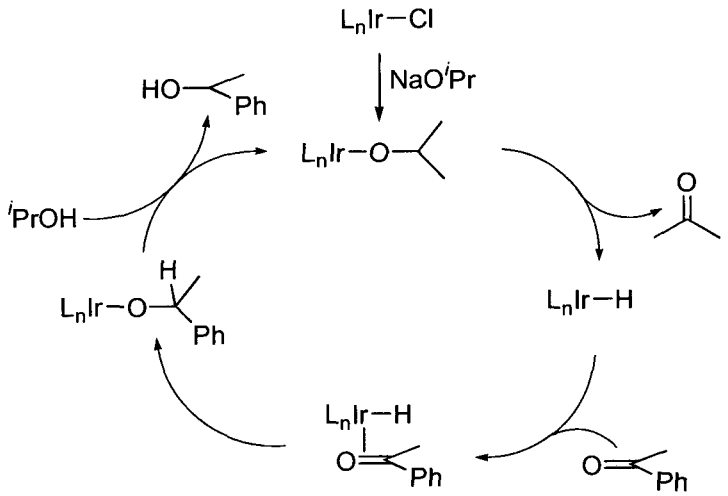

Scheme 87: Catalytic cycle for the transfer hydrogenation of acetophenone

A solution of either **137** or **145** in 5 mL IPA, with one equivalent of NaO^{i}Pr as base and the required amount of acetophenone (100 molar equivalents), were sealed under partial vacuum in a Youngs ampoule and heated to the desired temperature. Samples were taken at the denoted times and analysed by ^{1}H NMR. The yield was measured by integrating the resonance due to the acetophenone methyl group (a singlet at 2.50 ppm) relative to that of the 1-phenylethanol methyl group (a doublet at 1.38 ppm). The data are presented in tables 55 and 56.

Temp (°C)	Time (h)	Conv. (%)
80	3	83
80	20	93
50	3	88
50	20	96
RT	3	61
RT	20	81

Table 55: Catalytic data for the reduction of acetophenone with complex **137**. Conditions: 2 mmol acetophenone, 0.02 mmol **137**, NaO^{i}Pr, 5 mL IPA

Temp (°C)	Time (h)	Conv. (%)
80	3	94
80	20	94
50	3	95
50	20	95
RT	3	78
RT	20	>90

Table 56: Catalytic data for the reduction of acetophenone with complex **145**. Conditions: 2 mmol acetophenone, 0.02 mmol **145**, NaO^{i}Pr, 5 mL IPA

The data clearly shows that whilst both complexes are active catalysts, complex **145** is superior to **137**. At elevated temperatures, conversion is complete after three hours with **145** whereas with **137** it is only about 90% complete. At room temperature both complexes are slower, but complex **145** still manages a respectable 78% yield after three hours, increasing to over 90% after 20 hours.

The reaction with complex **145** was rerun at 40 °C and samples were taken every 30 minutes to monitor the conversion (Table 57).

Time (min)	30	60	90	120	150	180
Conv. (%)	49	78	85	92	94	95

Table 57: Catalytic data for the reduction of acetophenone with complex **145**. Conditions: 2 mmol acetophenone, 0.02 mmol **137**, NaO^{i}Pr, 5 mL IPA, 40 ℃.

The data shows the reaction is essentially complete after 2 hours. This is good in comparison to other Ir NHC complexes which utilise lower catalyst loadings but higher temperatures.[141, 142]

Reducing the catalyst loading to 0.1 mol% (1000 equivalents acetophenone) resulted in a substantial loss of activity at 40 °C, with only 30% conversion observed after 3 hours. An increased conversion of 82% was noted after 20 hours, but the reaction had still not reached the end point after this time. This is in contrast to the higher catalyst loading where the end point was reached after 3 hours at 40 °C.

6.5 – Summary

The reactivity of complex **40** with NaN_3 has been investigated, with an unexpected Ru(IV) peroxide being formed. Unfortunately, it was not possible to decompose the azides to form Ru(IV) and (VI) species. Unexpectedly, no Ru complex of ligand **58** could be isolated. A Rh(I) complex of **58** was isolated, but the ligand did not act as a pincer ligand.

A new (CNC) complex of Ir(I), **137**, was synthesised and its reactivity investigated. Much like Rh complex **42**, it is susceptible to oxidation to an Ir(III) complex by the oxidative addition of C–Cl bonds. It readily reacts with halide abstractors in the presence of simple donor ligands (*e.g.* CO, ethylene, acetonitrile) forming 4- and 5-coordinate cationic species.

Novel decomposition products were observed from the reaction of **137** with $NaNH_2$ and TlOTf. A bis(ligand)iridium species was observed in each case, although the oxidation state of the Ir centre was +1 when $NaNH_2$ was used and +3 when TlOTf was used. The proposed mechanism of formation occurs *via* an unprecedented binding mode for NHCs which was observed from the reaction of **137** with KPF_6 in acetone. The unsaturated backbone of an imidazol-2-ylidene ring acted as a 2-electron donor to another Ir centre. Also observed was a triple C–H activation of an ^{i}Pr group of a DiPP moiety; presumably the driving force was relief of steric strain.

Reaction of **137** with $NaO^{i}Pr$ led to the formation of a (CNC)IrH complex through spontaneous loss of acetone. Complex **137** and cationic species **145** were tested as catalysts for the transfer hydrogenation of acetophenone and proved to have good activity at reasonably low temperatures (92% conversion after 2 hours at 40 °C), although it dropped off as the catalyst loading was decreased.

Chapter 7

Conclusions

The known (CNC) pincer ligand **36** underwent decomposition *via* C–H activation of the 3- and 5-positions of the pyridine ring in certain reactions with Fe and Ir complexes. To inhibit these activation reactions, a novel methylated (CNC) pincer ligand **58** was synthesised and fully characterised (Scheme 88). Both **36** and **58** were used to synthesise a range of transition metal complexes from titanium to iridium. The metal complexes were fully characterised and their stoichiometric reactivity was explored.

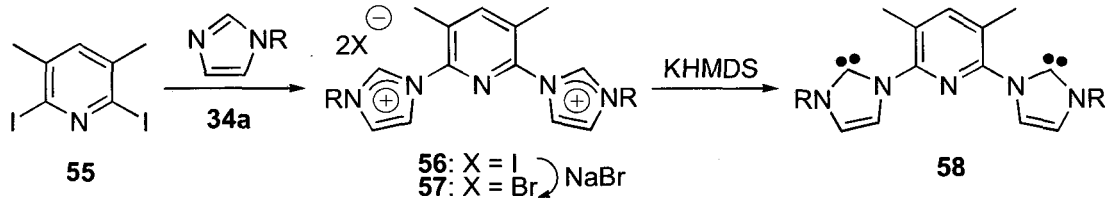

Scheme 88: Synthesis of novel (CNC) ligand **58**, R = DiPP

The effect of adding electron-donating groups to the pyridine moiety of the (CNC) pincer ligand was investigated by using the Ti=N bond as a spectroscopic handle. 6-coordinate Ti(IV) pincer complexes of **36**, **58** and the known (PNP) ligand **60** were synthesised and characterised. The Ti=N IR stretch and the Ti=N bond length were consistent with the idea that (CNC) ligands were better σ-donating ligands than (PNP) ligands, and that the extra methyl groups on the pyridine ring of **58** resulted in it being a better σ-donor than **36** (Figure 77).

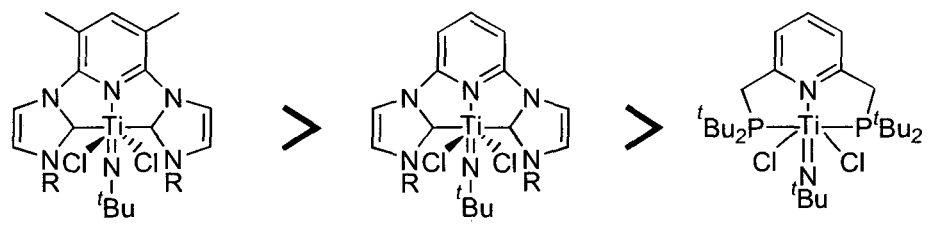

65, ν(Ti=N) = 1025 cm^{-1} **64**, ν(Ti=N) = 1037 cm^{-1} **66**, ν(Ti=N) = 1043 cm^{-1}

Figure 77: σ-Donating properties of ligands **36**, **58** and **60**: a comparison of the Ti=N bond in Ti(IV) imido dichloride complexes **64**, **65** and **66**, R = DiPP

However, similar investigations on 5-coordinate Fe(0) dicarbonyl complexes of **36**, **58** and **60** using CO as the spectroscopic handle indicated that (PNP) ligands were stronger σ-donating ligands than (CNC) ligands (Figure 78). This unexpected finding was consistent with a previous report[121] but inconsistent with the majority of literature data, although no explanation can yet be offered for this apparent abnormality.

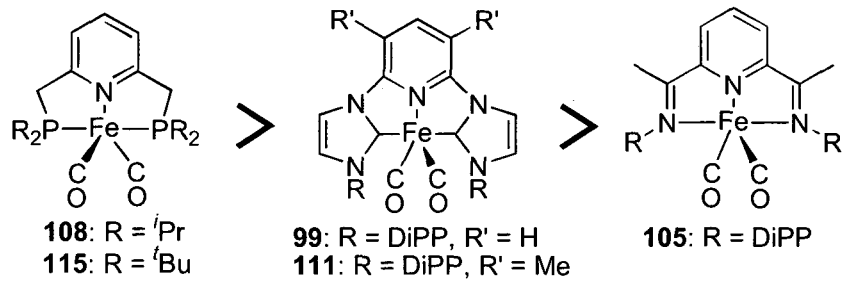

Figure 78: σ-Donating properties of ligands **36**, **58**, **60**, **102** and **106a** based on a comparison of the CO bond in Fe(0) dicarbonyl complexes **99**, **111**, **115**, **105** and **108** respectively

The synthesis of high oxidation state (CNC) metal complexes of first row transition metals through the oxidation of lower oxidation state metal complexes was accomplished by oxidising V(II) and V(III) species to V(IV) (Scheme 89).

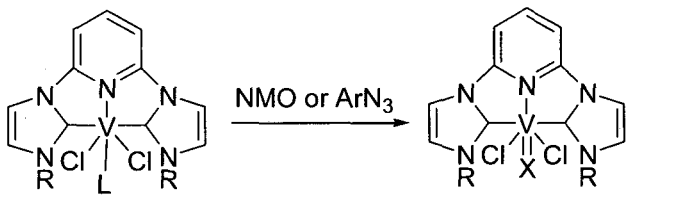

Scheme 89: Synthesis of V(IV) oxo and imido species, R = DiPP

Unfortunately, the +4 oxidation state was not attainable starting from Cr(III) and Mn(II) complexes of ligands **36** and **58**. However, the oxidation of Cr(II) complex **74** with NMO did afford Cr(III) complex **63** and Co(II) complex **82** was oxidised to Co(III) complexes **83** and **84** (Scheme 90).

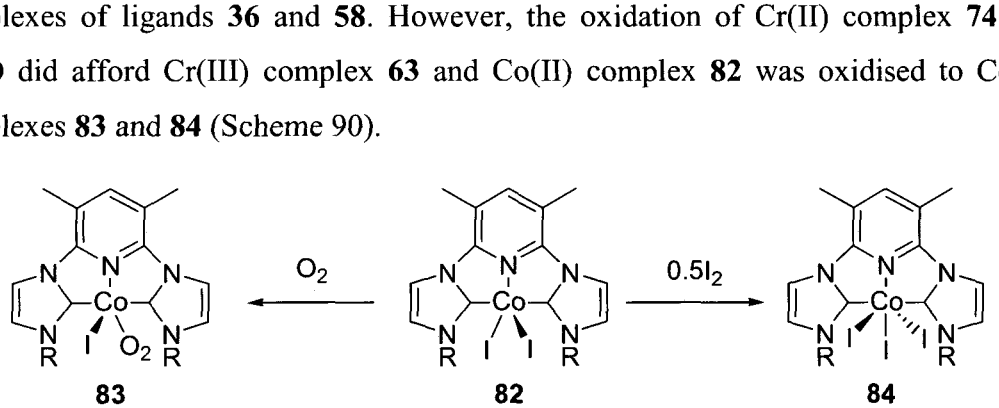

Scheme 90: Oxidation of **82** to Co(III) complexes, R = DiPP

The reaction of **36** with $NiBr_2$(DME) led to the synthesis of the first (CNC) pincer complex of nickel (Scheme 91). Substitution of one or both bromides was possible by judicious choice of halide abstractor. An octahedral Ni(II) complex was formed when **86** was reacted with AgOTf. However, the reaction of **36** with $NiMe_2$(TMEDA) led to an unexpected decomposition product where one of the NHC rings was completely destroyed (Scheme 91).

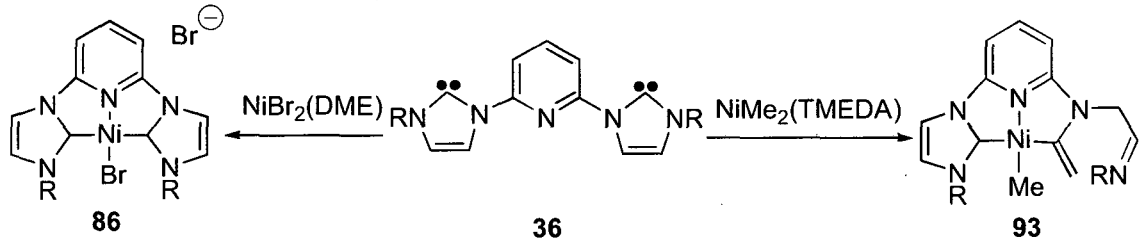

Scheme 91: Synthesis of (CNC)Ni pincer complexes, R = DiPP

The synthesis of Ni(II) complexes of **58** was accomplished in two ways: though the use of free ligand **58** and Ag complex **59**, forming Ni complexes **97** and **95** respectively. The reaction of complex **95** with Ag(OTf) led to an unprecedented "reverse transmetallation" reaction taking place whereby pincer ligand **58** was transferred from Ni to Ag. However, reaction of **97** with TlOTf led to only the non-coordinating bromide anion being substituted.

The reactivity of the published Fe(0) dinitrogen complex **48**[79] has been further explored. It accomplished the C–H activation of benzaldehyde anilide but was unreactive towards other sp^2 C–H bonds, instead forming the decomposition product **119**. It also reduced CO_2 to CO (Scheme 92), although the mechanism for this transformation is poorly understood.

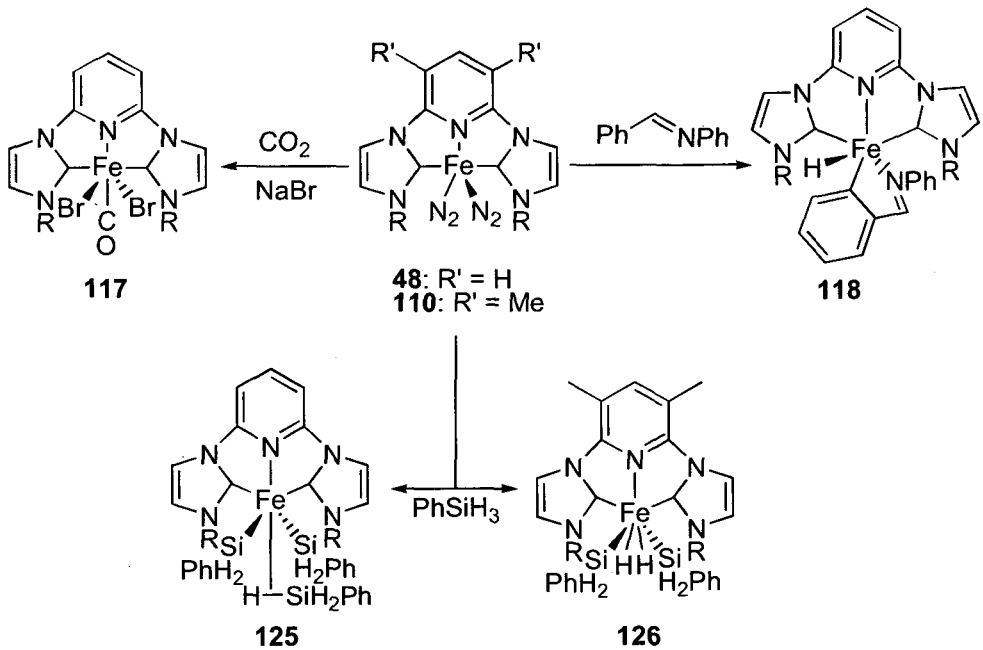

Scheme 92: Reactivity of dinitrogen complexes **48** and **110**, R = DiPP

Si–H activation of aromatic silanes has also been accomplished by **48** and **110** (Scheme 92) with substantially different products obtained depending on the starting dinitrogen complex. Both complexes **125** and **126** contain two phenylsilyl groups in addition to a

(CNC) ligand, but complex **125** is an Fe(II) species with an η^2-H–SiH_2Ph moiety occupying the position *trans* to the pyridine ring whereas complex **126** is an Fe(IV) species with two hydrides occupying the position *trans* to the pyridine ring.

Other aromatic silanes react in an analogous manner: diphenylsilane, mesitylsilane and *o*-tolylsilane all react with **48** and **110** affording a range of products with a variety of ligands (H_2, N_2, η^2-silane) in the position *trans* to the pyridine nitrogen.

The postulated mechanism of formation indicates that a double Si–H activation takes place, followed by reductive elimination of H_2 and substitution by the appropriate ligand. In the case of complex **126**, the strong σ-donating ligand **58** is capable of stabilising the dihydride before it reductively eliminates H_2, although the reason for this is not known.

A Ru(IV) peroxo species was formed by refluxing the literature complex **40**[62] with one equivalent of NaN_3 in THF under aerobic conditions. However, when two equivalents of NaN_3 were used, loss of PPh_3 was not observed (Scheme 93). Neither azide complex underwent photolytic or thermal decomposition to Ru nitride complexes.

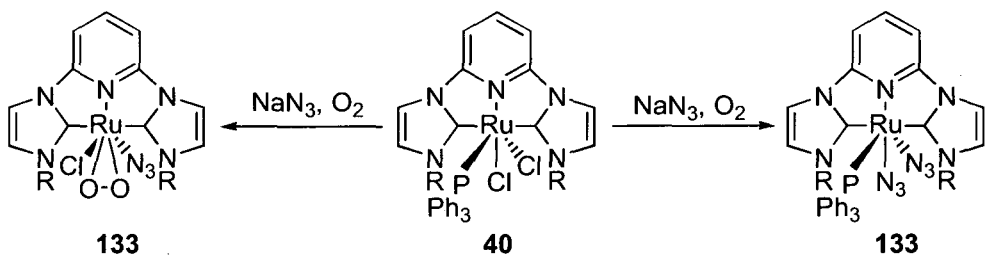

Scheme 93: Reactivity of **40** towards O_2 in the presence of NaN_3, R = DiPP

Previous attempts at synthesising Ir complexes of (CNC) ligands had resulted in ligand decomposition *via* C–H activation at the *meta* positions of the pyridine ring. However, ligand **58** contained methyl groups in the *meta* positions of the pyridine ring, enabling the synthesis of complex **137**, the first (CNC) pincer complex of iridium. The chloride in **137** was labile and a variety of cationic Ir(I) complexes were synthesised (Scheme 94), in addition to Ir(III) products formed through oxidative addition of, for example, DCM.

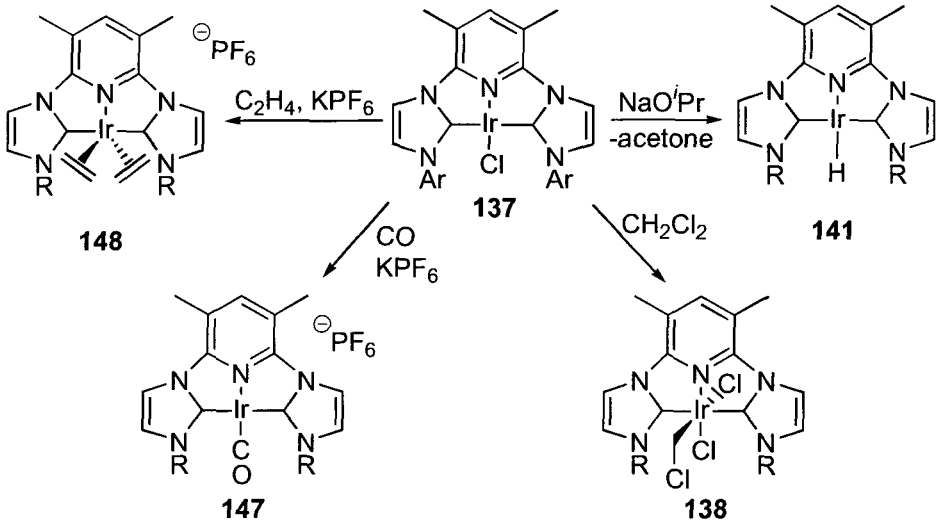

Scheme 94: Reactivity of novel Ir complex **137**, R = DiPP

An unprecedented coordination mode for NHCs was observed when complex **137** was reacted with KPF_6 in acetone. The unsaturated backbone of one NHC ring coordinated to another metal centre in an η^2 fashion (Scheme 95). Also observed was a novel decomposition product where one NHC ring was completely destroyed, forming a vinyl group. The oxidation state of the product depended on the reactant with an Ir(I) species obtained with $NaNH_2$ and an Ir(III) species obtained with TlOTf.

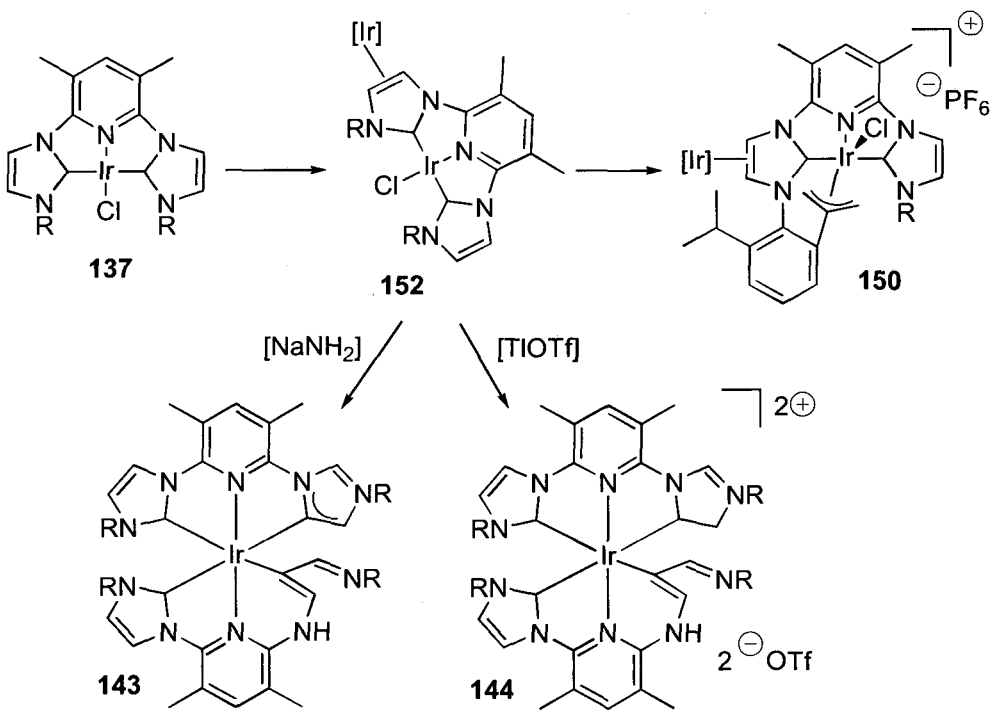

Scheme 95: Novel coordination mode and decomposition products observed for NHC rings, R = DiPP, [Ir] = $(CNC_{ab})IrCl$

Chapter 8

Experimental

8.1 - Instrumentation and Experimental Techniques

Unless otherwise stated, all reactions and manipulations were carried out under dry OFN using standard Schlenk line techniques, or in an inert atmosphere drybox (Braun UNILAB) containing OFN with constant monitoring of O_2 levels. Glassware was dried in a preheated oven (>160 °C) for at least 16 hours prior to use.

THF, petroleum ether (the fraction boiling between 40 and 60 °C), diethyl ether, pentane and benzene were distilled from purple/blue solutions of sodium benzophenone ketyl. DCM and MeCN were distilled from CaH_2; toluene and MeOH were distilled over Na and NaOMe respectively. Deuterated solvents were dried (C_6D_6 over NaK; CD_2Cl_2 and CD_3CN over CaH_2; $CDCl_3$ and $(CD_3)_2CO$ over 4Å molecular sieves, C_4D_8O over Na/benzophenone), distilled and degassed by freeze-pump-thaw cycles prior to use. Unless otherwise stated, commercial reagents were used as received from Acros, Aldrich, Avocado, Fisher or Lancaster. KHMDS was synthesised from the reaction of KH with $HN(SiMe_3)_2$ in refluxing PhMe; after filtration and removal of solvents, the resulting white solid was washed with PE and dried *in vacuo*. Purifications were carried out according to standard procedures.[143]

The following compounds were synthesised according to published procedures: 2,6-DiPP imidazole,[144] $Ti(N^tBu)Cl_2(py)_3$,[145] $Ti(NMes)Cl_2(NHMe_2)_2$,[91] $[Zr(\mu\text{-}NMes)Cl_2(THF)_2]_2$,[92] **67**, **62**,[76] *p*-tolyl azide,[146] **79**,[147] $Co(HMDS)_2$,[148] $NiMe_2(TMEDA)$,[116] $Fe(HMDS)_2$,[148] $FeBr_2(THF)_{1.5}$,[149] **45**,[77] **48**,[79] *o*-tolylsilane,[150] mesityl silane,[151] **40**,[62] $[RuCl_2(nbd)(py)_2]$,[152] $[Rh(COD)Cl]_2$,[153] $[Ir(COE)_2Cl]_2$,[154] $PhICl_2$[155] and $NaBAr^F$.[156]

Proton (^1H) and carbon ($^{13}C\{^1H\}$) NMR spectra were recorded on Bruker AV–300 or DPX–400 spectrometers at 300 K. ^1H NMR spectra were referenced to the residual protio-solvent signal and $^{13}C\{^1H\}$ spectra were referenced to the solvent signal. Chemical shifts are recorded in ppm (δ) downfield from $SiMe_4$, coupling constants (*J*) are expressed in Hz and approximated to the nearest 0.5 Hz. When reporting splitting patterns, the following abbreviations are used: (s) singlet, (d) doublet, (t) triplet, (q) quartet, (br) broad and (fs) fine splitting. $^{13}C\{^1H\}$ NMR spectra are reported as C, CH, CH_2 and CH_3, depending on the number of attached protons (0, 1, 2, 3 respectively); this being determined by DEPT-135 experiments. 2D spectra (H–H and H–C

correlation) were routinely used to assign signals from ^{1}H and $^{13}C\{^{1}H\}$ spectra and have not been specifically documented.

$^{19}F\{^{1}H\}$ and $^{31}P\{^{1}H\}$ NMR spectra were run on a Bruker AV–300 spectrometer at 300 K and referenced to an external sample of $CFCl_3$ or an 85% solution of H_3PO_4 respectively. $^{29}Si\{^{1}H\}$ NMR spectra were run on a Bruker DPX–400 spectrometer at 300 K and referenced to an external TMS sample.

Elemental analyses were carried out by Dr. Stephen Boyer at London Metropolitan University.

Magnetic susceptibilities were measured on a Johnson-Matthey balance or by using the Evans method[157] and are expressed in Bohr Magnetons (B.M.).

Infra-red spectra were recorded on a Perkin-Elmer 983G spectrometer as nujol mulls between KBr plates. Absorptions of relevance are given in wavenumbers (cm^{-1}).

Mössbauer spectra were recorded as a solid sample in zero magnetic field, at 80 and 273 K, on an ES-Technology MS–105 Mössbauer spectrometer with a 440 MBq ^{57}Co source in a rhodium matrix at ambient temperature. Spectra were referenced to a 25 μm iron foil at 298 K and spectral parameters were obtained by fitting with Lorentzian curves. The solid powder was prepared by grinding with boron nitride under an atmosphere of nitrogen. Thanks to Dr. David Evans at the John Innes Centre, Department of Biological Chemistry, for collecting the Mössbauer data.

X-ray datasets were collected on an Enraf Nonius KappaCCD area detector diffractometer with rotating FR591 anode and an Oxford Cryosystems low-temperature device operating in omega scanning mode with phi and omega scans to fill the Ewald sphere. The crystals were mounted on a glass fibre with silicon grease from Fomblin® vacuum oil (average MW = 3300, Aldrich catalogue number 317950). The programs used for control and integration were Collect, Scalepack and Denzo.[158, 159] All solutions and refinements were performed using PLATON[160] and the WinGX package and all software packages within.[161] CIFs were edited for publication using enCIFer.[162] Compounds **58**, **70**, **92**, **93**, **127**, **129**, **136**, **138**, **144**, **148** and **150** were collected on a Bruker SMART APEX2 CCD diffractometer at Daresbury station 9.8 or 16.9.[163]

H atoms were placed in geometrically assigned positions with fixed bond lengths of 0.95 Å (aromatic CH, terminal CH_2), 1.00 Å (methine CH), 0.99 Å (methylene CH_2) and 0.98 Å (CH_3) and refined using a riding model with a U_{iso}(H) value of $1.2U_{eq}$ (CH, CH_2) or $1.5U_{eq}$ (CH_3) of the parent atom. H atoms bonded to heteroatoms (N, Si, Fe, Ir) were located from the difference map and refined isotropically. Acknowledgements go to Drs. Mark Light, Joseph Wright, Neoklis Stylianides and Stephen Downing for their assistance in collecting and solving datasets, also to Prof. W. Clegg at the EPSRC single crystal synchrotron service at Daresbury for collecting datasets.

8.2 - Experimental for chapter 2

2,6-Dibromo-3,5-dimethylpyridine (**51**)

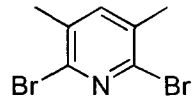

The title compound was synthesised following the procedure of Dunn and Guillermic[164] in an improved yield of 64%.

δ_H (400.0 MHz, $CDCl_3$): 7.32 (1H, s, Ar), 2.27 (6H, s, Me) ppm.
δ_C (100.6 MHz, $CDCl_3$): 141.26 (CH), 139.63, 134.36 (C), 21.09 (CH_3) ppm.

2,6-Diiodo-3,5-dimethylpyridine (**55**)

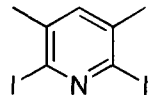

Compound **51** (15.0 g, 56.6 mmol), anhydrous NaI (34.1 g, 227.7 mmol), CuI (1.1 g, 5.7 mmol) and DMEDA (1.2 mL, 11.3 mmol) were suspended in refluxing 1,4-dioxane (250 mL) for 40 hours. After this time, the reaction was cooled, water (100 mL) was added and the solution extracted with DCM (3 × 50 mL). The combined organics were dried, filtered and the solvent was removed, affording a pale orange solid which was recrystallised from EtOH, yielding 16.77 g of white crystals in 83% yield.

δ_H (400.0 MHz, $CDCl_3$): 7.20 (1H, s, Ar), 2.30 (6H, s, Me) ppm.
δ_C (100.6 MHz, $CDCl_3$): 138.69 (C), 137.49 (CH), 119.38 (C), 25.20 (CH_3) ppm.
Analysis: Calc. for $C_7H_7NI_2$: C 23.42; H 1.97; N 3.90. Found: C 23.27; H 2.10; N 3.80.

(2,6-Bis(2,6-diisopropylphenyl)imidazolium)-3,5-dimethylpyridine diiodide (**56**)

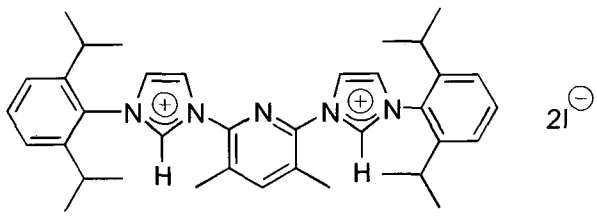

Compound **55** (5.0 g, 13.9 mmol) and 2,6-diisopropylphenyl imidazole (9.5 g, 41.7 mmol) were heated to 190 °C under vacuum in a sealed ampoule and stirred for 7 days. After this time, the solid was dissolved in a minimum amount of DCM, before adding Et_2O with vigorous stirring. The resulting grey solid was recovered by filtration, washed with Et_2O and dried azeotropically with toluene affording 17.0 g of the title compound as a pale grey powder in 96% yield. Crystallisation occurred from slow diffusion of Et_2O into a concentrated DCM solution.

δ_H (400.0 MHz, $CDCl_3$): 10.83 (2H, s, imidazolium CH), 9.11 (2H, s, Ar), 8.02 (1H, s, Ar), 7.56 (2H, t, J = 8.0 Hz, Ar), 7.42–7.35 (6H, m, Ar), 2.67 (6H, s, py-Me), 2.42 (4H, septet, J = 7.0 Hz, ^{i}Pr CH), 1.27, 1.20 (each 12H, d, J = 7.0 Hz, ^{i}Pr CH_3) ppm.
δ_C (100.6 MHz, $CDCl_3$): 147.61 (CH, Ar), 145.10, 142.09 (C, Ar), 138.27, 132.15 (CH, Ar), 131.60, 129.73 (C, Ar), 125.10, 124.76, 124.15, 123.98 (CH, Ar), 28.82 (CH, ^{i}Pr), 24.49, 24.13 (CH_3, ^{i}Pr), 18.23 (CH_3, py-Me) ppm.
Analysis: Calc. for $C_{37}H_{47}N_5I_2$: C 54.49; H 5.81; N 8.59. Found: C 54.58; H 5.85; N 8.51.

(2,6-Bis(2,6-diisopropylphenyl)imidazolium)-3,5-dimethylpyridine dibromide (**57**)

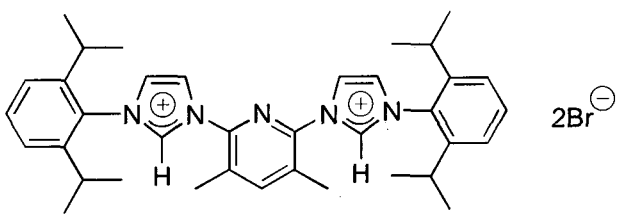

Compound **56** (20.0 g, 24.5 mmol) was dissolved in MeOH (300 mL) and a solution of NaBr (100.0 g, 980 mmol) in water (100 mL) was added. The reaction was stirred at RT for 6 hours after which time the solvents were removed, the solid extracted into a minimum amount of DCM, dried ($MgSO_4$) and filtered. Et_2O was added with vigorous stirring and the grey solid formed was isolated by filtration, washed with Et_2O and dried azeotropically with toluene, yielding 17.2 g of the title product as a pale grey powder in 97% yield. Crystallisation occurred from slow diffusion of Et_2O into a concentrated DCM solution.

δ_H (400.0 MHz, $CDCl_3$): 10.95 (2H, s, imidazolium CH), 9.14 (2H, s, Ar), 7.97 (1H, s, Ar), 7.47 (2H, t, J = 6.0 Hz, Ar), 7.33 (2H, s, Ar), 7.24 (4H, br s, Ar), 2.62 (6H, s, py-

Me), 2.33 (4H, septet, J = 6.5 Hz, ^{i}Pr CH), 1.18, 1.12 (each 12H, d, J = 6.5 Hz, ^{i}Pr CH_3) ppm.

δ_C (100.6 MHz, $CDCl_3$): 147.51 (CH, Ar), 144.79, 141.82 (C, Ar), 138.24, 131.83 (CH, Ar), 130.97, 129.53, 128.71, 127.91 (C, Ar), 124.90, 124.46, 124.01 (CH, Ar), 28.56 (CH, ^{i}Pr), 24.22, 23.82 (CH_3, ^{i}Pr), 18.06 (CH_3, py-Me) ppm.

Analysis: Calc. for $C_{37}H_{47}N_5Br_2$: C 61.58; H 6.56; N 9.71. Found: C 61.66; H 6.65; N 9.85.

(2,6-Bis(2,6-diisopropylphenyl)imidazol-2-ylidene)-3,5-dimethylpyridine (**58**)

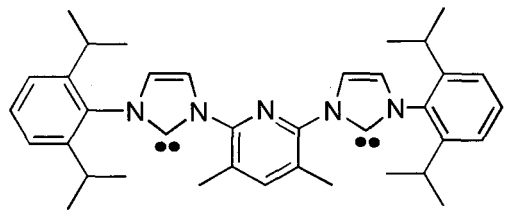

KHMDS (580 mg, 2.91 mmol) and compound **57** (1.0 g, 1.38 mmol) were cooled to –78 °C and cold (–78 °C) PE (50 mL) was added. The suspension was stirred at –78 °C for 15 mins then warmed to RT and stirred for 72 hours. After this time the solution was filtered, the solid washed with petrol (20 mL) and the combined petrol fractions were concentrated *in vacuo*, affording 600 mg of a pale yellow solid in 77% yield. Crystallisation occurred by cooling a saturated PE solution to –35 °C.

δ_H (400.0 MHz, C_6D_6): 7.73 (2H, d, J = 1.5 Hz, imidazol-2-ylidine), 7.36–7.30 (2H, m, Ar), 7.23–7.19 (3H, m, Ar), 6.62 (2H, d, J = 1.5 Hz, imidazol-2-ylidine), 2.92 (4H, septet, J = 7.0 Hz, ^{i}Pr CH), 2.76 (6H, s, py-Me), 1.25, 1.15 (each 12H, d, J = 7.0 Hz, ^{i}Pr CH_3) ppm.

δ_C (100.6 MHz, C_6D_6): 221.70 (C, C_{NHC}), 148.81 (C, Ar), 146.66 (CH, Ar), 146.43, 138.90, 129.34 (C, Ar), 129.12 (CH, Ar), 128.57, 125.70, 125.03 (C, Ar), 123.79, 121.21, 119.83 (CH, Ar), 28.66, 24.63 (CH_3, ^{i}Pr), 23.88 (CH, ^{i}Pr), 20.42 (CH_3, py-Me) ppm.

Analysis: Calc. for $C_{37}H_{45}N_5$: C 79.39; H 8.10; N 12.51. Found: C 79.50; H 8.13; N 12.44.

Bis((2,6-bis(2,6-diisopropylphenyl)imidazol-2-ylidene)-3,5-dimethylpyridine silver) (hexasilver octaiodide) (**59**)

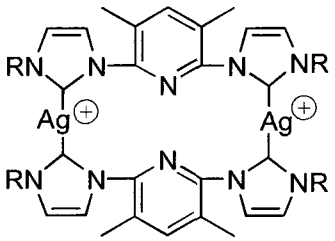

$[Ag_6I_8]^{2\ominus}$
R = DiPP

Ag_2O (232 mg, 1.00 mol) and compound **56** (816 mg, 1.00 mmol) were mixed as powders, dissolved in DCM (40 mL) and stirred for 4 hours with the exclusion of light. After this time the solution was filtered through celite, concentrated to ca. 10 mL and Et_2O (200 mL) was added to precipitate. The white solid formed was filtered and dried *in vacuo*, yielding 476 mg of the title compound in 92% yield. Crystallisation occurred from slow diffusion of Et_2O into a $CDCl_3$ solution, affording colourless crystals which decomposed slowly through solvent loss when removed from the mother liquor.

δ_H (400.0 MHz, C_6D_6): 7.87–7.66 (2H, m, Ar), 7.48–7.39 (2H, m, Ar), 7.32–7.18 (3H, m, Ar), 7.15–6.96 (4H, m, Ar), 2.51 (4H, br s, ^{i}Pr CH), 2.40 (6H, s, py-Me), 1.24, 1.14 (each 12H, br s, ^{i}Pr CH_3) ppm.

δ_C (100.6 MHz, C_6D_6): 188.27 (C, C_{NHC}), 147.51, 147.25 (C, Ar), 146.58, 146.25 (CH, Ar), 145.82, 145.08, 134.80 (C, Ar), 130.82, 130.58, 124.34, 123.71, 122.41 (CH, Ar), 28.42 (CH, ^{i}Pr), 24.81, 24.49 (CH_3, ^{i}Pr), 19.01 (CH_3, py-Me) ppm.

LRMS (ES$^+$, MeCN): 667.3 (M^{2+}, 100%)

Analysis: Calc. for $C_{74}H_{90}N_{10}Ag_8I_8$: C 29.65; H 3.03; N 4.67. Found: C 29.77, H 3.10; N 4.63.

8.3 - Experimental for chapter 3

(2,6-Bis(2,6-diisopropylphenyl)imidazol-2-ylidene)pyridine titanium(IV) *tert*-butylimido dichloride (**64**)

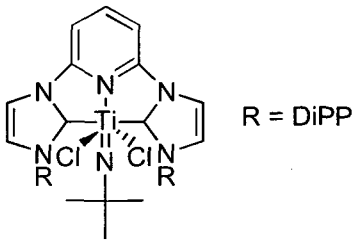

To a solution of Ti(N^{t}Bu)$Cl_2(py)_3$ (161 mg, 0.38 mmol) in THF (5 mL) was added a solution of **36** (200 mg, 0.38 mmol) in THF (15 mL). The reaction was stirred for 16 hours then the solvent was removed, the resultant solid washed with PE and dried *in vacuo*, affording 285 mg of the title compound as an orange powder in 95% yield. Crystallisation occurred by slow diffusion of petrol into a THF solution.

δ_H (300.1 MHz, C_6D_6): 7.23–7.03 (6H, m, Ar), 6.80 (2H, br s, Ar), 6.62 (1H, br t, J = 6.0 Hz, Ar), 6.43 (2H, d, J = 7.5 Hz, imidazol-2-ylidene CH), 6.36 (2H, d, J = 1.5 Hz, imidazol-2-ylidene CH), 3.27 (4H, septet, J = 6.5 Hz, ^{i}Pr CH), 1.68, 1.02 (each 12H, d, J = 6.5 Hz, ^{i}Pr CH_3), 0.54 (9H, s, ^{t}Bu CH_3) ppm.

δ_C (75.5 MHz, C_6D_6): 200.72 (C, C_{NHC}), 148.18, 146.76 (C, Ar), 141.96 (CH, Ar), 137.42 (C, Ar), 130.29, 128.34, 124.88, 124.57, 123.53 (CH, Ar), 114.55, 107.79 (CH, imidazol-2-ylidene), 67.83 (C, ^{t}Bu), 31.91 (CH_3, ^{t}Bu); 28.62, 25.87 (CH_3, ^{i}Pr); 24.16 (CH, ^{i}Pr) ppm.

LRMS (ES$^+$, MeCN): 721.3 ([M + H]$^+$, 100%)

IR (nujol mull): Ti=N 1037 cm^{-1}

Analysis: Calc. for $C_{39}H_{50}N_6TiCl_2$: C 64.91; H 6.98; N 11.65. Found: C 65.01, H 7.05; N 11.60.

(2,6-Bis(2,6-diisopropylphenyl)imidazol-2-ylidene)-3,5-dimethylpyridine titanium(IV) *tert*-butylimido dichloride (**65**)

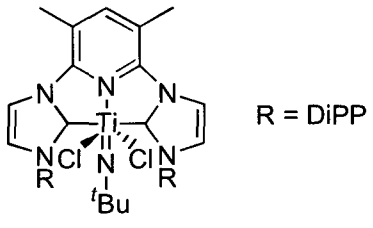

$Ti(N^tBu)Cl_2(py)_3$ (91 mg, 0.21 mmol) and **58** (120 mg, 0.21 mmol) were mixed as powders, dissolved in THF (20 mL) and stirred for 16 hours. After this time the solvent was removed, the resulting solid was washed with PE (20 mL) and dried *in vacuo*, affording 147 mg of the title compound as an orange powder in 92% yield. Crystallisation occurred by slow diffusion of petrol into a THF solution.

δ_H (400.0 MHz, C_6D_6): 7.29 (2H, br s, imidazol-2-ylidene CH), 7.23–7.03 (7H, m, Ar), 7.08 (2H, br s, imidazol-2-ylidene CH), 3.34 (4H, septet, J = 7.0 Hz, ^{i}Pr CH), 1.86 (6H, s, py-Me), 1.67, 1.05 (each 12H, d, J = 7.0 Hz, ^{i}Pr CH_3), 0.49 (9H, s, ^{t}Bu) ppm.
δ_C (100.6 MHz, C_6D_6): 200.86 (C, C_{NHC}); 149.90 (CH, Ar), 146.96, 145.53, 137.89 (C, Ar), 130.12, 124.62 (CH, Ar), 123.92 (CH, imidazol-2-ylidene), 120.27 (C, Ar), 117.92 (CH, imidazol-2-ylidene), 66.60 (C, ^{t}Bu), 32.04 (CH_3, ^{t}Bu), 28.65 (CH, ^{i}Pr), 26.04, 24.23 (CH_3, ^{i}Pr), 20.11 (CH_3, py-Me) ppm.
IR (nujol mull): Ti=N 1025 cm^{-1}
Analysis: Calc. for $C_{41}H_{54}N_6TiCl_2$: C 65.69; H 7.26; N 11.21. Found: C 65.61, H 7.29; N 11.07.

(2,6-Bis(di-*tert*-butylphosphinomethyl)pyridine) titanium(IV) *tert*-butylimido dichloride (**66**)

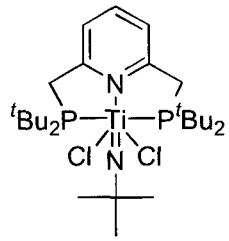

To a solution of $Ti(N^tBu)Cl_2(py)_3$ (218 mg, 0.51 mmol) in THF (5 mL) was added a solution of **60** (200 mg, 0.51 mmol) in THF (15 ml) at 0 °C. The reaction was stirred for 15 mins at 0 °C and then for 16 hours at RT. After this time solvents were removed, the resultant solid was washed with PE (20 mL) and dried *in vacuo*, affording 143 mg of an orange solid in 47% yield.

δ_H (400.0 MHz, C_6D_6): 7.22–7.10 (3H, m, Ar), 3.04 (4H, d, J = 3.5 Hz, CH_2), 1.05 (45H, d, J = 10.5 Hz, ^{t}Bu) ppm.

δ_C (100.6 MHz, C_6D_6): 160.21 (C, d, J = 15 Hz Ar); 136.61 (CH, Ar); 119.44 (CH, d, J = 10 Hz, Ar); 31.03 (CH_2, d, J = 26 Hz, CH_2); 30.49 (C, d, J = 24 Hz, P^{t}Bu); 29.45 (CH_3, N^{t}Bu); 28.54 (CH_3, d, J = 14 Hz, P^{t}Bu); 24.4 (C, N^{t}Bu) ppm.

δ_P (121.5 MHz, C_6D_6): 35.9 ppm.

IR (nujol mull): Ti=N 1043 cm^{-1}

Analysis: Calc. for $C_{27}H_{52}N_2Cl_2TiP_2$: C 55.39; H 8.95; N 4.79. Found: C 55.51; H 9.03; N 4.92.

(2,6-Bis(2,6-diisopropylphenyl)imidazol-2-ylidene)pyridine vanadium(II) dibromide, THF adduct (**68**)

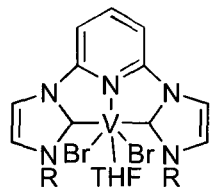

R = DiPP

To a stirred solution of **67** (225 mg, 0.31 mmol) in THF (20 mL) at –78 °C was added mesitylmagnesium bromide (0.53 mL of a 1.3 M soln. in THF, 0.69 mmol) dropwise. The solution was warmed slowly to RT and stirred for 72 hours. After this time, the solution was filtered through Celite, solvents were removed *in vacuo* and the resulting solid was crystallised by layering a THF solution with PE.

μ_{eff}: 3.83 B.M.

Analysis: Calc. for $C_{39}H_{49}N_5OBr_2V$: C 57.50; H 6.06; N 8.60. Found: C 57.46; H 6.20; N 8.40.

(2,6-Bis(2,6-diisopropylphenyl)imidazol-2-ylidene)pyridine vanadium(IV) oxide dichloride (**70**)

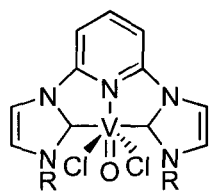

R = DiPP

To a stirred suspension of **62** (1.10 g, 1.60 mmol) in THF (100 mL) under a counterflow of N_2 was added NMO (0.21 g, 1.76 mmol) and the reaction was stirred for 16 hours at

RT. After this time, a green solution with a dark precipitate had formed which was diluted with THF (50 mL), filtered through Celite and concentrated *in vacuo*, affording 965 mg of the title compound as a green solid in 90% yield. Diffraction quality crystals were grown by layering a THF solution with petrol.

LRMS (ES$^+$, MeCN): 266.6 ($[M + 2H - VOCl_2]^{2+}$, 31%), 633.1 ($[M - Cl]^+$, 100%)

μ_{eff}: 1.66 B.M.

IR (nujol mull): V=O 974 cm^{-1}

Analysis: Calc. for $C_{35}H_{41}N_5OCl_2V$: C 62.78; H 6.17; N 10.46. Found: C 62.54; H 6.24; N 10.54.

(2,6-Bis(2,6-diisopropylphenyl)imidazol-2-ylidene)pyridine vanadium(IV) oxide bis(tetrafluoroborate), bis(acetonitrile) adduct (**71**)

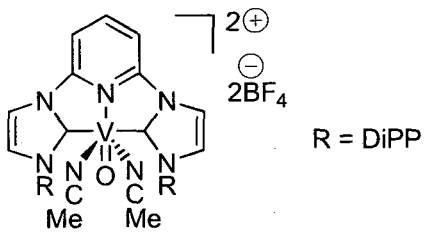

Compound **70** (150 mg, 0.22 mmol) and $AgBF_4$ (92 mg, 0.47 mmol) were mixed as solids with the exclusion of light, dissolved in MeCN (15 mL) and stirred for 4 hours at RT. After this time, a blue solution with a white precipitate had formed which was filtered through celite and concentrated *in vacuo*, affording 191 mg of the title compound as a blue-green solid in 97% yield. Crystallisation occurred by slow diffusion of Et_2O into a concentrated MeCN solution.

LRMS (ES$^+$, MeCN): 299.2 ($[M - 2MeCN]^{2+}$, 100%)

μ_{eff}: 1.79 B.M.

IR (nujol mull): 976 cm^{-1}

Analysis: Calc. for $C_{39}H_{47}N_7B_2F_8V$: C 54.82; H 5.54; N 11.48. Found: C 54.74, H 5.41; N 11.65.

(2,6-Bis(2,6-diisopropylphenyl)imidazol-2-ylidene)pyridine vanadium(IV) *para*-tolylimido dichloride (**72**)

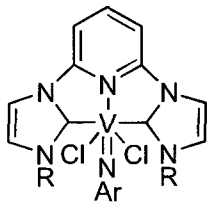

R = DiPP
Ar = *p*-C_6H_4Me

To a stirred suspension of **67** (200 mg, 0.28 mmol) in THF (20 mL) under a counterflow of dry N_2 was added *p*-tolylazide (37 mg, 0.28 mmol) and the reaction was stirred for 72 hours at RT. After this time, a brown solution had formed which was concentrated *in vacuo*, affording 150 mg of the title compound as a brown solid in 72% yield. Brown needles were grown by layering a THF solution with PE, which were exceptionally sensitive to solvent loss.

LRMS (ES^+, MeCN): 614.2 ($[M - C_7H_7NCl_2 + O_2]^+$, 70%), 722.3 ($[M - Cl]^+$, 100%)

μ_{eff}: 1.66 B.M.

IR (nujol mull): V=N 970 cm^{-1}

Analysis: Calc. for $C_{42}H_{48}N_6Cl_2V$: C 66.49; H 6.38; N 11.08. Found: C 66.32; H 6.50; N 10.97.

(2,6-Bis(2,6-diisopropylphenyl)imidazol-2-ylidene)pyridine niobium(III) trichloride (**73**)

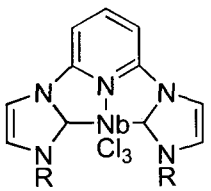

R = DiPP

A solution of **36** (1.98 g, 2.25 mmol) in THF (50 mL) at –78 °C was added to a solution of $NbCl_3$(DME) (0.65 g, 2.25 mmol) in THF (40 mL). The reaction was stirred for 15 mins then warmed to RT and stirred for 4 hours. After this time, the solution was filtered through celite and solvents were removed *in vacuo*, affording 1.56 g of a purple powder in 95% yield. Crystallisation occurred from layering a THF solution with PE.

μ_{eff}: 2.04 B.M.

Analysis: Calc. for $C_{39}H_{49}N_5ONbCl_3$: C 57.51; H 5.65; N 9.58. Found: C 57.58; H 5.79; N 9.42

(2,6-Bis(2,6-diisopropylphenyl)imidazol-2-ylidene)pyridine chromium(II) dichloride, THF adduct (**74**)

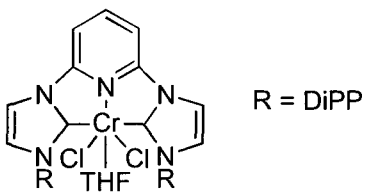

To a suspension of $CrCl_2$ (231 mg, 1.88 mmol) in THF (25 mL) was added a solution of **36** (1.0 g, 1.88 mmol) in THF (75 mL) at –78 °C. The reaction was stirred for 15 mins, then warmed to RT and stirred for 16 hours. After this time, the solvent was removed under partial vacuum (solid decomposed if exposed to high vacuum) affording 1.26 g of a purple solid in 92% yield.

μ_{eff}: 4.89 B.M.

Analysis: Calc. for $C_{39}H_{49}N_5OCrCl_2$: C 64.45; H 6.80; N 9.64. Found: C 64.57; H 6.75; N 9.60

(2,6-Bis(2,6-diisopropylphenyl)imidazol-2-ylidene)pyridine molybdenum(VI) dioxide chloride (chloride) (**75**)

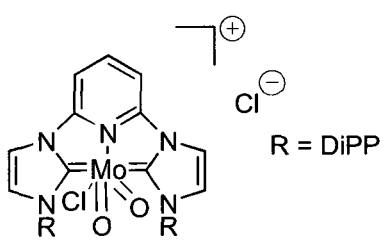

MoO_2Cl_2 (75 mg, 0.38 mmol) and **36** (200 mg, 0.38 mmol) were dissolved in THF (25 mL) and stirred for 16 hours at RT. After this time, the solution was filtered and crystallised by slow diffusion of PE, yielding 242 mg of purple microcrystals in 88% yield.

δ_H (400.0 MHz, CD_2Cl_2): 9.73, 9.21 and 8.61 (all 1H, br s, Ar), 7.53–7.21 (10H, m, Ar), 2.68 and 2.22 (both 2H, br s, ^{i}Pr CH), 1.39–1.01 (24H, m, ^{i}Pr CH_3) ppm.

δ_C (100.6 MHz, CD_2Cl_2): 181.86 (C, C_{NHC}), 148.33 (CH, Ar), 146.91 (C, Ar), 141.92 (CH, Ar), 135.98, 133.24 (C, Ar), 127.95, 125.34, 125.14 (CH, Ar), 29.22, 26.16, 25.93, 24.99, 23.42, 23.12 (CH/CH_3, ^{i}Pr) ppm.

IR (nujol mull): Mo=O 951 and 941 cm^{-1}

Analysis: Calc. for $C_{35}H_{41}N_5O_2MoCl_2$: C 57.34; H 5.66; N 9.59. Found: C 57.44; H 5.54; N 9.70.

(2,6-Bis(2,6-diisopropylphenyl)imidazol-2-ylidene)pyridine manganese(II) dibromide (**77**)

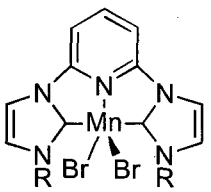

R = DiPP

To a stirred suspension of $MnBr_2$ (0.61 mg, 2.8 mmol) in THF (20 mL) at –78 °C was added a solution of **36** (1.50 g, 2.8 mmol) in THF (40 mL) at –78 °C. The solution was stirred at –78 °C for 15 minutes then warmed to RT and stirred for 16 hours. After this time, solvents were removed *in vacuo*, affording 2.15 g of the title compound as an orange-yellow powder in 93% yield. Crystallisation occurred by slow diffusion of PE into a concentrated THF solution.

μ_{eff}: 5.87 B.M.

Analysis: Calc. for $C_{35}H_{41}N_5MnBr_2 \cdot C_4H_8O$: C 57.22; H 6.03; N 8.56. Found: C 57.11; H 6.00; N 8.47.

(2,6-Bis(2,6-diisopropylphenyl)imidazol-2-ylidene)-3,5-dimethylpyridine manganese(II) dibromide (**78**)

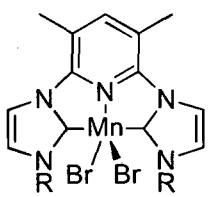

R = DiPP

$MnBr_2$ (96 mg, 0.45 mmol) was suspended in THF (10 mL) and a solution of **58** (250 mg, 0.45 mmol) in THF (20 mL) was added at RT. The resulting suspension was stirred for 16 hours at RT, after which time all the $MnBr_2$ had dissolved. Solvents were then

removed *in vacuo*, affording 326 mg of the title compound as an orange powder in 94% yield. Crystallisation occurred from slow diffusion of Et_2O into a concentrated DCM solution.

μ_{eff}: 5.95 B.M.

Analysis: Calc. for $C_{37}H_{45}N_5MnBr_2$: C 57.38; H 5.86; N 9.04. Found: C 57.33; H 5.75; N 8.95.

Dimethyl manganese(II) bis(1,3-di*iso*propyl-4,5-dimethylimidazol-2-ylidene) (**80**)

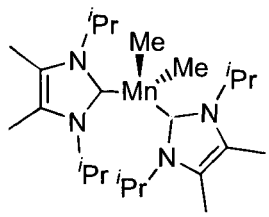

To a solution of $Mn(acac)_3$ (251 mg, 0.70 mmol) in Et_2O (15 mL) was added a solution of **79** (252 mg, 1.40 mmol) in Et_2O (15 mL) at –78 °C, then dropwise MeLi (1.3 mL of a 1.6 M soln. in Et_2O, 2.10 mmol). The reaction was stirred for 15 mins, then warmed to RT and stirred for 4 hours. After this time a grey precipitate was filtered, solvents removed and the resulting solid extracted into petrol. Crystallisation occurred at -35 °C from a concentrated petrol solution. Yield: 127 mg of an orange solid, 93%. The orange crystals reacted with Fomblin® with evolution of gas whilst attempting to mount them onto a pip for structural characterisation.

μ_{eff}: 5.88 B.M.

Analysis: Calc. for $C_{20}H_{38}N_4Mn$: C 61.68; H 9.83; N 14.39. Found: C 61.79; H 9.97; N 14.27.

8.4 - Experimental for chapter 4

(2,6-Bis(2,6-diisopropylphenyl)imidazol-2-ylidene)pyridine cobalt(II) diiodide (**82**)

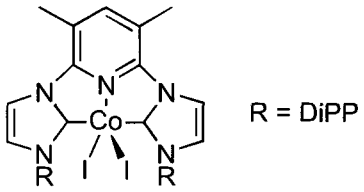

R = DiPP

Imidazolium salt **56** (250 mg, 0.31 mmol) and $Co(HMDS)_2$ (109 mg, 0.31 mmol) were mixed as powders and cold (–78 °C) THF (20 mL) was added. The solution was stirred for five minutes at –78 °C then warmed to RT and stirred for 72 hours. After this time, the solvents were removed *in vacuo*, the solid was washed with PE (15 mL) and dried, affording 229 mg of the title compound as a red-brown solid in 86% yield.

μ_{eff}: 2.95 B.M.

Analysis: Calc. for $C_{37}H_{45}N_5CoI_2$: C 50.93; H 5.20; N 8.03. Found: C 50.98; H 5.15; N 7.93.

(2,6-Bis(2,6-diisopropylphenyl)imidazol-2-ylidene)pyridine cobalt(III) iodide peroxide (**83**)

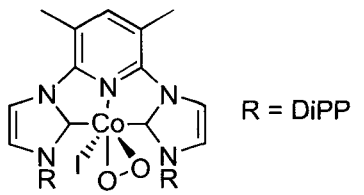

R = DiPP

Compound **82** (150 mg, 0.17 mmol) was dissolved in THF (10 mL) and PE was slowly diffused into the solution. After 14 days, 92 mg of purple crystals were deposited in 46% yield.

δ_H (400.0 MHz, CD_2Cl_2): 8.41 (2H, d, J = 2.0 Hz, imidazol-2-ylidene), 7.58 (1H, s, py), 7.34–7.30 (4H, m, Ar and imidazol-2-ylidene), 7.13 (4H, d, J = 8.0 Hz, Ar), 3.40 (4H, septet, J = 6.5 Hz, ^{i}Pr CH), 2.84 (6H, s, py-Me), 1.16, 1.07 (each 12H, d, J = 6.5 Hz, ^{i}Pr CH_3) ppm.

δ_C (100.6 MHz, CD_2Cl_2): 198.00 (C, C_{NHC}), 150.09 (C, Ar), 148.36 (CH, Ar), 147.75, 137.03 (C, Ar), 129.83, 128.89, 123.58, 118.77 (CH, Ar), 118.40 (C, Ar), 28.35 (CH, ^{i}Pr), 25.87, 22.91 (CH_3, ^{i}Pr), 19.19 (CH_3 py-Me) ppm.

Analysis: Calc. for $C_{37}H_{45}N_5O_2CoI$: C 57.15; H 5.83; N 9.01. Found: C 57.06; H 5.91; N 9.09.

(2,6-Bis(2,6-diisopropylphenyl)imidazol-2-ylidene)pyridine cobalt(III) triiodide (**84**)

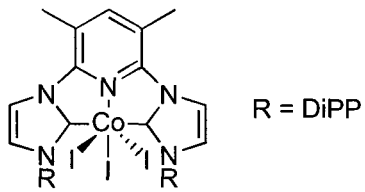

To a stirred solution of **82** (250 mg, 0.29 mmol) in THF (25 mL) was added I_2 (36 mg, 0.14 mmol) under a counterflow of N_2. The reaction was stirred for 16 hours then solvents were removed *in vacuo*, the solid extracted into Et_2O, concentrated and cooled to 5 °C. 144 mg of the title compound was isolated as a brown powder in 50% yield.

δ_H (400.0 MHz, CD_2Cl_2): 8.45 (2H, d, J = 2.0 Hz, imidazol-2-ylidene), 7.65 (1H, s, py), 7.37–7.29 (4H, m, Ar and imidazol-2-ylidene), 7.14 (4H, d, J = 7.5 Hz, Ar), 3.28 (4H, septet, J = 6.5 Hz, ^{i}Pr CH), 2.90 (6H, s, py-Me), 1.15, 1.09 (each 12H, d, J = 6.5 Hz, ^{i}Pr CH_3) ppm.

δ_C (100.6 MHz, CD_2Cl_2): 195.25 (C, C_{NHC}), 149.91 (C, Ar), 148.97 (CH, Ar), 146.96, 136.73 (C, Ar), 130.03, 129.22, 123.67 (CH, Ar), 119.52 (C, Ar), 119.40 (CH, Ar), 28.51 (CH, ^{i}Pr), 25.95, 22.82 (CH_3, ^{i}Pr), 19.43 (CH_3 py-Me) ppm.

Analysis: Calc. for $C_{37}H_{45}N_5CoI_3$: C 44.46; H 4.54; N 7.01. Found: C 44.57; H 4.59; N 7.14.

(2,6-Bis(di-^{t}butylphosphinomethyl)pyridine) cobalt(II) dibromide (**85**)

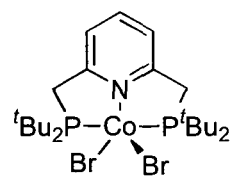

To a stirred solution of ligand **60** (200 mg, 0.51 mmol) in THF (15 ml) at 0 °C was added a solution of $CoBr_2(THF)_2$ (185 mg, 0.51 mmol) in THF (5 mL). The solution was warmed to RT then stirred for 16 hours. After this time, the solvent was removed *in vacuo*, affording 252 mg of a dark purple powder in 80% yield. Crystallisation occurred from slow diffusion of Et_2O into a saturated DCM solution.

μ_{eff}: 1.71 B.M.

Analysis: Calc. for $C_{23}H_{43}NCoBr_2P_2$: C 44.97; H 7.06; N 2.28. Found: C 45.09; H 7.13; N 2.35.

(2,6-Bis(2,6-diisopropylphenyl)imidazol-2-ylidene)pyridine nickel(II) dibromide (**86**)

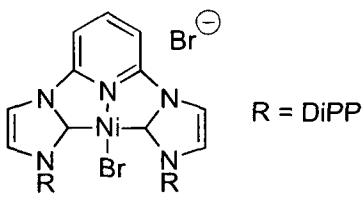

To a solution of $NiBr_2(DME)$ (116 mg, 0.38 mmol) in THF (15 mL) was added a solution of **36** (200 mg, 0.38 mmol) in THF (15 mL) at 0 °C. The reaction was stirred for 15 mins, then warmed to RT and stirred for 16 hours. After this time, solvents were removed under vacuum and the solid obtained was pure enough for further reactivity studies. Yield: 210 mg of an orange solid, 74%. Crystallisation occurred from slow diffusion of Et_2O into a concentrated DCM solution.

δ_H (300 MHz, CD_2Cl_2): 9.22–6.08 (13H, br m, Ar), 3.00–0.51 (28H, br m, ^{i}Pr CH/CH_3) ppm.

δ_C (75.5 MHz, CD_2Cl_2): 164.62, 150.88, 144.55, 134.00, 130.09, 127.86, 123.58, 118.41, 109.83 (C/CH, Ar), 28.60, 24.42, 22.91 (CH/CH_3, ^{i}Pr) ppm.

Analysis: Calc. for $C_{35}H_{41}N_5NiBr_2$: C 56.03; H 5.51; N 9.33. Found: C 55.97; H 5.41; N 9.41.

(2,6-Bis(2,6-diisopropylphenyl)imidazol-2-ylidene)pyridine nickel(II) bis(tetrafluoroborate), acetonitrile adduct (**87**)

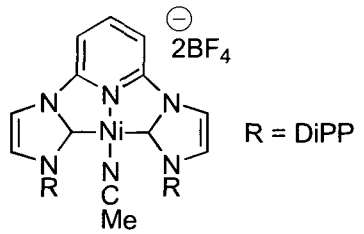

Compound **86** (250 mg, 0.33 mmol) and $AgBF_4$ (136 mg, 0.70 mmol) were dissolved in MeCN (25 mL) and stirred for 16 hours. After this time the solution was filtered through Celite, solvents were removed *in vacuo* and the solid obtained was crystallised by the slow diffusion of Et_2O into a concentrated MeCN solution. Yield: 247 mg of green crystals, 92%.

δ_H (300.1 MHz, CD_3CN): 8.46 (1H, t, J = 8.5 Hz, *p*–py), 8.14 (2H, d, J = 2 Hz, imidazol-2-ylidene), 7.72 (2H, d, J = 8.5 Hz, *o*–py), 7.42 (2H, dd, J = 8.5, 7.0 Hz, Ar), 7.34–7.27 (6H, m, Ar), 2.54 (4H, septet, J = 7.0 Hz, ^{i}Pr CH), 1.94 (3H, s, MeCN), 1.19, 1.08 (each 12H, d, J = 7.0 Hz, ^{i}Pr CH_3) ppm.

δ_C (100.6 MHz, CD_3CN): 151.81 (C, Ar), 149.33 (CH, Ar), 145.92, 132,64 (C, Ar), 132.25, 128.32, 125.12, 118.67, 109.92 (CH, Ar), 28.72 (CH, ^{i}Pr), 23.90, 23.62 (CH_3, ^{i}Pr) ppm.

δ_F (282.4 MHz, CD_3CN): –151.27 ppm.

Analysis: Calc. for $C_{37}H_{44}N_6NiB_2F_8$: C 55.20; H 5.51; N 10.44. Found: C 55.27; H 5.59; N 10.51.

(2,6-Bis(2,6-diisopropylphenyl)imidazol-2-ylidene)pyridine nickel(II) bis(triflate), THF adduct (**88**)

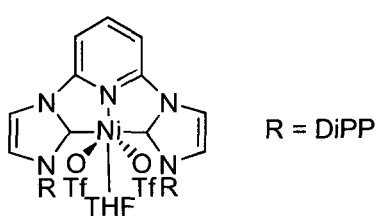

Compound **86** (250 mg, 0.33 mmol) and AgOTf (171 mg, 0.66 mmol) were dissolved in THF (25 mL) and stirred for 4 hours. After this time, the solution was filtered through Celite, the solvent was removed under vacuum and the solid was crystallised by the

slow diffusion of PE into a concentrated THF solution. Yield: 300 mg of green crystals, 94%.

μ_{eff}: 2.86 B.M.

Analysis: Calc. for $C_{41}H_{49}N_5O_7F_6NiS_2$: C 51.26; H 5.14; N 7.29. Found: C 51.18; H 5.23; N 7.16.

Methyl nickel 2-[(3-(2,6-diisopropylphenyl)-imidazol-2-ylidene]-6-[2-(2,6-diisopropylphenyl)iminomethyl vinyl amine]pyridine (**93**)

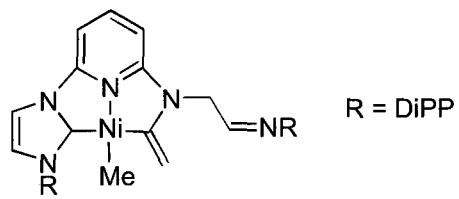

Compound **36** (250 mg, 0.47 mmol) and $NiMe_2(TMEDA)$ (96 mg, 0.47 mmol) were dissolved in cold (–78 °C) THF (20 mL), then warmed to RT and stirred for 16 hours. After this time, solvents were removed *in vacuo*, the solid was extracted into Et_2O, filtered and cooled to –35 °C, affording 131 mg of the title compound as brown crystals in 45% yield.

δ_H (400.0 MHz, C_6D_6): 7.38–6.96 (11H, m, Ar), 5.97 (1H, dd, J = 12.0, 10.0 Hz, imine CH), 5.59 and 5.25 (each 1H, br s, olefin CH_2), 3.36 (1H, septet, J = 6.5 Hz, ^{i}Pr CH), 3.08 (1H, br s, ^{i}Pr CH), 2.85 (2H, br s, ^{i}Pr CH), 2.36 (2H, s, CH_2), 2.12 (3H, s, Ni-Me), 1.24–0.89 (24H, m, ^{i}Pr CH_3) ppm.

δ_C (100.6 MHz, C_6D_6): 186.95 (C, C_{NHC}), 168.21 (C, imine), 157.48, 148.37, 145.68, 144.67, 138.61 (C, Ar), 137.15 (CH, Ar), 136.10 (C, Ar), 134.83, 130.22 (CH, Ar), 128.70, 127.40 (C, Ar), 126.07, 125.04, 124.61, 124.14, 123.95, 123.69 (CH, Ar), 104.41 (C, olefin), 100.01 (CH_2, olefin), 58.42 (CH_2, CH_2), 46.05 (CH, ^{i}Pr), 28.81, 28.28, 24.55, 23.93 (CH_3, ^{i}Pr), 15.62 (CH, iPr), -7.63 (CH_3, Ni–Me) ppm.

Analysis: Calc. for $C_{37}H_{47}N_5Ni$: C 71.62; H 7.63; N 11.29. Found: C 71.71; H 7.70; N 11.33.

(2,6-Bis(2,6-diisopropylphenyl)imidazol-2-ylidene)pyridine nickel(II) bromide, hexafluorophosphate (**94**)

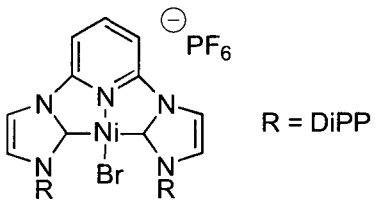

Compound **86** (150 mg, 0.20 mmol) and KPF_6 (171 mg, 0.66 mmol) were dissolved in THF (20 mL) and stirred for 16 hours. After this time solvents were removed *in vacuo*, the solid extracted into DCM, filtered through Celite and concentrated. Crystallisation occurred from slow diffusion of Et_2O into a concentrated DCM solution. Yield: 150 mg of orange crystals, 92%.

δ_H (400.0 MHz, CD_2Cl_2): 8.43 (1H, t, J = 8.0 Hz, py-4), 7.95 (2H, s, imidazol-2-ylidine CH), 7.69 (2H, d, J = 8.0 Hz, py-3,5), 7.36 (2H, t, J = 8.0 Hz, Ph-4), 7.13 (4H, d, J = 8.0 Hz, Ph-3,5), 7.00 (2H, s, imidazol-2-ylidine CH), 2.49 (4H, septet, J = 7.0 Hz, ^{i}Pr CH), 1.21, 1.07 (each 12H, d, J = 7.0 Hz, ^{i}Pr CH_3) ppm.

δ_C (100.6 MHz, CD_2Cl_2): 165.22 (C, C_{NHC}), 150.76 (C, Ar), 146.53 (CH, Ar), 144.61, 133.94 (C, Ar), 130.36 (CH, Ar), 128.32 (CH, imidazol-2-ylidene), 123.75 (CH, Ar), 116.21 (CH, imidazol-2-ylidene), 108.32 (CH, Ar), 28.76 (CH, ^{i}Pr), 24.48, 23.03 (CH_3, ^{i}Pr) ppm.

Analysis: Calc. for $C_{35}H_{41}N_5BrF_6NiP$: C 51.56; H 5.07; N 8.59. Found: C 51.43; H 5.16; N 8.65.

Bis((2,6-bis(2,6-diisopropylphenyl)imidazol-2-ylidene)-3,5-dimethylpyridine nickel(II) bromide) (disilver tetraiodide) (**95**)

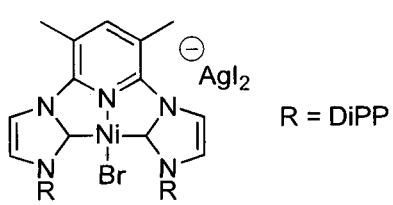

Compound **59** (450 mg, 0.44 mmol) and $NiBr_2$(DME) (136 mg, 0.44 mmol) were dissolved in THF (10 mL each). The solution of **59** was added to the $NiBr_2$(DME) solution and the reaction was stirred for 72 hours. After this time, the solution was filtered through Celite, concentrated to dryness and crystallised by the slow diffusion of

PE into a concentrated THF solution, affording 404 mg of the title compound in 87% yield.

δ_H (400.0 MHz, C_4D_8O): 8.45–8.41 (3H, m, Ar), 7.46–7.36 (4H, m, Ar), 7.23–7.18 (4H, m, Ar), 3.02 (6H, s, py-Me), 2.76 (4H, septet, J = 6.5 Hz, ^{i}Pr CH), 1.36, 1.19 (each 12H, d, J = 6.5 Hz, ^{i}Pr CH_3) ppm.

δ_C (100.6 MHz, C_4D_8O): 168.60 (C, Ar), 154.23 (CH, Ar), 150.09, 146.73, 137.12 (C, Ar), 131.70, 129.69, 125.36 (CH, Ar), 122.29 (C, Ar), 121.41 (CH, Ar), 30.60 (CH, ^{i}Pr), 26.39, 24.98 (CH_3, ^{i}Pr), 20.57 (CH_3, py-Me) ppm.

Analysis: Calc. for $C_{37}H_{45}N_5NiBrAgI_2$: C 41.92; H 4.28; N 6.61. Found: C 41.81, H 4.15; N 6.55.

Bis((2,6-bis(2,6-diisopropylphenyl)imidazol-2-ylidene)-3,5-dimethylpyridine silver) bis(triflate) (**96**)

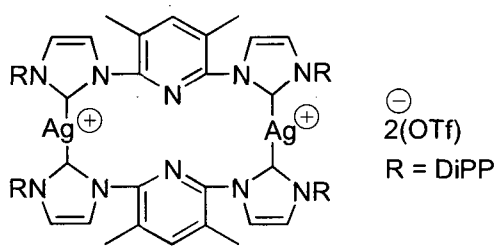

Compound **95** (100 mg, 0.13 mmol) and AgOTf (67 mg, 0.26 mmol) were mixed under nitrogen and cooled to –78°C. Cold (–78 °C) THF (25 mL) was added and the reaction was stirred for five minutes, then warmed to RT and stirred for 48 hours. After this time, the reaction was filtered through Celite, solvents were removed *in vacuo* and the resulting brown solid was crystallised by the slow diffusion of PE into a THF solution.

δ_H (400.0 MHz, C_6D_6): 7.87–7.66 (2H, m, Ar), 7.48–7.41 (2H, m, Ar), 7.33–7.18 (3H, m, Ar), 7.05–6.86 (4H, m, Ar), 2.54 (4H, br s, ^{i}Pr CH), 2.40 (6H, s, py-Me), 1.21, 1.16 (each 12H, br s, ^{i}Pr CH_3) ppm.

δ_C (100.6 MHz, C_6D_6): 188.47 (C, C_{NHC}), 147.41, 147.15 (C, Ar), 146.52, 146.03 (CH, Ar), 145.52, 145.28, 134.44 (C, Ar), 130.82, 130.52, 124.31, 123.91, 123.41 (CH, Ar), 29.41 (CH, ^{i}Pr), 24.91, 24.79 (CH_3, ^{i}Pr), 19.33 (CH_3, py-Me) ppm.

Analysis: Calculated for $C_{84}H_{106}Ag_2N_{10}F_6O_8S_2$: C 56.75; H 6.01; N 7.88. Found: C 54.97; H 5.94 N; 7.13.

(2,6-Bis(2,6-diisopropylphenyl)imidazol-2-ylidene)3,5-dimethylpyridine nickel(II) dibromide (**97**)

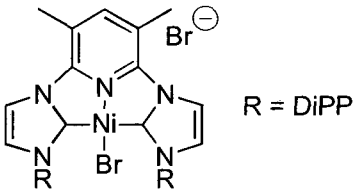

Ligand **58** (250 mg, 0.45 mmol) and $NiBr_2$(DME) (96 mg, 0.45 mmol) were suspended in THF (20 mL) and stirred for 16 hours at RT. After this time, solvents were removed *in vacuo*, affording 326 mg of the title compound as an orange powder in 94% yield. Crystallisation occurred from the slow diffusion of Et_2O into a concentrated DCM solution.

δ_H (400.0 MHz, C_6D_6): 8.32 (1H, s, py-H), 8.28 (2H, br s, imidazol-2-ylidene), 7.35 (2H, t, J = 7.5 Hz, Ar), 7.11 (4H, br d, J = 7.5 Hz, Ar), 7.01 (2H, br s, imidazol-2-ylidene), 2.89 (6H, s, py-Me), 2.46 (4H, septet, J = 6.5 Hz, ^{i}Pr CH), 1.19, 1.05 (each 12H, d, J = 6.5 Hz, ^{i}Pr CH_3) ppm.

δ_C (100.6 MHz, C_6D_6): 182.18 (C, C_{NHC}), 167.10 (C, Ar), 152.86 (CH, Ar), 148.58, 145.21, 134.98 (C, Ar), 130.91, 128.55, 124.38 (CH, Ar), 120.91 (C, Ar), 119.63 (CH, Ar), 29.42 (CH, ^{i}Pr), 25.26, 23.68 (CH_3, ^{i}Pr), 19.50 (CH_3, py-Me) ppm.

Analysis: Calc. for $C_{37}H_{45}N_5NiBr_2$: C 57.10; H 5.83; N 9.00. Found: C 56.96; H 5.69; N 8.82.

(2,6-Bis(2,6-diisopropylphenyl)imidazol-2-ylidene)3,5-dimethylpyridine nickel(II) bromide, triflate (**98**)

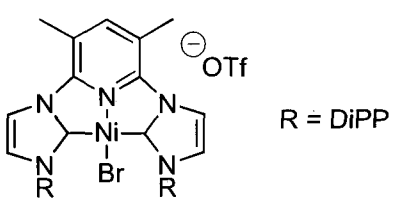

Compound **97** (250 mg, 0.32 mmol) and TlOTf (226 mg, 0.64 mmol) were suspended in THF (20 mL) and stirred for 16 hours at RT. After this time, the reaction was filtered through Celite and the solvents were removed *in vacuo*, affording 326 mg of the title compound as an orange powder in 94% yield. Crystallisation occurred from the slow diffusion of PE into a concentrated THF solution.

δ_H (400.0 MHz, C_6D_6): 8.04 (2H, d, J = 2.0 Hz, imidazol-2-ylidene), 8.02 (1H, s, py-H), 7.35 (2H, t, J = 7.5 Hz, Ar), 7.16–7.09 (4H, m, Ar), 6.98 (2H, d, J = 2.0 Hz, imidazol-2-ylidene), 2.78 (6H, s, py-Me), 2.46 (4H, septet, J = 7.0 Hz, ^{i}Pr CH), 1.19, 1.05 (each 12H, d, J = 2.0 Hz, ^{i}Pr CH_3) ppm.

δ_C (100.6 MHz, C_6D_6): 167.22 (C, Ar), 152.44 (CH, Ar), 148.60, 145.23, 134.97 (C, Ar), 130.98, 128.55, 124.43 (CH, Ar), 120.77 (C, Ar), 119.08 (CH, Ar), 29.45 (CH, ^{i}Pr), 25.24, 23.68 (CH_3, ^{i}Pr), 18.90 (CH_3, py-Me) ppm.

δ_F (282.4 MHz, C_6D_6): –78.89 ppm.

Analysis: Calc. for $C_{38}H_{45}N_5O_3F_3SNiBr$: C 53.86; H 5.35; N 8.26. Found: C 53.79; H 5.31; N 8.31.

8.5 - Experimental for chapter 5

(2,6-Bis(2,6-diisopropylphenyl)imidazol-2-ylidene)-3,5-dimethylpyridine iron(II) diiodide (**109**)

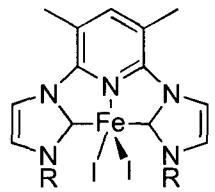

R = DiPP

$Fe(HMDS)_2$ (0.46 g, 1.23 mmol) and imidazolium salt **56** (1.00 g, 1.23 mmol) were mixed as solids and cold (–78 °C) THF (25 mL) was added. The reaction was stirred at –78 °C for 15 minutes then warmed to RT and stirred for 16 hours. After this time solvents were removed, the solid washed with petrol and dried *in vacuo*, yielding 1.02 g of a purple solid in 96% yield. Crystallisation occurred from slow diffusion of petrol into a concentrated THF solution.

μ_{eff}: 4.84 B.M.

Analysis: Calc. for $C_{37}H_{45}N_5FeI_2$: C 51.11; H 5.22; N 8.06. Found: C 51.16; H 5.31; N 8.15.

(2,6-Bis(2,6-diisopropylphenyl)imidazol-2-ylidene)-3,5-dimethylpyridine iron(0) *bis*(dinitrogen) (**110**)

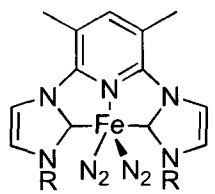

R = DiPP

Compound **109** (250 mg, 0.29 mmol) was dissolved in THF (20 mL) above 0.4 wt.% Na/Hg (9 g, 1.84 mmol) and stirred for 4 hours after which time an olive green solution had formed. The solution was decanted away from unreacted amalgam and the solvent was removed. The residue was extracted into Et_2O, filtered through Celite and concentrated to ca. 10 mL. Crystallisation occurred at 4 °C, affording 185 mg of a dark green complex in 96% yield.

δ_H (400.0 MHz, C_6D_6): 7.82 (2H, s, imidazol-2-ylidene), 7.25–7.17 (6H, m, Ar), 6.76 (2H, s, imidazol-2-ylidene), 6.64 (1H, s, Ar), 3.21 (4H, septet, J = 6.5 Hz, ^{i}Pr CH), 2.38 (6H, s, py-Me), 1.30, 1.15 (each 12H, d, J = 6.5 Hz, ^{i}Pr CH_3) ppm.

δ_C (100.6 MHz, C_6D_6): 204.64 (C, C_{NHC}), 147.68, 140.21, 137.58 (C, Ar), 129.73, 128.35, 124.78, 124.25, 123.92, 113.90 (CH, Ar), 110.88 (C, Ar), 28.54 (CH, ^{i}Pr), 25.81, 23.43 (CH_3, ^{i}Pr), 18.91 (CH_3, py-Me) ppm.

IR (nujol mull): N≡N 2107, 2026 cm^{-1}

Analysis*: Calc. for $C_{39}H_{45}N_5O_2Fe$: C 66.16; H 6.75; N 18.77. Found: C 72.26, H 7.31; N 11.49.

* = analyses to $C_{37}H_{45}N_5Fe$ after loss of 2 N_2 ligands

(2,6-Bis(2,6-diisopropylphenyl)imidazol-2-ylidene)-3,5-dimethylpyridine iron(0) dicarbonyl (**111**)

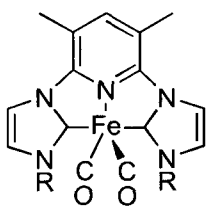

R = DiPP

Complex **109** (250 mg, 0.29 mmol) was reduced following the method for complex **110**. The THF solution was decanted from the unreacted amalgam and CO was bubbled through for 15 minutes. After this time the solvent was removed, the solid extracted into a 1:1 mix of Et_2O and petrol (*ca.* 50 mL), filtered and concentrated *in vacuo* to *ca.* 10 mL. Crystallisation occurred upon standing for 16 hours, affording 177 mg of pink crystals in 92% yield.

δ_H (400.0 MHz, C_6D_6): 7.70 (2H, br s, imidazol-2-ylidene), 7.25–7.13 (6H, m, Ar), 6.73 (2H, br s, imidazol-2-ylidene), 6.57 (1H, s, Ar), 3.10 (4H, septet, J = 6.5 Hz, ^{i}Pr CH), 2.31 (6H, s, py-Me), 1.39, 1.11 (each 12H, d, J = 6.5 Hz, ^{i}Pr CH_3) ppm.

δ_C (100.6 MHz, C_6D_6): 215.86 (C, CO), 210.84 (C, C_{NHC}), 147.56, 140.44, 137.42 (C, Ar), 129.95, 128.36, 127.80, 124.76, 124.15, 113.95 (CH, Ar), 110.76 (C, Ar), 28.67 (CH, ^{i}Pr), 26.25, 23.04 (CH_3, ^{i}Pr), 18.83 (CH_3, py-Me) ppm.

IR (nujol mull): C≡O 1925, 1858 cm^{-1}

Analysis: Calc. for $C_{39}H_{45}N_5O_2Fe$: C 69.74; H 6.75; N 10.43. Found: C 69.79, H 6.82; N 10.36.

(2,6-Bis(di-*tert*-butylphosphinomethyl)pyridine) iron(II) dibromide (**112**)

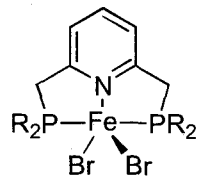

A solution of $FeBr_2(THF)_{1.5}$ (152 mg, 0.51 mmol) in ^{i}PrOH (15 mL) at –18 °C was added to a solution of ligand **60** (200 mg, 0.51 mmol) in ^{i}PrOH (15 mL). The reaction was warmed to RT and stirred for 16 hours. After this time, a yellow solid had formed which was isolated by filtration and dried *in vacuo*, affording 219 mg of the title compound in 68% yield. Yellow crystals suitable for X-ray diffraction were obtained by slow diffusion of Et_2O into a concentrated CH_2Cl_2 solution.

μ_{eff}: 6.09 B.M.

Analysis: Calc. for $C_{23}H_{43}NBr_2FeP_2$: C 45.20; H 7.09; N 2.29. Found: C 45.29; H 6.90; N 2.19.

(2,6-Bis(di-*tert*-butylphosphinomethyl)pyridine) iron(II) dichloride (**113**)

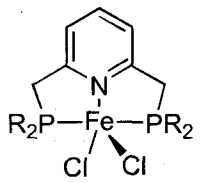

A solution of $FeCl_2$ (65 mg, 0.51 mmol) in ^{i}PrOH (15 mL) at –18 °C was added to a solution of ligand **60** (200 mg, 0.51 mmol) in ^{i}PrOH (15 mL). The reaction was warmed to RT and stirred for 16 hours. After this time, a yellow solid had formed which was isolated by filtration and dried *in vacuo*, affording 240 mg of the title compound in 91% yield. Yellow crystals suitable for X-ray diffraction were obtained by slow diffusion of Et_2O into a concentrated CH_2Cl_2 solution.

μ_{eff}: 5.94 B.M.

Analysis: Calc. for $C_{23}H_{43}NCl_2FeP_2$: C 52.89; H 8.30; N 2.68. Found: C 52.89; H 8.20; N 2.63.

(2,6-Bis(di-*tert*-butylphosphinomethyl)pyridine) iron(0) dicarbonyl (**115**)

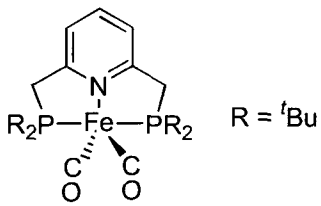

A Fischer-Porter bottle was charged in the glovebox with compound **113** (200 mg, 0.38 mmol) and 0.4 wt.% Na/Hg (13.2 g, 2.28 mmol). The Fischer-Porter bottle was purged with CO, CO-saturated THF (20 mL) was added, the pressure was increased to 1 bar CO and the reaction was stirred for 4 hours. After this time, the green-brown solution was decanted away from unreacted amalgam and the solvent was removed. The residue was extracted into PE, filtered through Celite and concentrated to dryness. Crystallisation occurred by cooling a saturated PE solution to –35 °C, affording 89 mg of the title compound as green crystals in 46% yield.

δ_H (300.0 MHz, $(CD_3)_2CO$): 7.51 (1H, t, J = 7.5 Hz, Ar), 7.17 (2H, d, J = 7.5 Hz, Ar), 2.99 (4H, d, J = 3.0 Hz, CH_2), 1.14 (36H, d, J = 11.0 Hz, ^{t}Bu) ppm.
δ_C (100.6 MHz, C_6D_6): 204.68 (C, d, J = 19 Hz, CO), 160.50 (C, Ar), 135.12, 119.79 (CH, Ar), 30.99 (CH_2, d, J = 26.0 Hz, CH_2), 30.86 (C, d, J = 23.0 Hz, ^{t}Bu), 28.62 (CH_3, ^{t}Bu) ppm.
δ_P (121.5 MHz, $(CD_3)_2CO$): 37.3 ppm.
IR (nujol mull): C≡O 1847, 1797 cm^{-1}.
Analysis: Calc. for $C_{25}H_{43}NFeO_2P_2$: C 58.94; H 8.90; N 2.75. Found: C 58.89; H 8.88; N 2.70.

(2,6-Bis(2,6-diisopropylphenyl)imidazol-2-ylidene)pyridine iron(0) bis(2,6-xylyl isocyanide) (**116**)

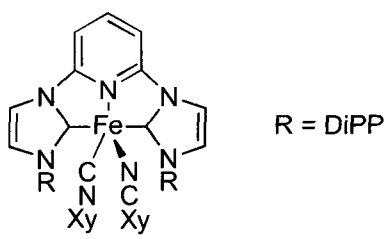

A freshly-reduced solution of **48** (173 mg, 0.27 mmol) in THF (20 mL) was added to a quartz flask containing 2,6-xylyl isocyanide (70 mg, 0.54 mmol). The reaction was

exposed to 254 nm UV light for 10 mins then stirred at RT for 2 hours. After this time, solvents were removed *in vacuo*, the solid extracted with toluene (20 mL) and filtered through Celite. The toluene was removed *in vacuo*, the brown solid was dissolved in petrol (10 mL) and cooled: crystallisation occurred at −18 °C affording the title compound as dark crystals in 56% yield.

δ_H (300.1 MHz, C_6D_6): 7.61 (2H, br s, Ar), 7.25–7.20 (4H, m, Ar), 7.01 (4H, d, J = 7.0 Hz, imidazol-2-ylidene), 6.95–6.90 (2H, m, Ar), 6.84–6.81 (7H, m, Ar), 3.30 (4H, septet, J = 5.0 Hz, ^{i}Pr CH), 2.05 (12H, s, isocyanide CH_3), 1.34, 1.14 (12H, d, J = 5.0 Hz, ^{i}Pr CH_3) ppm.

δ_C (75.5 MHz, C_6D_6): 208.56 (C, C_{NHC}), 203.56 (C, C_{CN}), 146.79, 141.26, 138.81, 134.67, 133.54 (C, Ar), 128.72, 128.34, 127.14, 126.67, 123.60, 123.12, 115.26, 110.38, 98.56 (CH, Ar), 28.64 (CH, ^{i}Pr), 25.70, 23.23 (CH_3, ^{i}Pr), 20.64 (CH_3, isocyanide) ppm.

IR (nujol mull): C=N 1901, 1837 cm^{-1}.

Analysis: Calc. for $C_{48}H_{52}N_6Fe$: C 74.90; H 7.00; N 11.54. Found: C 74.81; H 6.95; N 11.39.

(2,6-Bis(2,6-diisopropylphenyl)imidazol-2-ylidene)pyridine iron(II) carbonyl dibromide (**117**)

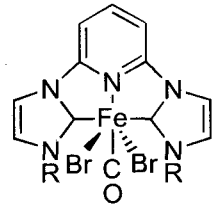

R = DiPP

CO was bubbled through a solution of compound **45** (250 mg, 0.31 mmol) in THF (25 mL) for 30 minutes. After this time the solvent was removed, the solid dissolved in Et_2O and cooled to −35 °C, yielding 209 mg of the title compound as brown crystals in 80% yield. Crystallisation also occurred from slow diffusion of Et_2O into a concentrated DCM solution.

μ_{eff}: 4.79 B.M.

IR (nujol mull): C≡O 1975 cm^{-1}

Analysis: Calc. for $C_{36}H_{41}N_5OFeBr_2$: C 55.76; H 5.33; N 9.03. Found: C 55.66; H 5.41; N 8.90.

(2,6-Bis(2,6-diisopropylphenyl)imidazol-2-ylidene)pyridine iron(II) (κ^2-(*ortho*-phenylimine)phenyl) hydride (**118**)

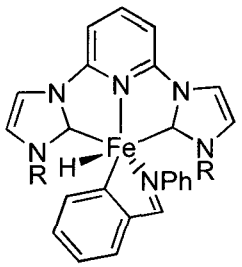

R = DiPP

A freshly reduced solution of **48** (173 mg, 0.27 mmol) in THF (20 mL) was added to a quartz flask containing benzaldehyde anilide (49 mg, 0.27 mmol). The reaction was exposed to 254 nm UV light and stirred at RT for 2 hours, during which time the colour changed from green to dark brown. After 2 hours, solvents were removed *in vacuo* and the solid extracted with toluene (20 mL) and filtered. The toluene was removed *in vacuo*, then solid was dissolved in petrol (10 mL), filtered and crystallisation occurred at –35C.

δ_H (300.1 MHz, C_6D_6): 8.24 (1H, s, imine CH), 7.85 (1H, d, J = 7.5 Hz, imidazol-2-ylidene), 7.41 (1H, d, J = 7.5 Hz, imidazol-2-ylidene), 7.24 (5H, br s, Ar), 7.19–7.15 (5H, m, Ar), 7.00–6.79 (5H, m, Ar), 6.68 (1H, d, J = 8.0 Hz, Ar), 6.62–6.58 (2H, m, Ar), 6.19 (2H, d, J = 7.5 Hz, imidazol-2-ylidene), 3.11 (2H, septet, J = 7.0 Hz, ^{i}Pr CH), 2.44 (2H, septet, J = 7.0 Hz, ^{i}Pr CH), 1.60 (6H, d, J = 7.0 Hz, ^{i}Pr CH_3), 1.14 (6H, d, J = 7.0 Hz, ^{i}Pr CH_3), 1.03 (12H, d, J = 7.0 Hz, ^{i}Pr CH_3), –14.14 (1H, s, Fe–H) ppm.

δ_C (75.5 MHz, C_6D_6): 225.14 (C, Fe–C_{Ph}), 214.49 (C, C_{NHC}), 167.03 (CH, C=N), 153.86, 150.52 (C, Ar), 147.20 (CH, imidazol-2-ylidene), 146.38, 145.25, 144.72, 137.76 (C, Ar), 129.08 (CH, imidazol-2-ylidene), 128.97, 128.32, 128.10, 127.03, 123.62, 123.55, 122.71, 122.01 (CH, Ar), 121.19 (CH, imidazol-2-ylidene), 116.67, 111.88, 99.39 (CH, Ar), 28.16, 27.88 (CH, ^{i}Pr), 26.07, 25.73, 23.14, 21.84 (CH_3, ^{i}Pr) ppm.

Analysis: Calc. for $C_{48}H_{52}N_6Fe$: C 74.99; H 6.82; N 10.93. Found: C 74.83; H 7.00; N 11.02.

(2,6-Bis(2,6-diisopropylphenyl)imidazol-2-ylidene)pyridine (κ^2(2-(2,6-diisopropylphenyl)imidazol-2-ylidene)-6-(2,6-diisopropylphenylimidazolium)-3-pyridyl iron(II) (**119**)

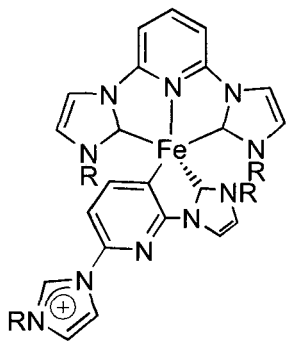

R = DiPP

A Fischer-Porter bottle was charged in the glovebox with compound **45** (200 mg, 0.34 mmol) and 0.4 wt.% Na/Hg (13.2 g, 2.28 mmol). The Fischer-Porter bottle was purged with Ar, Ar-saturated THF (20 mL) was added, the pressure was increased to 5 bar Ar and the reaction was stirred for 4 hours. After this time, the brown solution was decanted away from unreacted amalgam and the solvent was removed. The brown solid was extracted into Et_2O and crystallisation occurred at 5 °C.

Analysis: Calc. for $C_{70}H_{82}N_{10}Fe$: C 75.11; H 7.38; N 12.51. Found: C 75.24; H 7.41; N 12.60.

(2,6-Bis(2,6-diisopropylphenyl)imidazol-2-ylidene)pyridine iron (II) bis(phenylsilyl) (η^2-phenylsilane) (**125**)

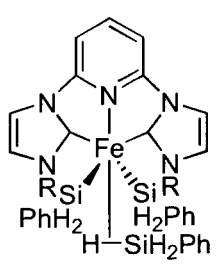

R = DiPP

To a solution of **48** (173 mg, 0.27 mmol) in THF (20 mL) was added phenylsilane (0.5 mL, 4.05 mmol). After no more gas was evolved, the reaction was stirred for 30 minutes then the solvent was removed and the solid extracted into toluene. The toluene solution was concentrated and crystallisation occurred at –35 °C, yielding 210 mg of the title compound as orange crystals in 85% yield.

δ_H (300.1 MHz, C_6D_6): 7.14–6.93 (13H, m, Ar), 6.77–6.70 (7H, m, Ar), 6.5 (4H, d, J = 7.0 Hz, Ar), 6.39 and 6.10 (each 2H, d, J = 8.0 Hz, imidazol-2-ylidine), 4.97 (2H, s, silane SiH_2), 4.62 (4H, s, silyl SiH_2), 3.44 (4H, septet, J = 6.5 Hz, ^{i}Pr CH), 1.42, 1.01 (each 12H, d, J = 6.5 Hz, ^{i}Pr CH_3), –12.03 (1H, s, Fe–H) ppm.

δ_C (75.5 MHz, C_6D_6): 211.92 (C, C_{NHC}), 147.85, 147.23, 144.98, 141.99, 137.11 (C, Ar), 136.05, 134.65, 130.40, 129.61, 129.16, 128.58, 128.35, 126.83, 126.57, 126.49, 126.36 (CH, Ar), 125.70 (C, Ar), 124.13 (CH, Ar), 112.47, 101.73 (C, Ar), 28.65 (CH, ^{i}Pr), 26.73, 22.39 (CH_3, ^{i}Pr) ppm.

δ_{Si} (79.5 MHz, C_4D_8O): –1.18 (Si, silane), –19.35 (Si, silyl)

Analysis: Calc. for $C_{53}H_{63}N_5FeSi_3$: C 69.94; H 6.98; N 7.69. Found: C 69.82; H 7.10; N 7.56.

(2,6-Bis(2,6-diisopropylphenyl)imidazol-2-ylidene)-3,5-dimethylpyridine iron(II) bis(phenylsilyl) dihydide (**126**)

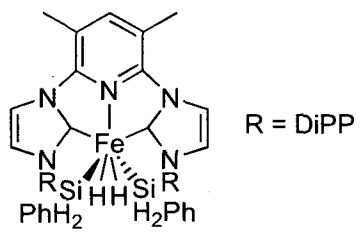

Complex **109** (250 mg, 0.29 mmol) was reduced as for complex **110**. The THF solution was decanted from the unreacted amalgam, $PhSiH_3$ (0.5 mL, 4.05 mmol) was added and the solution stirred for 16 hours at RT. After this time the solvent was removed, the solid extracted into Et_2O, filtered and concentrated *in vacuo* to *ca.* 10 mL. Crystallisation occurred at 5 °C, affording 201 mg of orange-yellow crystals in 92% yield.

δ_H (300.1 MHz, C_6D_6): 7.35–7.30 (2H, m, Ar), 7.22 (6H, br s, Ar), 7.00 (2H, dd, J = 7.5, 7.0 Hz, Ar), 6.83 (4H, dd, J = 7.5, 7.0 Hz, Ar), 6.87–6.53 (6H, m, Ar), 6.35 (1H, s, Ar), 4.56 (4H, s, Si–H), 3.50 (4H, septet, J = 6.5 Hz, ^{i}Pr CH), 2.04 (6H, s, py-Me), 1.54, 1.18 (each 12H, d, J = 6.5 Hz, ^{i}Pr CH_3), –12.92 (2H, br s, Fe–H_2) ppm.

δ_C (100.6 MHz, C_6D_6): 218.81 (C, C_{NHC}), 146.96, 145.63, 142.54, 136.72 (C, Ar), 134.38, 134.09, 129.73, 128.36, 126.32, 125.94, 125.71, 124.25, 114.57 (CH, Ar), 112.12 (C, Si-C), 28.72, 26.97 (CH_3, ^{i}Pr Me), 23.01 (CH, ^{i}Pr CH), 18.60 (CH_3, py-Me) ppm.

Analysis: Calc. for $C_{49}H_{61}N_5FeSi_2$: C 70.73; H 7.39; N 8.42. Found: C 70.56, H 7.34; N 8.33.

(2,6-Bis(2,6-diisopropylphenyl)imidazol-2-ylidene)pyridine iron (II) bis(diphenylsilyl) (η^2-dihydrogen) (**127**)

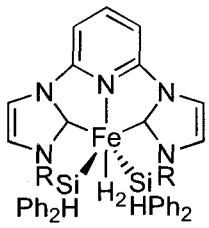

R = DiPP

To a solution of **48** (173 mg, 0.27 mmol) in THF (20 mL) was added diphenylsilane (0.25 mL, 1.35 mmol). After no more gas was evolved, the reaction was stirred for 16 hours then the solvent was removed and the solid extracted into toluene. After filtration, the toluene solution was concentrated to *ca.* 10 mL and crystallisation occurred at –35 °C, yielding 166 mg of the title compound as orange crystals in 64% yield.

δ_H (300.1 MHz, C_6D_6): 6.93-7.14 (10H, m, Ar), 6.70-6.77 (6H, m, Ar), 6.5 (4H, d, J = 7.0 Hz, Ar), 6.39 and 6.10 (each 2H, d, J = 8.0 Hz, imidazol-2-ylidine), 4.72 (2H, s, Si–H), 3.21 (4H, septet, J = 6.5 Hz, ^{i}Pr CH), 1.22, 1.01 (each 12H, d, J = 6.5 Hz, ^{i}Pr CH_3), –12.63 (2H, s, Fe–H) ppm.

δ_C (75.5 MHz, C_6D_6): 147.85, 144.98, 137.11 (C, Ar), 136.05, 134.65, 130.40, 129.61, 129.16, 128.58, 128.35, 126.83, 126.57, 126.49, 126.36 (CH, Ar), 125.70 (C, Ar), 124.13 (CH, Ar), 112.47 (C, Ar), 28.65 (CH, ^{i}Pr), 26.73, 22.39 (CH_3, ^{i}Pr) ppm.

Analysis: Calc. for $C_{59}H_{65}N_5FeSi_2$: C 74.27; H 6.65; N 7.34. Found: C 74.11; H 6.61; N 7.27.

(2,6-Bis(2,6-diisopropylphenyl)imidazol-2-ylidene)-3,5-dimethylpyridine iron (II) bis(*ortho*tolylsilyl) (η^2-*ortho*tolylsilane) (**128**)

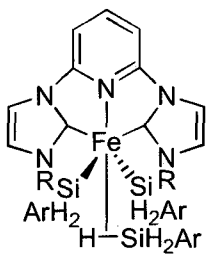

R = DiPP
Ar = *o*-tolyl

Complex **109** (250 mg, 0.29 mmol) was reduced as for complex **110**. The THF solution was decanted from the unreacted amalgam and *ortho*-tolylsilane (147 mg, 1.20 mmol) was added. After no more gas was evolved, the reaction was stirred for 16 hours then the solvent was removed, the solid dissolved in toluene and filtered through Celite. The toluene solution was concentrated and crystallisation occurred on standing, yielding 210 mg of orange crystals in 85% yield.

δ_H (400.0 MHz, C_4D_8O): 8.20–8.15 (2H, m, Ar), 7.59 (1H, d, J = 7.0 Hz, Ar), 7.41–7.18 (3H, m, Ar), 7.14 (2H, d, J = 2.0 Hz, Ar), 6.94 (1H, t, J = 7.5 Hz, Ar), 6.91–6.76 (6H, m, Ar), 6.71 (1H, d, J = 7.0 Hz, Ar), 6.65 (2H, t, J = 7.0 Hz, Ar), 6.58 (2H, d, J = 7.5 Hz, Ar), 6.42 (1H, t, J = 6.0 Hz, Ar), 6.29 (2H, d, J = 7.0 Hz, Ar), 4.54 (2H, s, silane SiH_2), 4.52 (4H, s, silyl SiH_2), 3.55 (4H, septet, J = 6.5 Hz, ^{i}Pr CH), 2.32 (6H, s, py-Me), 2.04 (3H, s, silane CH_3), 1.70 (6H, s, silyl CH_3), 1.39, 1.04 (each 12H, d, J = 6.5 Hz, ^{i}Pr CH_3), –13.62 (1H, s, Fe–H) ppm.
δ_C (100.6 MHz, C_4D_8O): 213.55 (C, C_{NHC}), 149.35, 148.98, 146.72, 144.74, 143.38, 141.75 (C, Ar), 139.59 (CH, Ar), 139.00 (C, Ar), 138.55, 137.12, 136.82, 130.93, 130.24, 128.80, 128.12, 127.95, 125.75, 125.53, 124.65, 124.55, 117.22 (CH, Ar), 114.90 (C, Ar), 30.25 (CH, iPr), 28.15 (CH3, iPr), 24.63 (CH_3, silyl Me), 24.34 (CH_3, silane Me), 23.98 (CH_3, iPr), 20.83 (CH_3, py-Me) ppm.
Analysis: Calc. for $C_{58}H_{73}N_5FeSi_3$: C 71.06; H 7.51; N 7.14. Found: C 71.11; H 7.44; N 7.18.

(2,6-Bis(2,6-diisopropylphenyl)imidazol-2-ylidene)pyridine iron (II) bis(mesitylsilyl) dinitrogen (**129**)

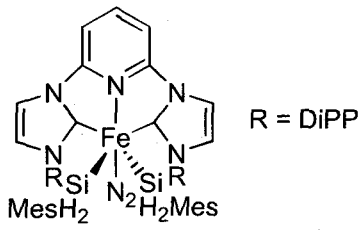

To a solution of **48** (173 mg, 0.27 mmol) in THF (20 mL) was added mesitylsilane (250 mg, 1.35 mmol). After no more gas was evolved, the reaction was stirred for 30 minutes then the solvent was removed and the solid dissolved in toluene. The toluene solution was concentrated and crystallisation occurred at –35 °C, yielding 166 mg of orange crystals in 64% yield.

IR (nujol mull): N≡N 2149 cm^{-1}

Analysis: Calc. for $C_{53}H_{67}N_7FeSi_2$: C 69.63; H 7.39; N 10.73. Found:* C 71.86; H 7.71; N 7.98.

* = Analysis consistent with loss of N_2 from the molecule

8.6 - Experimental for chapter 6

(2,6-Bis(2,6-diisopropylphenyl)imidazol-2-ylidene)pyridine ruthenium(II) chloride azide peroxide (**132**)

R = DiPP

Compound **40** (200 mg, 0.21 mmol) and NaN_3 (14 mg, 0.21 mmol) were dissolved in THF (20 mL) and refluxed for 16 hours in aerobic conditions. After this time the solvent was evaporated, the residue dissolved in DCM and filtered. Crystallisation occurred by the slow diffusion of Et_2O into a DCM solution, affording 156 mg of the title compound as red crystals in 86% yield.

δ_H (400.0 MHz, CD_2Cl_2): 8.01–6.93 (13H, br m, Ar), 3.03–2.66 (4H, m, ^{i}Pr CH), 1.04–0.89 (24H, br m, ^{i}Pr CH_3) ppm.

δ_C (100.6 MHz, CD_2Cl_2): 146.84 (C, Ar), 134.17, 132.09 (CH, Ar), 131.99, 130.27 (C, Ar), 128.66, 128.54, 123.84, 123.51 (CH, Ar), 28.50, 28.08, 25.96, 23.17, 22.71 (CH/CH_3, ^{i}Pr) ppm. (C_{NHC} not observed)

Analysis*: Calc. for $C_{35}H_{41}N_8O_{1.5}RuCl$: C 57.25; H 5.63; N 15.10. Found: C 59.75; H 5.89; N 11.93.

* = analyses to $C_{35}H_{41}N_6O_{1.5}RuCl$ after loss of N_2 from the azide.

(2,6-Bis(2,6-diisopropylphenyl)imidazol-2-ylidene)pyridine ruthenium(II) triphenylphosphine diazide (**133**)

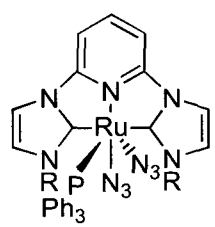

R = DiPP

Compound **40** (188 mg, 0.19 mmol) and NaN_3 (63 mg, 0.97 mmol) were dissolved in THF (20 mL) and stirred for 16 hours. After this time the solvent was evaporated, the residue dissolved in DCM and filtered through Celite. Crystallisation occurred by the

slow diffusion of Et_2O into a DCM solution, affording 156 mg of the title compound as red crystals in 86% yield.

δ_H (300.1 MHz, CD_2Cl_2): 8.25–7.93 (1H, m, Ar), 7.77–6.98 (23H, m, Ar), 6.88–6.76 (4H, m, Ar), 2.82–2.14 (4H, m, ^{i}Pr CH), 1.34–0.70 (24H, m, ^{i}Pr CH_3) ppm.

δ_C (75.5 MHz, CD_2Cl_2): 157.43, 148.97, 136.20 (C, Ar), 134.14 (CH, d, J = 10.0 Hz, *o*-PPh_3), 132.67, 131.12, 130.17, 129.74 (CH, Ar), 129.35 (CH, *p*-PPh_3), 129.22 (C, Ar), 128.70 (CH, Ar), 128.47 (CH, d, J = 9.0 Hz, *m*-PPh_3), 125.30, 124.72, 123.77, 116.09, 105.35 (CH, Ar), 26.53, 26.30, 22.48, 22.23 (CH/CH_3, ^{i}Pr) ppm.

δ_P (121.5 MHz, CD_2Cl_2): –151.27 ppm.

Analysis*: Calc. for $C_{53}H_{56}N_{11}RuP$: C 65.01; H 5.76; N 15.74. Found: C 68.91; H 6.06; N 10.49.

* = analyses to $C_{53}H_{56}N_7RuP$ after loss of 2 * N_2 from the azides.

(2,6-Bis(2,6-diisopropylphenyl)imidazol-2-ylidene)pyridine ruthenium(II) pyridine dichloride (**134**)

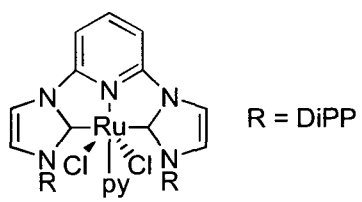

$[RuCl_2(nbd)(py)_2]$ (300 mg, 0.71 mmol) and complex **36** (377 mg, 0.71 mmol) were dissolved in THF (30 mL) and stirred for 6 hours. After this time the solvent was evaporated and the residue washed with PE (20 mL). Crystallisation occurred by the slow diffusion of Et_2O into a DCM solution, affording 431 mg of the title compound as red-brown crystals in 78% yield.

δ_H (400.0 MHz, CD_2Cl_2): 8.42 (2H, dd, *J* = 6.5, 1.5 Hz, Ar), 7.96 (2H, d, *J* = 2.0 Hz, Ar), 7.63–7.52 (2H, m, Ar), 7.41–7.28 (7H, m, Ar), 7.19–7.08 (2H, m, Ar), 7.03 (1H, d, *J* = 2.0 Hz, Ar), 6.94 (2H, d, *J* = 8.0 Hz, Ar), 3.07 (4H, septet, *J* = 7.0 Hz, ^{i}Pr CH), 0.97, 0.91 (each 12H, d, *J* = 7.0 Hz, ^{i}Pr CH_3) ppm.

δ_C (100.6 MHz, CD_2Cl_2): 204.33 (C, C_{NHC}), 157.96 (C, Ar), 154.98 (CH, Ar), 148.44, 147.67, 136.91 (C, Ar), 134.16, 132.50 (CH, Ar), 130.95 (C, Ar), 130.25 (CH, Ar), 126.48 (C, Ar), 126.37, 125.32, 124.75, 123.91, 121.46, 116.57, 104.16 (CH, Ar), 28.28 (CH, ^{i}Pr), 26.52, 22.90 (CH_3, ^{i}Pr) ppm.

Analysis: Calc. for $C_{40}H_{46}N_6Ru$: C 61.37; H 5.92; N 10.74. Found: C 61.29; H 5.88; N 10.62.

(2,6-Bis(2,6-diisopropylphenyl)imidazol-2-ylidene)-3,5-dimethylpyridine iridium(I) chloride (**137**)

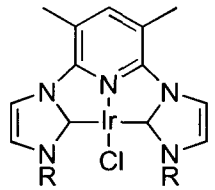

R = DiPP

A solution of ligand **58** (200 mg, 0.36 mmol) in THF (10 mL) at –78 °C was added to a solution of $[IrCl(COE)_2]_2$ in THF (10 mL) at –78 °C, stirred for 15 mins, warmed to RT and stirred for 16 hours. After this time, the solvent was removed and the solid washed with petrol, yielding 209 mg of a green solid in 74% yield.

δ_H (400.0 MHz, C_6D_6): 7.64 (2H, d, J = 2.0 Hz, imidazol-2-ylidene), 7.31–7.08 (7H, m, Ar), 6.59 (2H, d, J = 2.0 Hz, imidazol-2-ylidene), 3.11 (4H, septet, J = 7.0 Hz, ^{i}Pr CH), 2.16 (6H, s, py-Me), 1.31, 1.13 (each 12H, d, J = 7.0 Hz, ^{i}Pr CH_3) ppm.
δ_C (100.6 MHz, C_6D_6): 188.43 (C, C_{NHC}), 153.36, 145.67, 136.98 (C, Ar), 131.36, 129.63, 124.51, 123.72, 116.91 (CH, Ar), 114.48 (C, Ar), 28.95 (CH, ^{i}Pr), 24.73 and 24.17 (CH_3, ^{i}Pr), 18.29 (CH_3, py-Me) ppm.
Analysis: Calc. for $C_{37}H_{45}N_5IrCl$: C 56.43; H 5.76; N 8.89. Found: C 56.54, H 5.80; N 8.86.

(2,6-Bis(2,6-DiPP)imidazol-2-ylidene)-3,5-dimethylpyridine iridium(III) chloromethyl dichloride (**138**)

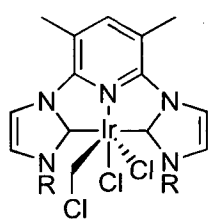

R = DiPP

Compound **137** (75 mg, 0.10 mmol) was dissolved in DCM (20 mL) and stirred for 1 hour. After this time, the solvent was removed and the solid was crystallised by slow diffusion of Et_2O into a DCM solution, yielding 80 mg of yellow needles in 96% yield.

δ_H (400.0 MHz, C_6D_6): 8.06 (2H, d, J = 2.0 Hz, imidazol-2-ylidene), 7.44 (1H, s, py-Me), 7.34–7.26 (4H, m, Ar), 7.19–7.10 (2H, m, Ar), 7.02 (2H, d, J = 2.0 Hz, imidazol-2-ylidene), 3.29 (2H, septet, J = 6.5 Hz, ^{i}Pr CH), 2.77 (6H, s, py-Me), 2.63 (2H, septet, J = 6.5 Hz, ^{i}Pr CH), 1.47 (2H, s, CH_2Cl), 1.19, 1.13, 1.08, 0.95 (each 6H, d, J = 6.5 Hz, ^{i}Pr CH_3) ppm.

δ_C (100.6 MHz, C_6D_6): 175.57 (C, C_{NHC}), 152.09, 147.52 (C, Ar), 147.21 (CH, Ar), 145.21, 134.17 (C, Ar), 129.60, 124.90, 123.68, 122.96, 118.94 (CH, Ar), 116.66 (C, Ar), 29.26, 28.07, 26.05, 25.81, 22.93, 22.54 (CH/CH_3, ^{i}Pr), 19.29 (CH_3, py-Me), 13.46 (CH_2, CH_2Cl) ppm.

Analysis: Calc. for $C_{38}H_{47}N_5IrCl_3$: C 52.32; H 5.43; N 8.03. Found: C 52.44, H 5.45; N 8.14.

(2,6-Bis(2,6-diisopropylphenyl)imidazol-2-ylidene)-3,5-dimethylpyridine iridium (III) chloride (**139**)

R = DiPP

Compound **137** (150 mg, 0.19 mmol) was dissolved in THF (20 mL) and $PhICl_2$ (58 mg, 0.19 mmol) was added under a counterflow of N_2. The solution was stirred for 16 hours, filtered and solvents were removed *in vacuo*. The residue was dissolved in the minimum amount of DCM and Et_2O (50 mL) was added, precipitating 110 mg of a yellow powder in 67% yield.

δ_H (400.0 MHz, C_6D_6): 8.68 (1H, s, py-Me), 8.32 (2H, d, J = 6.5 Hz, imidazol-2-ylidene), 7.54 (2H, d, J = 6.5 Hz, imidazol-2-ylidene), 7.41 (4H, d, J = 8.0 Hz, Ar), 7.24 (2H, t, J = 8.0 Hz, Ar), 3.04 (4H, septet, J = 6.5 Hz, ^{i}Pr CH), 2.95 (6H, s, py-Me), 1.22, 1.11 (each 12H, d, J = 6.5 Hz, ^{i}Pr CH_3) ppm.

δ_C (100.6 MHz, C_6D_6): 167.72 (C, C_{NHC}), 153.10 (CH, Ar), 147.25 (C, Ar), 138.29 (CH, Ar), 135.16 (C, Ar), 132.03 (CH, Ar), 128.10 (C, Ar), 127.66, 125.06 (CH, Ar), 120.38 (C, Ar), 28.88 (CH, ^{i}Pr), 26.68, 22.14 (CH_3, ^{i}Pr), 19.97 (CH_3, py-Me) ppm.

Analysis: Calc. for $C_{37}H_{45}N_5IrCl_3$: C 51.77; H 5.28; N 8.16. Found: C 51.71, H 5.23; N 8.10.

(2,6-Bis(2,6-diisopropylphenyl)imidazol-2-ylidene)-3,5-dimethylpyridine iridium (I) hydride (**141**)

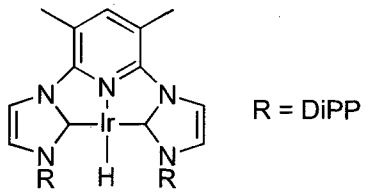

Complex **137** (75 mg, 0.10 mmol) and NaO^{i}Pr (10 mL of a 0.01 M soln. in IPA, 0.10 mmol) were dissolved in THF (10 mL) and stirred for 16 hours at RT. After this time, solvents were removed *in vacuo* and the resulting solid was crystallised from Et_2O at 5 °C, affording 69 mg of the title compound as a brown solid in 92% yield.

δ_H (400.0 MHz, $(CD_3)_2CO$): 8.42 (2H, d, J = 2.5 Hz, imidazol-2-ylidene), 7.42–7.25 (5H, m, Ar + imidazol-2-ylidene), 7.14 (4H, d, J = 8.0 Hz, Ar), 2.90 (6H, s, py-Me), 2.73 (4H, septet, J = 7.0 Hz, ^{i}Pr CH), 1.11, 1.03 (each 12H, d, J = 7.0 Hz, ^{i}Pr CH_3), –12.97 (1H, s, Ir-H) ppm.

δ_C (100.6 MHz, $(CD_3)_2CO$): 187.81 (C, C_{NHC}), 147.71, 147.44, 138.46 (C, Ar), 137.34, 129.82, 124.43, 123.06, 117.66 (CH, Ar), 112.92 (C, Ar), 29.17 (CH, ^{i}Pr), 25.16, 24.23 (CH_3, ^{i}Pr), 19.51 (CH_3, py-Me) ppm.

Analysis: Calc. for $C_{37}H_{46}N_5Ir$: C 59.02; H 6.16; N 9.30. Found: C 58.93; H 6.10; N 9.17.

(2,6-Bis(2,6-diisopropylphenyl)imidazol-2-ylidene)-3,5-dimethylpyridine iridium(I) pyridine tetrakis[3,5-bis(trifluoromethyl)phenyl]borate (**145**)

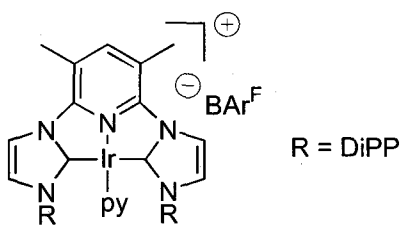

Complex **137** (250 mg, 0.32 mmol) and NaBAr^F (281 mg, 0.32 mmol) were dissolved in pyridine (10 mL) and stirred for 16 hours at RT. After this time, solvents were removed *in vacuo*, the resulting solid was dissolved in Et_2O and filtered through Celite. Crystallisation occurred by the slow diffusion of PE into a THF solution, affording 402 mg of the title compound as a dark green powder in 74% yield.

δ_H (400.0 MHz, $(CD_3)_2CO$): 8.47 (2H, d, J = 2.5 Hz, imidazol-2-ylidene), 8.04 (1H, s, Ar), 7.85 (1H, d, J = 5.0 Hz, Ar), 7.72 (8H, br s, *o*-BAr^F), 7.60 (4H, br s, *p*-BAr^F), 7.44 (2H, d, J = 2.5 Hz, imidazol-2-ylidene), 7.10–7.01 (4H, m, Ar), 6.87 (4H, d, J = 8.0 Hz, Ar), 6.47 (2H, dd, J = 8.0, 5.0 Hz, Ar), 2.86 (4H, septet, J = 7.0 Hz, ^{i}Pr CH), 2.81 (6H, s, py-Me), 1.03, 0.95 (each 12H, d, J = 7.0 Hz, ^{i}Pr CH_3) ppm.

δ_C (100.6 MHz, $(CD_3)_2CO$): 188.57 (C, C_{NHC}), 162.82 (C, q, J_{C-B} = 49.5 Hz, *i*-BAr^F), 155.48 (CH, Ar), 145.93 (C, Ar), 143.99 (CH, Ar), 136.20 (C, Ar), 135.76, 135.30, 131.26 (CH, Ar), 130.24 (C, q, J_{C-F} = 32.0 Hz, CF_3), 126.95 (C, Ar), 126.49, 125.23, 124.71 (CH, Ar), 124.25 (C, Ar), 120.32, 118.65 (CH, Ar), 116.50 (C, Ar), 29.06 (CH, ^{i}Pr), 25.57, 22.89 (CH_3, ^{i}Pr), 19.01 (CH_3, py-Me) ppm.

δ_F (282.4 MHz, acetone): –63.21 ppm.

Analysis: Calc. for $C_{74}H_{62}N_6BF_{24}Ir$: C 52.46; H 3.69; N 4.96. Found: C 52.53; H 3.57; N 4.83.

(2,6-Bis(2,6-diisopropylphenyl)imidazol-2-ylidene)-3,5-dimethylpyridine iridium(I) carbonyl hexafluorophosphate (**147**)

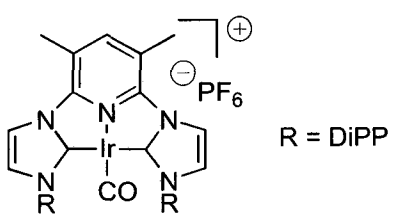

Compound **137** (75 mg, 0.10 mmol) and KPF_6 (18 mg, 0.10 mmol) were dissolved in THF (15 mL) and CO was bubbled through the solution for 5 mins, resulting in the formation of a brown solution. The reaction was stirred for 15 minutes and a colour change from brown to purple was observed. After this time, solvents were removed and the resulting solid was dissolved in MeCN, filtered through Celite and crystallised by the slow diffusion of Et_2O into the MeCN solution, affording 74 mg of the title compound as purple needles in 84% yield.

δ_H (400.0 MHz, $(CD_3)_2CO$): 8.30 (2H, d, J = 2.5 Hz, imidazol-2-ylidene), 7.97 (1H, s, py-H), 7.57 (2H, d, J = 2.5 Hz, imidazol-2-ylidene), 7.42 (2H, t, J = 8.0 Hz, *p*-Ar), 7.26 (4H, d, J = 8.0 Hz, *m*-Ar), 2.77 (6H, s, py-Me), 2.63 (4H, septet, J = 7.0 Hz, ^{i}Pr CH), 1.16, 1.13 (each 12H, d, J = 7.0 Hz, ^{i}Pr CH_3) ppm.

δ_C (100.6 MHz, $(CD_3)_2CO$): 193.08 (C, CO), 189.69 (C, C_{NHC}), 153.86 (CH, Ar), 153.22, 146.21, 135.44 (C, Ar), 131.52, 125.45, 124.98, 121.87 (CH, Ar), 119.71 (C, Ar), 29.13 (CH, ^{i}Pr), 24.43, 24.08 (CH_3, ^{i}Pr), 18.48 (CH_3, py-Me) ppm.

IR (nujol mull): C≡O 1983 cm^{-1}

Analysis: Calc. for $C_{38}H_{45}N_5OF_6PIr$: C 49.34; H 4.90; N 7.57. Found: C 49.19; H 4.92; N 7.48.

(2,6-Bis(2,6-diisopropylphenyl)imidazol-2-ylidene)-3,5-dimethylpyridine iridium(I) bis(ethylene) hexafluorophosphate (**148**)

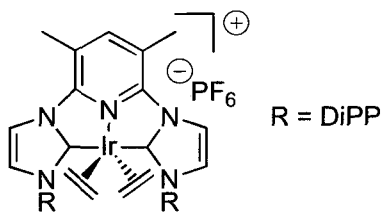

Compound **137** (75 mg, 0.10 mmol) and KPF_6 (18 mg, 0.10 mmol) were dissolved in THF (15 mL) and ethylene was bubbled through the solution for 15 minutes, resulting in a colour change from green to orange. After this time, solvents were removed *in vacuo*, the resulting solid was dissolved in Et_2O, filtered through Celite, concentrated and crystallised by slow diffusion of PE into a THF solution, affording 81 mg of the title compound as yellow needles in 89% yield.

δ_H (400.0 MHz, $(CD_3)_2CO$): 8.50 (2H, d, J = 2.5 Hz, imidazol-2-ylidene), 8.07 (1H, s, py-H), 7.47 (2H, t, J = 8.0 Hz, *p*-Ar), 7.39 (2H, d, J = 2.5 Hz, imidazol-2-ylidene), 7.30 (4H, d, J = 8.0 Hz, *m*-Ar), 2.97 (6H, s, py-Me), 2.23 (4H, septet, J = 7.0 Hz, ^{i}Pr CH), 1.90 (8H, s, ethylene), 1.28, 0.97 (each 12H, d, J = 7.0 Hz, ^{i}Pr CH_3) ppm.

δ_C (100.6 MHz, $(CD_3)_2CO$): 167.89 (C, C_{NHC}), 150.28 (C, Ar), 149.04 (CH, Ar), 147.05, 134.66 (C, Ar), 131.67, 126.42 (CH, Ar), 125.04 (C, Ar), 124.23, 120.80 (CH, Ar), 118.42 (C, Ar), 32.51, 30.99 (CH_2, ethylene), 28.91, 27.14, 21.76 (CH/CH_3, ^{i}Pr), 19.35 (CH_3, py-Me) ppm.

IR (nujol mull): $H_2C=CH_2$ 1598 cm^{-1}

Analysis: Calc. for $C_{41}H_{53}N_5F_6PIr$: C 51.67; H 5.61; N 7.35. Found: C 51.61; H 5.50; N 7.29.

(2,6-Bis(2,6-diisopropylphenyl)imidazol-2-ylidene)-3,5-dimethylpyridine iridium (I) acetonitrile hexafluorophosphate (**149**)

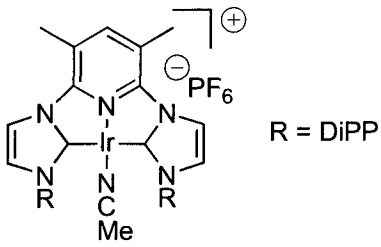

Compound **137** (150 mg, 0.19 mmol) and KPF_6 (35 mg, 0.19 mmol) were dissolved in MeCN (10 mL) and stirred for 16 hours at RT. After this time, solvents were removed *in vacuo* and the resulting solid was crystallised by slow diffusion of Et_2O into a MeCN solution, affording 144 mg of the title compound as dark green crystals in 81% yield.

δ_H (400.0 MHz, $(CD_3)_2CO$): 8.44 (2H, d, J = 2.5 Hz, imidazol-2-ylidene), 8.03 (1H, s, py-4), 7.54 (2H, d, J = 2.5 Hz, imidazol-2-ylidene), 7.49–7.45 (2H, m, *p*-D^{i}PP), 7.35 (4H, d, J = 7.5 Hz, *m*-D^{i}PP), 2.84 (6H, s, py-Me), 2.79 (4H, septet, J = 7.0 Hz, ^{i}Pr CH), 1.77 (3H, s, MeCN), 1.15, 1.12 (each 12H, d, J = 7.0 Hz, ^{i}Pr CH_3) ppm.
δ_C (100.6 MHz, $(CD_3)_2CO$): 188.71 (C, C_{NHC}), 155.22, 147.04 (C, Ar), 145.02 (CH, Ar), 135.91 (C, Ar), 131.36, 124.67, 120.71 (CH, Ar), 116.80 (C, Ar), 29.16 (CH, ^{i}Pr), 24.29, 24.14 (CH_3, ^{i}Pr), 18.57 (CH_3, py-Me), 3.11 (CH_3, MeCN) ppm.
Analysis: Calc. for $C_{39}H_{48}N_6F_6IrP$: C 49.94; H 5.16; N 8.96. Found: C 49.85; H 5.15; N 9.01.

Representative procedure for the transfer hydrogenation of acetophenone

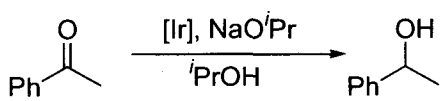

A Youngs ampoule was charged with iridium complex **145** (34 mg, 0.02 mmol). Acetophenone (0.23 mL, 2.0 mmol), IPA (3 mL) and NaO^{i}Pr (2 mL of a 0.01 M soln. in IPA, 0.02 mmol) were added; the ampoule was partially evacuated and heated to the desired temperature. Samples were taken after 3 and 20 hours and analysed by ^{1}H NMR spectroscopy.

Chapter 9

References

1. Hine, J., *Divalent Carbon.*; Ronald Press: New York, 1964.
2. Geuther, A., *Justus Liebigs Ann. Chem.* **1862,** 123, 121.
3. Hine, J., *J. Am. Chem. Soc.* **1950,** 72, 2438-2445.
4. Nef, J. U., *Justus Liebigs Ann. Chem.* **1897,** 298, 367.
5. Kirmse, W., *Carbene Chemistry.* 1st ed.; Academic Press: New York, 1964.
6. Nozaki, H.; Takaya, H.; Moriuti, S.; Noyori, R., *Tetrahedron* **1968,** 24, 3655-3669.
7. Fischer, E. O.; Maasböl, A., *Angew. Chem. Int. Ed.* **1964,** 4, 580-581.
8. Schrock, R., *J. Am. Chem. Soc.* **1975,** 97, 6577-6578.
9. Wanzlick, H. W., *Angew. Chem. Int. Ed.* **1962,** 1, 75-80.
10. Öfele, K., *J. Organomet. Chem.* **1968,** 12, P42-43.
11. Wanzlick, H. W.; Schönherr, H. J., *Angew. Chem. Int. Ed.* **1968,** 7, 141-142.
12. Arduengo III, A. J.; Harlow, R. L.; Kline, M., *J. Am. Chem. Soc.* **1991,** 113, 361-363.
13. Alder, R. W.; Allen, P. R.; Murray, M.; Orpen, A. G., *Angew. Chem. Int. Ed.* **1996,** 35, 1121-1123.
14. Kirmse, W., *Angew. Chem. Int. Ed.* **2003,** 42, 2117-2119.
15. Iwamoto, E.; Hirai, K.; Tomioka, H., *J. Am. Chem. Soc.* **2003,** 125, 14664-14665.
16. Kawano, M.; Hirai, K.; Tomioka, H.; Ohashi, Y., *J. Am. Chem. Soc.* **2007,** 129, 2383-2391.
17. Scholl, M.; Ding, S.; Lee, C. W.; Grubbs, R. H., *Org. Lett.* **1999,** 1, 953-956.
18. Herrmann, W. A.; Köcher, C., *Angew. Chem. Int. Ed.* **1997,** 36, 2162-2187.
19. Jacobsen, H.; Correa, A.; Costabile, C.; Cavallo, L., *J. Organomet. Chem.* **2006,** 691, 4350-4358.
20. Marion, N.; Díez-González, S.; Nolan, S. P., *Angew. Chem. Int. Ed.* **2007,** 46, 2988-3000.
21. Mayr, M.; Wurst, K.; Ongania, K.-H.; Buchmeiser, M. R., *Chem. Eur. J.* **2004,** 10, 1256-1266.
22. Michelin, R. A.; Zanotto, L.; Braga, D.; Sabatino, P.; Angelici, R. J., *Inorg. Chem.* **1988,** 27, 85-92.
23. Stylianides, N.; Danopoulos, A. A.; Tsoureas, N., *J. Organomet. Chem.* **2005,** 690, 5948-5958.
24. Arnold, P. L.; Pearson, S., *Coord. Chem. Rev.* **2007,** 251, 596-609.
25. Martin, D.; Baceiredo, A.; Gornitzka, H.; Schoeller, W. W.; Bertrand, G., *Angew. Chem. Int. Ed.* **2005,** 44, 1700-1703.

26. Tumanskii, B.; Pine, P.; Apeloig, Y.; Hill, N. J.; West, R., *J. Am. Chem. Soc.* **2005,** 127, 8248-8249.
27. Gudat, D.; Gans-Eichler, T.; Nieger, M., *Chem. Commun.* **2004**, 2434-2435.
28. Arduengo III, A. J.; Davidson, F.; Dias, H. V. R.; Goerlich, J. R.; Khasnis, D.; Marshall, W. J.; Prakasha, T. K., *J. Am. Chem. Soc.* **1997,** 119, 12742-12749.
29. Gnanamgari, D.; Moores, A.; Rajaseelan, E.; Crabtree, R. H., *Organometallics* **2007,** 26, 1226-1230.
30. Krahulic, K. E.; Enright, G. D.; Parvez, M.; Roesler, R., *J. Am. Chem. Soc.* **2005,** 127, 4142-4143.
31. Hahn, F. E.; Wittenbecher, L.; Boese, R.; Bläser, D., *Chem. Eur. J.* **1999,** 5, 1931-1935.
32. Weiss, R.; Reichel, S.; Handke, M.; Hampel, F., *Angew. Chem. Int. Ed.* **1998,** 37, 344-347.
33. Alcarazo, M.; Roseblade, S. J.; Cowley, A. R.; Fernández, R.; Brown, J. M.; Lassaletta, J. M., *J. Am. Chem. Soc.* **2005,** 127, 3290-3291.
34. Weskamp, T.; Böhm, V. P. W.; Herrmann, W. A., *J. Organomet. Chem.* **2000,** 600, 12-22.
35. Ruiz, J.; Garcia, G.; Mosquera, M. E. G.; Perandones, B. F.; Gonzalo, M. P.; Vivanco, M., *J. Am. Chem. Soc.* **2005,** 127, 8584-8585.
36. Fürstner, A.; Alcarazo, M.; César, V.; Lehmann, C. W., *Chem. Commun.* **2006**, 2176-2178.
37. Lin, I. J. B.; Vasam, C. S., *Coord. Chem. Rev.* **2007,** 251, 642-670.
38. Danopoulos, A. A.; Winston, S.; Gelbrich, T.; Hursthouse, M. B.; Tooze, R. P., *Chem. Commun.* **2002**, 482-483 and references therein.
39. Mata, J. A.; Poyatos, M.; Peris, E., *Coord. Chem. Rev.* **2007,** 251, 841-859.
40. Downing, S. P.; Danopoulos, A. A., *Organometallics* **2006,** 25, 1337-1340.
41. Chiu, P. L.; Lee, H. M., *Organometallics* **2005,** 24, 1692-1702.
42. Kernbach, U.; Ramm, M.; Luger, P.; Fehlhammer, W. P., *Angew. Chem. Int. Ed.* **1996,** 35, 310-312.
43. Hu, X.; Meyer, K., *J. Organomet. Chem.* **2005,** 690, 5474-5484.
44. Mas-Marza, E.; Peris, E.; Castro-Rodriguez, I.; Meyer, K., *Organometallics* **2005,** 24, 3158-3162.
45. Moulton, C. J.; Shaw, B. L., *J. Chem. Soc. Dalton Trans.* **1976**, 1020-1024.
46. Matsumura, N.; Kawano, J.; Fukunishi, N.; Inoue, H., *J. Am. Chem. Soc.* **1995,** 117, 3623-3624.

47. Chen, J. C. C.; Lin, I. J. B., *J. Chem. Soc. Dalton Trans.* **2000**, 839-840.
48. Schneider, N.; Cesar, V.; Bellemin-Laponnaz, S.; Gade, L. H., *Organometallics* **2005,** 24, 4886-4888.
49. Wright, J. A.; Danopoulos, A. A.; Motherwell, W. B.; Carroll, R. J.; Ellwood, S., *J. Organomet. Chem.* **2006,** 691, 5204-5210.
50. Pugh, D.; Danopoulos, A. A., *Coord. Chem. Rev.* **2007,** 251, 610-641.
51. Grundemann, S.; Albrecht, M.; Loch, J. A.; Faller, J. W.; Crabtree, R. H., *Organometallics* **2001,** 20, 5485-5488.
52. Danopoulos, A. A.; Tulloch, A. A. D.; Winston, S.; Eastham, G.; Hursthouse, M. B., *Dalton Trans.* **2003**, 1009-1015.
53. Hahn, F. E.; Jahnke, M. C.; Pape, T., *Organometallics* **2007,** 26, 150-154.
54. Andavan, G. T. S.; Bauer, E. B.; Letko, C. S.; Hollis, T. K.; Tham, F. S., *J. Organomet. Chem.* **2005,** 690, 5938-5947.
55. Rubio, R. J.; Andavan, G. T. S.; Bauer, E. B.; Hollis, T. K.; Cho, J.; Tham, F. S.; Donnadieu, B., *J. Organomet. Chem.* **2005,** 690, 5353-5364.
56. Hahn, F. E.; Jahnke, M. C.; Gomez-Benitez, V.; Morales-Morales, D.; Pape, T., *Organometallics* **2005,** 24, 6458-6463.
57. Simons, R. S.; Custer, P.; Tessier, C. A.; Youngs, W. J., *Organometallics* **2003,** 22, 1979-1982.
58. Nielsen, D. J.; Cavell, K. J.; Skelton, B. W.; White, A. H., *Inorg. Chim. Acta* **2002,** 327, 116-125.
59. Tulloch, A. A. D.; Danopoulos, A. A.; Tizzard, G. J.; Coles, S. J.; Hursthouse, M. B.; Hay-Motherwell, R. S.; Motherwell, W. B., *Chem. Commun.* **2001**, 1270-1271.
60. Douthwaite, R. E.; Houghton, J.; Kariuki, B. M., *Chem. Commun.* **2004**, 698-699.
61. Moser, M.; Wucher, B.; Kunz, D.; Rominger, F., *Organometallics* **2007,** 26, 1024-1030.
62. Danopoulos, A. A.; Winston, S.; Motherwell, W. B., *Chem. Commun.* **2002**, 1376-1377.
63. McGuinness, D. S.; Gibson, V. C.; Wass, D. F.; Steed, J. W., *J. Am. Chem. Soc.* **2003,** 125, 12716-12717.
64. McGuinness, D. S.; Gibson, V. C.; Steed, J. W., *Organometallics* **2004,** 23, 6288-6292.
65. Inamoto, K.; Kuroda, J.; Hiroya, K.; Noda, Y.; Watanabe, W.; Sakamoto, T., *Organometallics* **2006,** 25, 3095-3098.

66. Poyatos, M.; Mata, J. A.; Falomir, E.; Crabtree, R. H.; Peris, E., *Organometallics* **2003,** 22, 1110-1114.
67. Son, S. U.; Park, K. H.; Lee, Y.-S.; Kim, B. Y.; Choi, C. H.; Lah, M. S.; Jang, Y. H.; Jang, D.-J.; Chung, Y. K., *Inorg. Chem.* **2004,** 43, 6896-6898.
68. Poyatos, M.; Mas-Marza, E.; Mata, J. A.; Sanau, M.; Peris, E., *Eur. J. Inorg. Chem.* **2003**, 1215-1221.
69. Wilson, J. M.; Sunley, G. J.; Adams, H.; Haynes, A., *J. Organomet. Chem.* **2005,** 690, 6089-6095.
70. Peris, E.; Loch, J. A.; Mata, J.; Crabtree, R. H., *Chem. Commun.* **2001**, 201-202.
71. Loch, J. A.; Albrecht, M.; Peris, E.; Mata, J.; Faller, J. W.; Crabtree, R. H., *Organometallics* **2002,** 21, 700-706.
72. Churruca, F.; SanMartin, R.; Inés, B.; Tellitu, I.; Domínguez, E., *Adv. Synth. Catal.* **2007,** 348, 1836-1840.
73. Wright, J. A.; Danopoulos, A. A.; Motherwell, W. B.; Carroll, R. J.; Ellwood, S.; Saßmannshausen, J., *Eur. J. Inorg. Chem.* **2006**, 4857-4865.
74. Danopoulos, A. A.; Tsoureas, N.; Green, J. C.; Hursthouse, M. B., *Chem. Commun.* **2003**, 756-757.
75. Nielsen, D. J.; Magill, A. M.; Yates, B. F.; Cavell, K. J.; Skelton, B. W.; White, A. H., *Chem. Commun.* **2002**, 2500-2501.
76. Pugh, D.; Wright, J. A.; Freeman, S.; Danopoulos, A. A., *Dalton Trans.* **2006**, 775-782.
77. Danopoulos, A. A.; Tsoureas, N.; Wright, J. A.; Light, M. E., *Organometallics* **2004,** 23, 166-168.
78. Danopoulos, A. A.; Wright, J. A.; Motherwell, W. B.; Ellwood, S., *Organometallics* **2004,** 23, 4807-4810.
79. Danopoulos, A. A.; Wright, J. A.; Motherwell, W. B., *Chem. Commun.* **2005**, 784-786.
80. Wright, J. A.; Danopoulos, A. A., Unpublished results.
81. Schlosser, M.; Rausis, T., *Eur. J. Org. Chem.* **2004**, 1018-1024.
82. Gros, P.; Viney, C.; Fort, Y., *Synlett* **2002,** 4, 628-630.
83. Sedelmeier, J.; Bolm, C., *J. Org. Chem.* **2005,** 70, 6904-6906.
84. Pugh, D., *Acta Cryst.* **2006,** C62, o590-592.
85. Shimizu, G. K. H.; Enright, G. D.; Ratcliffe, C. I.; Preston, K. F.; Reid, J. L.; Ripmeester, J. A., *Chem. Commun.* **1999**, 1485-1486.

86. Caballero, A.; Díez-Barra, E.; Jalón, F. A.; Merino, S.; Rodríguez, A. M.; Tejeda, J., *J. Organomet. Chem.* **2001,** 627, 263-264.
87. Kawatsura, M.; Hartwig, J. F., *Organometallics* **2001,** 20, 1960-1964.
88. Hagadorn, J. R.; Arnold, J., *Organometallics* **1999,** 17, 1355-1368.
89. Jagirdar, B. R.; Murugavel, R.; Schmidt, H.-G., *Inorg. Chim. Acta* **1999,** 292, 105-107.
90. Leuthäußer, S.; Schwarz, D.; Plenio, H., *Chem. Eur. J.* **2007,** 13, 7195-7203 and references therein.
91. Adams, N.; Bigmore, H. R.; Blundell, T. L.; Boyd, C. L.; Dubberley, S. R.; Sealey, A. J.; Cowley, A. R.; Skinner, M. E. G.; Mountford, P., *Inorg. Chem.* **2005,** 44, 2882-2894.
92. Arney, D. J.; Bruck, M. A.; Huber, S. R.; Wigley, D. E., *Inorg. Chem.* **1992,** 31, 3749-3755.
93. Jeske, P.; Haselhorst, G.; Weyhermüller, T.; Wieghardt, K.; Nuber, B., *Inorg. Chem.* **1994,** 33, 2462-2471.
94. Hart, R.; Levason, W.; Patel, B.; Reid, G., *J. Chem. Soc. Dalton Trans.* **2002,** 3153-3159.
95. Vidyaratne, I.; Gambarotta, S.; Korobkov, I., *Inorg. Chem.* **2005,** 44, 1187-1189.
96. Cavell, K. J.; McGuinness, D. S., *Coord. Chem. Rev.* **2004,** 248, 671-681.
97. Abernethy, C. D.; Codd, G. M.; Spicer, M. D.; Taylor, M. K., *J. Am. Chem. Soc.* **2003,** 125, 1128-1129.
98. Hills, A.; Hughes, D. L.; Leigh, G. J.; Prieto-Alcón, R., *J. Chem. Soc. Dalton Trans.* **1993,** 3609-3617.
99. Herrmann, W. A.; Lobmaier, G. M.; Elison, M., *J. Organomet. Chem.* **1996,** 520, 231-234.
100. Shivaiah, V.; Das, S. K., *Angew. Chem. Int. Ed. Eng.* **2006,** 45, 245-248.
101. Venkataramanan, N. S.; Kuppuraj, G.; Rajagopal, S., *Coord. Chem. Rev.* **2005,** 249, 1249-1268.
102. Addison, A. W.; Rao, T. N.; Reedijk, J.; van Rijn, J.; Verschoor, G. C., *J. Chem. Soc. Dalton Trans.* **1984,** 1349-1356.
103. Seyferth, K.; Taube, R., *J. Organomet. Chem.* **1982,** 229, C19-23.
104. Howard, C. G.; Girolami, G. S.; Wilkinson, G.; Thornton-Pett, M.; Hursthouse, M. B., *J. Chem. Soc., Chem. Commun.* **1983,** 1163-1164.
105. Gallo, E.; Solari, E.; Floriani, C.; Chiesi-Villa, A.; Rizzoli, C., *Inorg. Chem.* **1997,** 36, 2178-2186.

106. Greenwood, N. N.; Earnshaw, A., *Chemistry of the Elements*. 1st ed.; Pergamon Press Ltd.: 1985; p 1315.

107. Rahman, A. F. M. M.; Jackson, W. G.; Willis, A. C., *Inorg. Chem.* **2004,** 43, 7558-7560.

108. Müller, G.; Klinga, M.; Leskelä, M.; Rieger, B., *Z. Anorg. Allg. Chem.* **2002,** 628, 2839-2846.

109. Winston, S.; Stylianides, N.; Tulloch, A. A. D.; Wright, J. A.; Danopoulos, A. A., *Polyhedron* **2004,** 23, 2813-2820.

110. Taube, R.; Langlotz, J.; Sieler, J.; Gelbrich, T.; Tittes, K., *J. Organomet. Chem.* **2000,** 597, 92-104.

111. Blake, A. J.; Brechin, E. K.; Codron, A.; Gould, R. O.; Grant, C. M.; Parsons, S.; Rawson, J. M.; Winpenny, R. E. P., *J. Chem. Soc., Chem. Commun.* **1995**, 1983-1985.

112. Halcrow, M. S.; Sun, J.-S.; Huffman, J. C.; Christou, G., *Inorg. Chem.* **1995,** 34, 4167-4177.

113. Atkins, A. J.; Blake, A. J.; Schröder, M., *J. Chem. Soc. Chem. Commun.* **1993**, 1662-1665.

114. Escuer, A.; Font-Bardía, M.; Kumar, S. B.; Solans, X.; Vicente, R., *Polyhedron* **1999,** 18, 909-914.

115. Schlager, O.; Wieghardt, K.; Rufinska, A.; Nuber, B., *J. Chem. Soc. Dalton Trans.* **1996**, 1659-1668.

116. Connor, E. F.; Younkin, T. R.; Henderson, J. I.; Waltman, A. W.; Grubbs, R. H., *Chem. Commun.* **2003**, 2272-2273.

117. Waltman, A. W.; Ritter, T.; Grubbs, R. H., *Organometallics* **2006,** 25, 4238-4239.

118. Herrmann, W. A.; Schneider, S. K.; Öfele, K.; Sakamoto, M.; Herdtweck, E., *J. Organomet. Chem.* **2004,** 689, 2441-2449.

119. Kovacevic, A.; Gründemann, S.; Miecznikowski, J. R.; Clot, E.; Eisenstein, O.; Crabtree, R. H., *Chem. Commun.* **2002**, 2580-2581.

120. Bart, S. C.; Lobkovsky, E.; Chirik, P. J., *J. Am. Chem. Soc.* **2004,** 126, 13794-13807.

121. Trovitch, R. J.; Lobkovsky, E.; Chirik, P. J., *Inorg. Chem.* **2006,** 45, 7252-7260.

122. Baker, R. T.; Morton, J. R.; Preston, K. F.; Williams, A. J.; Le Page, Y., *Inorg. Chem.* **1991,** 30, 113-116.

123. Karlin, K. D., *Progress in Inorganic Chemistry: Nonclassical Carbonyls*, John Wiley and Sons: 2007; **49**; 1-112.

124. Chadwell, S. J.; Coles, S. J.; Edwards, P. G.; Hursthouse, M. B., *J. Chem. Soc. Dalton Trans.* **1996**, 1105-1112.

125. Sellman, D.; Kleine-Kleffman, U.; Zapf, L., *J. Organomet. Chem.* **1984,** 263, 321-331.

126. Brookhart, M.; Chandler, W. A.; Pfister, A. C.; Santini, C. C.; White, P. S., *Organometallics* **1992,** 11, 1263-1274.

127. Geier, S.; Goddard, R.; Holle, S.; Jolly, P. W.; Krüger, C.; Lutz, F., *Organometallics* **1997,** 16, 1612-1620.

128. Jones, W. D.; Foster, G. P.; Putinas, J. M., *Inorg. Chem.* **1987,** 26, 2120-2127.

129. Gibson, D. H., *Chem. Rev.* **1996,** 96, 2063-2095.

130. Ellis, E. J., *Inorg. Chem.* **2006,** 45, 3167-3186.

131. Kubas, G. J., Metal dihydrogen and σ-bond complexes. 1st ed.; Kluwer Academic/Plenum Publishers: New York, 2001.

132. Clemente, M. E. N.; Saavedra, P. J.; Vásquez, M.; Paz-Sandoval, M. A.; Arif, A. M.; Ernst, R. D., *Organometallics* **2002,** 21, 592-605.

133. Bruce, M. I.; Hall, B. C.; Zaitseva, N. N.; Skelton, B. W.; White, A. H., *J. Chem. Soc. Dalton Trans.* **1998**, 1793-1803.

134. Hunter, C. A.; Lawson, K. R.; Perkins, J.; Urch, C. J., *J. Chem. Soc. Perkin Trans. 2* **2001**, 651-669.

135. Wiley, J. S.; Oldham Jr., W. J.; Heinekey, D. M., *Organometallics* **2000,** 19, 1670-1676.

136. Carmona, D.; Ferrer, J.; Lalaguna, E.; Lorenzo, M.; Lahoz, F. J.; Elipe, S.; Oro, L. A., *Eur. J. Inorg. Chem.* **2002**, 259-263.

137. Blake, A. J.; Halcrow, M. S.; Schröder, M., *J. Chem. Soc. Dalton Trans.* **1994**, 1631-1639.

138. Steed, J. W.; Anderson, K. M. http://www.dur.ac.uk/zprime/

139. Rice, F. O.; Vollrath, R. E., *Proc. Natl. Acad. Sci.* **1929,** 15, 702-705.

140. Freeman, G. R., *Proc. Roy. Sci. A* **1958,** 245, 40-48.

141. Albrecht, M.; Miecznikowski, J. R.; Samuel, A.; Faller, J. W.; Crabtree, R. H., *Organometallics* **2002,** 21, 3596-3604.

142. Stylianides, N. Ph.D. Thesis. University of Southampton, 2007.

143. Armarego, W. L. F.; Perrin, D. D., *Purification of Laboratory Chemicals*. 4th ed.; Butterworth Heinemann: 1997.

144. Johnson, A. L. U.S. Patent 3637731, 1972.

145. Blake, A. J.; Collier, P. E.; Dunn, S. C.; Li, W.-S.; Mountford, P.; Shishkin, O. V., *J. Chem. Soc. Dalton Trans.* **1997**, 1549-1558.
146. Baum, K., *J. Org. Chem.* **1968,** 33, 4333-4335.
147. Kuhn, N.; Kratz, T., *Synthesis* **1993**, 561-562.
148. Andersen, R. A.; Faegri Jr., K.; Green, J. C.; Haaland, A.; Lappert, M. F.; Leung, W.-P.; Rypdal, K., *Inorg. Chem.* **1988,** 27, 1782-1786.
149. Aresta, M.; Nobile, C. F.; Petruzzelli, D., *Inorg. Chem.* **1977,** 16, 1817-1818.
150. Selin, T. G.; West, R., *J. Am. Chem. Soc.* **1962,** 84, 1856-1859.
151. Soeldner, M.; Sandor, M.; Schier, A.; Schmidbauer, H., *Chem. Ber.* **1997,** 130, 1671-1676.
152. Akotsi, O. M.; Metera, K.; Reid, R. D.; McDonald, R.; Bergens, S. H., *Chirality* **2000,** 12, 514-522.
153. Chatt, J.; Venanzi, L. M., *J. Chem. Soc.* **1957**, 4735-4741.
154. van der Ent, A.; Onderdelinden, A. L., *Inorg. Synth.* **1990,** 28, 90-92.
155. Ranganathan, S.; Ranganathan, D.; Ramachandran, P. V., *Tetrahedron* **1984,** 40, 3145-3151.
156. Yakelis, N. A.; Bergman, R. G., *Organometallics* **2005,** 24, 3579-3581.
157. Evans, D. F., *J. Chem. Soc.* **1959**, 2003-2005.
158. Hooft, R.; COLLECT, *Nonius BV* **1997-2000**.
159. Otwinowski, Z.; Minor, W.; SCALEPACK, D., *Methods Enzymol.* **1997**, 276, 307.
160. Spek, A. L., *J. Appl. Cryst.* **2003,** 36, 7-13.
161. Farrugia, L. J. J., *Appl. Cryst.* **1999,** 32, 83.
162. Allen, F. H.; Johnson, O.; Shields, G. P.; Smith, B. R.; Towler, M., *J. Appl. Cryst.* **2004,** 37, 335-338.
163. Cernik, R. J.; Clegg, W.; Catlow, C. R. A.; Bushnell-Wye, G.; Flaherty, J. V.; Greaves, G. N.; Hamichi, M.; Burrows, I.; Taylor, D. J.; Teat, S. J., *J. Synchrotron Radiation* **1997,** 4, 279-286.
164. Dunn, A. D.; Guillermic, S., *Z. Chem.* **1988,** 28, 59-60.

Appendix I

CIF data for structurally characterised complexes

Compound	**35a**	**51**	**55**	**56**	**58**	**59**
Formula	$C_{35}H_{43}Br_2N_5$[a]	$C_7H_7Br_2N$	$C_7H_7I_2N$	$C_{37}H_{47}I_2N_5$[b]	$C_{37}H_{45}N_5$	$C_{74}H_{90}Ag_8I_8N_{10}$[c]
T/K	120(2)	120(2)	120(2)	120(2)	120(2)	120(2)
Crystal system	Monoclinic	Orthorhombic	Orthorhombic	Trigonal	Monoclinic	Monoclinic
Space group	$P2_1/c$	$P2_12_12_1$	Pbcn	R-3	$P2_1/c$	$P2_1/n$
a/ Å	13.5859(5)	10.5429(3)	7.6194(3)	52.325(4)	15.058(3)	13.6353(4)
b/ Å	17.2106(5)	12.4821(4)	14.6296(6)	52.325(4)	24.920(6)	22.1211(6)
c/ Å	24.6022(9)	12.6458(3)	8.1057(2)	9.4345(5)	10.967(3)	17.0640(5)
α/°	90	90	90	90	90	90
β/°	105.2940(10)	90	90	90	91.360(3)	98.0900(10)
γ/°	90	90	90	120	90	90
V/ Å^3	5548.8(3)	1664.16(8)	903.53(6)	22370(3)	4114.2(17)	5095.8(3)
Z	4	8	4	18	4	2
Density (calculated)	1.204 Mg/m^3	2.115 Mg/m^3	2.639 Mg/m^3	1.356 Mg/m^3	0.904 Mg/m^3	2.050 Mg/m^3
μ/mm^{-1}	1.762	9.665	6.890	1.563	0.054	3.972
F(000)	2070	1008	648	9120	1208	2976
Reflections collected	53445	14709	7765	40406	22457	78859
Independent reflections	12678	2175	1049	11431	5879	11729
R_{int}	0.1042	0.0431	0.0348	0.0842	0.0579	0.0516
Final R indices [I>2σ(I)]	R1 = 0.0732	R1 = 0.0255	R1 = 0.0212	R1 = 0.0665	R1 = 0.0700	R1 = 0.0560
	wR2 = 0.1649	wR2 = 0.0470	wR2 = 0.0452	wR2 = 0.1500	wR2 = 0.1937	wR2 = 0.1026
R indices (all data)	R1 = 0.1677	R1 = 0.0307	R1 = 0.0256	R1 = 0.1396	R1 = 0.1048	R1 = 0.0753
	wR2 = 0.1900	wR2 = 0.0487	wR2 = 0.0469	wR2 = 0.1754	wR2 = 0.2125	wR2 = 0.1121

a: contains ($C_4H_{10}O$) and 2.8(CH_2Cl_2), b: contains 1.6($CHCl_3$), c: contains 2($C_4H_{10}O$)

Compound	**64**	**65**	**68**	**70**	**71**
Formula	$C_{39}H_{49}Cl_2N_6Ti$	$C_{49}H_{70}Cl_2N_6O_2Ti$[a]	$C_{39}H_{49}Br_2N_5OV$	$C_{35}H_{41}Cl_2N_5OV$	$C_{41}H_{50}B_2F_8N_8OV$[b]
T/K	120(2)	120(2)	120(2)	120(2)	120(2)
Crystal system	Orthorhombic	Orthorhombic	Monoclinic	Monoclinic	Monoclinic
Space group	$P2_12_12_1$	Pbca	$P2_1/c$	$P2_1/n$	$P2_1/c$
a/ Å	10.802(9)	23.7970(8)	15.6919(15)	16.699(5)	16.851(3)
b/ Å	13.630(13)	16.5122(6)	14.6332(15)	19.125(5)	12.707(4)
c/ Å	32.45(2)	24.8086(8)	17.1157(12)	22.226(6)	21.564(4)
α/°	90	90	90	90	90
β/°	90	90	102.828(7)	97.012(4)	100.152(13)
γ/°	90	90	90	90	90
V/ Å^3	4778(7)	9748.3(6)	3832.1(6)	7045(3)	4545.1(18)
Z	4	8	4	8	4
Density (calculated)	1.002 Mg/m^3	1.218 Mg/m^3	1.412 Mg/m^3	1.263 Mg/m^3	1.309 Mg/m^3
μ/mm^{-1}	0.319	0.329	2.381	0.467	0.292
F(000)	1524	3824	1676	2808	1860
Reflections collected	28273	39418	36118	34114	66201
Independent reflections	4712	8551	8801	7369	10463
R_{int}	0.1106	0.1225	0.0883	0.1383	0.0687
Final R indices [I>2σ(I)]	R1 = 0.0852	R1 = 0.1059	R1 = 0.0755	R1 = 0.0763	R1 = 0.0604
	wR2 = 0.1929	wR2 = 0.1728	wR2 = 0.1573	wR2 = 0.1795	wR2 = 0.1382
R indices (all data)	R1 = 0.1183	R1 = 0.1951	R1 = 0.1398	R1 = 0.1342	R1 = 0.0957
	wR2 = 0.2087	wR2 = 0.2122	wR2 = 0.1831	wR2 = 0.2073	wR2 = 0.1564

a: contains 2(C_4H_8O), b: contains CH_3CN, c: contains (C_4H_8O), d: contains 3(C_3H_6O)

Compound	73	76	77	78	80
Formula	$C_{39}H_{49}Cl_3N_5NbO$ [c]	$C_{44}H_{61}Mo_6N_5O_{22}$ [d]	$C_{39}H_{49}Br_2MnN_5O$ [c]	$C_{39}H_{49}Br_2Cl_4MnN_5$	$C_{24}H_{46}MnN_4$
T/K	120(2)	120(2)	120(2)	120(2)	120(2)
Crystal system	Monoclinic	Triclinic	Monoclinic	Monoclinic	Monoclinic
Space group	$P2_1/c$	P-1	$P2_1/c$	$P2_1/c$	$P2_1/n$
a/ Å	10.803(7)	11.0498(4)	10.6948(8)	19.1593(4)	12.4893(6)
b/ Å	18.707(11)	15.6439(4)	18.7188(14)	14.7913(3)	15.9613(6)
c/ Å	18.838(17)	16.1858(4)	19.2039(19)	16.0236(2)	13.2704(5)
α/°	90	97.518(2)	90	90	90
β/°	92.61(6)	96.3940(10)	93.796(9)	108.1680(10)	91.700(2)
γ/°	90	91.447(2)	90	90	90
V/ Å^3	3803(5)	2754.35(14)	3836.1(6)	4314.56(14)	2644.23(19)
Z	4	2	4	4	4
Density (calculated)	1.403 Mg/m^3	1.914 Mg/m^3	1.417 Mg/m^3	1.454 Mg/m^3	1.119 Mg/m^3
μ/mm^{-1}	0.565	1.406	2.464	2.439	0.515
F(000)	1672	1576	1684	1924	972
Reflections collected	26634	54253	26916	45693	24819
Independent reflections	8730	12668	6754	9869	6064
R_{int}	0.1325	0.1878	0.0661	0.0569	0.0760
Final R indices [I>2σ(I)]	R1 = 0.0902	R1 = 0.0775	R1 = 0.0874	R1 = 0.0587	R1 = 0.0670
	wR2 = 0.1446	wR2 = 0.0984	wR2 = 0.2042	wR2 = 0.1037	wR2 = 0.1251
R indices (all data)	R1 = 0.1973	R1 = 0.1745	R1 = 0.1373	R1 = 0.0905	R1 = 0.1091
	wR2 = 0.1774	wR2 = 0.1158	wR2 = 0.2333	wR2 = 0.1178	wR2 = 0.1401

a: contains 2(C_4H_8O), b: contains CH_3CN, c: contains (C_4H_8O), d: contains 3(C_3H_6O)

Compound	**83**	**85**	**86**	**88**	**89**
Formula	$C_{37}H_{45}CoIN_5O_2$	$C_{23}H_{43}Br_2CoNP_2$	$C_{36}H_{43}Br_2Cl_2N_5Ni$[a]	$C_{49}H_{65}F_6N_5NiO_9S_2$[b]	$C_{20}H_{32}F_{12}Ni_4O_{20}S_4$
T/K	120(2)	120(2)	120(2)	120(2)	120(2)
Crystal system	Trigonal	Triclinic	Triclinic	Monoclinic	Tetragonal
Space group	R-3	P-1	P-1	C2/c	I41/a
a/ Å	30.2494(5)	12.1267(2)	12.7728(5)	22.7194(19)	15.77860(10)
b/ Å	30.2494(5)	15.2373(2)	13.6700(5)	25.510(3)	15.77860(10)
c/ Å	22.6059(8)	15.7810(2)	25.2292(10)	14.1716(13)	17.5089(3)
α/°	90	95.1970(10)	87.286(2)	90	90
β/°	90	91.7130(10)	75.428(2)	125.520(4)	90
γ/°	120	99.7470(10)	71.776(2)	90	90
V/ Å^3	17913.7(8)	2859.04(7)	4047.2(3)	6685.2(11)	4359.09(8)
Z	18	4	4	4	4
Density (calculated)	1.297 Mg/m^3	1.427 Mg/m^3	1.371 Mg/m^3	1.098 Mg/m^3	1.803 Mg/m^3
μ/mm^{-1}	1.242	3.517	2.616	0.415	2.012
F(000)	7164	1260	1704	2320	2384
Reflections collected	32602	64688	69924	28442	45911
Independent reflections	8902	13103	18589	7590	2502
R_{int}	0.0872	0.0395	0.1227	0.0715	0.0705
Final R indices [I>2σ(I)]	R1 = 0.0729	R1 = 0.0312	R1 = 0.0900	R1 = 0.0869	R1 = 0.0552
	wR2 = 0.1388	wR2 = 0.0662	wR2 = 0.1668	wR2 = 0.1959	wR2 = 0.1458
R indices (all data)	R1 = 0.1296	R1 = 0.0429	R1 = 0.1837	R1 = 0.1390	R1 = 0.0641
	wR2 = 0.1604	wR2 = 0.0696	wR2 = 0.1947	wR2 = 0.2181	wR2 = 0.1509

a: contains CH_2Cl_2, b: containsC_4H_9O, c: contains $C_4H_{10}O$, d: contains 2(C_4H_9O)

Compound	**92**	**93**	**94**	**95**	**96**	**98**
Formula	$C_{38}H_{45}N_5Ni$	$C_{41}H_{57}N_5NiO$[c]	$C_{35}H_{41}BrF_6N_5NiP$	$C_{37}H_{45}AgBrI_2N_5Ni$	$C_{84}H_{106}Ag_2F_6N_{10}O_8S_2$[d]	$C_{38}H_{45}BrF_3N_5NiO_3S$
T/K	120(2)	120(2)	120(2)	120(2)	120(2)	120(2)
Crystal system	Triclinic	Triclinic	Monoclinic	Monoclinic	Triclinic	Triclinic
Space group	P-1	P-1	C2/c	C2/c	P-1	P-1
a/ Å	8.2121(16)	9.907(2)	35.7904(8)	41.413(2)	12.7012(3)	8.6147(3)
b/ Å	12.417(3)	13.813(3)	8.6403(2)	8.1837(4)	13.0999(3)	14.2268(7)
c/ Å	32.452(7)	15.330(3)	23.4502(5)	23.0900(11)	13.2765(3)	16.2224(8)
α/°	92.18(3)	111.24(3)	90	90	89.4130(10)	101.802(2)
β/°	92.16(3)	93.82(3)	99.3100(10)	104.661(2)	74.8100(10)	98.787(3)
γ/°	95.77(3)	99.87(3)	90	90	80.2370(10)	96.327(3)
V/ Å^3	3287.1(13)	1907.3(7)	7156.2(3)	7570.7(6)	2099.59(8)	1902.67(15)
Z	4	2	8	8	1	2
Density (calculated)	1.274 Mg/m^3	1.210 Mg/m^3	1.514 Mg/m^3	1.860 Mg/m^3	1.406 Mg/m^3	1.479 Mg/m^3
μ/mm^{-1}	0.625	0.546	1.768	3.735	0.590	1.673
F(000)	1344	748	3344	4144	924	876
Reflections collected	36665	18662	41758	42239	42521	27224
Independent reflections	19426	9332	8207	8691	9617	6686
R_{int}	0.0372	0.0377	0.0568	0.0734	0.0435	0.1479
Final R indices [I>2σ(I)]	R1 = 0.0484	R1 = 0.0498	R1 = 0.0394	R1 = 0.0667	R1 = 0.0381	R1 = 0.1050
	wR2 = 0.1099	wR2 = 0.1154	wR2 = 0.0722	wR2 = 0.1858	wR2 = 0.0889	wR2 = 0.1744
R indices (all data)	R1 = 0.0773	R1 = 0.0797	R1 = 0.0583	R1 = 0.1067	R1 = 0.0476	R1 = 0.1853
	wR2 = 0.1217	wR2 = 0.1286	wR2 = 0.0781	wR2 = 0.2119	wR2 = 0.0932	wR2 = 0.2085

a: contains CH_2Cl_2, b: containsC_4H_8O, c: contains $C_4H_{10}O$, d: contains 2(C_4H_9O)

Compound	**109**	**110**	**111**	**112**	**113**
Formula	$C_{37}H_{45}FeI_2N_5$	$C_{41}H_{55}FeN_9O$[a]	$C_{39}H_{45}FeN_5O_2$	$C_{23}H_{43}Br_2FeNP_2$	$C_{23}H_{43}Cl_2FeNP_2$
T/K	120(2)	120(2)	120(2)	120(2)	120(2)
Crystal system	Monoclinic	Triclinic	Monoclinic	Triclinic	Monoclinic
Space group	$P2_1$	P-1	$P2_1/c$	P-1	$P2_1/n$
a/ Å	8.8591(4)	8.75940(10)	16.7597(4)	12.1603(2)	12.1029(3)
b/ Å	18.4412(11)	14.5429(3)	8.66210(10)	15.2569(3)	15.5317(5)
c/ Å	11.3826(7)	16.0312(3)	24.5438(6)	15.7158(2)	14.5111(4)
α/°	90	100.4120(10)	90	94.4130(10)	90
β/°	91.177(4)	93.2570(10)	101.0080(10)	92.0750(10)	91.026(2)
γ/°	90	98.1720(10)	90	99.3910(10)	90
V/ Å^3	1859.21(18)	1980.99(6)	3497.57(13)	2864.60(8)	2727.34(13)
Z	2	2	4	4	4
Density (calculated)	1.553 Mg/m^3	1.250 Mg/m^3	1.276 Mg/m^3	1.417 Mg/m^3	1.272 Mg/m^3
μ/mm^{-1}	2.098	0.425	0.472	3.438	0.877
F(000)	868	796	1424	1256	1112
Reflections collected	22960	41463	68261	61571	36718
Independent reflections	4403	9089	8118	13154	6250
R_{int}	0.1095	0.0352	0.1785	0.0488	0.0326
Final R indices [I>2σ(I)]	R1 = 0.0666	R1 = 0.0377	R1 = 0.0819	R1 = 0.0363	R1 = 0.0284
	wR2 = 0.1090	wR2 = 0.0912	wR2 = 0.1178	wR2 = 0.0728	wR2 = 0.0663
R indices (all data)	R1 = 0.0885	R1 = 0.0511	R1 = 0.1346	R1 = 0.0571	R1 = 0.0390
	wR2 = 0.1153	wR2 = 0.0975	wR2 = 0.1319	wR2 = 0.0779	wR2 = 0.0710

a: contains $C_4H_{10}O$, b: contains CH_2Cl_2

Compound	**115**	**116**	**117**	**118**	**119**
Formula	$C_{25}H_{43}FeNO_2P_2$	$C_{53}H_{58.50}FeN_7$	$C_{37}H_{43}Br_2Cl_2FeN_5O^b$	$C_{48}H_{52}FeN_6$	$C_{70}H_{82}FeN_{10}$
T/K	120(2)	120(2)	120(2)	120(2)	120(2)
Crystal system	Orthorhombic	Triclinic	Monoclinic	Triclinic	Monoclinic
Space group	$P2_12_12_1$	P-1	$P2_1/c$	P-1	$P2_1/c$
a/ Å	11.7566(6)	12.091(3)	10.60920(10)	11.5045(11)	12.6784(12)
b/ Å	14.5937(9)	13.626(4)	18.6753(2)	18.0009(13)	21.467(2)
c/ Å	15.3337(8)	14.446(2)	18.9664(2)	19.7074(9)	27.096(3)
α/°	90	84.619(19)	90	83.719(5)	90
β/°	90	86.191(17)	96.2100(10)	81.106(5)	90.944(9)
γ/°	90	76.301(15)	90	80.497(6)	90
V/ Å^3	2630.8(3)	2299.6(9)	3735.76(7)	3962.1(5)	7373.6(12)
Z	4	2	4	4	4
Density (calculated)	1.281 Mg/m^3	1.227 Mg/m^3	1.530 Mg/m^3	1.289 Mg/m^3	1.008 Mg/m^3
μ/mm^{-1}	0.716	0.372	2.723	0.423	0.246
F(000)	1088	903	1752	1632	2392
Reflections collected	14450	38960	88327	56331	39036
Independent reflections	5989	10526	8574	18237	9903
R_{int}	0.0770	0.0917	0.0496	0.0678	0.0703
Final R indices [I>2σ(I)]	R1 = 0.0530	R1 = 0.0706	R1 = 0.0327	R1 = 0.0600	R1 = 0.0731
	wR2 = 0.1034	wR2 = 0.1401	wR2 = 0.0741	wR2 = 0.1207	wR2 = 0.1942
R indices (all data)	R1 = 0.0720	R1 = 0.1326	R1 = 0.0470	R1 = 0.1320	R1 = 0.1172
	wR2 = 0.1106	wR2 = 0.1623	wR2 = 0.0796	wR2 = 0.1459	wR2 = 0.2132

a: contains $C_4H_{10}O$, b: contains CH_2Cl_2

Compound	**125**	**126**	**127**	**128**	**129**
Formula	$C_{53}H_{63}FeN_5Si_3$	$C_{49}H_{61}FeN_5Si_2$	$C_{59}H_{65}FeN_5Si_2$	$C_{58}H_{73}FeN_5Si_3$	$C_{53}H_{67}FeN_7Si_2$
T/K	120(2)	120(2)	120(2)	120(2)	120(2)
Crystal system	Monoclinic	Orthorhombic	Monoclinic	Monoclinic	Monoclinic
Space group	$P2_1/c$	Pbca	C_2/c	$P2_1/n$	C_2/c
a/ Å	18.195(19)	12.2235(4)	23.466(5)	14.6347(5)	19.556(5)
b/ Å	14.27(3)	19.7035(8)	10.382(2)	17.4275(7)	17.102(5)
c/ Å	19.696(9)	37.4328(13)	22.594(4)	20.4980(7)	15.405(4)
α/°	90	90	90	90	90
β/°	101.44(7)	90	111.47(3)	90.266(2)	107.316(3)
γ/°	90	90	90	90	90
V/ Å^3	5013(11)	9015.5(6)	5123(2)	5227.9(3)	4919(2)
Z	4	8	4	4	4
Density (calculated)	1.206 Mg/m^3	1.226 Mg/m^3	1.240 Mg/m^3	1.246 Mg/m^3	1.234 Mg/m^3
μ/mm^{-1}	0.412	0.427	0.385	0.400	0.398
F(000)	1936	3552	2032	2096	1952
Reflections collected	55154	99536	17951	60685	17290
Independent reflections	9215	10340	5426	11952	5048
R_{int}	0.1625	0.1130	0.0398	0.0959	0.0627
Final R indices [I>2σ(I)]	R1 = 0.0830	R1 = 0.0553	R1 = 0.0407	R1 = 0.0684	R1 = 0.0693
	wR2 = 0.1149	wR2 = 0.1102	wR2 = 0.0985	wR2 = 0.1279	wR2 = 0.1901
R indices (all data)	R1 = 0.1635	R1 = 0.1162	R1 = 0.0572	R1 = 0.1251	R1 = 0.1131
	wR2 = 0.1345	wR2 = 0.1303	wR2 = 0.1065	wR2 = 0.1468	wR2 = 0.2172

a: contains $C_4H_{10}O$, b: contains CH_2Cl_2

Compound	**132**	**133**	**134**	**136**	**138**
Formula	$C_{35}H_{41}ClN_8O_{1.5}Ru$	$C_{53}H_{56}N_{11}PRu$	$C_{40}H_{46}Cl_2N_6Ru$	$C_{53}H_{69}Cl_2N_5Rh_2$	$C_{39}H_{49}Cl_5IrN_5$[a]
T/K	120(2)	120(2)	120(2)	120(2)	120(2)
Crystal system	Monoclinic	Trigonal	Monoclinic	Monoclinic	Monoclinic
Space group	$P2_1/c$	R-3	$P2_1/c$	$P2_1/n$	$P2_1/c$
a/ Å	18.9874(17)	28.1159(7)	19.390(4)	10.3726(19)	10.9651(18)
b/ Å	10.2038(9)	28.1159(7)	15.960(3)	39.191(7)	19.437(3)
c/ Å	19.2212(17)	36.6687(18)	12.590(2)	13.469(3)	19.241(3)
α/°	90	90	90	90	90
β/°	109.567(4)	90	103.46(3)	104.905(2)	97.490(2)
γ/°	90	120	90	90	90
V/ Å^3	3508.9(5)	25103.3(15)	3789.1(12)	5291.1(18)	4065.8(11)
Z	4	18	4	4	4
Density (calculated)	1.390 Mg/m^3	1.166 Mg/m^3	1.372 Mg/m^3	1.322 Mg/m^3	1.564 Mg/m^3
μ/mm^{-1}	0.564	0.352	0.591	0.763	3.647
F(000)	1520	9180	1624	2184	1920
Reflections collected	19667	25620	25139	54970	28967
Independent reflections	7939	12819	8593	15629	7136
R_{int}	0.0546	0.0945	0.1291	0.0627	0.0613
Final R indices [I>2σ(I)]	R1 = 0.0694	R1 = 0.0815	R1 = 0.0775	R1 = 0.0439	R1 = 0.0347
	wR2 = 0.1546	wR2 = 0.1767	wR2 = 0.1305	wR2 = 0.1007	wR2 = 0.0923
R indices (all data)	R1 = 0.1155	R1 = 0.1526	R1 = 0.1659	R1 = 0.0587	R1 = 0.0390
	wR2 = 0.1742	wR2 = 0.2034	wR2 = 0.1562	wR2 = 0.1062	wR2 = 0.0959

a: contains CH_2Cl_2, b: contains 0.5(CH_2Cl_2), c: contains CH_3CN, d: contains 0.5($C_4H_{10}O$), e: contains 2(C_3H_6O)

Compound	**141**	**143**	**144**	**145**	**147**
Formula	$C_{37}H_{46}IrN_5$	$C_{74}H_{91}IrN_{10}$	$C_{76.5}H_{92}ClF_6IrN_{10}O_6S_2$[b]	$C_{74}H_{62}BF_{24}IrN_6$	$C_{40}H_{48}F_6IrN_6OP$[c]
T/K	120(2)	120(2)	120(2)	120(2)	120(2)
Crystal system	Triclinic	Monoclinic	Monoclinic	Triclinic	Triclinic
Space group	P-1	$P2_1/n$	$P2_1/n$	P-1	P-1
a/ Å	11.7002(4)	15.4729(2)	18.394(3)	12.90010(10)	8.3881(7)
b/ Å	12.2554(4)	18.0377(2)	20.416(3)	16.6745(2)	14.5928(14)
c/ Å	12.7077(5)	24.8736(3)	21.987(3)	19.7485(3)	17.1949(17)
α/°	83.460(2)	90	90	109.0790(10)	106.162(4)
β/°	80.693(2)	100.9550(10)	95.928(2)	99.9180(10)	96.835(6)
γ/°	71.350(2)	90	90	103.0800(10)	94.952(6)
V/ Å^3	1699.98(10)	6815.60(14)	8213(2)	3767.99(9)	1991.4(3)
Z	2	4	4	2	2
Density (calculated)	1.471 Mg/m^3	1.279 Mg/m^3	1.337 Mg/m^3	1.493 Mg/m^3	1.611 Mg/m^3
μ/mm^{-1}	3.959	2.007	1.777	1.876	3.461
F(000)	760	2728	3396	1692	968
Reflections collected	31429	84696	61947	65917	32449
Independent reflections	7776	15557	14500	17240	9126
R_{int}	0.0410	0.0406	0.0915	0.0620	0.0790
Final R indices [I>2σ(I)]	R1 = 0.0358	R1 = 0.0328	R1 = 0.0516	R1 = 0.0480	R1 = 0.0718
	wR2 = 0.0676	wR2 = 0.0649	wR2 = 0.1250	wR2 = 0.1152	wR2 = 0.1287
R indices (all data)	R1 = 0.0490	R1 = 0.0419	R1 = 0.0785	R1 = 0.0542	R1 = 0.1096
	wR2 = 0.0736	wR2 = 0.0684	wR2 = 0.1359	wR2 = 0.1198	wR2 = 0.1466

a: contains CH_2Cl_2, b: contains 0.5(CH_2Cl_2), c: contains CH_3CN, d: contains 0.5($C_4H_{10}O$), e: contains 2(C_3H_6O)

Compound	**148**	**149**	**150**
Formula	$C_{41}H_{53}F_6IrN_5P$	$C_{41}H_{53}F_6IrN_6O_{0.5}P$[d]	$C_{80}H_{99}Cl_2F_6Ir_2N_{10}O_2P$[e]
T/K	120(2)	120(2)	120(2)
Crystal system	Triclinic	Triclinic	Triclinic
Space group	P-1	P-1	P-1
a/ Å	8.5051(6)	17.0076(2)	16.618(5)
b/ Å	15.1440(10)	20.5915(2)	17.523(5)
c/ Å	16.5098(11)	24.7477(2)	18.315(5)
α/°	105.8720(10)	99.6300(10)	65.338(3)
β/°	101.4970(10)	100.3820(10)	70.541(3)
γ/°	91.0240(10)	90.6060(10)	66.844(3)
V/ Å^3	1998.5(2)	8397.50(14)	4364(2)
Z	2	8	2
Density (calculated)	1.584 Mg/m^3	1.542 Mg/m^3	1.395 Mg/m^3
μ/mm^{-1}	3.445	3.283	3.186
F(000)	960	3928	1844
Reflections collected	21458	142467	41356
Independent reflections	11584	38358	21172
R_{int}	0.0420	0.0536	0.0298
Final R indices [I>2σ(I)]	R1 = 0.0334	R1 = 0.0544	R1 = 0.0322
	wR2 = 0.0849	wR2 = 0.0994	wR2 = 0.0801
R indices (all data)	R1 = 0.0362	R1 = 0.0827	R1 = 0.0394
	wR2 = 0.0864	wR2 = 0.1132	wR2 = 0.0830

a: contains CH_2Cl_2, b: contains 0.5(CH_2Cl_2), c: contains CH_3CN, d: contains 0.5($C_4H_{10}O$), e: contains 2(C_3H_6O)

Appendix II

Additional characterisation and structural data

2,6-Bis(2,6-diisopropylphenyl)imidazolium-3,5-dimethylpyridine dibromide (**57**)

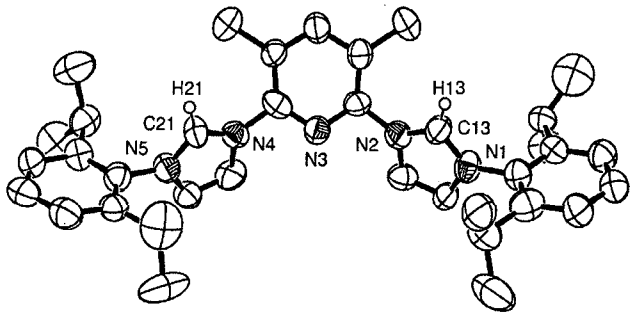

Titanium(IV) mesitylimido dichloride bis(dimethylamine) (**154**)

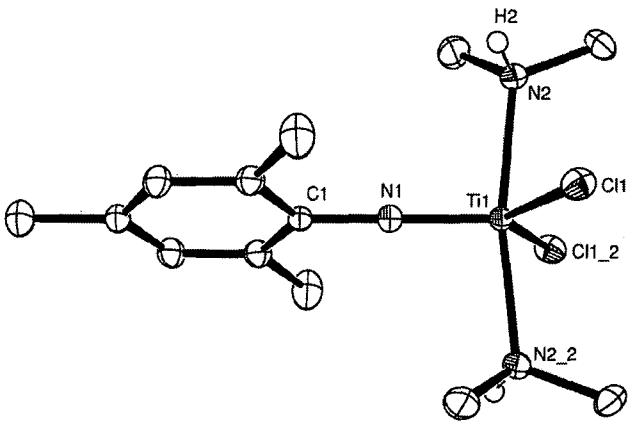

Following the procedure of Adams *et al.*,[91] to a solution of $Ti(NMe_2)_2Cl_2$ (1.04 g, 5.0 mmol) in benzene (20 mL) was added mesityl amine (0.7 mL, 5.0 mmol) and the reaction was stirred for 16 hours. After this time the solvent was removed, affording 1.7 g of a brown solid in 99% yield.

δ_H (300.0 MHz, C_6D_6): 6.67 (2H, s, Ar), 2.76 (6H, s, *o*-Me), 2.25 (12H, d, $J = 4.5$ Hz, NMe), 2.11 (3H, s, *p*-Me) ppm.

δ_C (75.5 MHz, C_6D_6): 159.07 (C, C–N), 133.74 (C, Ar), 131.59 (C, Ar), 128.08 (CH, Ar), 40.75 (CH_3, NMe), 21.01 (CH_3, *p*-Me), 19.47 (CH_3, *o*-Me)

Analysis: Calc. for $C_{13}H_{25}N_3TiCl_2$: C 45.64; H 7.37; N 12.28. Found: C 45.51; H 7.45; N 12.18.

Bis[zirconium(IV) (μ^2-mesitylimido) dichloride bis(tetrahydrofuran)] (**155**)

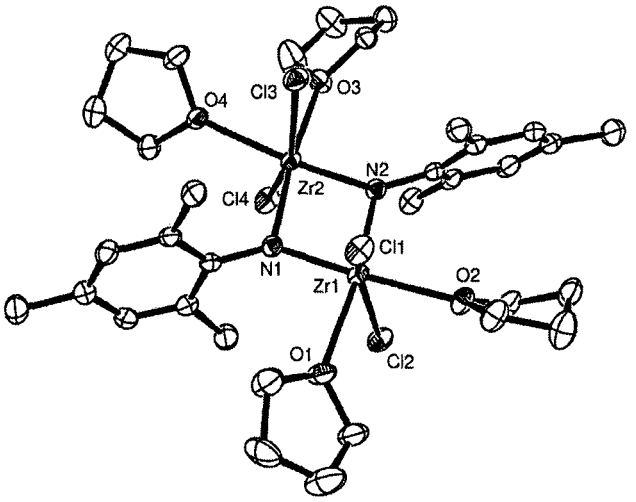

Following the procedure of Arney *et al.*,[92] a solution of $ZrCl_4(THF)_2$ (1.50 g, 3.98 mmol) in THF (40 mL) was added dropwise to a solution of lithium mesitylamide (3.0 g, 21.0 mmol) in THF (10 mL) and the reaction was stirred for 16 hours at RT. After this time the solvent was removed *in vacuo*, the resulting oil was dissolved in PhMe (30 mL) and filtered through Celite. The solvent was removed *in vacuo*, the resulting oil was dissolved in THF (60 mL) and transferred to an ampoule. TMSCl (1.06 mL, 8.3 mmol) was added and the reaction was stirred at 65 °C for 16 hours. After this time the solution was cooled, THF removed, and the solid triturated with pentane. After drying *in vacuo*, 1.7 g of a bright yellow solid in 97% yield was isolated. Crystallisation occurred from the slow diffusion of PE into a THF solution.

δ_H (300.0 MHz, C_6D_6): 6.84 (2H, s, Ar), 3.67 (8H, br s, OCH_2), 3.27 (6H, s, *o*-CH_3), 2.21 (3H, s, *p*-CH_3), 1.21 (8H, br s, CH_2) ppm.

δ_C (75.5 MHz, C_6D_6): 149.53 (C, C–N), 130.86 (C, Ar), 130.73 (C, Ar), 128.88 (CH, Ar), 70.85 (CH_2, OCH_2), 25.13 (CH_2, THF CH_2), 22.13 (CH_3, *o*-CH_3), 20.64 (CH_3, *p*-CH_3) ppm.

Analysis: Calc. for $C_{34}H_{54}N_2O_4Zr_2Cl_4$: C 46.45; H 6.19; N 3.19. Found: C 46.29; H 5.99; N 3.34.

(2,6-Bis(2,6-diisopropylphenyl)imidazol-2-ylidene)pyridine chromium(III) trichloride (**63**)

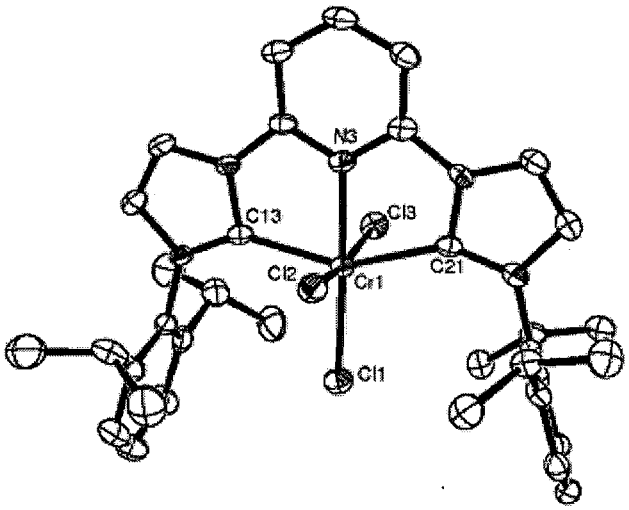

Compound	**57**	**154**	**155**	**63**
Formula	$C_{37}H_{47}Br_2N_5$	$C_{13}H_{25}Cl_2N_3Ti$	$C=H_{70}Cl_4N_2O_6Zr_2$	$C_{39}H_{49}Cl_3CrN_5O$[a]
T/K	120(2)	120(2)	120(2)	120(2)
Crystal system	Trigonal	Monoclinic	Monoclinic	Monoclinic
Space group	R-3	C_2/c	$P2_1/c$	$P2_1/c$
a/ Å	52.1838(13)	13.9749(9)	17.6060(7)	10.880(7)
b/ Å	52.1838(13)	11.7855(7)	14.0480(6)	18.88(3)
c/ Å	9.4150(3)	12.7931(9)	21.8334(8)	18.44(3)
α/°	90	90	90	90
β/°	90	121.171(2)	118.619(3)	94.53(10)
γ/°	120	90	90	90
V/ Å^3	22203.5(11)	1802.8(2)	4740.3(3)	3777(8)
Z	18	4	4	4
Density (calculated)	0.971 Mg/m^3	1.261 Mg/m^3	1.434 Mg/m^3	1.340 Mg/m^3
μ/mm^{-1}	1.666	0.763	0.710	0.553
F(000)	6732	720	2128	1604
Reflections collected	60773	5222	56589	57205
Independent reflections	8591	2038	10861	8673
R_{int}	0.0739	0.0256	0.0561	0.1563
Final R indices [I>2σ(I)]	R1 = 0.0995	R1 = 0.0275	R1 = 0.0397	R1 = 0.0853
	wR2 = 0.2847	wR2 = 0.0690	wR2 = 0.0727	wR2 = 0.1331
R indices (all data)	R1 = 0.1366	R1 = 0.0336	R1 = 0.0728	R1 = 0.1534
	wR2 = 0.3094	wR2 = 0.0715	wR2 = 0.0825	wR2 = 0.1540

Appendix III

List of publications

Publications:

'Pincer' dicarbene complexes of some early transition metals and uranium; David Pugh, Joseph A. Wright, Sandra Freeman and Andreas A. Danopoulos; *Dalton Trans.*; **2006**; 775-782

2,6-Dibromo-3,5-dimethylpyridine and 2,6-diiodo-3,5-dimethylpyridine; David Pugh; *Acta Cryst.* (2006); **C62**; o590-o592

'Pincer' pyridine dicarbene complexes of nickel and their derivatives: unexpected ring-opening of a coordinated imidazol-2-ylidene; David Pugh, Aimee Boyle and Andreas A. Danopoulos; *Dalton Trans.*; **2008**; 1087-1094.

Reviews:

Metal complexes with 'pincer'-type ligands incorporating N-heterocyclic carbene functionalities; David Pugh and Andreas A. Danopoulos; *Coord. Chem. Rev.*; **2007**; 251; 610-641